The Impact of Portland Cement on the Performance of Cold In-Place Recycled Pavement

by

Taha Younes

A thesis

presented to the University of Waterloo

in fulfilment of the

thesis requirement for the degree of

Doctor of Philosophy

in

Civil Engineering

Waterloo, Ontario, Canada, 2022

Examining Committee Membership

The following served on the Examining Committee for this thesis. The decision of the Examining Committee is by majority vote.

External Examiner	Dr. Leila Hashemian Professor Department of Civil & Environmental Engineering, University of Alberta
Supervisor	Dr. Susan Tighe Professor Civil & Environmental Engineering University of Waterloo
Supervisor	Dr. Shunde Yin Professor Civil & Environmental Engineering University of Waterloo
Internal Member	Dr. Hassan Baaj Professor Civil & Environmental Engineering University of Waterloo
Internal Member	Dr. Steve Goodman Professor Civil & Environmental Engineering University of Waterloo
Internal-external Member	Dr. Kaan Inal Professor Mechanical & Mechatronics Engineering University of Waterloo

Author’s Declaration

I hereby declare that I am the sole author of this thesis. This is a true copy of the thesis, including any required final revisions, as accepted by my examiners. I understand that my thesis may be made electronically available to the public.

Abstract

In place recycling of existing asphalt pavement is a rehabilitation strategy, which the Ministry of Transportation Ontario (MTO) adopted decades ago. Asphalt emulsion is the most common type of bitumen stabilizing agent incorporated into recycled mixtures in Ontario. Active fillers such as Portland cement, hydrated lime and fly ash can be added to a volume fraction of less than 1% to the recycled mixtures to improve dispersion of the bitumen in the mixtures and to increase the stiffness of the mixtures and the rate of strength gain. This study is a project of the Centre for Pavement and Transportation Technology (CPATT) laboratory at the University of Waterloo in partnership with the MTO and various industry partners in Ontario. Cationic Slow Setting Emulsion (CSS-1H) and Anionic High Float Emulsion (HF-150) emulsions were mixed with typical Reclaimed Asphalt Pavement materials (RAP), which are pulverized (HL8 and HL3) in the CPATT laboratory at the University of Waterloo. To improve the dispersion of the bitumen in the mixes and to increase the stiffness of the mixtures and the rate of strength gain, different percentages of Portland cement (0%, 0.5%, 1.5% and 3%) were added to the mixes. Four mixes were prepared. Mixture 1 (M1) was developed using the cationic slow setting emulsion-CSS-1H that was mixed with a pulverized HL8 RAP material; for the second mixture (M2), the Anionic High Float Emulsion (HF-150) was mixed with a pulverized HL8 RAP material. However, for the third mixture (M3), the cationic slow setting emulsion-CSS-1H was mixed with pulverized HL3 RAP material, and for the fourth mixture (M4), the Anionic High Float Emulsion (HF-150) was mixed with pulverized HL3 RAP material. These mixes were tested and evaluated using Indirect Tensile, Dynamic Modulus, Fatigue and Thermal Stress Restrained Specimen Tests. Furthermore, the moisture susceptibility was controlled by conditioning the specimens for 24 hours at 25 degrees Celsius before testing. The results showed that increasing the percentage of Portland cement led to an increase in strength. For the Cold In-Place Recycled Asphalt (CIR) mixes, the addition of Portland cement increased the stiffness. For M1 and M2 mixes, there was a tradeoff relationship between the stiffness and fatigue life. Adding amounts of Portland cement between 0.5% and 1.5% to these mixes increased the stiffness significantly with only a small reduction in fatigue life. As Portland cement was added to M3 and M4 mixtures, the stiffness increased until the cement content reached 1.5%. Additions above 1.5% did not produce a noticeable increase in stiffness. Also, the tensile strength and moisture resistance improved significantly with the addition of Portland

cement. However, the low-temperature fracture properties of the mixtures deteriorated due to increased brittleness and the development of shrinkage cracks that caused the mixtures to fail at higher temperatures and lower fracture stresses. In all cases, adding amounts of Portland cement between 0.5% and 1.5% enhanced the stiffness, tensile strength, and moisture susceptibility resistance of the mixes with only a small reduction in fatigue life. Finally, a classic Maxwell model, a rheological model comprised of a spring and dashpot in a series of materials, was used to simulate either the stress-strain behaviour of the material or the force-deformation relationship of a test specimen. The model, once calibrated using the stress-strain data from a single specimen fatigue test, accurately described the stress-strain histories for all tests. Features described by the model included the stress-strain hysteresis loop shape, the relaxation of mean stress to zero under controlled strain cycling and the decrease of stress range with cyclic straining. The latter gave accurate predictions of the reduction of the initial stiffness to one-half its initial value, which was used as the definition of failure.

Acknowledgements

First and foremost, I would like to thank and praise Allah for helping and guiding me through this work and giving me the patience and health necessary to complete my PhD degree.

I would like to express my sincere gratitude and appreciation to my supervisor Prof. Susan Tighe for her patience, help, understanding, guidance, and an outstanding supervision. "Her courage, devotion, and patience, have deeply inspired me". I am really greatfull to be one of her students. She was always there for me to answer all my questions and inquires. Also, I would like to thank Professor Tim Topper, Shunde Yin for their support, help and encouragement throughout my PhD.

I would also like to acknowledge the technical assistance of laboratory technicians Peter Volcic, Richard Morrison and Douglas Hirst. I would like to acknowledge the committee members for their time in reading my thesis. Special thanks to all my family, friends and CPATT Group for their help and support. Finally, I would like to thank both the Ministry of Transportation Ontario (MTO), Coco and Mcasphslt companies for funding the project and feedback for the project.

Table of Contents

List of Figures

List of Tables

List of Abbreviations

AASHTO	American Association of State Highway Transportation Officials
AC	Asphalt Cement
PDR	Partial Depth Reclamation
CIR	Cold In-Place Recycled Pavement
CIREAM	Cold In-Place Recycling with Expanded Asphalt Mixture
CPATT	Centre for Pavement and Transportation Technology
E*	Dynamic Modulus
HMA	Hot Mix Asphalt
HF-150	Anionic High Float Emulsion
MTO	Ministry of Transportation Ontario
PG	Performance Graded
RAP	Recycled Asphalt Pavement
SGC	Superpave Gyratory Compactor
CSS-1H	Cationic Slow Setting Emulsion
TSRST	Thermal Stress Restrained Specimen Test
δ	Phase Angle
M1	Mixture # 1 where CSS-1H mixed with pulverized HL8 RAP
M2	Mixture # 2 where HF-150 mixed with pulverized HL8 RAP
M3	Mixture # 3 where CSS-1H mixed with pulverized HL3 RAP
M4	Mixture # 4 where HF-150 mixed with pulverized HL3 RAP

1 Introduction

1.1 Background

Road construction maintenance and repair cost the government of Ontario a substantial portion of its budget every year. An increase in the population requires improvements in the quality of our roads. However, sometimes due to limitations of budget, contractors, and government agencies have to maintain and rehabilitate the roads at a low cost and hence lower than optimum quality. Adopting cost-effectiveness and environmentally friendly techniques to improve the quality of road rehabilitation and maintenance has become one of the priorities for governments and many contractors (Johnson, 2000). The classic method of road maintenance and rehabilitation is to lay a new layer of hot mix asphalt (HMA) after preparing the old pavement. In some cases, when a road is severely distressed, milling off the top layer of the pavement is required, and then a new HMA layer is placed (Abiodun, 2014). This traditional way of maintenance and rehabilitation provides a good surface quality; however, it has drawbacks. Some of these drawbacks are the users' delays caused by the required long construction period of HMA, the high cost and the large amount of energy needed to produce the HMA and reconstruct the base layer. Furthermore, the traditional way of rehabilitation is not considered environmentally friendly due to the greenhouse gasses that are released during the process. For the above-mentioned reasons, governments, contractors, and designers have put much effort into overcoming these disadvantages. Designers have been driven to utilize more environmentally friendly alternatives. Designs have been made to improve the efficiency of the pavement structure and to reduce traffic and construction delays (Alkins et al., 2008). In the light of this scenario, recycling methods have become more acceptable around the world (Lewis et al., 1999). Reclaiming methods for asphalt include hot in-place recycling and cold in-place recycling for partial and full-depth reclamation (Abiodun, 2014).

Partial Depth Reclamation (PDR) is one of the rehabilitation techniques in which 100% of Reclaimed Asphalt Pavement (RAP) is used. This technique is carried out in place (Bhavsar, 2015). There are several benefits of using PDR technique, such as: reducing project costs since there is no off-site hauling of aggregate (Alkins et al., 2008), and the fuel consumption and the emissions of carbon dioxide and nitrous oxide are reduced as well (Chesner, 2011). The Partial Depth Reclamation is a sustainable rehabilitation technique in terms of environmental and economic benefits (Mallick et al., 2008). In Ontario, there are two rehabilitation techniques with PDR. The two techniques, which involve removing and milling about 70% - 75% of the existing pavement, are Cold In- Place Recycling (CIR) and Cold In-Place Recycling with Expanded Asphalt Mixture (CIREAM). The focus of this study is to investigate the effect on pavement behaviour of adding Portland Cement to CIR mixtures in amounts that do not compromise the stiffness or fatigue life. Through this study, recommendations to advance the state-of-the-art or CIR mixture design procedure have been provided. Finally, guidelines to encourage and promote the use of CIR technique, which is considered cost-effective and environmentally friendly mixtures are proposed.

1.2 Problem Statement

CIR has been used in Canada, particularly in Ontario, for many years. Fillers such as Portland cement are added (<1%) to the recycled mixture to improve the dispersion of the bitumen in the mixture and as a result, increase the stiffness and rate of the early strength gain.

The main purpose of adding Portland Cement is to increase the short-term strength and shorten the curing time of the mixture. The author has found no previous published data on the effect of Portland Cement on CIR mixtures in Ontario. The optimum cement content is still unknown. Excessive amounts of Portland Cement cause sudden and premature cracks. Moreover, the behaviour of the CIR mixture under cyclic loading with the addition of Portland Cement is not fully understood. Therefore, the main objective of this study is to investigate the impact of the addition of Portland Cement on the mechanical behaviour of CIR mixtures. In addition, the goal of this study is to experimentally determine the applicability of the Classic Maxwell Model to simulating the viscos-elastic deformation behaviour exhibited by CIR mixture when subjected to cyclic loading.

1.3 Scope and Objectives

Cement materials tend to behave in a brittle manner and crack due to shrinkage, which affects the performance of asphalt pavement. However, by determining the optimum cement content, moisture content, and accurate mix design these cracks can be minimized.

In this research, Portland Cement additives will be added to the CIR in order to determine the optimum cement content and to evaluate the properties of resulting asphalt mixtures. The Portland Cement will be introduced in powder form. In summary, the main objectives of the proposed research are as follows:

- To find the optimum cement content added to CIR mixtures (for the combinations of different of emulsion types and aggregates used in this study) without significantly compromising either the stiffness or fatigue life of the pavement.
- To compare the effect of different gradations of the (RAP) on the mechanical behaviours of the mixtures.
- To provide recommendations about the optimum Portland Cement percentages that should be used.
- To develop a numerical model in order to predict the performance of in-place recycled asphalt pavement and compare the model predictions with laboratory testing data.

1.4 Research hypothesis

The fundamental aim underlying the present research is to improve the performance of CIR mixture that is stabilized with Portland Cement. In particular, the intention is to enhance the stiffness of these mixtures without degrading the fatigue strength by finding an optimum cement content for CIR mixture. The specific assumptions are as follows:

1- An optimum emulsion content and asphalt cement content of CIR mixture leads to a significant improvement in workability and compatibility of the mixtures.

2- An optimum cement content of the CIR mixture leads to a significant improvement in the performance of the mixtures.

3- The classic Maxwell rheological model of a material can be applied to simulate either the stress-strain behaviour of the material or the force-deformation relationship of a test specimen.

4- HL3 is more stable under load than HL8 and is used where stresses are high (typically in surface courses). However, HL3 requires more emulsion to blind the mixture.

1.5 Thesis Organization

This thesis consists of seven chapters as follows:

Chapter 1: This chapter explains the overall and the objectives of the research.

Chapter 2: This chapter provides a literature review concerning Partial Depth Reclamation (PDR): Cold In-Place recycling (CIR) and some case studies.

Chapter 3: This chapter provides the methodology used in this research, the experimental program of the research as well as a laboratory performance evaluation of CIR mixtures. Also, in this chapter, Indirect Tensile, Dynamic Modulus and Fatigue Tests are explained.

Chapter 4: This chapter provides the result of the experimental program and discusses the main findings of the research as well as the relationship between fatigue strength and stiffness.

Chapter 5: This chapter addresses the applicability of the Classic Maxwell Model to simulating the viscous-elastic deformation behaviour exhibited by a CIR mixture subjected to cyclic loading.

Chapter 6: This chapter describes the contributions of the study to the behaviour of Partial Depth Reclamation (PDR)under various loading conditions and gives an insight into the design of PDR with acceptable performance for regions with cold climatic conditions.

Chapter 7: This chapter provides a summary of the main findings of the research as well as recommendations for future work.

2 Literature Review

2.1 Rehabilitation Techniques

In Ontario, there are two in-place rehabilitation techniques with PDR. The two techniques, which involve removing by milling about 70% of the existing pavement, are Cold In-Place Recycling (CIR) and Cold In-Place Recycling with an Expanded Asphalt Mixture (CIREAM).

CIR is a pavement rehabilitation technique that reuses the existing asphalt pavement to reduce the life cycle cost and environmental impact of the pavement structure. This rehabilitation technique processes the recycling of pavement materials in situ. CIR is used to rehabilitate pavement distresses such as transverse, thermal failures, and reflective cracks, producing a flexible layer of pavement that has a crack mitigating property. The process may involve partial depth recycling. In partial depth recycling, the process reuses only the existing asphalt pavement and the depth of recycling ranges from 65 to 150 mm. Partial depth recycling is used when the pavement is not severely cracked or distressed, so the base and underlying layers may be left intact. In the case of a heavily distressed pavement having deep cracks and/or rutting of the existing asphalt, full depth reclaiming is applied. This process is performed at a depth ranging from 150 to 300mm. Generally, PDR is used when 70-75% of asphalt pavement is reclaimed (mainly asphalt pavement layer). However, FDR includes two or more different pavement layer materials (Wirtgen Cold Recycling Technology, 2012). The PDR process is all carried out on the site without the need for heating and uses 100% of RAP that is generated during the process. This process allows for the preservation of aggregates and asphalt cement (Davidson et al., 2003). The nature of the process has significant benefits when compared with traditional rehabilitation techniques (Mallick et al., 2002). CIR minimizes the harmful impact of a repair on the environment, reduces the consumed energy and conserves non-renewable resources. Also, cold in-place recycling fills the cracked surface, eliminates rutting, potholes, and ravelling, and thus improves pavement cross-slope and profile. Furthermore, cold in-place recycling corrects problems associated with the existing aggregate gradation and asphalt binder by adding new corrective aggregate and stabilizing additives. In overall terms, cold in-place recycling improves safety and production rate, reduces and delays reflective cracks, and minimizes the cost of the paving process. CIR is a cost-effective rehabilitation alternative to traditional methods. It was reported by the State of Oregon that the annual cost of CIR projects varies from 37 to 82% of the cost of the 50mm hot mix overlay alternative (De Larrard et al, 1993). CIR is a good rehabilitation technique when cracking and permanent deformations are found in the existing asphalt. In some cases, additional operations such as road profiling and supplementing of aggregate may be needed before the recycling process. The primary purpose of adding corrective sized aggregate is to modify the gradation and improve the strength of recycled material. The cold in-place recycling procedure includes a series of steps. Generally, the process is done by cold milling the existing pavement layer and mixing it with a binder (or stabilizers). After which, the mixture is placed on the milled surface, compacted, and allowed to cure. The cold in-place recycling process is carried out by using a single unit train or multi-unit train with different equipment and configuration (Brayton et al., 2001). Generally, the train contains a pulverizing/mixing drum, which is inside the mixing chamber, as shown in Figure (2.1). Tankers attached to the mixing chamber add the stabilizer and water to the pulverized materials (RAP) (Recycling, A., & Reclaiming Association, 2001). Usually, both the stabilizing agents and the cementitious additives are mixed with the milled material in the mixing chamber. These stabilizing agents include bitumen emulsion and foamed bitumen. However, the cementitious additives are lime, fly ash, and cement slurry (Romanoschi, 2003).

Figure 2.1 Recycling Train (Davidson et al., 2003)

2.1.1 Cold In-Place Recycling with Expanded Asphalt Mix (CIREAM)

In 2003, an innovation in the cold in-place recycling technology was introduced. It consisted of using expanded (foamed) asphalt rather than emulsified asphalt to bind the mix (Lane et al., 2014). The idea of asphalt foaming dates back to 1956 and is attributed to L. Csanyi of Iowa State University (Goh et al., 2011). In the foaming process, a small quantity of cold water is injected into the hot asphalt bitumen at temperatures between 150°C and 180°C. At this temperature, the water is vaporized, which in turn causes foamed asphalt. As the asphalt foams, its volume increases 10-30 times, and the viscosity is greatly reduced (Abiodun, 2014). The combination of Cold In-Place Recycling and Expanded Asphalt technologies is termed Cold In-Place Recycling with Expanded Asphalt Mix (CIREAM).

CIREAM involves pumping the hot asphalt cement through a chamber, where a small amount of water is added. Then the added water vaporizes immediately and creates bubbles in the mixture causing the hot mixture to expand. Foam is rapidly created and mixed with the reclaimed asphalt pavement, providing adhesion between the recycled aggregates (Chan et al., 2009).

Compared to CIR, CIREAM presents the advantage of shorter curing periods. If the compaction and strength requirements are met, the new HMA can be applied over CIREAM after three days. In addition to this, CIREAM does not require warm and dry conditions (Lane and Kazmierowski, 2005). Therefore, CIREAM offers high early strength characteristics and reduces the curing time giving a significant reduction in construction cost compared to the CIR technique.

2.1.2 Cold-in-Place Recycling with Asphalt Emulsion (CIR)

Ontario has been using cold in-place recycling with emulsified asphalt binder (CIR) since 1990 (Lane et al., 2014). The CIR treatment depth depends on the type of recycling agent. For instance, if the recycling agent is only an asphalt emulsion or an emulsified recycling agent, the CIR treatment depth is usually between 65 and 100mm. However, when chemical additives such as Portland Cement, lime, and fly ash are used, the CIR depth would be 165 mm (Abiodun, 2014). Where there is reflective cracking, a minimum depth of (70%-75%) of the full depth of the existing pavement is required to be milled to mitigate reflective cracking (Davidson et al., 2003). Chemical additives are used to improve the early strength, reduce moisture damage, and achieve rapid curing of the recycled material, hence, allowing the road to remain unaffected by traffic before being overlaid with HMA or a Seal Coat (Mo et al., 2012). Emulsifying agents are chemicals that are used to stabilize a suspension of asphalt in water. The emulsified agents contain about 40% water and 60% asphalt (Abiodun, 2014). This ratio is important to obtain the maximum density, stability, and air voids (Kazmierowski et al., 1999). Some counties use the modified Marshall method for mixture design; the mixture design contains 3% water (consisting of emulsion water, RAP water content (0.3%) and additional water added to the mixture) and 2.5 to 4.5% by weight of the total mixture is bitumen emulsion. The volume fraction of air voids should be between 9 and 14%, which is considered the only design criterion for optimum bitumen emulsion content in this modified method (Kavussi & Modarres, 2010). According to the Ministry of Transportation Ontario (MTO) laboratory Standard, LS-300, the total liquid content (including emulsion or water) that is added to mixes is 4.5% asphalt cement (MTO-LS, 1996). According to Ontario Provincial Standard Specification (OPSS. PROV 333), the design rate of the emulsified asphalt shall be a minimum of 1.2%.

The emulsified agent added to stabilize a suspension of asphalt in water determines the type of emulsion formed (i.e. water-in-oil or oil-in-water type). The emulsified agent provides the right setting time, makes emulsification easier by reducing the interfacial tension between the bitumen and water, determines the charge on emulsion droplets, and influences the physical properties of the emulsion (Read et al., 2003). Emulsifying agents are made up of large organic molecules that consist of two parts, which are called head and tail. The head part consists of a set of atoms that have positively and negatively charged areas. The nature of some atoms in the head makes the head soluble in water. The tail part consists of a group of long-chain organic molecules that are soluble in organic substances like bitumen (Read et al., 2003). In cationic emulsifying agents, the negative area of the head reacts with water to leave a positively charged area on the surface of the droplet. This imparts a positive charge to all the droplets, which leads to a suspension of the droplets in the water since all the molecules have a positive charge and repel each other, as shown in Figure (2.2). However, in the anionic emulsion, as shown in Figure (2.3), the tail part aligns with the bitumen, and the positive area of the head reacts with water leaving a negative area at the surface of the droplets, which imparts a negative charge to all the droplets so that they repel each other and hence the bitumen droplets are kept suspended in the water (Read et al., 2003). Once the bitumen emulsion is added to the aggregate of the pulverized materials (RAP) to be mixed together, the charged droplets of the bitumen attract the oppositely charged aggregate, which causes the aggregate particles to be coated, especially the fine particles. Generally, the CIR with a Bitumen emulsion process includes adding emulsion to the milled materials that are mixed RAP materials, presumably giving rise to higher workability and durability of the mixture (Brayton et al., 2001). CIR has advantages such as ease of processing, wide availability in the industry, low temperature during the process, resistance to deformation, less expensive than new HMA and the availability of standard test methods and specifications. However, there are some disadvantages associated with it: the curing time is long; hence, the development of the strength is slow (Bhavsar, 2015). CIR presents two major limitations: the weather requirements during application and the curing period. CIR has to be carried out in dry and warm weather (Kazmierowski et al., 1999), and the Ministry of Transportation Ontario (MTO) specifies a minimum 14-days curing period for CIR to meet the requirements in terms of compaction and moisture before HMA overlay.

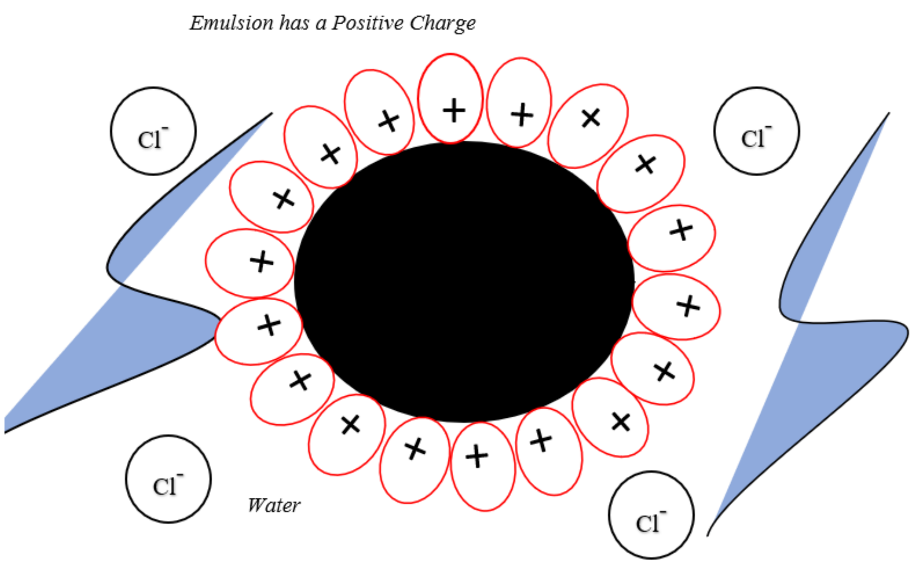

Figure 2.2 Cationic Emulsifying Agent (Read et al., 2003)

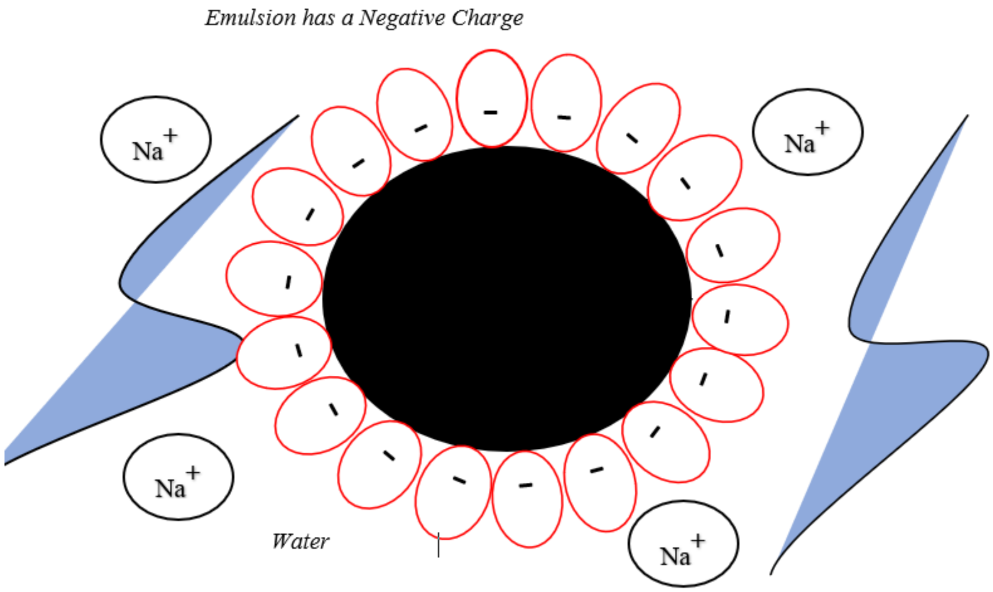

Figure 2.3 Anionic Emulsifying Agent (Read et al., 2003)

2.1.3 Stabilizing Agents and Additives

CIR has been used by many agencies; however, there have been problems associated with it, such as ravelling, thermal cracking, rutting, compaction, low early strength, extended curing time and stripping (Niazi & Jalili, 2009). For those reasons, some of these agencies have started using stabilizing agents and cementitious additives to improve some characteristics of pavement, such as strength, durability, stability, and water resistance (Mallick et al., 2002). Also, stabilizing agents can be used to overcome some deficiencies in the raw materials used in pavement construction (Jitareekul, 2009). Furthermore, stabilizing agents are used to upgrade the properties of existing recycled pavements (Jitareekul, 2009). As a result, there is no necessity to add new materials to improve the strength of recycled pavements.

For bituminous stabilization, asphalt emulsions and expanded asphalt are used as bituminous stabilizing agents. Cementitious additives such as Portland Cement, fly ash, and hydrated lime are utilized with the emulsions or expanded asphalt (Kearney and Huffman, 1999). Both bituminous stabilization agents and cementitious additives are used to bind the components of the pavement mixture, increase the strength, and improve the durability and stability of the mixtures (Jitareekul, 2009).

2.1.3.1 Bituminous Stabilizing Agent

Bituminous stabilizing agents are commonly utilized in the form of emulsions and foams. Bitumen emulsion is blended with pulverized recycled materials in the mixing chamber, as explained earlier. The emulsion stabilizer is used to provide a flexible pavement that has an outstanding fatigue resistance; however, it is considered more expensive than foamed asphalt stabilization and it extends the curing time of the pavement and delays the full-strength development (Mallick et al., 2002). Furthermore, the presence of high moisture content in the RAP materials, in addition to an asphalt emulsion, could lead to an increase in the moisture content to a higher than optimum value (Kearney and Huffman,1999), resulting in a decrease in the strength of the asphalt layers. Nowadays, there is more attention paid to foamed asphalt stabilization than to the bitumen emulsion since the foamed asphalt is considered to be less expensive (Moore, 2004). Table (2.1) shows the advantages and disadvantages of bituminous stabilizing agents (Wirtgen, 2004).

Table 2.1 Advantages and Disadvantages of Bituminous Stabilizing Agents (Wirtgen,2004)

Stabilizing with Bitumen (Emulsion and Foamed)	
Advantages	**Disadvantages**
1- Provides flexibility and creates a visco-elastic-plastic material. 2- Improves shear properties (cohesion and resistance to deformation. 3- Available in the industry 4- Mixtures stabilized with foam do not require a long time to gain strength; hence, they can be trafficked soon after placing and compaction. 5- Provides a durable mixture. A bitumen stabilized mixture tends to lock up the finer particles by encapsulating them in the bitumen. This would prevent the fine particles from reacting with water and any potential pumping.	1- Cost, the bitumen, and the emulsifiers are relatively expensive. 2- Bitumen emulsion is not normally manufactured on-site. 3- The manufacturing process requires strict quality control. 4- Foamed bitumen demands hot bitumen (above 160°C, which requires additional safety precautions 5- Mixtures stabilized with foam require strict grading (fraction smaller than 0.075 mm cannot be treated with foamed bitumen without pre-treatment. 6- The curing time of the mixtures stabilized with emulsified asphalt can be long; therefore, strength development is dictated by moisture loss.

2.1.3.1.1 Cationic Slow Setting Emulsion and Anionic High Float Emulsion

As mentioned in section (2.1.1), the asphalt emulsions can be categorized based on their surrounding electrical charges and breaking time (how fast the asphalt binder breaks from the water), which is generally a function of the surrounding temperature. A Slow-Setting Cationic Emulsion (CSS-1H) is produced to be used for several industrial applications and uses. Because it provides a strong bond between the asphalt lifts and does not deform under traffic loading, the CSS-1H emulsion can be used as a tack coat. In addition, CSS-1H can be thinned with water to reduce its viscosity, which improves its penetration into an existing asphalt surface to control dust. The CSS-1H emulsion is used for “fog sealing”, in which it is applied to an existing pavement surface to heal and seal the thin cracks. Also, it should be noted that for a fog seal treatment, the conventional sand blotting treatment is not required due to its rapid cure and non-tracking properties. CSS-1H emulsion is designed to increase the mixing time of the CIR mixture to provide a better workable mixture and a good coating of the RAP material used in the mixture.

The Anionic High Float Emulsion (HF-150) is also used for surface treatments. This type of emulsion is designed to break and cure faster than the slow setting emulsion yet allows sufficient time for aggregate mixing and wetting. After the water breaks from the asphalt particles, the HF-150 emulsion creates a gel-like structure within the asphalt residue. This leads to the generation of a thick asphalt film on the aggregate particles, providing an adequate coating of the aggregate particles and a reduction in moisture susceptibility. Moreover, the HF-150 emulsion provides good durable surface treatment and high rutting and crack resistance. In addition, the HF-150 allows for the usage of anti-stripping agents, thus, improving moisture resistance and increasing the bonds between the aggregate particles. The data sheets for both Slow-Setting Cationic Emulsion (CSS-1H) and Anionic High Float Emulsion (HF-150) are provided in Appendix-I.

2.1.3.2 Cementitious Additives

Cement, lime and fly ash and blast furnace slag are used successfully as recycling additives. Also, these materials are frequently used for cementitious additives. These additives provide early strength, increase the rutting resistance, and reduce the sensitivity of the mixture to moisture. Table (2.2) summarizes the advantages and disadvantages of cementitious additives (Wirtgen, 2004). Portland Cement and Limestone are one of the main cementitious additives used with the PDR technique. Once a cementitious treated road interacts with water, the components of the Portland Cement undergo a hydration process in which hydrated calcium silicate (C-S-H) and Calcium hydroxide are formed. C-S-H is the main component in the chemical reactions that contribute to the strength of the cementitious material. Equations (2.1), (2.2) ,(2,3) and (2,4) show the hydration process (Wirtgen, 2010).

$$(CaO)_3 SiO_2 + H_2O \longrightarrow (CaO)_x (SiO_2)_y (H_2O)_z + Ca(OH)_2 \quad \text{……………….(2.1)}$$

$$(CaO)_2 SiO_2 + H_2O \longrightarrow (CaO)_x (SiO_2)_y (H_2O)_z + Ca(OH)_2 \quad \text{……………….(2.2)}$$

$$(CaO)_3 Al_2 O_3 + H_2O \longrightarrow (CaO)_x (Al_2 O_3)_y (H_2O)_z \quad \text{……………….(2.3)}$$

$$(CaO)_4 Al_2 O_{3\,Fe2} O + H_2O \longrightarrow (CaO)_x (Al_2 O_3)_y (Fe_2 O_3)_z (H_2O)_w \quad \text{……………….(2.4)}$$

Table 2.2 Advantages and Disadvantages of Cementitious Additives (Wirtgen,2004)

Cementitious Additives (Cement)	
Advantages	**Disadvantages**
1- Availability, cement can be obtained worldwide. 2- Cost, cement is inexpensive relative to bitumen. 3- Cement is easy to deal with (cement can be spread by hand in the absence of spreaders). 4- Cement is well-known in the construction industry. 5- Slandered test methods and specifications are usually available. 6- Cement provides high compressive strength and durability.	1- Shrinkage cracks are unavoidable yet can be minimized. 2- Requires curing and protection from early traffic (especially heavy, slow-moving vehicles).

2.1.3.3 Combination of Cementitious Additives and Asphalt Stabilizing Agents

The combination of cementitious additives and bitumen stabilizing agents is thought to be efficient (Jitareekul, 2009). The most commonly used cementitious additives are Portland Cement, lime, and fly ash. Niazi and Jalili (2009) conducted an experiment to study the effect of Portland Cement on the properties of cold in-place recycled mixtures with an asphalt emulsion. Different Portland Cement percentages were used (0, 0.5, 1, 1.5, and 2). The results showed that Portland Cement can increase tensile strength and Marshall Stability, resistance to moisture damage, resilient modulus, and resistance to permanent deformation of CIR mixes. The increases in stability and strength of the pavement mixture are linked to the shorter curing time that is needed since the

Portland Cement reduced the breaking time of bitumen emulsions. Furthermore, it was found that the use of 2% of Portland Cement resulted in the highest resilient modulus value since Portland Cement stiffens the binder. However, they did not comment on the fatigue behaviour of the mixture.

It was reported by Salomon et al. (2000) that adding Cement to a recycled mixture with a bitumen emulsion led to an increase in the cohesion, resistance to permanent deformation, and stiffness. Cement additives are frequently thought to behave in a brittle manner, which might reduce the flexibility and fatigue behaviour of recycled mixes (Kavussi & Modarres, 2010). Mixing the cement with bitumen emulsion produces a crystallized pozzolanic structure, which has a brittle behaviour; therefore, the mixture is more likely to be susceptible to shrinkage and cracking. Another study was carried out by Modarres et al. (2011) to study the fatigue characteristics of a recycled mixture containing a bitumen emulsion and cement at different cement contents and temperatures. The amounts of cement used in the mixture were 1, 2 and 3% of the total weight of the mixture. The results showed that as the cement content increased and the temperature decreased, the resilient modulus increased, and the changes in fatigue life were dependent on the initial strain levels. At high initial strain levels, the fatigue life of the specimens that contained cement was lower than that of the control specimens. However, at low strain levels, the fatigue life of control specimens was lower than the cement-containing specimens. Moreover, the results showed that using an amount of cement of up to 3% had no significant effect on the on-temperature susceptibility of recycled mixes.

A study was conducted by Kavussi and Modarres (2010) to examine the fatigue behaviour of recycled mixtures with bitumen emulsion and cement. The main findings were that the effect of cement on fatigue life was linked to the strain level. It was noticed that at 300 micro-strain and higher, the addition of cement led to a reduction in fatigue life. On the other hand, below 300 micro-strains, the addition of cement caused an increase in fatigue life. Also, it was observed that at a low temperature and high cement content, a sudden cracking occurred. Finally, they found that there is no relationship between curing time and the slope of the load versus the fatigue life curve. Kavussi and Modarres (2010) carried out a study to determine the resilient modulus of recycled mixes with bitumen emulsion and cement. The amounts of cement used in the mixture were 1, 2 and 3% of the total weight of the mix. The results showed that as the curing time and cement content increased and the temperature of the test decreased, the indirect tensile test and resilient values increased. Also, it was observed that 90% of the final stiffness was achieved between 90-120 days of curing. It was stated that the stiffness after 120 days of curing is almost two or three times higher than the stiffness at seven days of curing. Some studies have been conducted to examine the behaviour of CIR and CIREAM without adding Portland Cement, as explained in the following section.

2.1.4 Case Study 1

In July 2003, the Ministry of Transportation Ontario constructed a trial section on highway7. The purpose of this study was to compare the performance of the CIR and CIREAM. The section is located approximately 90 Km southwest of Ottawa, Ontario, as shown in Figure (2.4). The length of the section was 15.4 Km. 8 Km of CIR and 5 Km of CIREAM were placed. The section is classified as a rural arterial undivided highway with an Average Annual Daily Traffic of 9000 vehicles as of 2004 and posted speed of 80 Km/h. A pavement investigation showed an average HMA thickness of 207 mm. The resurfacing consisted of 40 mm of recycled surface course over 40 mm of open-graded binder course (Lane & Kazmierowski, 2005). In 1995, the pavement had a condition index (PCI) of 55 out of 100 and a ride comfort rating of 6.2 out of 10. The highway had severe rutting in wheel paths, severe transverse cracking, and fatigue cracks (Bhavsar, 2015).

Figure 2.4 Highway 7 from Innisville to the Town of Perth (Bhavsar, 2015)

Falling weight deflectometer (FWD) test, indirect tensile strength (ITS) test and MTO's automatic road analyzer (ARAN) were conducted on both CIR and CIREAM after laying a 50mm overlay. The CIR and CIREAM performed similarly with the same cost. After a year from the construction time, there was little rutting or cracking. In addition, the overall RCR and PCI were 9 and 93 out of 10 and 100, respectively (Lane & Kazmierowski, 2005). Also, the other objective of the MTO was to compare the performance of CIR and CIREAM. They conducted ITS test. The results showed that the density of both CIR and CIREAM play an essential role in the tensile strength, as shown in Figure (2.5); the denser the specimen and more compact it is, the higher tensile strength it gains (Lane & Kazmierowski, 2005). Furthermore, 8 months after construction, a resilient modulus test was conducted on both CIR and CIREAM materials. The findings showed that the resilient modulus is similar for both CIR and CREAM materials (Lane & Kazmierowski, 2005). In summary, CIR was found to mitigate reflective cracks and extend pavement life, and the CIREAM seems to be a successful new rehabilitation technique. Therefore, CIR to a depth of 110 mm and 50 mm HMA overlay was chosen as an effective rehabilitation technique for this project.

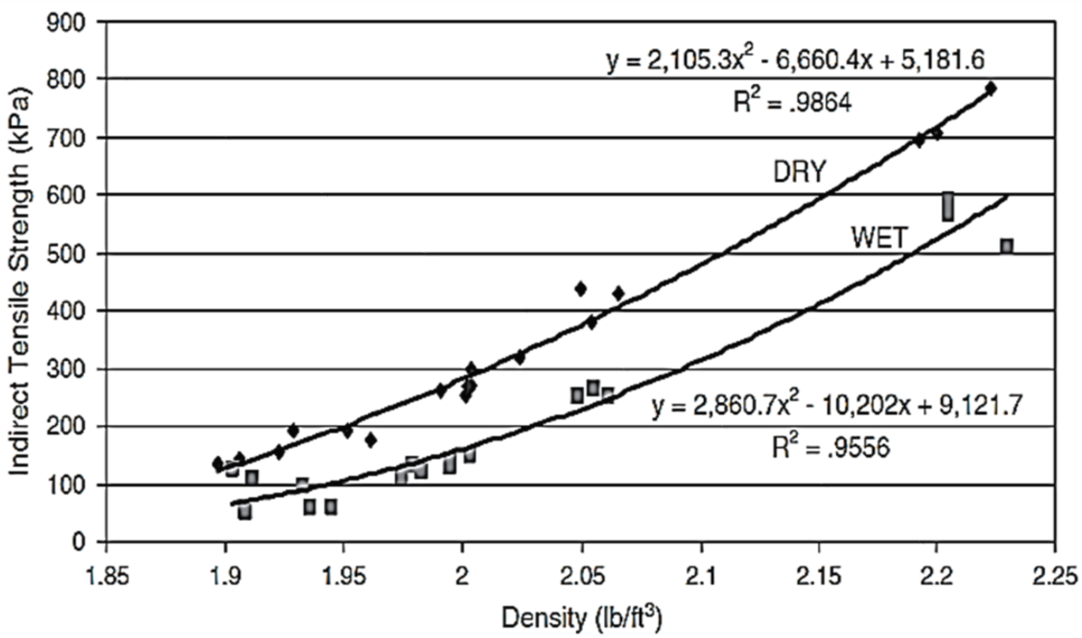

Figure 2.5 Indirect Tensile Strength versus Briquette Density for Samples of CIR and CIREAM (Lane & Kazmierowski, 2005)

2.1.5 Case Study 2

In 2015, a study was conducted by Bhavsar to compare CIR and CIREAM mixtures. The goal of this study is to determine the laboratory and field performance of CIR and CIREAM. The RAP material was provided by Miller Paving Limited from Southern and Northern Ontario (Highway 400, 401 projects). In this study, mixes with five different percentages of AC were prepared and tested. The percentage of AC varied from 1.2% to 3.2% of the mass of RAP material at an increment of 0.5% AC. The mixed samples of CIR and CIREAM were tested at different curing times to evaluate their overall strength, tension cracking and fatigue cracking performance. The samples were compacted and tested after different numbers of days to determine the optimum curing time. Table (2.3) shows the test matrix for the duration test. It is shown in the table that the “DT” in the sample IDs represents the Duration Test, and the “S” represents the use of Southern RAP. The number that follows the “S” is the number of days the mix was allowed to cure before compaction. The dynamic modulus test was carried out according to AASHTO TP 62-09(AASHTO, 2009) to determine the best curing time. The obtained results showed that the curing time of the CIR samples for 14 days after compaction led to an improvement in the test results for low frequencies, as shown in Figure (2.6). It is clearly shown from the Figure that sample DT-S0 has the highest stiffness at low frequency (10-7Hz to 10-4Hz). That indicates that the sample has a high resistance to rutting. However, at high frequency (105Hz to 108Hz), samples DT-S7 and DT-S14 have a slightly better fatigue resistance. Since the difference in rutting resistance performance of sample DT-S0 relative to other mixes is more significant than the difference in fatigue resistance performance of DT-S7 and DT-S14 relative to other mixes, the sample DT-S0 was selected as a better performance mixture.

Table 2.3 Curing Time (Bhavsar, 2015)

Sample ID	**Curing Time (Days)**	
	Before Compaction	**After Compaction**
DT-S0	0	14
DT-S2	2	14
DT-S7	7	7
DT-S14	14	7

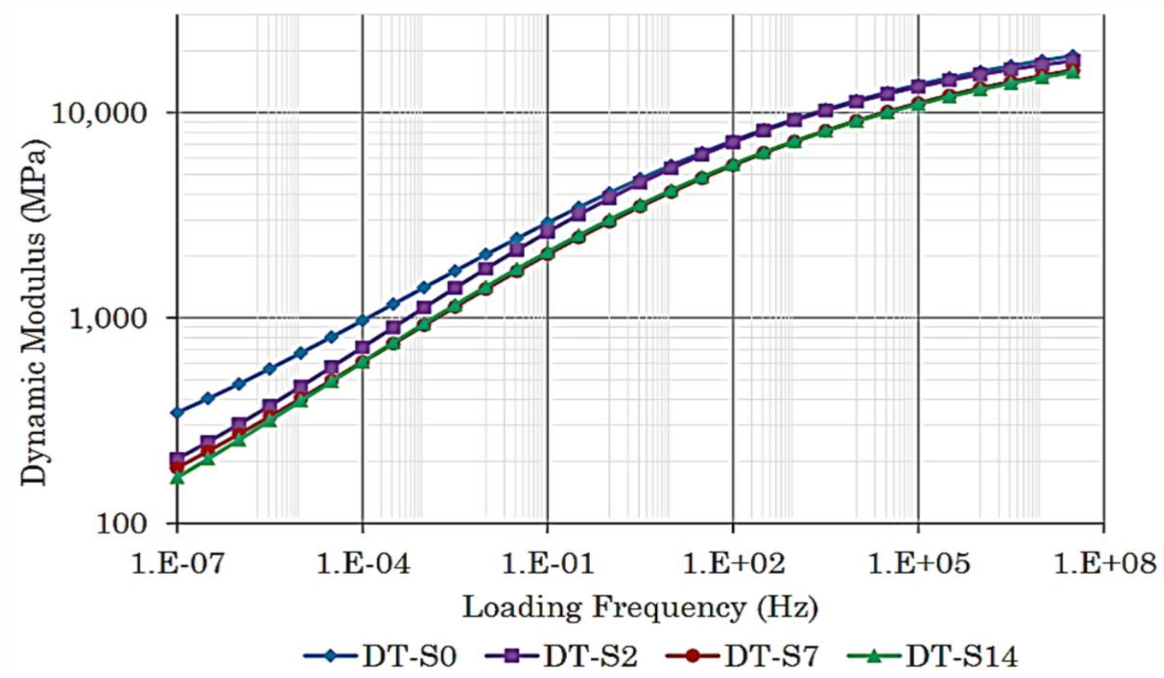

Figure 2.6 Dynamic Modulus Master Curve-Duration Testing (Bhavsar, 2015)

Also, laboratory testing of CIR materials using southern RAP and 3.2% bitumen within the mix resulted in overall better performance in comparison to other mixes, as shown in Figure (2.7). In the sample IDs, the "S" represents Southern Ontario RAP, and the number following it represents the mix's number. The number denotes the first increment of the percentage AC used (i.e., 1.2%). CIR-S5, which is the mixture with 3.2% AC, has a much higher dynamic modulus compared to the other mixes; as a result, a higher percentage of AC led to gain better rutting resistance and overall performance of the mix.

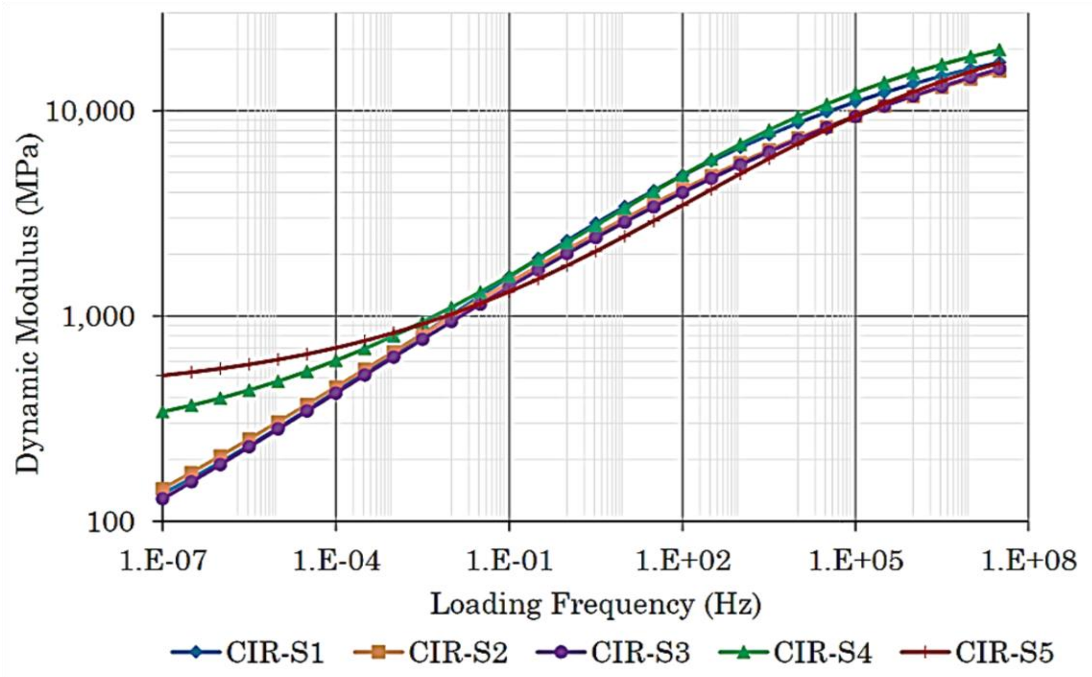

Figure 2.7 Dynamic Modulus Master Curve –CIR-S Samples (Bhavsar, 2015)

In addition, when a CIREAM mixture was mixed with 3.2% of bitumen, the results showed an improvement in the performance, as shown in Figure (2.8). It is shown in the Figure, in the low-frequency region (10-7 Hz to 10-4Hz), CIREAM-S5 has the highest percentage of AC (3.2%), resulting in a higher stiffness compared to other mixtures. On the other hand, at higher frequencies (102 Hz to 108 Hz), CIREAM-S5 (S represents southern RAP, and 5 donates for the highest AC percentage (3.2%)), exhibited a lower stiffness modulus. That indicted that the sample has good resistance to fatigue cracks; as a result, this mixture was selected as a good performance mixture. For the master curves developed for the CIR mixtures with north Ontario RAP, the results showed that there were no significant differences between any of the mixes. In summary, samples that mixed using HL3 RAP gave lower stiffness at low frequencies and similar stiffness at higher frequencies.

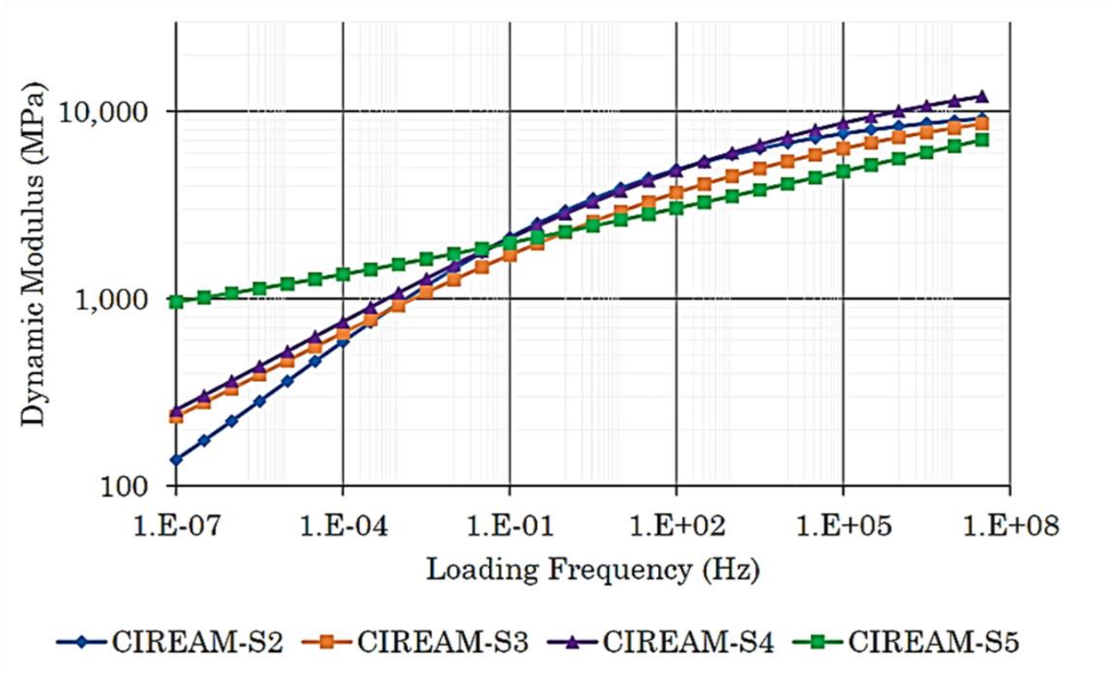

Figure 2.8 Dynamic Modulus Master Curve –CIREAM-S Samples (Bhavsar, 2015)

A four-point bending (FPB) fatigue beam test is used to estimate the fatigue life of both CIR and CIREAM samples using southern RAP and 3.2%; the results showed that both mixtures gave the same performance in terms of fatigue resistance, as shown in Figure (2.9). It is clearly shown that the average number of cycles to failure for both mixtures CIR and CIREAM are 19013 and 19513, respectively. That indicates that the two mixtures had a similar fatigue behaviour. Furthermore, when both mixtures CIR and CIREAM were tested using Thermal Stress Restrained Specimen Testing (TSRST) to estimate the failure temperature, the findings showed that both mixtures performed similarly, as shown in Figure (2.10). The temperature at failure for both mixtures was on average -28 °C and -27 °C for CIR and CIREAM, respectively. Since the Performance-Grade Asphalt Cement (PGAC) PG 58-28 was used for the emulsion and foamed asphalt, the failure temperature was expected to be around -28 °C. However, the tensile stresses of the CIR samples were much higher at failure than the stresses on CIREAM samples, as shown in Figure (2.11).

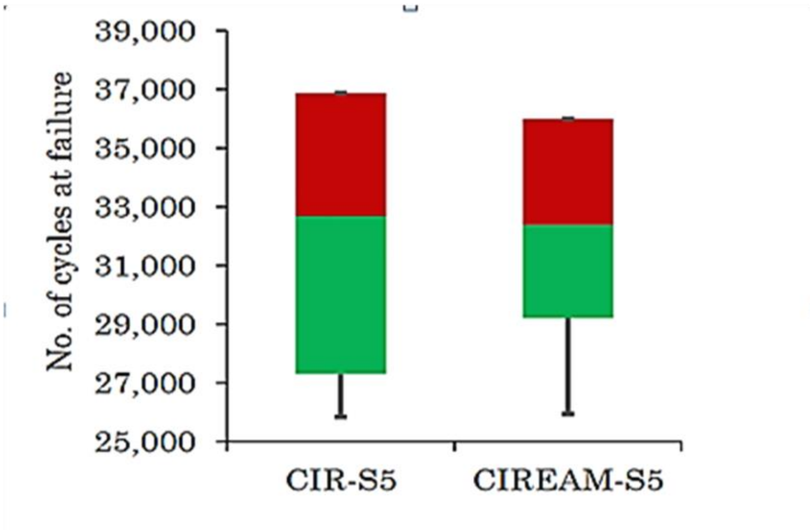

Figure 2.9 Cycles To Failure of Fatigue Test (Bhavsar, 2015)

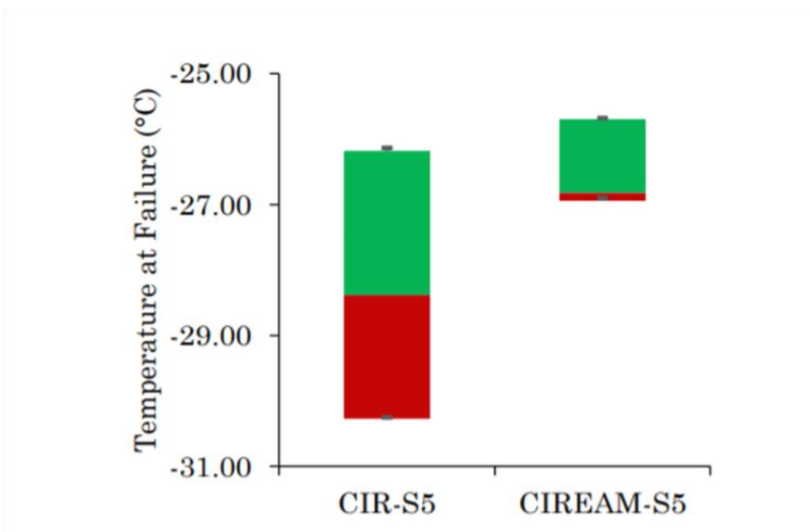

Figure 2.10 Temperature Recorded at Failure of CIR and CIREAM Samples (Bhavsar, 2015)

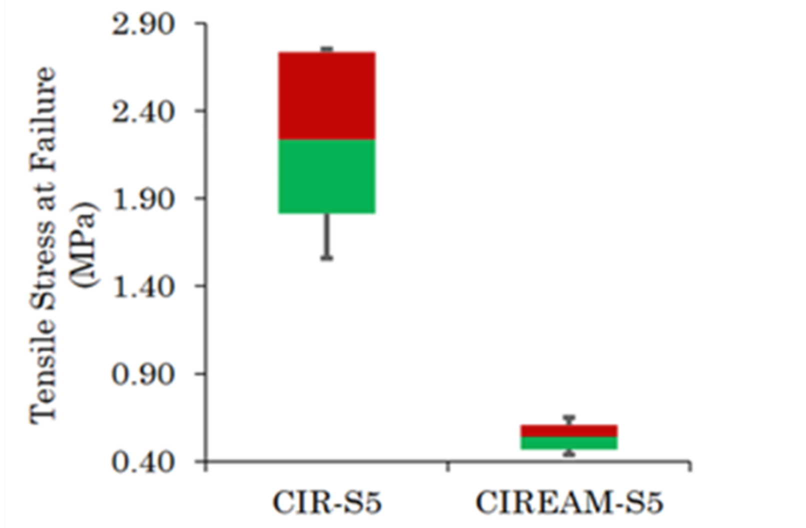

Figure 2.11 Tensile Stress at Failure of CIR and CIREAM (Bhavsar, 2015)

Finally, based on the information provided by MTO, the physical condition index values showed that the visually inspected sections with CIR and CIREAM performed well, and all of them were adequate. From visual inspections done in the municipalities, a large number of deteriorated regions were observed in both the CIR and the CIREAM road sections. Raveling, along with wheel path rutting and alligator cracking were a very common forms of deterioration observed on sections with poor drainage and/or improper road geometry. In conclusion, both CIR and CIREAM performed similarly in the field in comparison.

2.2 Mechanical behaviour of Asphalt Pavement

There are a number of modes that are used to characterize the asphalt material, such as elastic, plastic, viscoelastic, and viscoelastoplastic. Most engineering materials experience plasticity behaviour, in which permanent deformation occurs when the stress exceeds the elastic limit. The stress-strain relationship is explained in Figure (2.12).

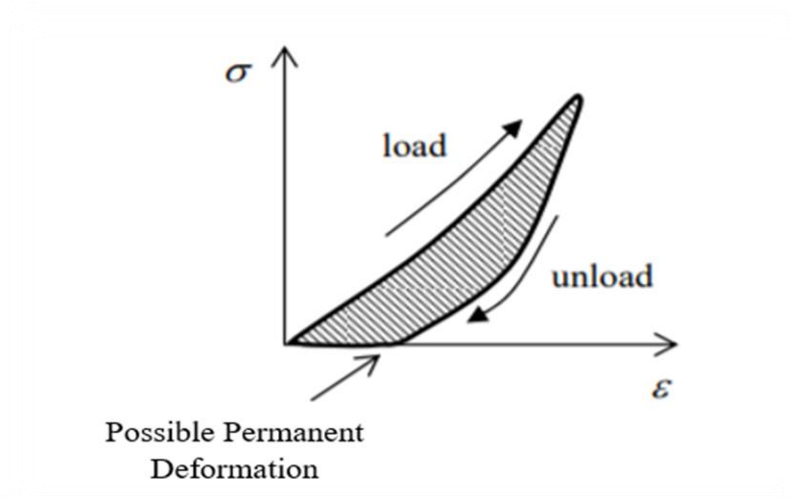

Figure 2.12 Stress Strain Response of Viscoelastic Materials (Kelly, 2014)

Unlike viscoelasticity, the stress-strain behaviour of plastic materials is rate-independent. Viscoelastic behaviour can be characterized by different rheological models such as classic or generalized Maxwell, Kelvin-Voigt, and Burgers models comprised of offspring and dashpot components, as shown in Figure (2.13). Elastic behaviour occurs at rapid loading rates, whereas viscoelastic behaviour will only appear at slower loading rates. Mechanical behaviour changes with changes in temperature and loading rates in viscoelastic materials. Furthermore, the mechanical properties of the asphalt materials are a function of stress amplitudes and strain rates (Onyango 2009).

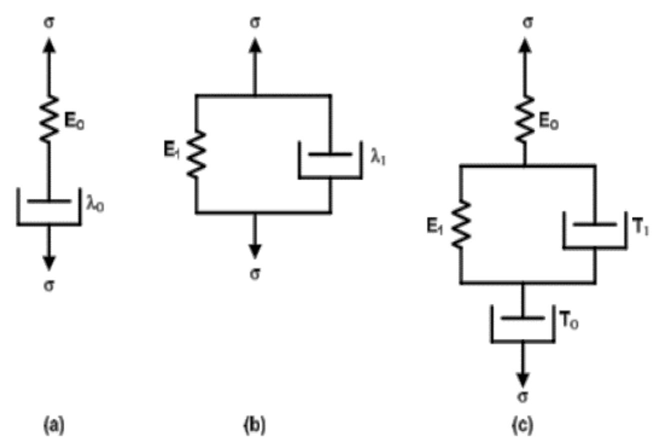

Figure 2.13 Mechanical models (a) Maxwell, (b) Kelvin-Voigt, and (c) Burger (Breakah 2009)

Figure 2.14 shows the typical behaviour of a viscoelastic material when the material is loaded at constant stress for a given time, followed by the removal of the load. At the beginning of loading, there is an instantaneous elastic straining. After that, the creep strain phase at which the strain increases over time. The creep strain increases at a decreasing strain rate, and later the steady-state of constant strain may be reached. However, some materials at high stresses do not reach this steady state but have a continuously increasing strain rate to failure. For the unloading phase, the elastic strain is recovered instantly. Then, an anelastic recovery phase occurs, during which the strain recovers over time. This anelastic strain is considerable in polymeric materials (Kelly, 2014).

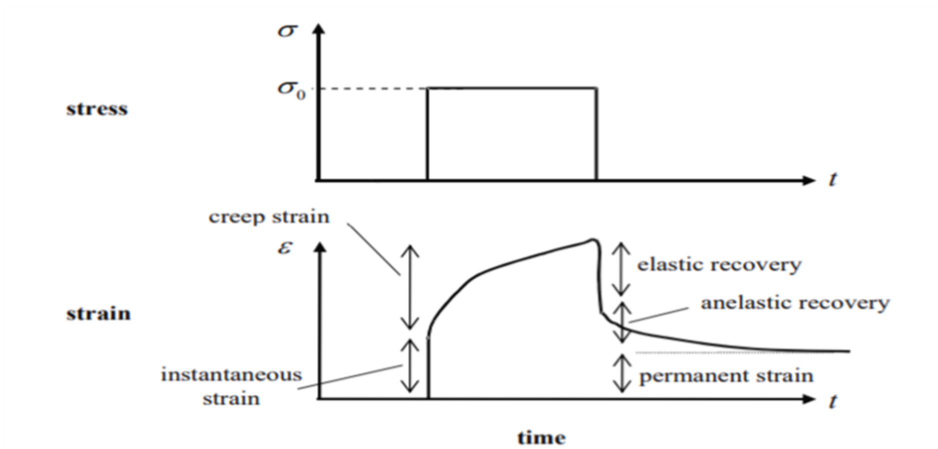

Figure 2.14 Strain Response to the Creep-Recovery Test (Kelly, 2014)

Figure (2.15) shows the stress relaxation under the application of a given strain which is then maintained. The stress that is needed to maintain the strain in the viscoelastic material decreases with time. This phenomenon of stress relaxation occurs due to a re-arrangement of the material atoms at the molecular levels (Kelly, 2014).

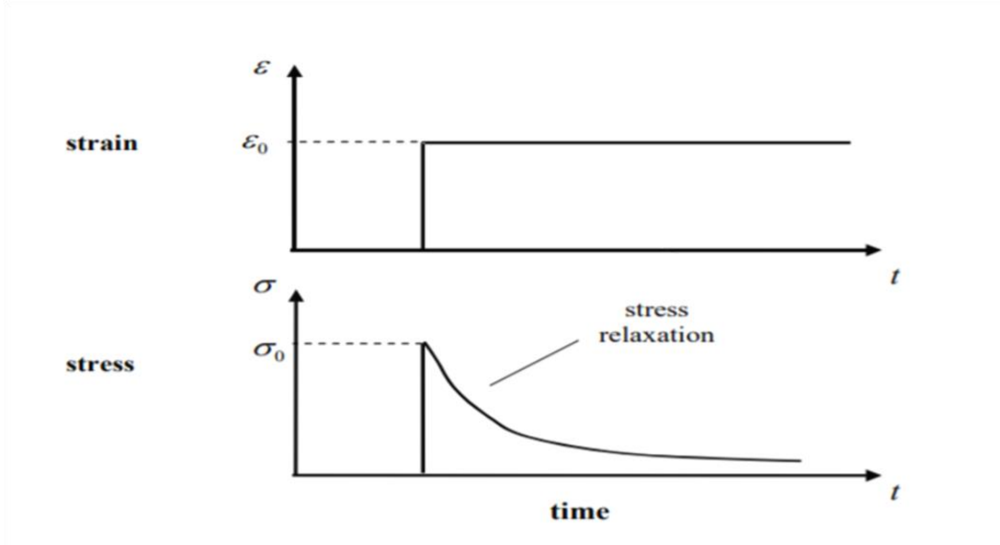

Figure 2.15 Stress Relaxation at Constant Strain (Kelly, 2014)

A Maxwell Model is often used to simulate the stable cyclic stress-strain behaviour displayed by viscous-elastic structural systems subjected to proportional constant straining. The model may be used to represent the relationship between applied forces and displacements or stresses and strains. The classic *Maxwell model* consists of a spring and dashpot connected in series shown in Figure (2.16). The classic maxwell model is described by the following Equation (2.3): Physically, this means that when stress (σ_0) is applied to the classic Maxwell model, the spring will immediately stretch. However, the dashpot will take time to react to the applied stress. As a result, the initial strain is $\varepsilon_0 = \sigma_0 / E$. The classic model can be applied to predict the stress-strain or load-deformation relationship of the pavement material.

Figure 2.16 Classic Maxwell Model (Zaoutsos et al., 2011)

2.3 Summary

Various studies have been conducted on the performance of CIR pavement rehabilitation. The CIR technique includes sizing an existing pavement, mixing the pavement with emulsified asphalt, and laying it back without off-site hauling and treatment. This technique was initially developed in order to reduce the cost of PDR and extend the service life of the pavement. There are many advantages to using CIR techniques for road rehabilitation, such as its being environmentally friendly, energy-efficient and cost-effective solutions. However, traditional techniques are preferred over the CIR technique because of the limited amount of information that is available regarding the behaviour and failure mechanisms of the PDR mixtures. The use of the CIR technique in Ontario is associated with a low early strength and moisture damage, which results in some extreme cases of ravelling and the formation of potholes. Two case studies, which were conducted in Ontario by MTO, and the university of waterloo in 2003 and 2015, respectively, are reported in sections (2.1.3) and (2.1.4. Although the studies were performed to study the mechanical behaviour of the CIR mixtures did not include an investigation of the effect of the addition of cementitious additives such as Portland Cement. Furthermore, the studies evaluated the mechanical properties of the CIR mixture using only one type of emulsion and gradation. Therefore, there was a decision by the MTO to sponsor an investigation that included two types of emulsion and the addition of various percentages of Portland Cement on the mechanical properties of the CIR mixture. It was also decided that the study would concentrate on the pavement produced using the PDR technique. It is expected that this investigation will provide further insight regarding fatigue, low-temperature thermal cracking and stiffness of CIR mixtures. In the study, the stiffness of the asphalt mix is increased by adding Portland Cement in different Percentages (0%, 0.5%, 1.5%, 3%) and verifying which combinations improve the stiffness without unduly compromising the fatigue life. Finally, a classic Maxwell rheological model was used to model the Stress-Strain history under fatigue testing (hysteresis loops).

3 Methodology and Experimental Program

3.1 Proposed Approach

The primary purpose of this study is to investigate the changes achieved in the performance of Cold In-Place Asphalt Recycled, in Ontario, by adding Portland Cement with different percentages. The literature findings call for the need to verify the impact that higher percentages of Portland Cement will have on CIR mixtures in Ontario. Studies on the performance of CIR mixtures are essential to recommend guidelines for the optimum cement content that should be used as cementitious additives. This study was conducted by examing the performance testing of several laboratory-prepared mixes. The focus of this study is the laboratory performance testing program. This project involved optimistic expectations as to the outcomes and thus carried some risk or uncertainty. The research structure and experimental test combinations to meet the outlined objectives of this study are shown in Figure (3.1).

Task 1:

Conduct a literature review on existing applications of cementitious additives such as Portland Cement. This involves a review of all existing available data about CIR that have been used in Canada and particularly in Ontario. The literature review also includes a review of all the mixture design methods and the cement contents that have been used.

Task 2:

In this task, the design requirement was to obtain an optimum bitumen emulsion that had a voids content that corresponded to high stability. The recommended air voids of the CIR mixture range from 10% to 12 %. The design amount of the emulsified asphalt was a minimum of 1.2% of the RAP materials. By using these criteria, the optimum value of the emulsion shall be determined.

Task 3:

This task involved the laboratory testing of specimens that contain different percentages of Portland Cement (0.5%,1.5% and 3%) in order to determine the optimum Portland Cement content. The design criteria for optimum Portland Cement content are based on the results of the indirect tensile test, indirect tensile strength ratio(wet/dry), which shall be maintained at a minimum of 50, dynamic modulus tests and fatigue tests. The dynamic modulus test will be evaluated at three different temperatures (-10˚C, 4˚C and 21˚C). However, the fatigue test will be conducted at 5˚C.

Furthermore, in this task, a thermal stress restrained specimen test was conducted on the CIR mixture that contains (0 %, 0.5 %, 1.5 %, and 3 % Portland Cement) to evaluate the effect of the temperature on the mechanical properties of the mixture. Furthermore, in this task, an extensive discussion will be presented as well as the test results for the proposed mixes. The optimum value of the Portland Cement will be reported.

Task 4

Predicting the stress-strain or the force-deformation behaviour and fatigue lives of the test specimens of the material, using a classic Maxwell model to describe stress-strain and force deformation behaviour.

Task 5

In this task, the main research findings and recommendations of the research will be presented.

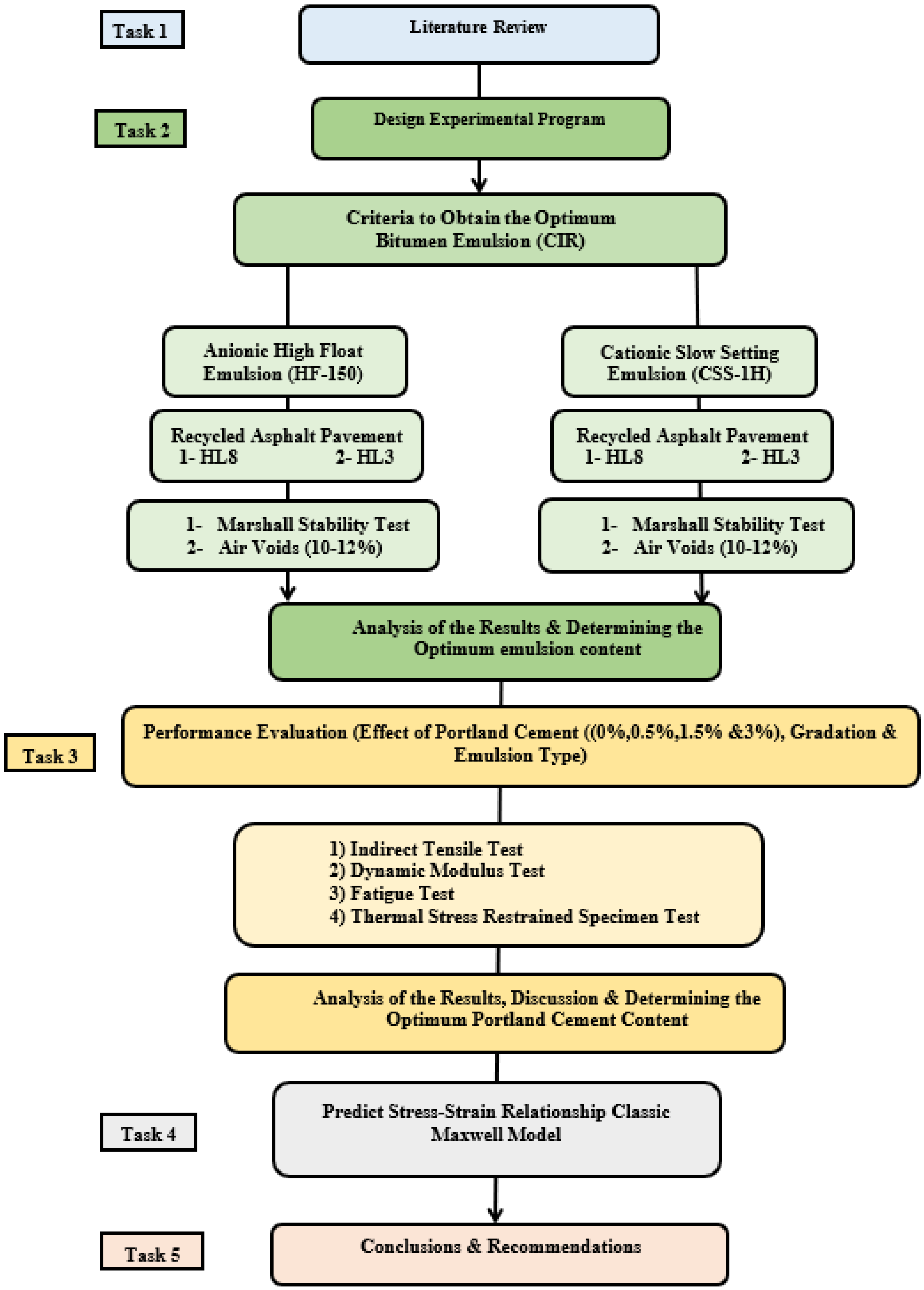

Figure 3.1 Research Methodology

3.2 Mix Preparation

3.2.1 Material Collection and Preparation

The reclaimed asphalt concrete mixture used in this research was pulverized RAP materials, HL8 and HL3. The RAP was first air-dried for 72 hours in order to decrease the moisture. Then, extraction and penetration tests were performed to determine the percent of asphalt binder in the RAP and the stiffness of the binder. The extraction and penetration tests were performed in accordance with MTO laboratory standard method LS-282 (MTO-LS, 2009). Higher values of penetration mean a softer binder consistency. The variation in the RAP's stiffness with the percent of the asphalt in the RAP materials was determined. The stiffness was determined by a penetration test on the two RAP materials, which gave values of 11 and 21 mm for the pulverized HL8 and HL3 materials, respectively. Also, the extraction test was performed on both RAP materials and it was found that the pulverized HL8 RAP contained 4.78% existing binder and the pulverized HL3 RAP contained 4.0% existing binder. The moisture in the pulverized RAP materials (HL8&HL3) was calculated to be 0.26% and 5.35%,respectively. The Performance-Grade of the pulverized RAP materials (HL8&HL3) was PG 58-28. Furthermore, the total liquid content (including emulsion or water) that was added to mixes was 4.5% asphalt cement (MTO-LS, 1996).

The RAP material mainly consisted of crushed rock material, trap rock, limestone, and some gravel. The gradation of the mixture was determined following the [ASTM C136] standard test method. The gradation for the pulverized HL8 RAP materials is presented in Table (3.1) and Figure (3.2). In addition, the gradation of the pulverized HL3 is presented in Table (3.2) and Figure (3.3). Furthermore, Table (3.3) shows the physical and chemical properties of the Portland Cement used in this study (Muhit,2014).

Table 3.1 HL8 Gradation (Pulverized)

Sieve Size	Weight Retained	Percent Retained	Cumulative Retained	Percent Passing
mm/mm	**(g)**	**(%)**	**(%)**	**(%)**
26.5	0.0	0.0	0.0	100.0
19	0.0	0.0	0.0	100.0
16	7.3	0.4	0.4	99.6
13.2	27.2	1.6	2.1	97.9
9.5	129.2	7.7	9.7	90.3
4.75	319.5	19.0	28.7	71.3
2.36	227.3	13.5	42.3	57.7
1.18	187.2	11.1	53.4	46.6
0.6	194.8	11.6	65.0	35.0
0.3	180.9	10.8	75.7	24.3
0.15	160.5	9.5	85.3	14.7
0.075	87.7	5.2	90.5	9.5
Pan	159.7	9.5	100.0	0.0
Total	1681.3 gm			

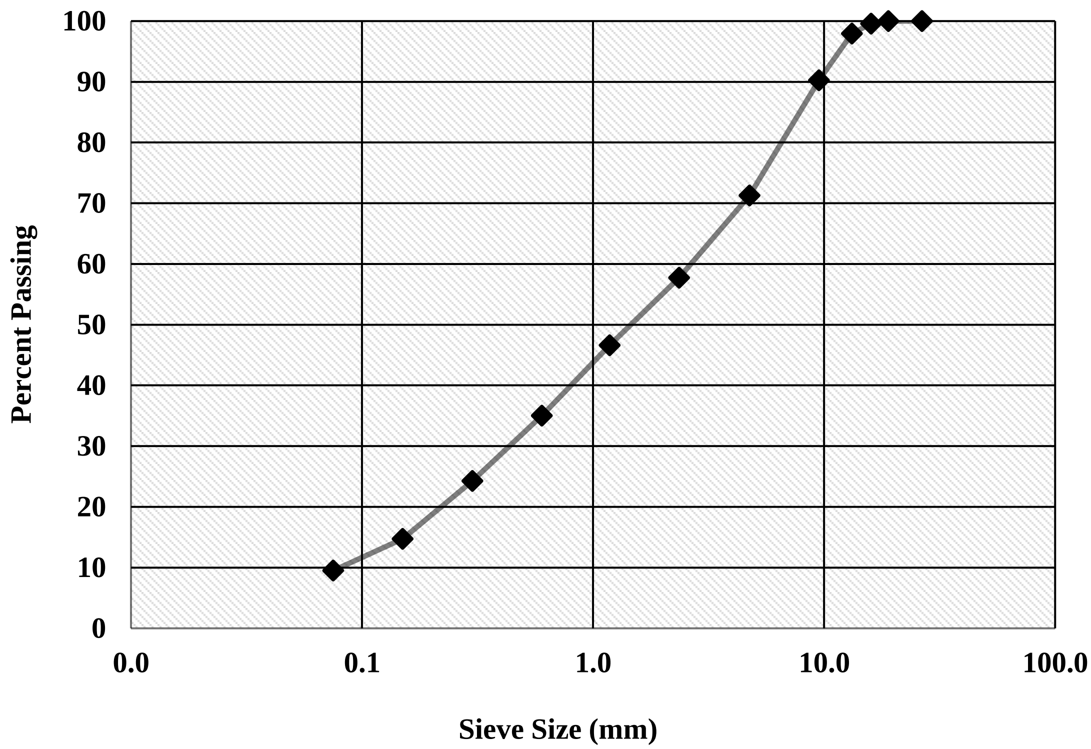

Figure 3.2 Gradation of HL8 RAP Materials (Pulverized)

Table 3.2 HL3 Gradation (Pulverized)

Sieve Size	Weight Retained	Percent Retained	Cumulative Retained	Percent Passing
mm/mm	**(g)**	**(%)**	**(%)**	**(%)**
26.5	0.0	0.0	0.0	100.0
19	0.0	0.0	0.0	100.0
16	0.0	0.0	0.0	100.0
13.2	8.1	0.5	0.5	99.5
9.5	93.8	6.0	6.5	93.5
4.75	372.1	23.9	30.5	69.5
2.36	237.1	15.2	45.7	54.3
1.18	172.0	11.1	56.8	43.2
0.6	152.6	9.8	66.6	33.4
0.3	181.6	11.7	78.2	21.8
0.15	135.0	8.7	86.9	13.1
0.075	73.6	4.7	91.7	8.3
Pan	129.9	8.3	100.0	0.0
Total	1555.8			

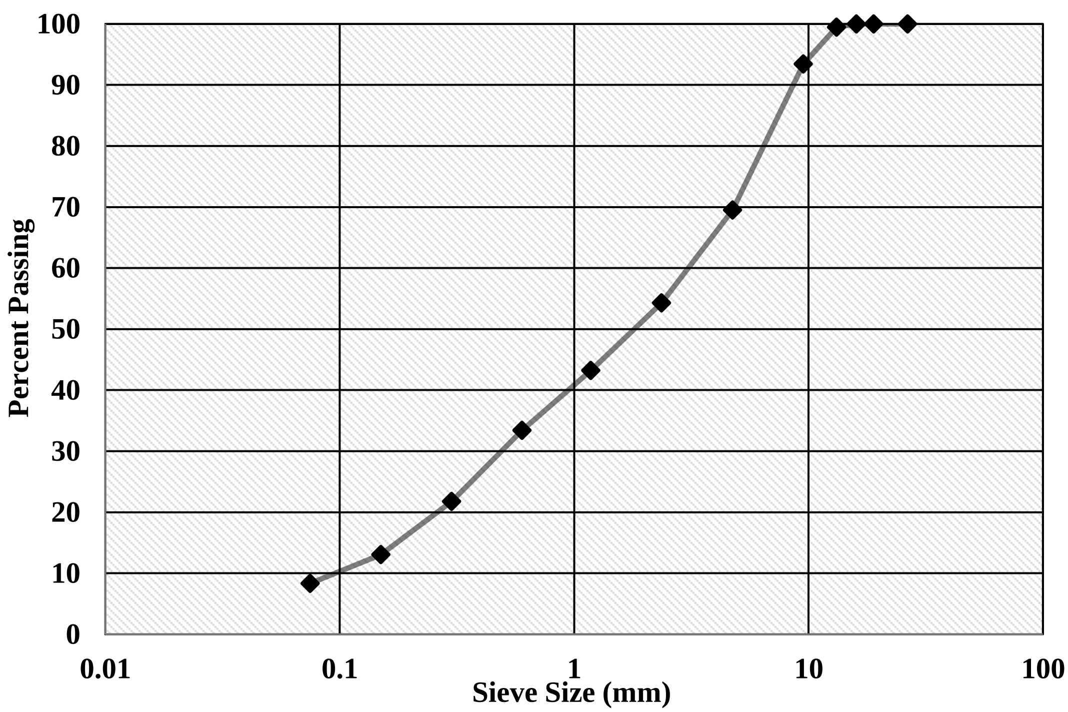

Figure 3.3 Gradation of HL3 RAP Materials (Pulverized

Table 3.3 Physical and Chemical Properties of Portland Cement

Physical Properties	
Initial Setting Time (Minute)	90
Fineness, 45μm Sieve, % Retained	4
28 Days Compressive Strength (Mpa)	40
Blaine Fineness, M2/Kg	383
Autocalve, % Expansion	0.05
Calcium Oxide (Cao)	62.26%
Silicon Dioxide (Sio2)	19.6%
Aluminum Oxide (Al2 O3)	5.0%
Sulphur Trioxide (So3)	3.90%
Ferric Oxide (Fe2o3)	3.30%
Magnesium Oxide (Mgo)	2.50%
Sodium Oxide (Na2o)	0.20%
Potassium Oxide (K2o)	0.45%
Loss Of Ignition	1.10%

3.2.2 Mix Design Preparation

In this study, four mixes were evaluated. Mix-1 (M1), in which the Cationic Slow Setting Emulsion (CSS-1H) was mixed with pulverized HL8 RAP material; mix-2 (M2), in which the pulverized HL8 RAP material was mixed with an Anionic High Float Emulsion (HF-150). However, for mix-3 (M3), the Cationic Slow Setting Emulsion (CSS-1H) was mixed with the pulverized HL3 RAP materials, and for mix-4 (M4), the pulverized HL3 RAP material was mixed with an Anionic High Float Emulsion (HF-150) as illustrated in Table (3.4). It is worth mentioning that the water content was 25-45% for the Slow Setting Emulsion (CSS-1H) and 15-45% for the Anionic High Float Emulsion (HF-150), respectively, as reported in the data sheets in Appendix-I.

To determine the optimum emulsion percentage and obtain a mixture that has the properties of new asphalt concrete, there are different methods for mixture design of cold-in-place recycled asphalt concrete. The most commonly used is the modified Marshall method. This method was used in this study. For both mixes, 4500 gm of RAP material was prepared and put in an oven at 40°C for an hour, and then water was added such that the total final liquid content of the mixture was 4.5% of the dry weight (MTO-LS, 1996). Then emulsion was added to the mixture and put in the oven to cure for 1 hour at 40 °C. Mixes with five different percentages of emulsion were prepared.

Table 3.4 Proposed Mixtures

Mixtures	M1	M2	M3	M4
Gradation & Emulsion Type	**HL8 + CSS-1H**	**HL8 + HF-150**	**HL3 + CSS-1H**	**HL3 + HF-150**
Portland Cement Content (%)	0	0	0	0
	0.5	0.5	0.5	0.5
	1.5	1.5	1.5	1.5
	3	3	3	3

To determine appropriate percentages of emulsion, a pilot study was performed using different percentages of emulsion for M1, M2, M3 and M4 mixtures. For M1 mix, the percentages of emulsion added were 2.5%, 3%, 3.5%,4% and 4.5 % of the mass of the reclaimed aggregate in increments of 0.5% AC. For M2 and M3 mixtures, the percentages of emulsion added were 2 %, 2.5%,3%, 3.5% and 4% of the mass of the reclaimed aggregate in increments of 0.5 % AC However, M4 was prepared with a different five percentages of emulsion (1.2 %, 1.5 %, 2%, 2.5 % and 3 %).

Five hundred grams (500 g) of the cured RAP material was taken for moisture content measurement, and its mass was recorded to the nearest 0.1 gm. Three replicates for each mix were prepared using a modified Marshall procedure to produce specimens with a height of 63 mm and a diameter of 100mm. Fifty blows per side were applied using a mechanical compactor. The specimens were then placed in an oven for 24 hours at 40 °C and re-compacted in the same order as previously with 25 blows on each side. Finally, the molded specimens were placed on their side in the oven for 24 hours at 40 °C. The mixes were all constructed in accordance with MTO LS-300 (MTO-LS, 1996) for CIR. Then, the bulk relative density (BRD) of the specimens was measured, and the maximum relative density (MRD) of the mixtures was measured. The BRD and MRD were conducted in accordance with MTO LS-262 (MTOLS, 1999) and LS-264 (MTO-LS, 2012), respectively, and the air voids content of the specimens was calculated. Then, the Marshall stability of the specimens was measured according to (ASTM D6927 – 15). Figures (3.4,3.5,3.6, and 3.7) show a Stability test for M1, M2, M3, and M4 mixtures. Figures (3.8, 3.9, 3.10 and 3.11) show the air voids for M1, M2, M3, and M4 mixtures.

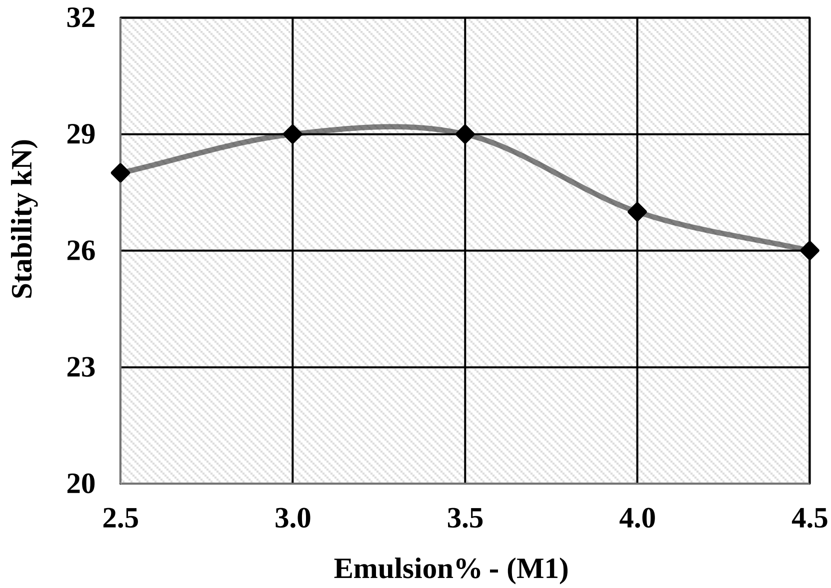

Figure 3.4 Stability and Emulsion Percentage(M1)

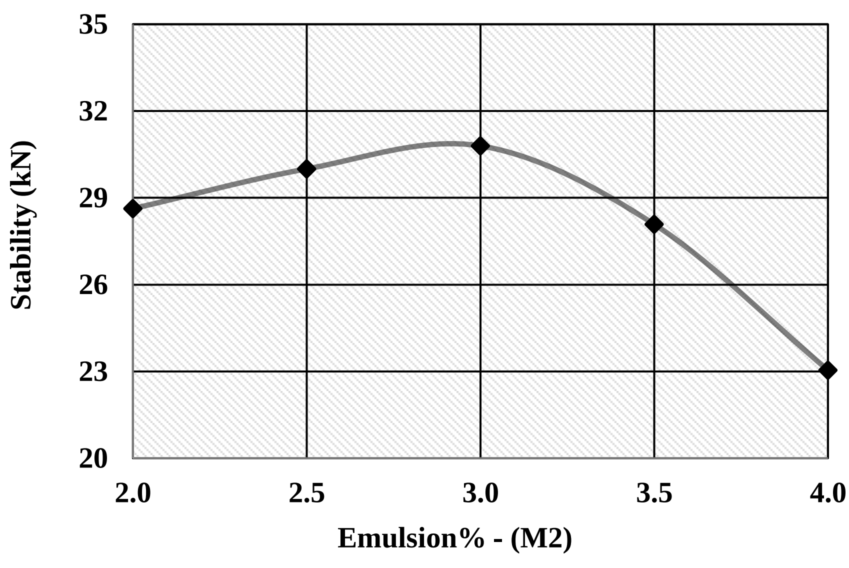

Figure 3.5 Stability and Emulsion Percentage (M2)

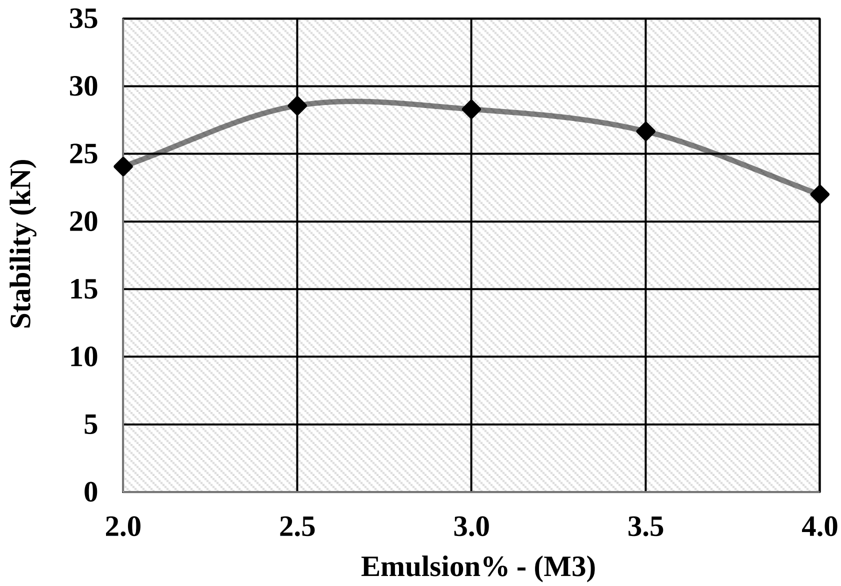

Figure 3.6 Stability and Emulsion Percentage (M3)

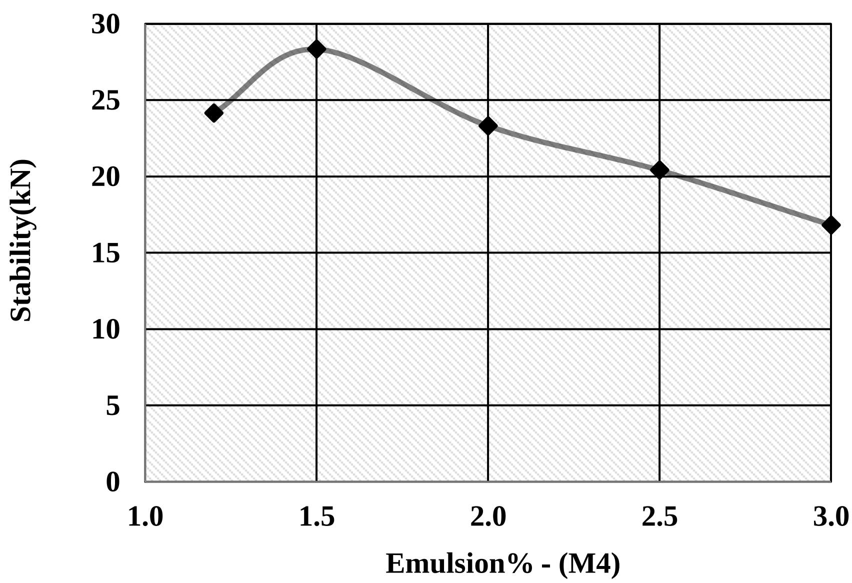

Figure 3.7 Stability and Emulsion Percentage (M4)

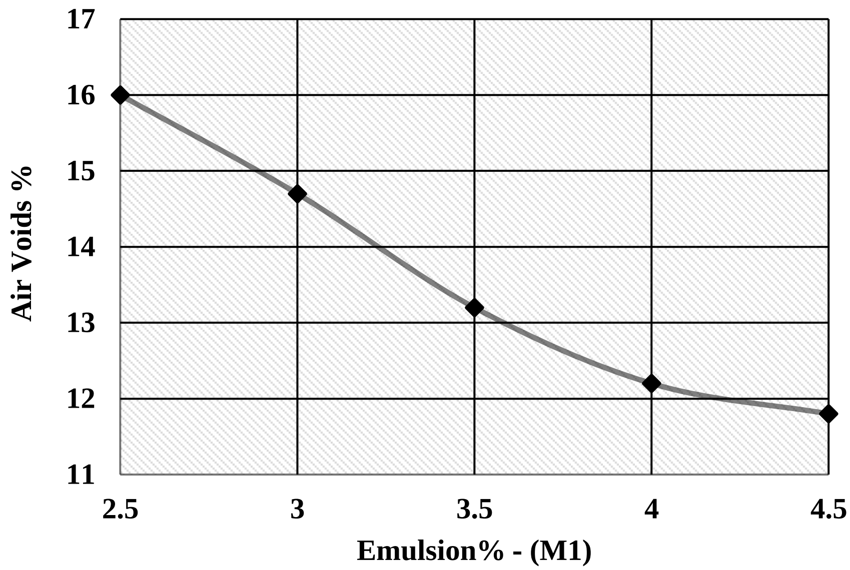

Figure 3.8 Air voids and Emulsion Percentages (M1)

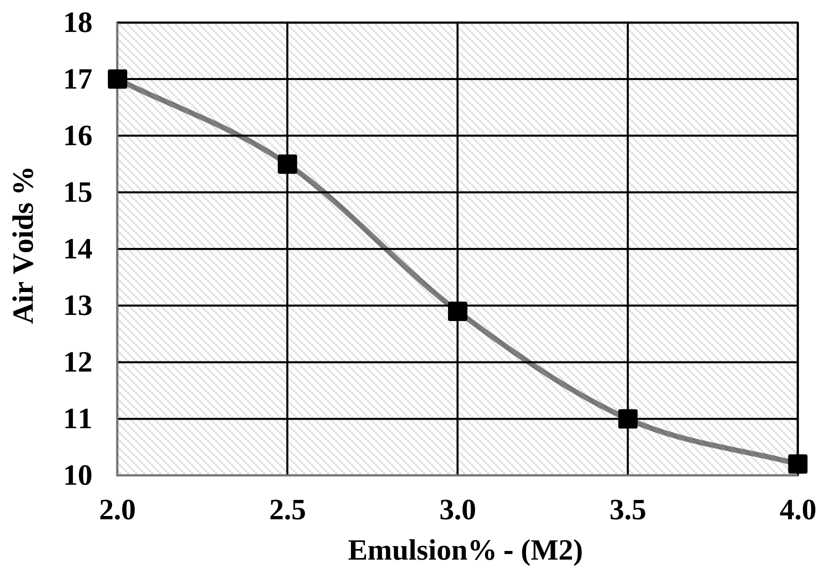

Figure 3.9 Air voids and Emulsion Percentages(M2)

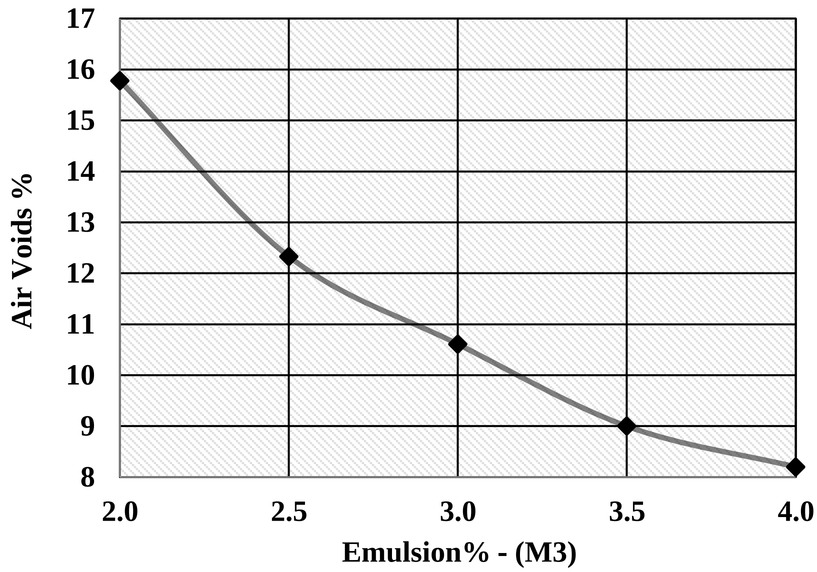

Figure 3.10 Air voids and Emulsion Percentages (M3)

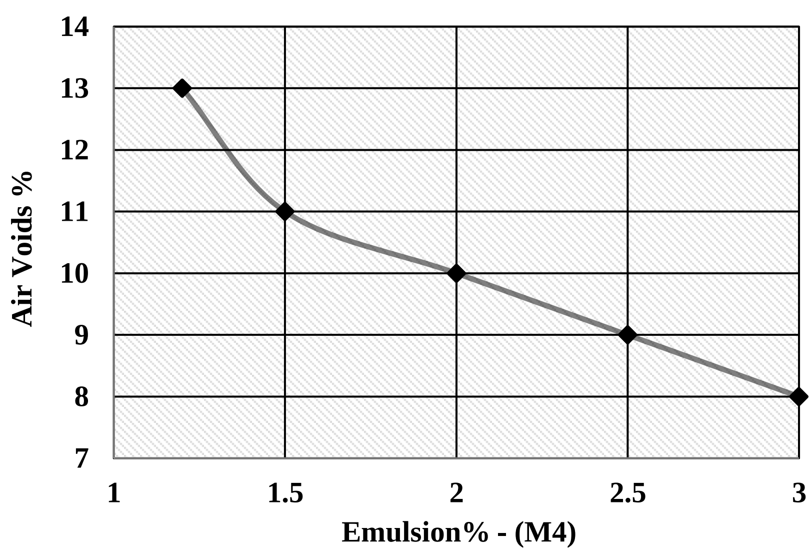

Figure 3.11 Air voids and Emulsion Percentages (M4)

The flow value was recorded at 0.25 mm increments at the same time the maximum load was recorded. For (M1) mix, a 3.8% emulsion content has met the CIR mix design requirements with air voids of 12.56%, stability of 27.9 kN, and a flow number of 24. However, for the (M2) mix, a 3% emulsion content was obtained with air voids of 13%, Stability of 25.1 kN, and flow number of 22. For (M3) mix, the optimum emulsion percentage was 2.6%, and the Marshal Stability was measured to be 29 kN with air voids of 11.8%. As for the M4 mix, the optimum emulsion percentage was 1.5%, with air voids of 11% and stability of 28.3 kN. The Marshall Stability and flow test provide a performance prediction measure for the Marshall Mix design method. The stability portion of the test measures the maximum load supported by the test specimen at a loading rate of 50.8 mm/minute, as shown in Figure (3.12).

Figure 3.12 Marshall Stability Test

Furthermore, after the optimum emulsion content had been determined, different percentages of Portland Cement (0%, 0.5%, 1.5% and 3%) were added to the mixture. The Specimens were made using a Superpave gyratory compactor. The vertical stress level and the angle of gyration for compacting the specimens were selected to be 600 kPa, and 1.25˚, respectively. After compaction, the specimens were cured for two weeks at room temperature.

3.3 Laboratory Evaluation of CIR Mixes

3.3.1 Indirect Tensile Test

The tensile strength of the asphalt mixtures was evaluated by loading a specimen along a diametral plane. The specimens were prepared using a Superpave Gyratory Compactor. The load was applied at a constant compressive loading rate using two strips on opposite sides. A relatively uniform tensile stress develops perpendicular to the direction of the applied load and causes the specimen to fail by splitting along the vertical diameter. The static indirect tensile strength of a specimen was measured using the procedure outlined in [ASTM D 6931].

A loading rate of 50.8 mm/minute was adopted. The test set up is shown in Figure (3.13). The maximum force required to fail the specimen was monitored, and the tensile strength of the mixtures was calculated using Equation.

$$\text{ITS} = \frac{2000 \times \text{P}}{\pi \times \text{T} \times \text{D}} \qquad (3.1)$$

Where:
ITS = strength, kPa
P = maximum load, N
T = specimen height immediately before test, mm, and
D = specimen diameter, mm

Figure 3.13 Indirect Tensile Test Setup

The specimens for the Indirect Tensile test were prepared according to the AASHTO T-283 method, except that the specimens were conditioned in water at 25˚C for 24 ±1 hours rather than at 60˚C because they fractured at 60˚C temperature. A total of 96 specimens, with a diameter of 150mm and a height of 95mm, were prepared and compacted using a Superpave Gyratory

Compactor in the CPATT laboratory. These 96 specimens were divided into four groups. Each mix design (M1, M2, M3, and M4) consisted of 24 specimens. These 24 specimens were divided into four groups containing 0%, 0.5%, 1.5%, and 3% Portland Cement by weight of the total mix. The group that contained 0% of Portland Cement served as a control. The mixes were compacted using a SuperPave Gyratory Compactor to achieve an air voids content of (7% ±0.5) (AASHTO T-283). Also, in each group, three specimens were non-conditioned (dry), and the other three remained conditioned in water at 25˚C for 24±1 hours to measure the water susceptibility of the mixtures. After that, the specimens were cured in an oven at 60ºC for 48 hours to allow the water to evaporate.

3.3.2 Dynamic Modulus

It was proposed in the 2002 Design Guide that the complex modulus of asphalt mixtures be used as a parameter in the design procedure. The complex modulus is a compressive test for asphalt specimens to predict rutting and fatigue cracking in asphalt pavements. As a result, an accurate determination of the complex modulus of asphalt mixtures has become an important priority (Marasteanu et al., 2003). The test is conducted over a wide range of temperatures and frequencies. The dynamic modulus of an asphalt mixture can be determined by conducting laboratory tests in either a stress-controlled or strain-controlled mode. Figure (3.14) shows a typical viscoelastic response of an asphalt mixture. The stress can be expressed by Equation (3.2):

$$\sigma = \sigma_o * \sin(\omega t) \tag{3.2}$$

Where: σ_o is the stress amplitude, and ω is related to frequency (f), $\omega = 2\pi f$

The strain can be expressed by Equation (3.3):

$$\varepsilon = \varepsilon_0 * (\omega t - \delta) \tag{3.3}$$

Where: ε_0 is the strain amplitude and δ is the phase angle related to the time the strain lags the stress

The phase angle is an indicator of the viscous (or elastic) properties of the material. For a purely elastic material, δ = 0º, and for purely viscous material, δ = 90º. The complex modulus is defined as a complex quantity and expressed by Equation (3.4):

$$E^*(i\omega) = \frac{\sigma^*}{\varepsilon^*} = \frac{\sigma_o}{\varepsilon_o} * e^{i\delta} = E' + iE'' \tag{3.4}$$

The real part (E') of the complex modulus is the storage modulus and the imaginary part (iE'') is the loss modulus. The complex dynamic modulus is the absolute value of the complex modulus and is expressed by Equation (3.5):

$$|E^*| = \frac{\sigma_o}{\varepsilon_o} \tag{3.5}$$

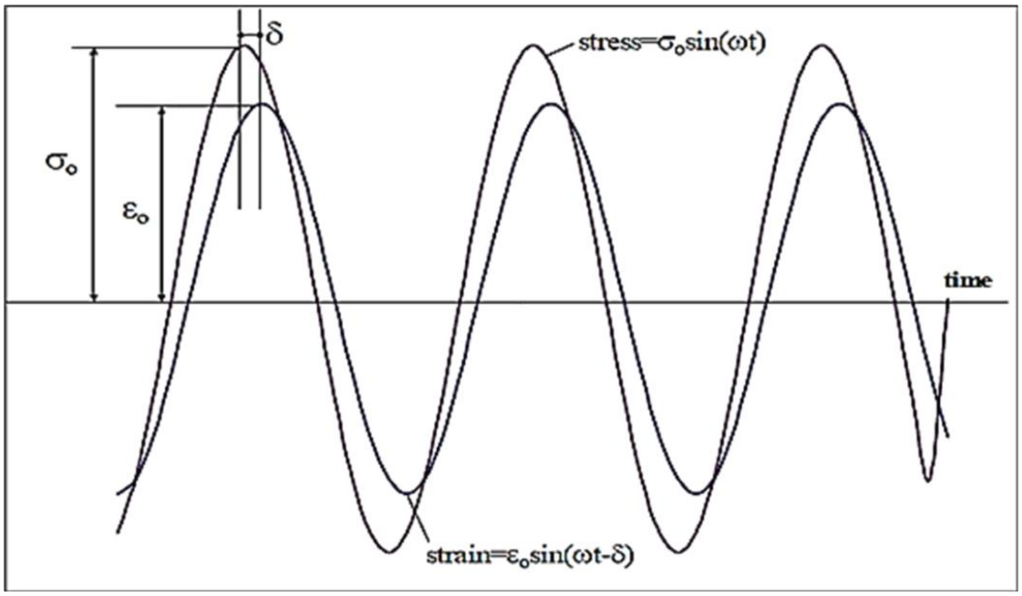

Figure 3.14 Stress and Strain in Dynamic Loading (Clyne et al., 2003)

An analysis of complex modulus test data often involves generating master curves. The development of a master curve provides a comparison of the stiffness of an asphalt mixture over extended ranges of frequencies and temperatures. In order to obtain the master curve, a shift factor should be applied to the experimental complex modulus (E*) values in order to normalize them to a reference temperature. The master curve for a material can be constructed using an arbitrarily selected reference temperature, to which all data are shifted (Marasteanu et al., 2003). Shifting of the values is performed using the principle of time-temperature super positioning with respect to time until the curves merge into a simple smooth function (Witczak, 2005).

The main objective of utilizing a dynamic modulus test is to evaluate the CIR mixture's properties under different temperatures and frequencies and to observe the effect of the emulsion type on their stiffness. The specimens were prepared and compacted using the Superpave Gyratory Compactor in the CPATT laboratory. The specimens were compacted with target air voids values of 8% ± 0.5%, which came down to about (7% ± 0.5%) once the samples were cored and cut. The compacted specimens were kept at room temperature for 24 hours to allow the mixture to lose moisture and gain strength. After that, the samples were put in an oven at 60ºC for 48 hours for curing purposes.

A total of 32 specimens, with a diameter of 100mm (after coring) and a height of 150mm, were prepared and compacted using a Superpave Gyratory Compactor in the CPATT laboratory. Each mix (M1, M2, M3, and M4) contains 8 specimens. Two replicates for each mixture were prepared for 0%, 0.5%, 1,5%, and 3% Portland Cement. The test was performed on all the mixes with their different dosages of Portland Cement (0%, 0.5%,1.5% and 3%) according to the procedure given in [AASHTO TP 6207], Standard Test Method for Determining Dynamic Modulus of Hot-Mix Asphalt Concrete Mixtures. The test specimens were subjected to a repetitive, compressive, sinusoidal loading. Three Linear Variable Differential Transducers (LVDTs) were used to measure the deformation of test specimens. For all mixtures (M1, M2, M3 and M4), the specimens were examined at six loading frequencies (0.1, 0.5, 1.0, 5.0, 10.0 and 25 Hz) and three temperatures (-10, 4, and 21˚C). For each temperature, the specimens were conditioned and then subjected to compression loading at the six frequencies. The test setup is shown in Figure (3.15).

Figure 3.15 Dynamic Modulus Setup

3.3.3 Flexural Beam Fatigue Test

Fatigue cracks are another major mode of pavement failure under cyclic traffic loading, in which micro-cracks initiate and progress to macrocracks. The fatigue life measures the resistance of the asphalt to fatigue cracking and is defined as the number of cycles to which the material can be subjected before failing. When repeated traffic loading acts on the pavement surface, tensile stresses will be induced at the bottom of the asphalt layer (Mun et al., 2004). Therefore, cracks initiate at the bottom of the asphalt layer and then propagate to the surface of the pavement under cyclic load applications, which is called bottom-up cracking. However, also, it has been suggested that fatigue cracks can be initiated at the pavement surface and propagate downwards under traffic loading and that is called (top-down cracking). These cracks are initiated due to the induced tensile stresses that result from the interaction between truck tires and the pavement surface (Ann et al., 2001). Figure (3.16) shows a typical example of fatigue cracking.

Figure 3.16 Typical Fatigue Cracks in Asphalt Pavement (Shaheen, 2016)

Four-point bending fatigue (FPB) beam test was used to determine the fatigue life of the asphalt mixtures M1, M2, M3 and M4. The test setup is shown in Figure (3.17). The test was carried out in accordance with the AASHTOT 321-07 specification (AASHTO,2007) (Method for Determining the Fatigue Life of Compacted Hot-Mix Asphalt (HMA) Subjected to Repeated Flexural Bending). For M1 and M2 mixes, a total of 68 specimens were prepared and tested. Each mixture (M1 and M2) consisted of 34 specimens. However, a total of 78 specimens were prepared for M3 and M4 mixtures. Both mixtures, M3 and M4, were comprised of 40 and 38 specimens, respectively. The tested beam dimensions are 380mm in length by 50mm in width by 63mm in height. The specimens were prepared using the special mold shown in Figure (3.18) as the specimens are too weak to be cut when using a PReSBOX® Shear Compactor. The specimens were compacted using a MTS machine. Then the air voids were determined to make sure they were in the 7±1% range. After preparing the specimens, they were cured in the oven for 48 hours at 60℃.

The fatigue test specimens were conditioned for two hours at a temperature of 5℃, that corresponded to the conditioning temperature of the dynamic modulus test specimens. The test specimens were subjected to a repeated cyclic flexural load at a loading frequency of 5 Hz. According to the specification that is outlined in AASHTO T 321-07, the failure criterion is a reduction of the beam stiffness to 50% of the initial stiffness. A higher number of cycles to failure indicates a more fatigue-resistant mixture (AASHTO,2007).

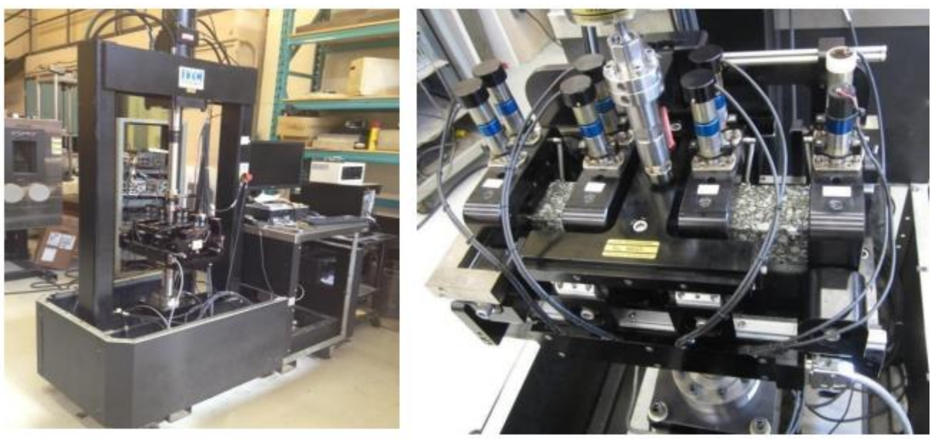

Figure 3.17 CPATT Repeated Flexural Fatigue Bending Test Setup

Figure 3.18 Fatigue Mold

In a four-point bending frame, the tested beams are subjected to repeated flexural loading. At each strain level, two to three replicate beam specimens were tested in order to obtain a Strain-Number of cycles curve. It is worthy of mention that 50 load cycles at a constant strain level were used to estimate the ratio of initial load to deflection(K*). The maximum stress and strain were calculated using the Equations (3.6 & 3.7). Different strain levels were applied - 600, 500, 400, 300, 250, 200 and 150 µm.

$$\sigma_t = \frac{0.357 \quad P}{b \;\; h^2} \tag{3.6}$$

$$\varepsilon_t = \frac{12 \quad \delta\, h}{3\, L^2 - 4a^2} \tag{3.7}$$

Where:

σ_t = *Maximum peak-to-peak stress, MPa,*
ε_t = *Maximum peak − to − peak strain, m/m,*
P = Peak load,
b = Average specimen width, m,
h = Average specimen height, m,
δ = Maximum deflection at the center of the beam, m.
L = Length of the specimen, 0.357 m, and
a = Length between the clamps (L/3 = 0.119 m)

$$S = \frac{\sigma_t}{\varepsilon} \tag{3.8}$$

$$\phi = 360\, fs \tag{3.9}$$

$$D = \pi \ \sigma_t \ \varepsilon_t \ \sin(\phi) \tag{3.10}$$

Where:
S = Stiffness Modulus, Pa,
ϕ = Phase angle, degrees,
f = Load frequency, Hz, s = Time lag between Pmax and δmax, seconds, and
D = Dissipated energy per cycle, J/m3

3.3.4 Thermal Stress Restrained Specimen Test (TSRST)

Thermal cracking of asphalt pavements has been a recognized problem for Canadian provinces since it is a common phenomenon that occurs in cold regions. Thermal cracks in asphalt, which are considered to be one of the main failure criteria for flexible pavements, occur due to a reduction and largely daily fluctuation in temperature. Figure (3.19) shows transverse cracks that extend across a pavement surface in response to cold ambient temperatures (Marasteanu et al., 2004). The cracking resistance of an asphalt mix is often evaluated by the Thermal Stress Restrained Specimen Test (TSRST), which is conducted according to AASTHO TP-10-93 specifications (AASHTO, 1993). A total of 48 specimens were prepared using the special mold shown in Figure (3.18) as the specimens are too weak to be cut when using a PReSBOX® Shear Compactor. The samples were compacted using a MTS machine. Then the air voids were determined to make sure they were in the 7±1% range. Then, the specimens were cured in the oven for 48 hours at 60°C before testing. The specimen dimensions are 50-mm width by 50 mm in height by 250 mm in length, and the specimen is glued to two aluminum end plates with epoxy, as shown in Figure (3.20). Two linear variable differential transducers (LVDT) used to measure the deformation during the cooling process are also shown in Figure (3.20). The temperature of the specimen is decreased using a liquid nitrogen coolant which is released into the chamber around the specimen at a rate that causes a decrease of 5°C per hour in the specimen temperature, as shown in Figure (3.20). The applied load on the specimen is recorded from the output of a load cell with a capacity of 100 kN. During the test, the applied load and the specimen temperature are recorded at intervals of one minute until failure. In addition, the fracture temperature and stress were recorded. Figure (3.21) from reference (Marasteanu et al., 2007) shows a typical temperature versus stress result for an asphalt mixture. A decrease in temperature induces tensile stresses in the specimen. The slope of the (dS/dT) temperature versus stress curve gradually increases until it reaches its maximum value at the transition temperature. In this region, the increasing stress tends to increase the creep rate while the decreasing temperature decreases the creep rate, resulting in a continuous decrease in creep rate and a continuous increase in (dS/dT). Below the transition temperature, the creep ceases, and the (dS/dT) slope is linear until fracture. Table (3.5) gives a summary of the mixtures and the number of each tested.

Figure 3.19 Typical Low-Temperature Cracks

Table 3.5 Summary of the Total Number of the Tested Specimens

Test Type	Mixture	Number of Specimens	Total
Indirect Tensile Test (ITS)	M1	24	96
	M2	24	
	M3	24	
	M4	24	
Dynamic Test	M1	8	32
	M2	8	
	M3	8	
	M4	8	
Fatigue Test	M1	34	146
	M2	34	
	M3	40	
	M4	38	
Thermal Crack	M1	12	48
	M2	12	
	M3	12	
	M4	12	

Figure 3.20 TSRST Test Setup

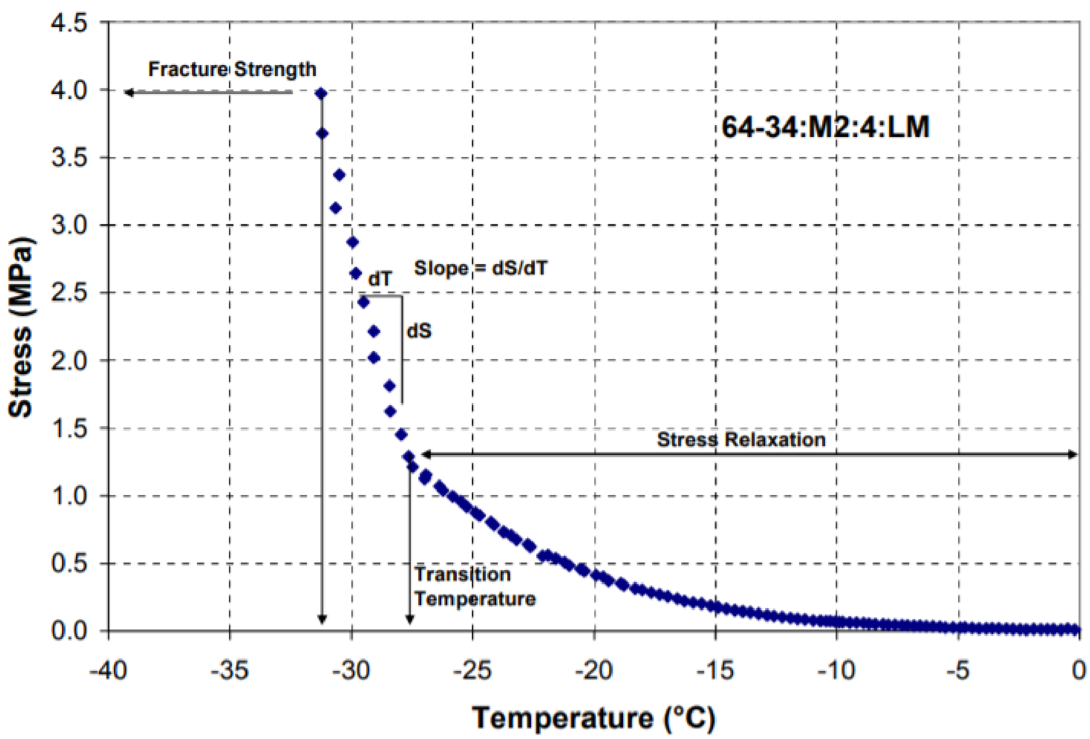

Figure 3.21 Stress versus Temperature(Marasteanu et al., 2007)

4 Experimental Program Results and Discussion

This chapter presents the test results for the Indirect Tensile, Dynamic Modulus, Fatigue, and Thermal Stress Restrained Specimen Tests. For M1, M2, M3, and M4 mixtures, the tensile strength and the tensile strength ratio are presented and discussed for each mix. Furthermore, a load-temperature master curve was developed for the M1, M2, M3, and M4 asphalt mixtures at Portland Cement Percentages of (0%, 0.5%, 1.5% and 3%) as explained later in the chapter. A four-point bending test was conducted to determine the endurance fatigue limit. The test was conducted on all mixes (M1, M2, M3, and M4), with different Portland Cement percentages (0%, 0.5%, 1.5% and 3%) under strain control and for different stain ranges (200 micro-strain to 600 micro-strain). Moreover, the results of Thermal Stress Restrained Specimen Tests for M1, M2, M3, and M4 mixtures with four different Portland Cement percentages (0%, 0.5%, 1.5% and 3%) were presented and discussed. Finally, a comparison was presented between the stiffness and fatigue life in order to obtain the best Portland Cement percentage. A trade-off relationship was obtained that gave a higher stiffness without compromising the fatigue life.

4.1 Indirect Tensile Tests

Table (4.1) provides a summary of the indirect tensile strengths for all mixtures (M1, M2, M3 and M4) both unconditioned and conditioned for all the tested specimens with their averages and standard deviations. Figure (4.1) shows the variation of the indirect tensile strength for unconditioned (dry) and conditioned (wet) specimens with the variation of cement content for M1 mix. It is clearly shown that as the percentage of Portland Cement increases, the indirect tensile strength increases, which will increase the load-carrying capacity of the pavement structure by providing early strength, increasing the rutting resistance and reducing the sensitivity of the mixture to moisture (ARRA,2017). However, as the Portland Cement increased, the pavement is more likely to develop shrinkage cracks. Shrinkage cracks can develop over the lifetime of a pavement due to the evaporation of the water from the emulsion and the changes in moisture and ambient temperature. Shrinkage of the cement can increase the tensile stress at the surface of the pavement and initiate cracks that propagate through the depth of the pavement leading to failure.

Figure (4.1) shows that the tensile strengths for the unconditioned (dry) mixtures containing 0.5%, 1.5% and 3% Portland Cement are 1.1, 1.4 and 1.8 times that of the control mix, respectively.

Similarly, there is a general trend for the conditioned specimens that as the amount of Portland Cement increases, the tensile strength of the specimens increase. The strengths of the specimens containing 0.5%, 1.5%, and 3% Portland Cement are 1.2 and 1.6, and 1.9 times that of the control mix, respectively.

Generally, there is a noticeable increase in the tensile strength with cement content for the unconditioned and conditioned specimens containing 0.5%, 1.5% and 3% Portland Cement. However, there is only a small increase in tensile strength between cement additions of 1.5% and 3.0%, as the additional amount of Portland Cements apparently acts as a filler in the mix. This may be attributed to the fact that the total liquid (including emulsion or water) content in the mix should not exceed 4.5%, according to the Ministry of Transportation Ontario (MTO) laboratory Standard, LS-300. As a result, there is not enough water to react with the Portland Cement to complete the hydration process, and the Portland Cement acts as a filler rather than playing the role of increasing the stiffness of the mixes.

Also, the ratios of indirect tensile test strengths (wet /dry) are shown in Figure (4.2). It is clearly shown that as the amount of Portland Cement increases, the ratio increases. This is because as the percentage of Portland Cement increases, the mixtures become stiffer and less ductile. That will reduce the deflection of the pavement and increases the rutting resistance of the pavement. Figure (4.3) shows the variation of the indirect tensile strength with the variation of cement content for M2 mix. Similarly, to M1 mix, as the percentage of Portland Cement increases, the indirect tensile strength increases. The Indirect tensile strength for the unconditioned (dry) mixes containing 0.5%, 1.5% and 3% Portland Cement was 1.01, 1.3 and 1.5 times that of the control mix, respectively. It is worth mentioning that the ratios of the indirect tensile test (wet/dry) do not change with the fraction of Portland Cement, as shown in Figure (4.4).

Figure (4.5) shows the tensile strength for the M3 mixture of conditioned and unconditioned specimens. As the percentage of Portland Cement increases, the strength increases for both wet and dry conditions, which suggests a corresponding increase in the load-carrying capacity, resistance to deformation (rutting resistance) and moisture sensitivity of the pavement. Adding Portland Cement in the amounts of 0.5%, 1.5%, and 3% to unconditioned specimens leads to increase in mixture’s strength. The increase was 1.2, 1.5 and 2.3 times that of the control mix, respectively. The addition of the same amounts of Portland Cement to the conditioned specimens increases the tensile strength by similar amounts (1.3, 1.7 and 2.5 times that of the control mix, respectively). The increase in strength as the Portland Cement portion increases results in the specimens being stronger (and more brittle) as they become stiffer.

Figure (4.6) shows the ratios of tensile strength wet /dry for the tests of the M3 mixture. The strength increases continuously with increasing Cement content; during the tensile testing, cracks developed along the diameter of the specimen and propagated to failure.

The tensile strength for the M4 mix increased as the Portland Cement increased, as shown in Figure (4.7). For both wet and dry conditions, the ratio of strengths increased with cement content. Furthermore, Figure (4.8) shows that an addition of Portland Cement increased the ratio of tensile strengths (wet/dry) by about the same amount for additions of 0.5%, 1.5% and 3%. The addition of 0.5% increases the ratio of wet/dry significantly, but further additions have almost no effect. This is probably due to the fact the amount of water was kept constant as the amount of Portland Cement increased. This would result in incomplete hydration of the Portland Cement, reducing its strengthening effect on the mixture.

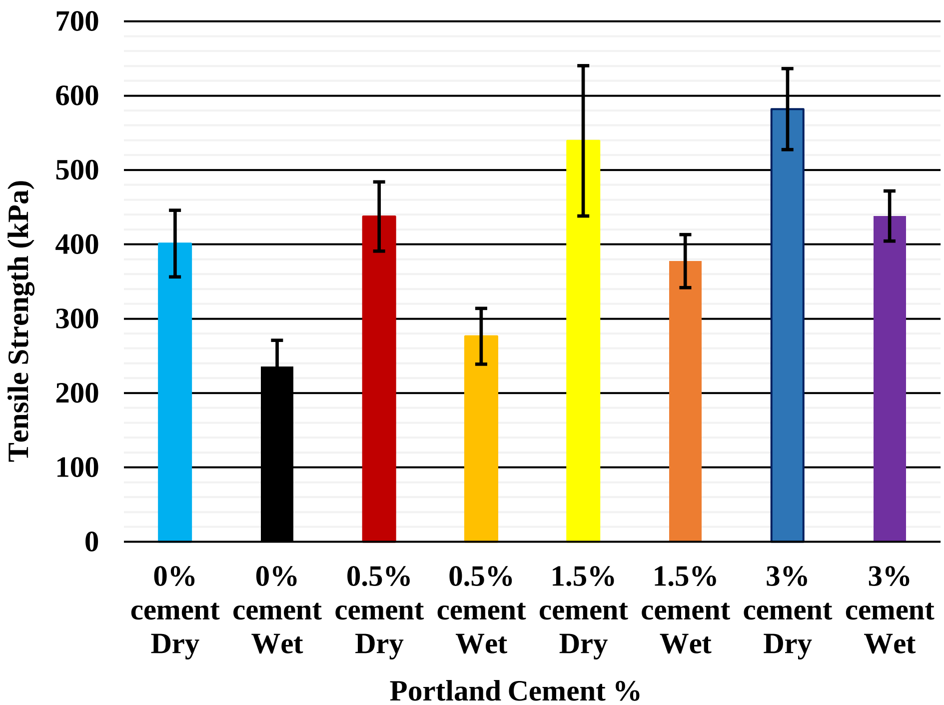

Figure 4.1 Indirect Tensile Strength for M1

Table 4.1 Indirect Tensile Strength for M1, M2,M3 and M4 for all the Tested Specimens

Mixture				***M1***				
Cement%	0		0.5		1.5		3	
Test	**ITS dry (kPa)**	**ITS wet (kPa)**	**ITS dry (kPa)**	**ITS wet (kPa)**	**ITS dry (kPa)**	**ITS wet (kPa)**	**ITS dry (kPa)**	**ITS wet (kPa)**
specimen 1	411.8	215.7	488.7	269.6	640.3	404.4	640.3	471.8
specimen 2	439.5	215.7	397.7	316.8	539.2	390.9	572.9	404.4
specimen 3	351.8	276.3	426.0	242.6	438.1	337.0	532.5	438.1
Average	401.0	235.9	437.4	276.3	539.2	377.4	581.9	438.1
Std	44.8	35.0	46.6	37.5		101.1		54.5
Mixture				***M2***				
Cement%	0		0.5		1.5		3	
Test	**ITS dry (kPa)**	**ITS wet (kPa)**	**ITS dry (kPa)**	**ITS wet (kPa)**	**ITS dry (kPa)**	**ITS wet (kPa)**	**ITS dry (kPa)**	**ITS wet (kPa)**
specimen 1	407.4	357.9	402.9	316.0	507.8	411.2	546.4	500.4
specimen 2	384.3	372.6	356.1	268.0	520.6	457.9	619.9	510.7
specimen 3	425.5	354.2	475.8	335.2	607.9	542.3	692.8	639.2
Average	405.7	361.6	411.6	306.4	545.4	470.5	619.7	550.1
Std	20.7	9.7	60.3	34.6	54.5	66.5	73.2	77.3
Mixture				***M3***				
Cement%	0		0.5		1.5		3	
Test	**ITS dry (kPa)**	**ITS wet (kPa)**	**ITS dry (kPa)**	**ITS wet (kPa)**	**ITS dry (kPa)**	**ITS wet (kPa)**	**ITS dry (kPa)**	**ITS wet (kPa)**
specimen 1	338.4	177.2	425.5	284.2	526.0	346.5	782.0	623.8
specimen 2	363.9	294.2	400.6	313.9	541.6	502.0	856.6	611.2
specimen 3	306.0	233.1	458.2	328.9	502.6	379.9	632.8	577.5
Ave	336.1	234.8	428.1	309.0	523.4	409.5	757.1	604.1
Std	29.0	58.6	28.9	22.7	19.6	81.9	113.9	23.9
Mixture				***M4***				
Cement%	0		0.5		1.5		3	
Test	**ITS dry (kPa)**	**ITS wet (kPa)**	**ITS dry (kPa)**	**ITS wet (kPa)**	**ITS dry (kPa)**	**ITS wet (kPa)**	**ITS dry (kPa)**	**ITS wet (kPa)**
specimen 1	246.7	154.1	211.2	211.2	262.3	262.3	659.3	473.0
specimen 2	187.7	91.5	219.0	219.0	269.3	269.3	535.5	466.6
specimen 3	281.5	105.0	188.2	188.2	237.4	237.4	496.1	425.5
Average	238.6	116.9	206.1	206.1	256.3	256.3	563.6	455.0
Std	47.4	32.9	16.0	16.0	16.7	16.7	85.1	25.8

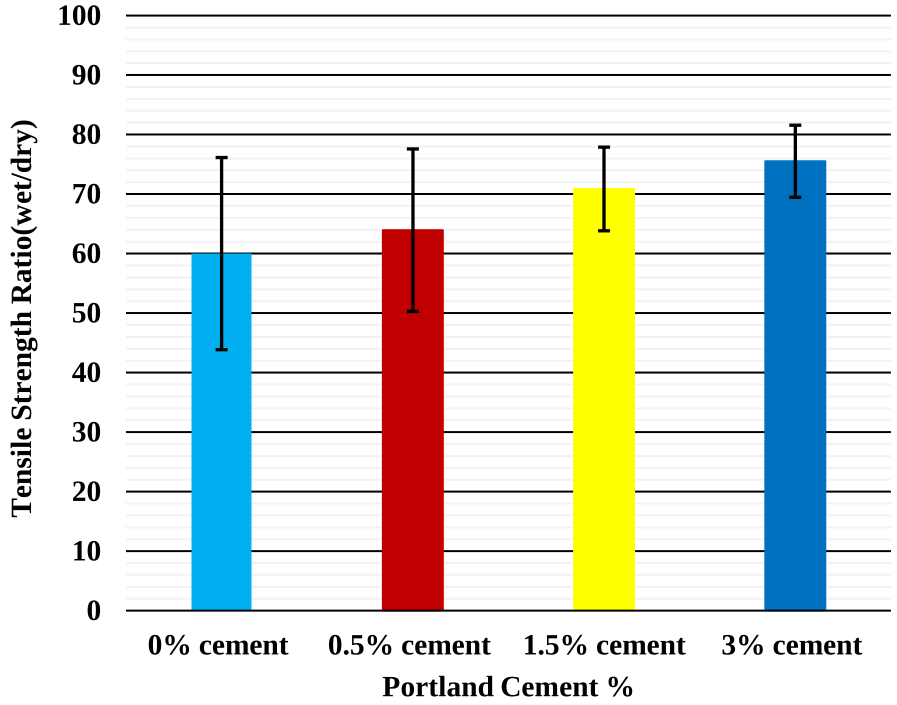

Figure 4.2 Ratio (Wet/Dry) of Indirect Tensile Strength for M1

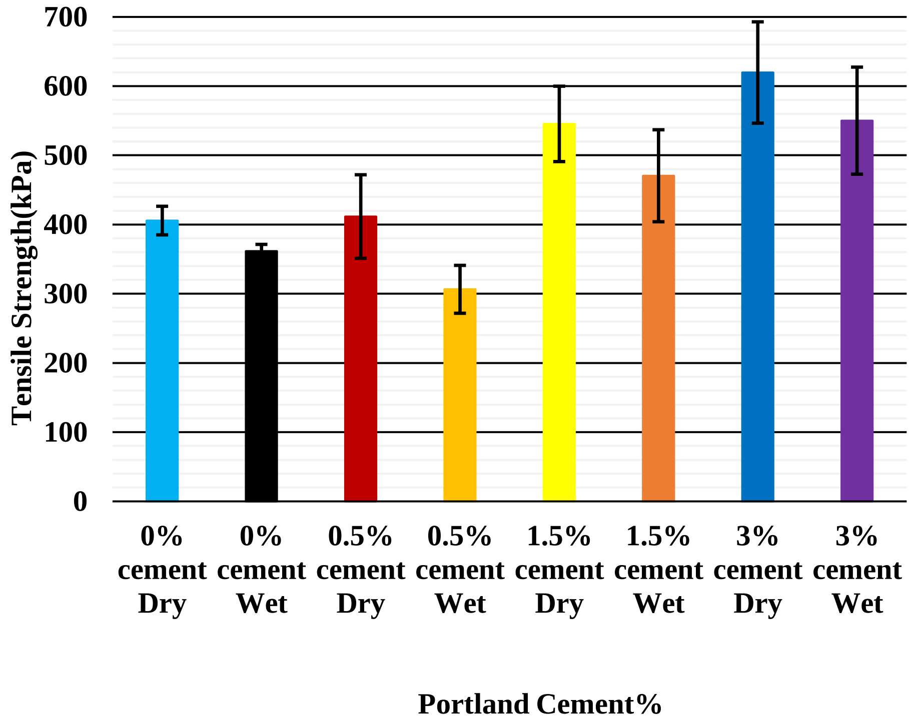

Figure 4.3 Indirect Tensile Strength M2

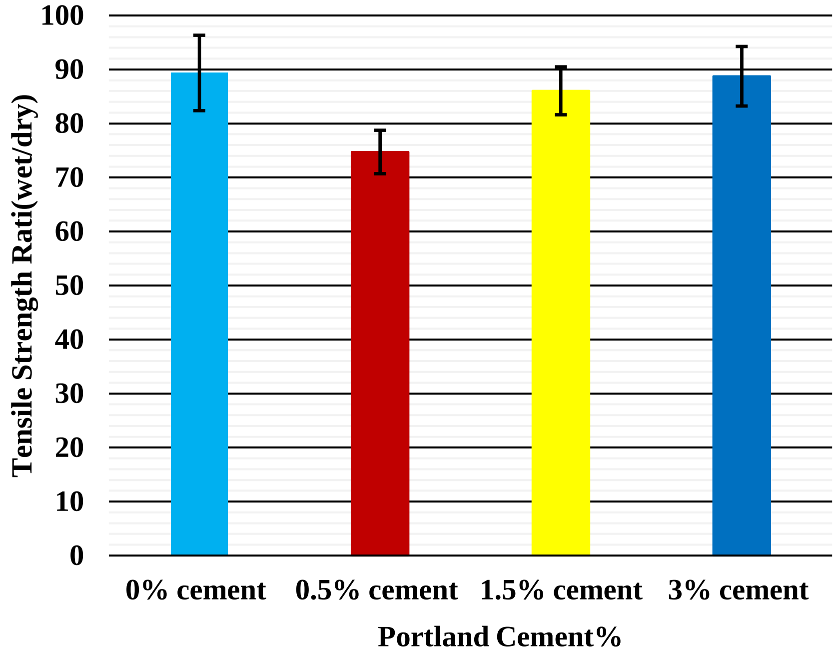

Figure 4.4 Ratio (Wet/Dry) of Indirect Tensile for M2

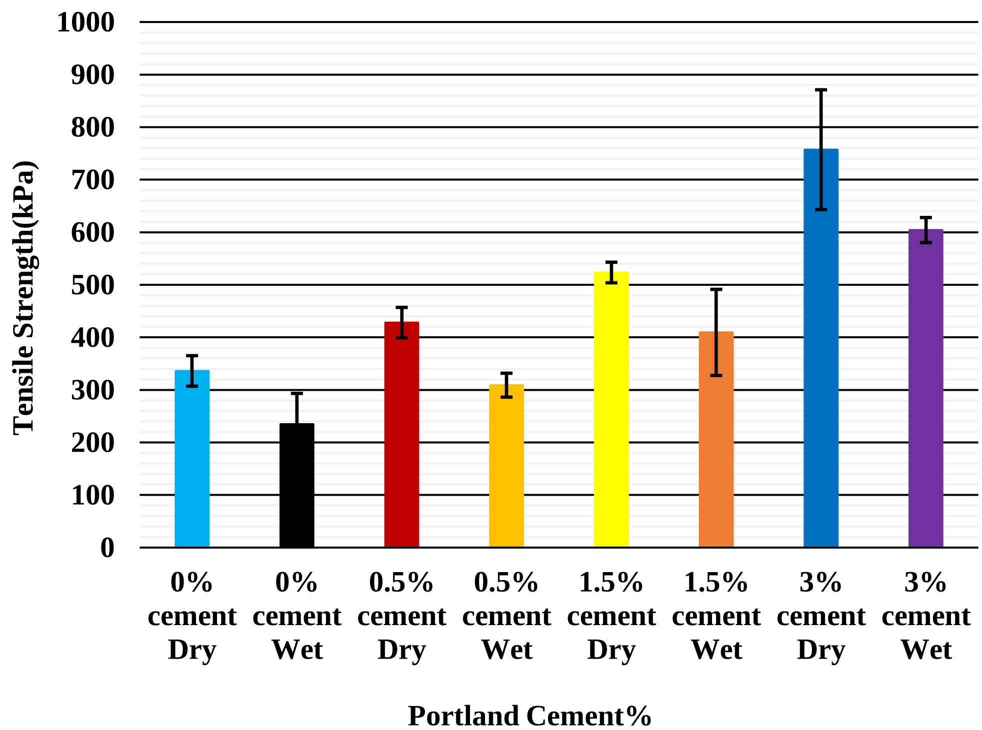

Figure 4.5 Indirect Tensile Strength for M3

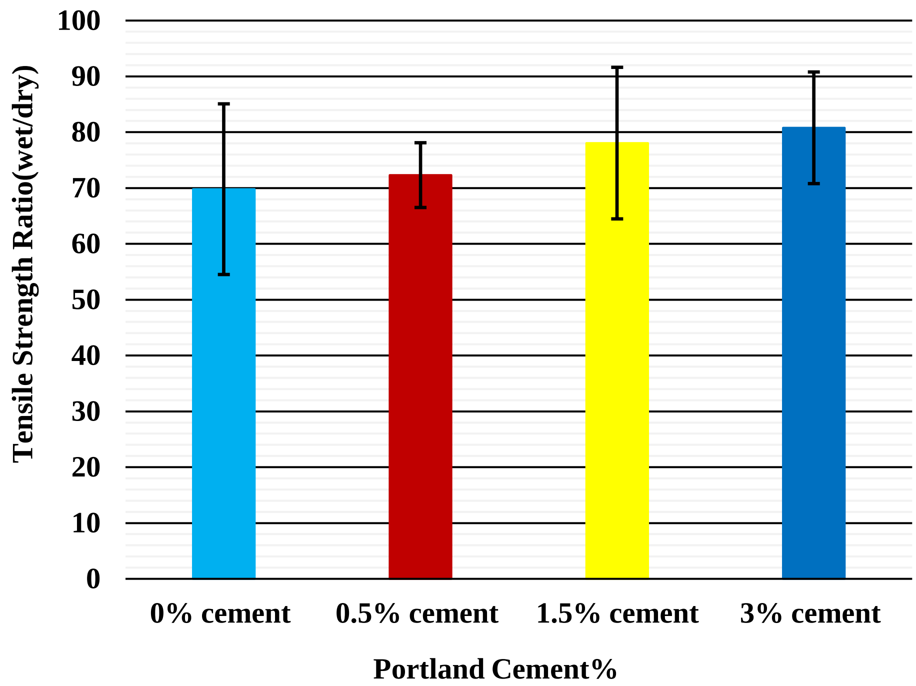

Figure 4.6 Ratio (Wet/Dry) of Indirect Tensile Strength for M3

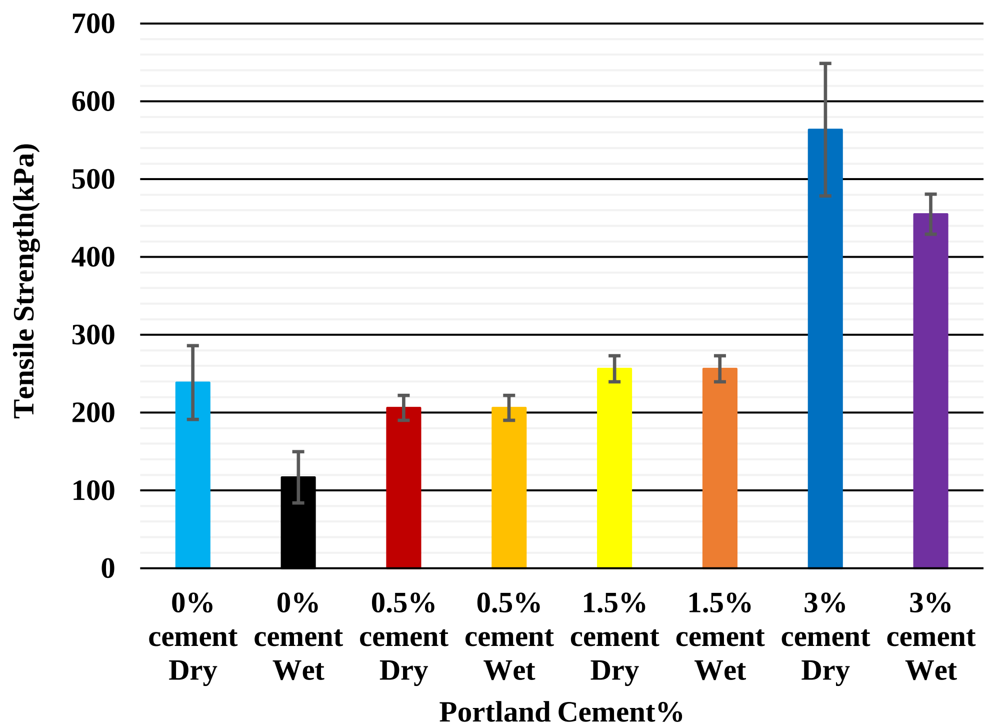

Figure 4.7 Indirect Tensile Strength for M4

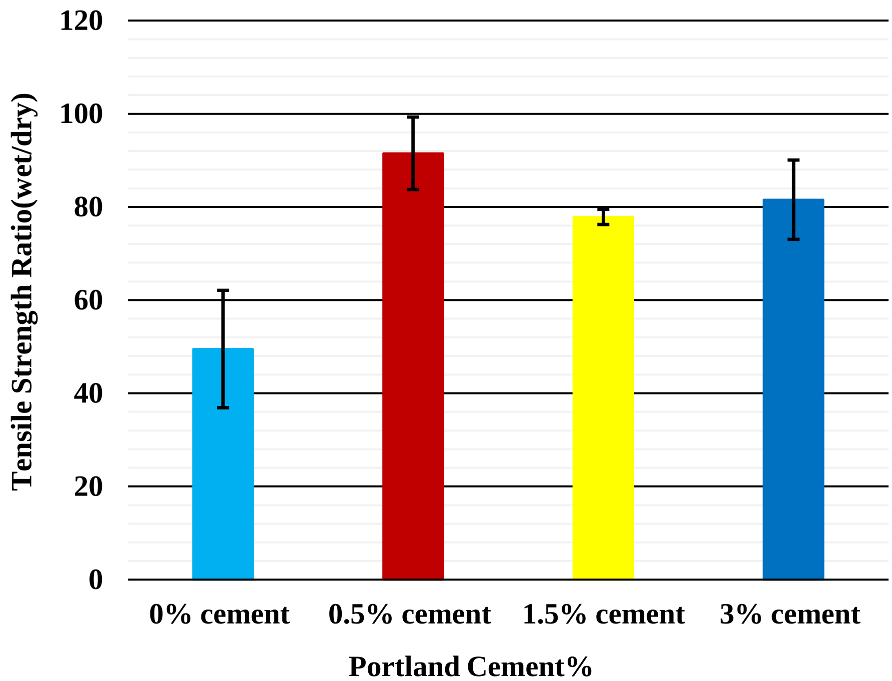

Figure 4.8 Ratio (Wet/Dry) of Indirect Tensile Strength for M4

It is seen in Figure (4.9) that the combinations of cationic slow setting emulsion with pulverized HL8 and HL3 RAP materials and rapid setting emulsion with pulverized HL8 RAP materials have about the same strength for all additions of Portland Cement. An outlier to this uniformity is a cationic slow setting emulsion with pulverized HL3 RAP materials aggregate, which has a higher strength than the other two combinations at a 3% Portland Cement addition. However, for the rapid setting emulsion and pulverized HL3 RAP materials, the tensile strength is significantly reduced for given percentages of Portland Cement addition until it reaches the strength level of the other combinations at a Portland Cement addition of 3%. It appears that the cationic slow setting emulsion provides sufficient bonding strength to hold the finer mixture together as well as, the coarser mixture when the Portland Cement addition reaches about 3%. In all cases, as the Portland Cement increases, the tensile strength increases. A linear regression statistical analysis was conducted to study the effect of Portland Cement on the CIR mixtures. As can be seen from the linear regression analysis for M1, M2 and M3, there is a strong relationship between the ITS and Portland Cement contents, with the adjusted R^2 ranging between 0.89 to 0.98. However, the R^2 adjusted value for M4 was 0.73, which suggests an approximately linear relationship between the Portland Cement contents and ITS values. The results are presented in Appendix II.

Figure (4.10) shows a similar trend for the wet indirect tensile strength test results. A linear regression analysis was conducted, and the results show that the adjusted R2 values for M1, M3, and M4 range between 0.93 and 0.99, indicating a linear relationship between their Portland Cement additions and ITS values. But for M2, the adjusted R^2 was found to be 0.76, indicating a semi-linear relationship. The analysis is presented in Appendix II as well.

Furthermore, for all mixes (M1, M2, M3, and M4), two modes of failure were observed. Some of the specimens failed by developing cracks along the diameter of the specimen, and others failed due to excessive deformation near the loading strip and cracking in the central section of the specimen, as shown in Figure (4.11). When the load was applied on the specimen through two loading strips, the applied load was transferred through two loading strips that have the same radius as that of the specimen. After transferring the load, the tensile stresses developed at the center of the vertical plane and perpendicular that causing the specimen to fail, as shown the Figure (4.11). As can be seen, some specimens developed a tensile failure (vertical)and others a deformation failure (cracks are distributed over the specimen).

In summary, as the amount of Portland Cement increases, the tensile strength increases. This leads to an increase in the stiffness of the asphalt mixture and reduces the deformation of the mixture; thus, the rutting resistance increases. On the other hand, an excessive amount of Portland Cement leads to the development of shrinkage cracks leading to premature cracking of the pavement. Shrinkage cracks are unavoidable but can be minimized by an appropriate mixing time and the use of sufficient water to complete the hydration process of the Portland Cement. It is recommended that the Portland Cement content should not exceed the emulsion content used in the mixture to ensure proper mixing of the mixture, achieve adhesion between the emulsion and the Portland Cement used, and reduce shrinkage cracks.

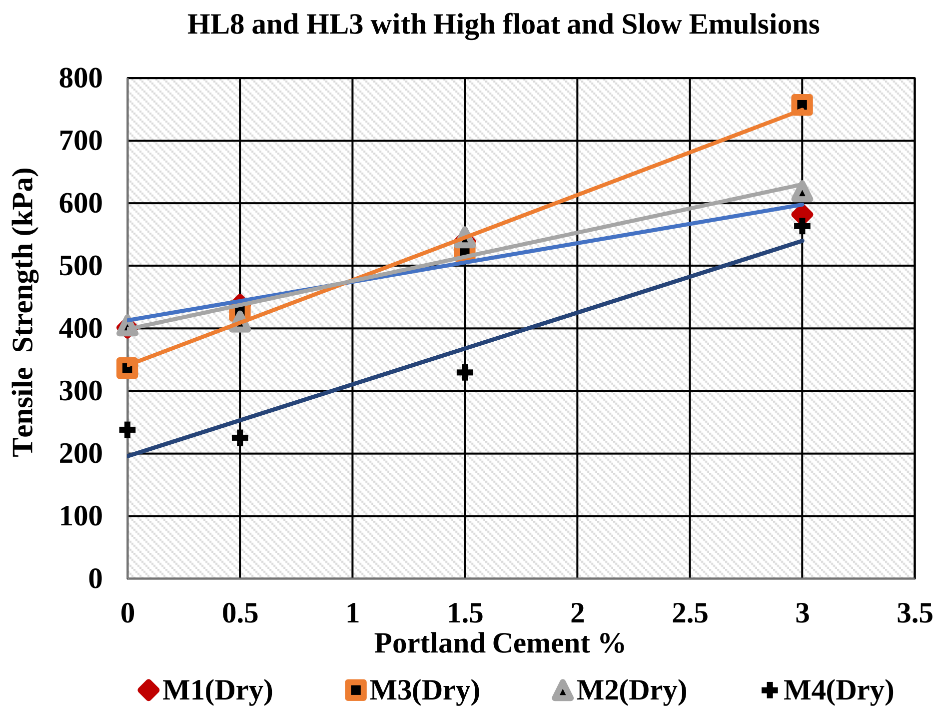

Figure 4.9 M1 ,M2 ,M3 and M4 Dry Vs Tensile Strength

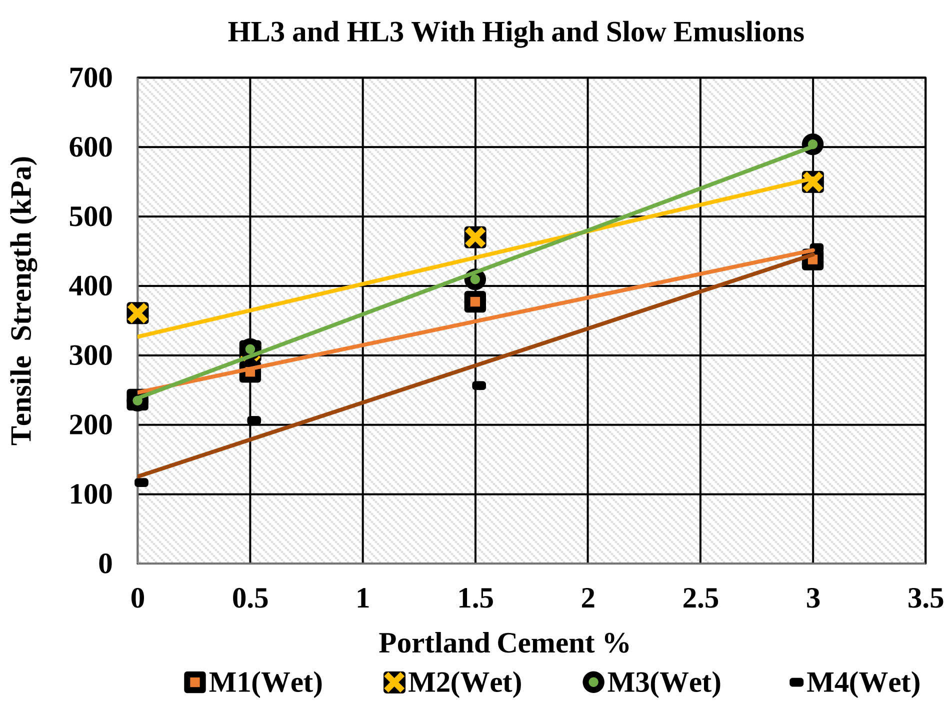

Figure 4.10 M1 ,M2 ,M3 and M4 Wet Tensile Strength Vs Portland Cement Percentage

Figure 4.11 Mode of Failure of Indirect Tensile Specimen

4.2 Dynamic Modulus

Figure (4.12) shows a Master Curve for the Dynamic modulus test results for M1mix. As can be seen, the results show that the dynamic modulus of the mixtures increases with increasing cement content and decreases with increasing temperature.

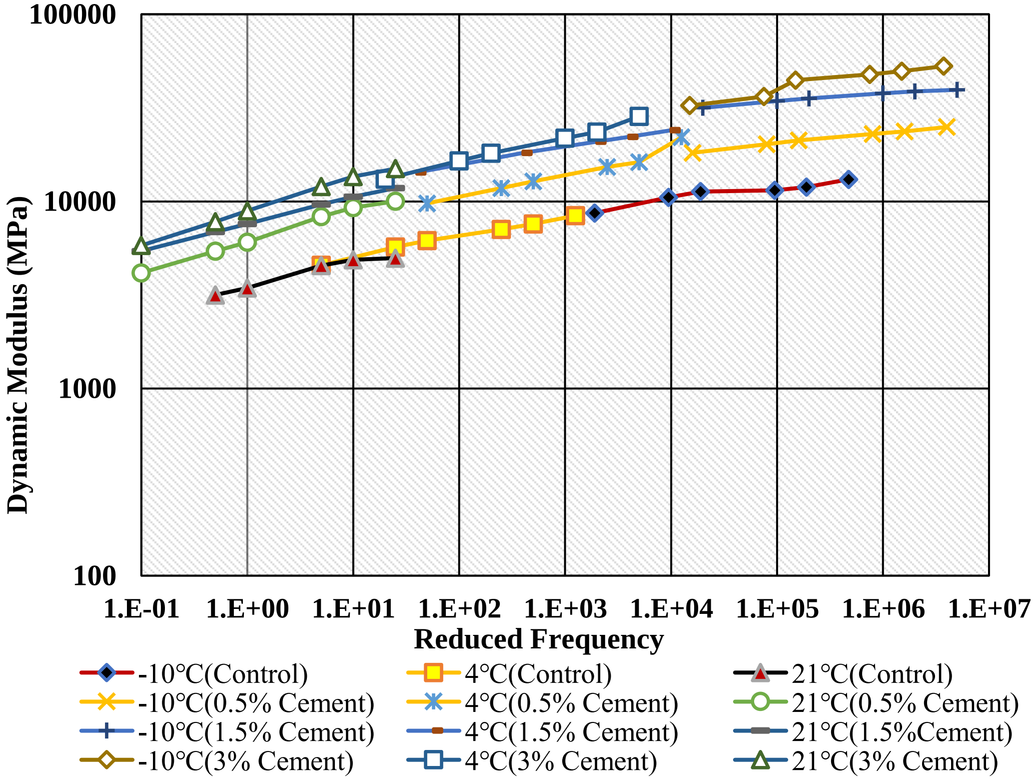

Figure 4.12 Master Curve of CIR Specimens with different Portland Cement for M1

Adding more cement to the mixture leads to a cementation effect which increases the bond between the aggregate particles resulting in increased stiffness of the mixtures. Also, as the temperature decreases, the emulsion stiffness increases, which results in an increase in the stiffness of the mixtures. Furthermore, it can be noted that as the temperature decreases, the rate of variation of the stiffness with cement content increases. This indicates that the effect of Portland Cement on the stiffness is more dominant at low temperatures. However, as the temperature increases, the emulsion becomes softer, and the stiffness of the mixture is reduced by this softening of the emulsion mortar. Therefore, the addition of Portland Cement is less effective in increasing the stiffness.

As it is difficult to visualize the differences between the samples in the log-log master curve, Figure (4.13) was used to better represent the influence of the cement on the stiffness. Each ratio value represents the stiffness of the mix with 3% cement (called E3%) divided by the stiffness of the control mix (called EControl). Figure (4.13) clearly shows that the complex modulus value for the mixes with 3% cement is approximately 4 times higher than that of control mixes at low temperatures. However, as the temperature goes higher, the stiffness values for the mixes with 3% cement decrease to about 3 times higher and 2.5 times higher for 4℃ and 21℃, respectively than that of the control mix.

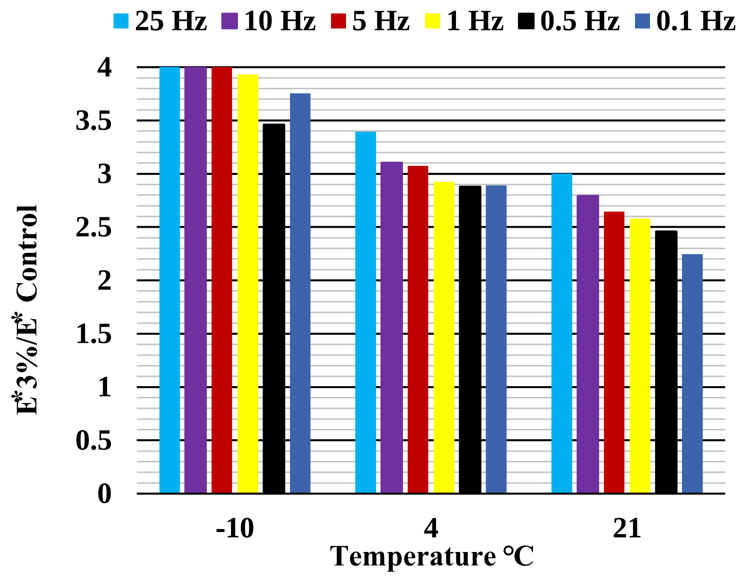

*Figure 4.13 Modulus Ratio Value (E*3 %/ E*control) of the Tested M1*

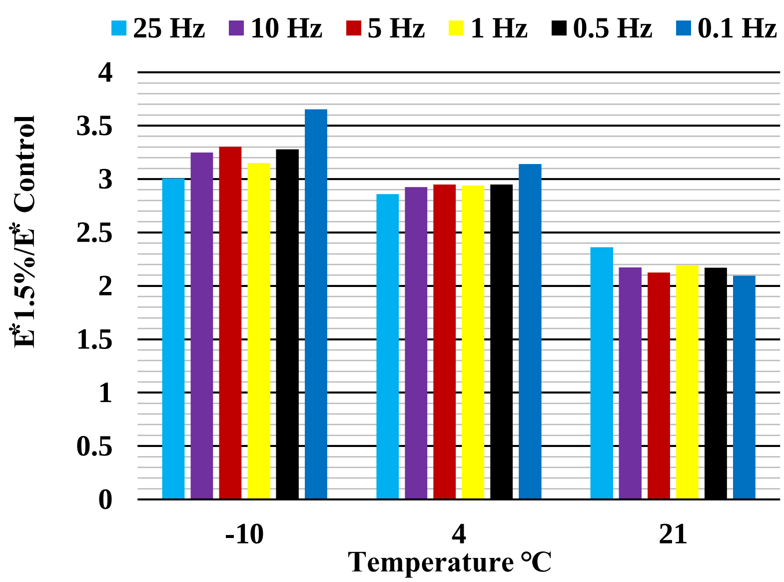

*Figure 4.14 Modulus Ratio Value (E*1.5%/ E*control) of the Tested M1*

Moreover, similarly, Figure (4.14) shows the effect of the ratio (E*1.5 cement /E*control) of adding 1.5% cement to the mixture. Each ratio value represents the stiffness of the mix with 1.5% cement (called E*1.5%) divided by the stiffness of the control mix (called E*control). It is shown that adding 1.5% cement led to an increase in the stiffness at low temperatures of -10℃ and 4℃ to approximately 3 times that of the control mixes. However, at a temperature of 21℃, the stiffness increased by only about 2 times that of the control mix. This is because at a higher temperature, the mixture becomes softer, and the effect of the emulsion mortar is greater than that at a low temperature; as a result, the addition of Portland Cement is less effective in increasing the stiffness.

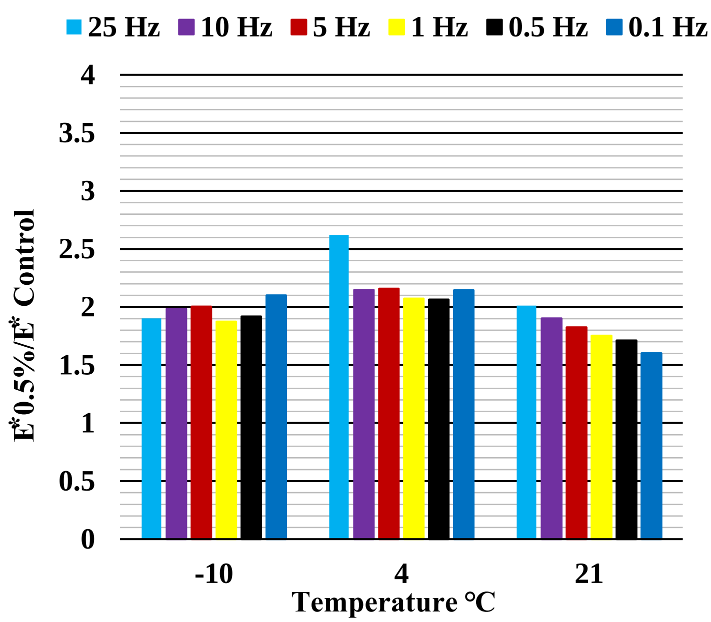

Figure 4.15 Modulus Ratio Value (E*0.5 %/ E*control) of the Tested M1

Furthermore, Figure (4.15) shows the ratio of stiffness of E*0.5% cement to that of E*control at temperatures of -10℃, 4℃ and 21℃. This ratio is about 2 at temperatures of -10℃, 4℃ but decreases to an average of about 1.75 at 21℃. Finally, there was not a noticeable increase in the stiffness when 3% Portland Cement was added compared to the value when 1.5% Portland Cement was added at high and low temperatures, as shown in Figure (4.16). This unexpected result may be due to material variation in the recycled material.In addition, Figure (4.17) shows a Master Curve for the Dynamic modulus test results for the M2 mix. It is evident that there is an increase in the stiffness when adding 0.5% Portland Cement; however, there are no noticeable further increases in the stiffness when adding 1.5% and 3% Portland Cement compared to 0.5% Portland Cement.

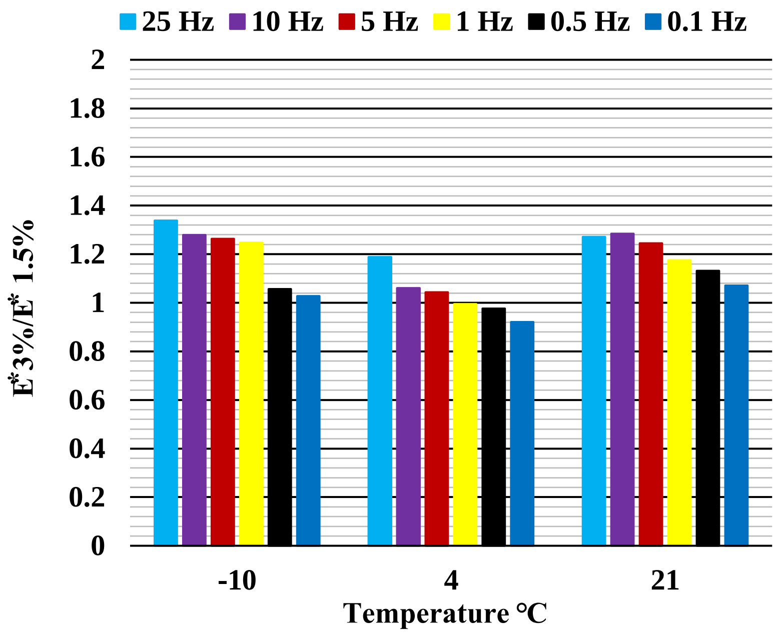

*Figure 4.16 Modulus Ratio Value (E*3%/ 1.5%E*) of the Tested M1*

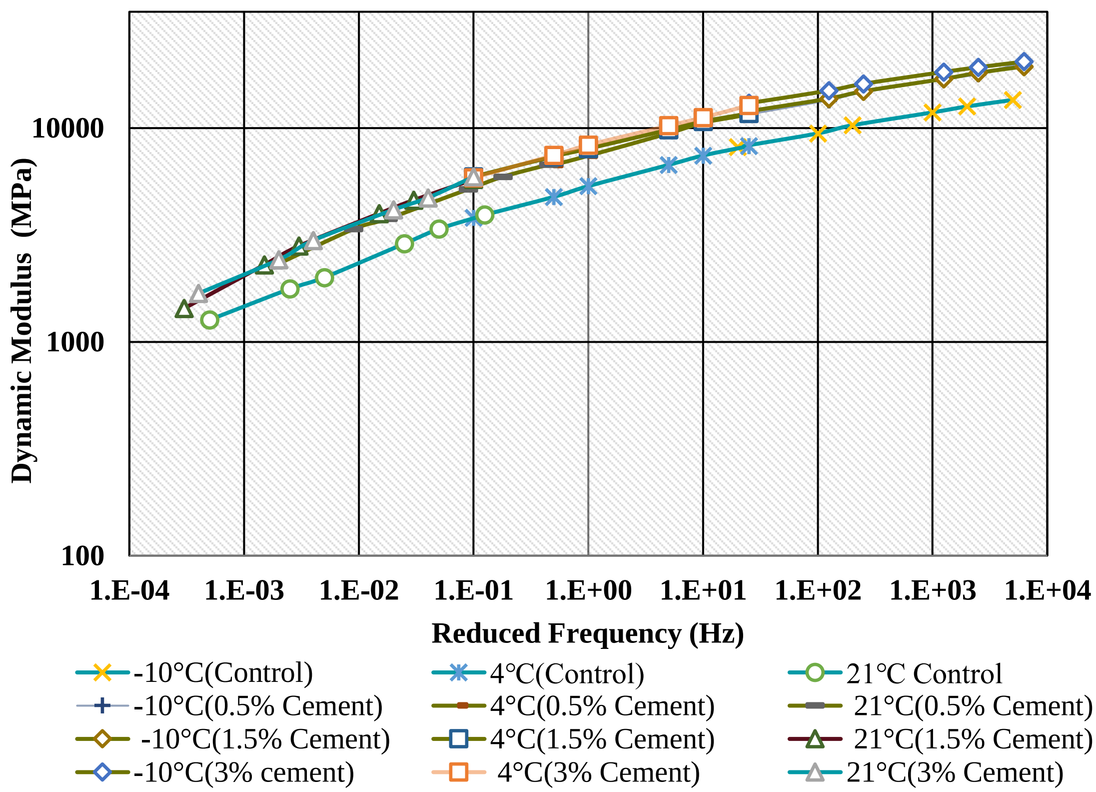

Figure 4.17 Master Curve of CIR Specimens with different Portland Cement Percentage for M2

For a better and more comprehensive understanding of the master curve for the M2 mix, Figure (4.18) was used to represent the ratio of the stiffness of the mix with 3% cement (called E*3%) divided by the stiffness of the control mix (called E*Control). Figure (4.18) shows that the complex modulus value for the M2 mix with 0.5%,1.5% and 3% cement is approximately 1.5 times higher than that of the control mix at all the temperatures examined. This indicates that there is no noticeable increase in stiffness due to adding more than 0.5% Portland Cement as shown in Figures (4.19& 4.20).

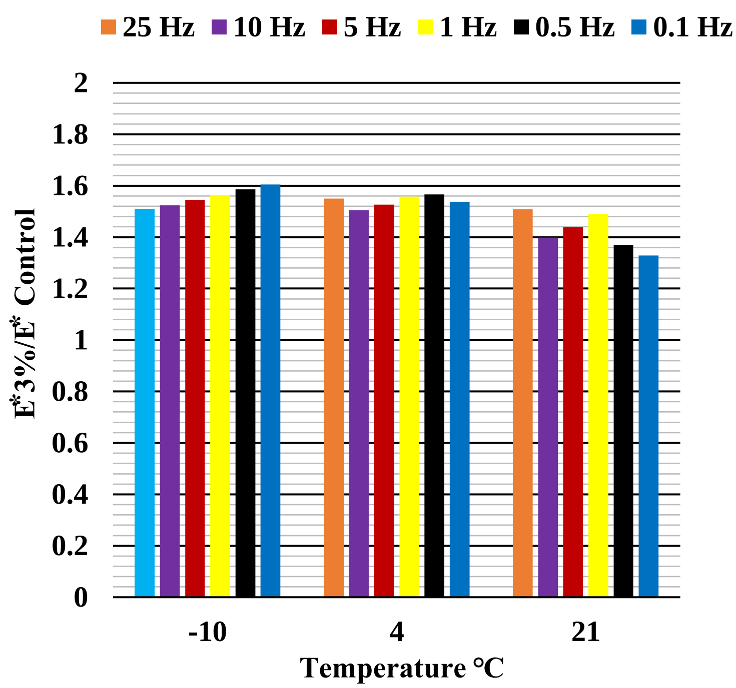

Figure 4.18 Modulus Ratio Value ($E^*3\%/E^*$Control) of the Tested M2

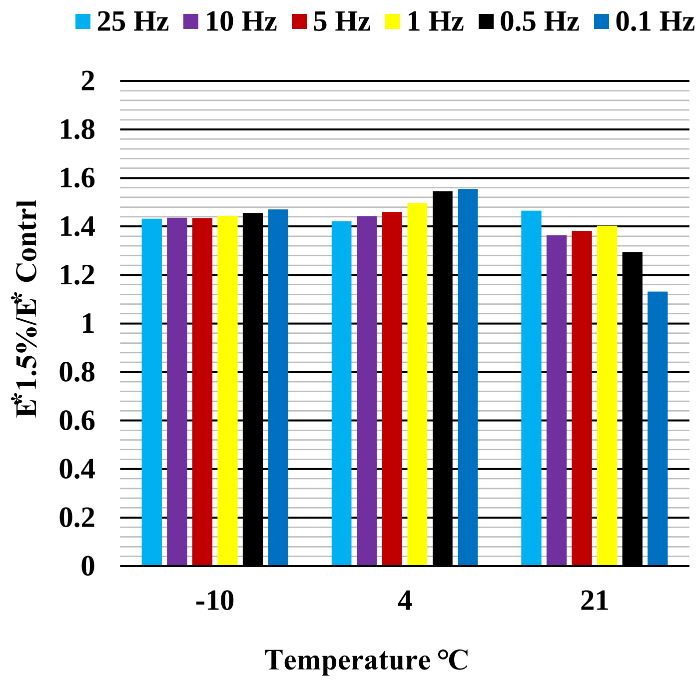

*Figure 4.19 Modulus Ratio Value (E*1.5%/E*Control) of the Tested M2*

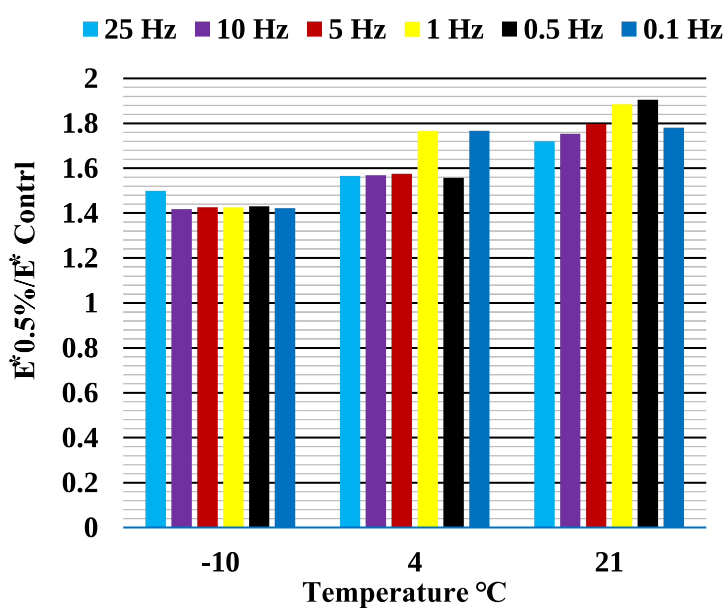

*Figure 4.20 Modulus Ratio Value (E*0.5%/E*Control) of the Tested M2*

The master Curve for the M3 mix was developed as shown in Figure (4.21). In order to explain the effect of Portland Cement, Figure (4.22) was produced. The Figure shows the ratio of the stiffness of the M3 mix that contains 3% Portland Cement (E*3%) divided by the stiffness of the control mix (E*Control). It is shown that the complex modulus value for these mixes at all the temperatures (-10℃, 4℃ and 21℃) is approximately 2 times higher than that of the control mix.

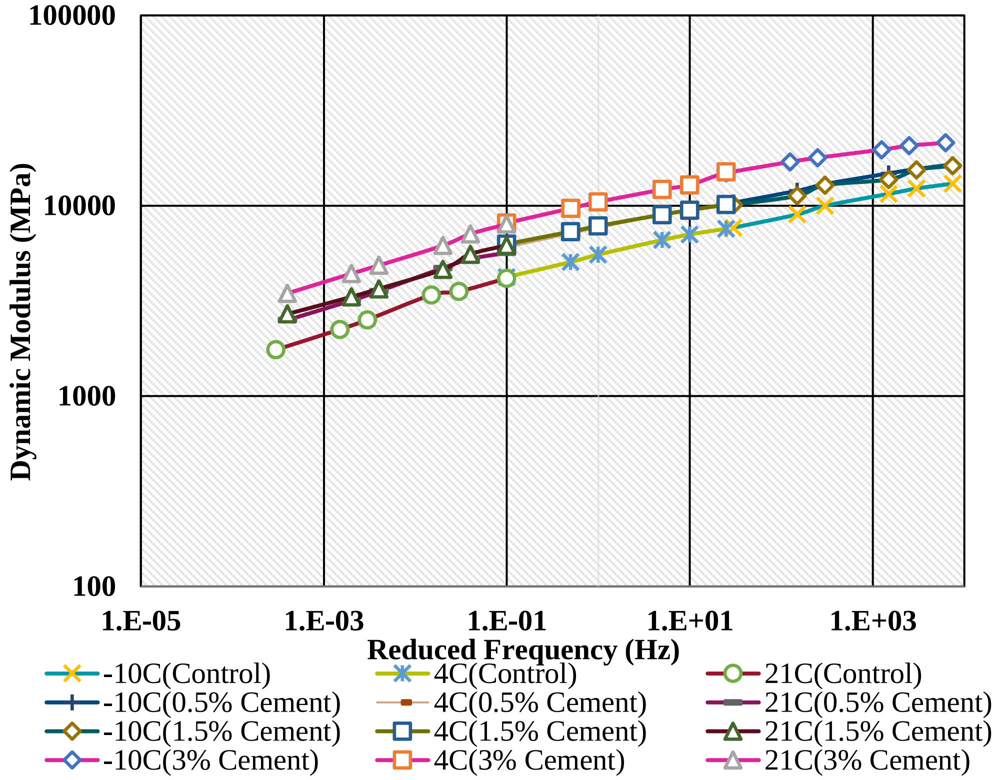

Figure 4.21 Master Curve of CIR Specimens with different Portland Cement Percentage for M3

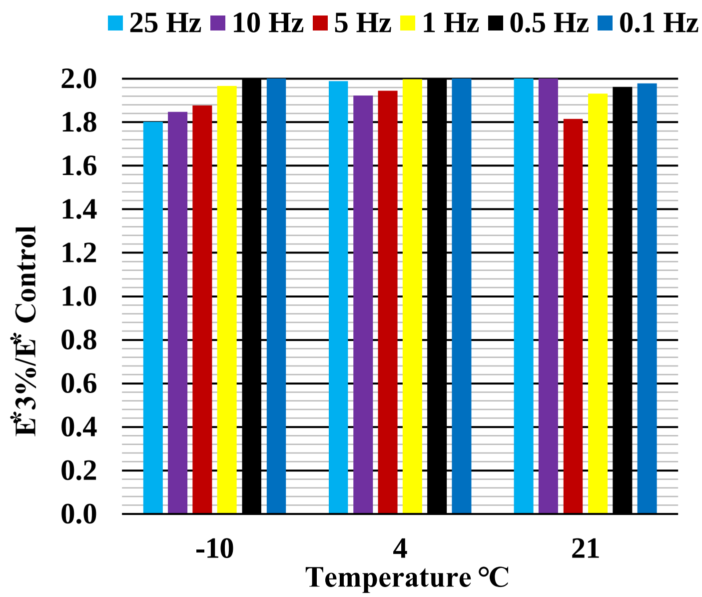

Figure 4.22 Modulus Ratio Value (E^{*}3 %/ E^{*}control) of the Tested M3

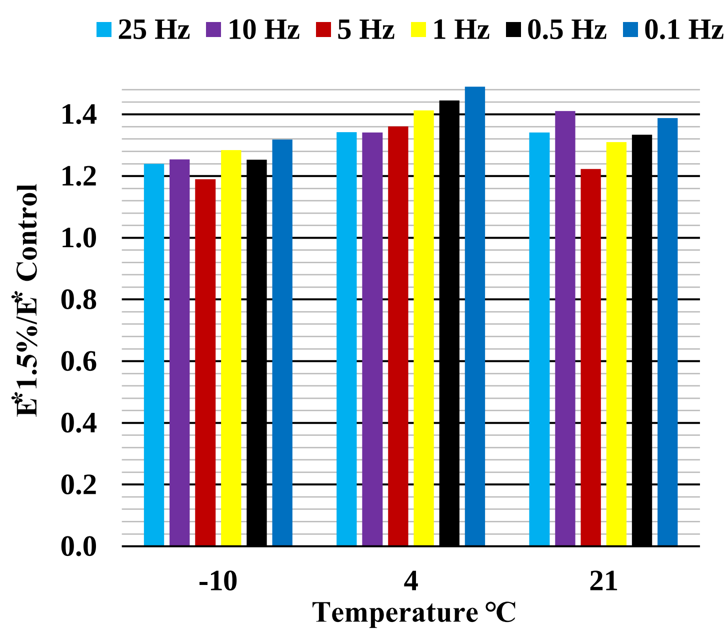

Figure 4.23 Modulus Ratio Value (E^{*}1.5%/ E^{*}control) of the Tested M3

Figure (4.23) shows the effect of the addition of 1.5% Portland Cement on the stiffness of the M3 mix at temperatures of (-10℃, 4℃ and 21℃). The stiffness compared to the control at -10℃ is about 1.25 increasing to 1.35 at 4℃ and 21℃.

The ratio of E*0.5% cement to E*control is presented in Figure (4.24). It shows that the stiffness was 1.3, 1.36 and 1.4 times higher than that of the control mix at -10℃, 4℃ and 21℃,respectively. The effects of variations in temperature and percentages of Portalnd Cement are small.

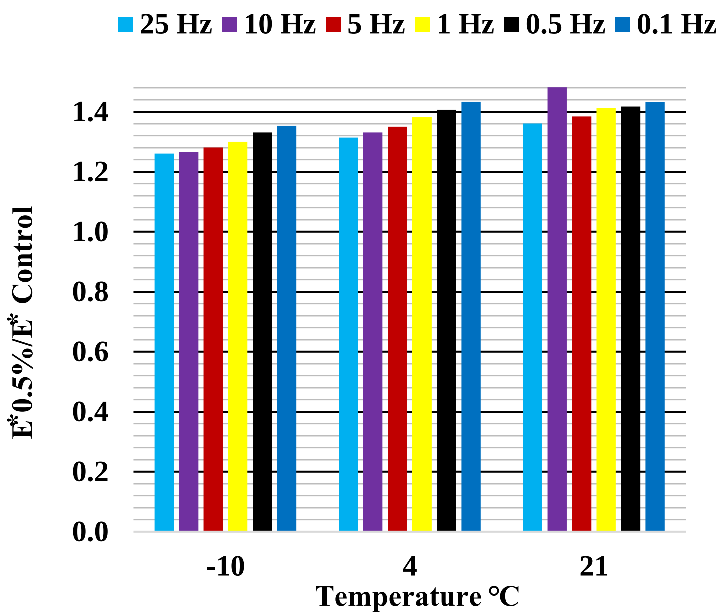

Figure 4.24 Modulus Ratio Value (E*0.5 %/ E *control) of the Tested M3

A master Curve was constructed for the M4 mix, as shown in Figure (4.25). As the amount of Portland Cement increases, the stiffness increases. Figure (4.26) was constructed to better explain the effect of Portland Cement on the mixture behaviour. Figure (4.26) shows the ratio of the stiffness of the mix with a 3% cement (called E*3%) divided by the stiffness of the control mix (called E*Control). Figure (4.26) shows that the stiffness increase due to the addintion of 3% of Portland Cement was to approximately 1.5 times that of the control mix at all the temperatures examined.

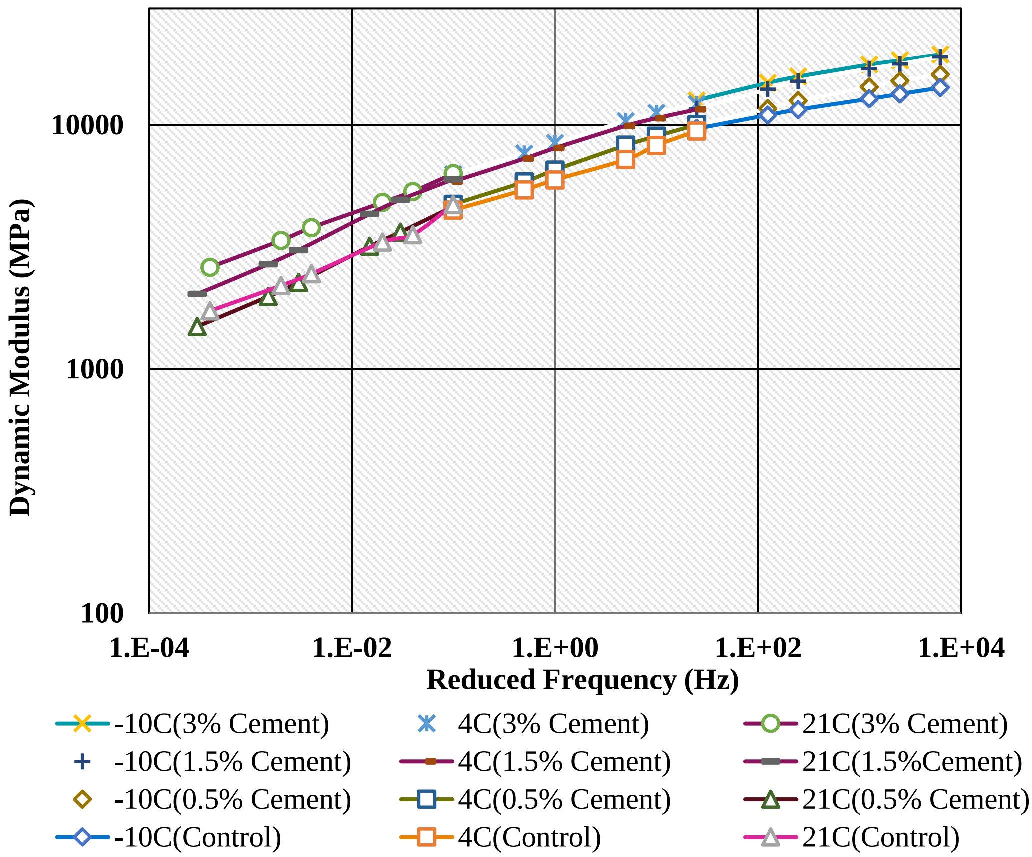

Figure 4.25 Master Curve of CIR Specimens with different Portland Cement Percentage for M4

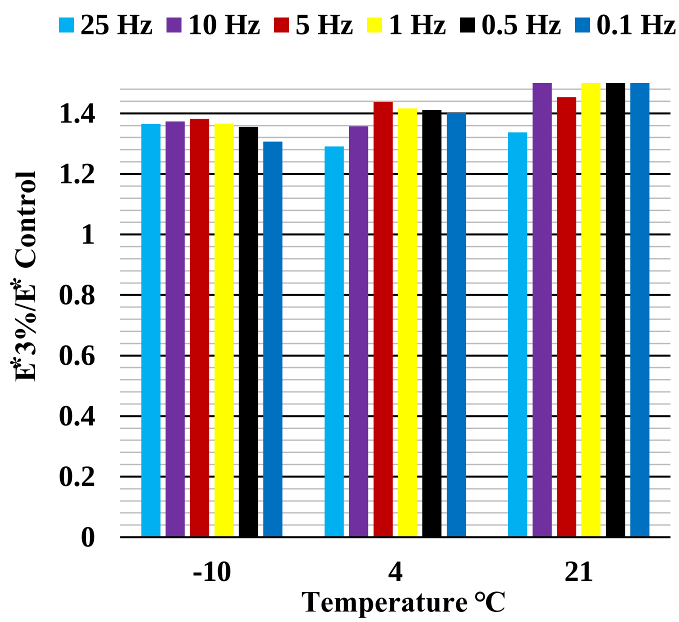

*Figure 4.26 Modulus Ratio Value (E*3%/E*Control) of the Tested M4*

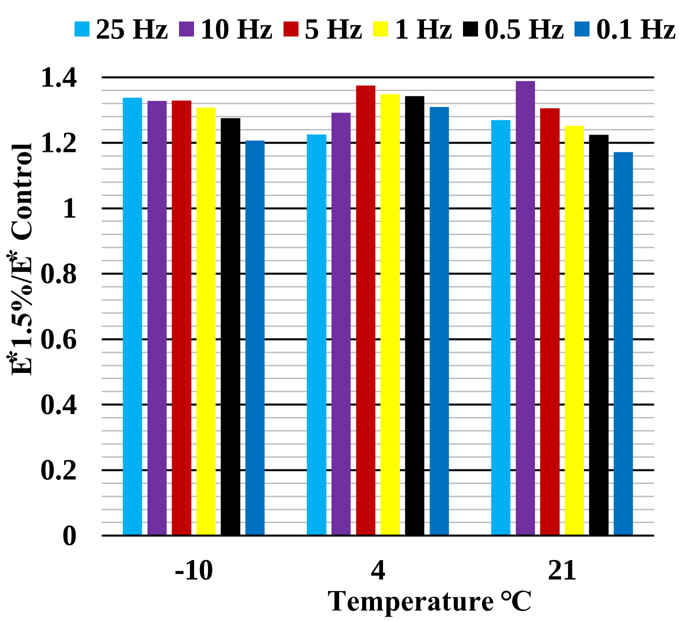

*Figure 4.27 Modulus Ratio Value (E*1.5%/E*Control) of the Tested M4*

In addition, the stiffness was increased to approximately 1.2 times that of the control mix at all temperatures examined when 1.5% of Portland Cement was added, as shown in Figure (4.27). When 0.5% Portland Cement was added, there was little change in stiffness at temperatures of -10℃ and 4℃ from that of the control mix. However, at a temperature of 21℃, the stiffness decreased by a small amount, as shown in Figure (4.28).

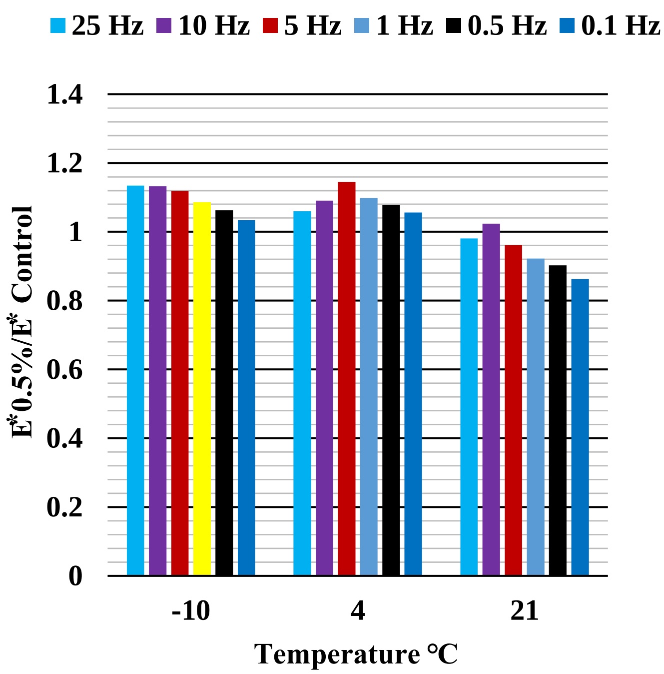

*Figure 4.28 Modulus Ratio Value (E*0.5%/E*Control) of the Tested M4*

4.3 Fatigue Test Results

An example of one set of data is shown in figures (4.29 & 4.30) of the normalized stiffness (E*/E0*) versus the number of cycles for various cement contents. The failure criterion is that failure occurs when the stiffness of a specimen reaches 50% of its initial stiffness. Since the deflection during the test does not stay constant, the obtained results must be corrected based on the actual maximum deflection by considering sample geometry.

The geometry was taken into consideration by using Equations (3.6 & 3.7) in chapter (3) to calculate the normalized stiffness (E*/E0*). The results illustrate a clear influence on the fatigue lifespan by increasing the percentage of Portland Cement. For both mixes (M1 and M2), it is shown that as the percentage of the Portland Cement increases, the fatigue life decreases. Table (4.2) summarizes the fatigue lives of all the tested beams of M1 and M2 mixes. For M1 and M2 mixes, the fatigue test results for the four sets of beams (0%, 0.5%, 1.5% and 3% Portland Cement) are plotted on logarithmic axes of strain range versus cycles to failure in Figures (4.31and 4.32). The strain ranges varied from 200 μm/m to 600 μm/m in 50 μm/m increments, and the failure criterion used was that failure occurred when the beam stiffness reached 50% of the original value of its stiffness. Two specimens are tested at each strain level for each set of beams.

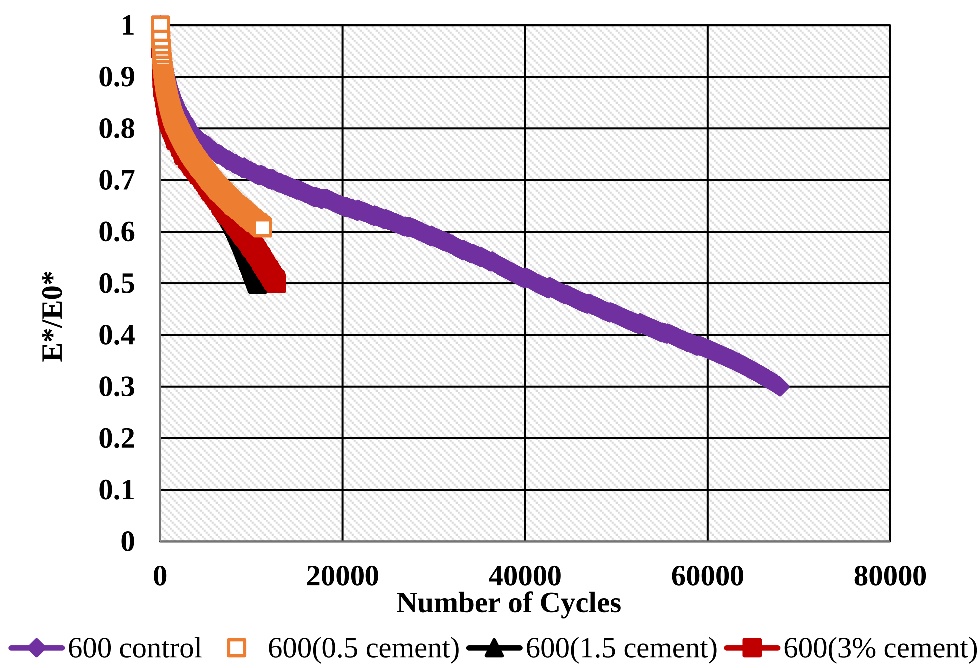

Figure 4.29 E*/E0* versus Nf50% at 600 μm/m For M1

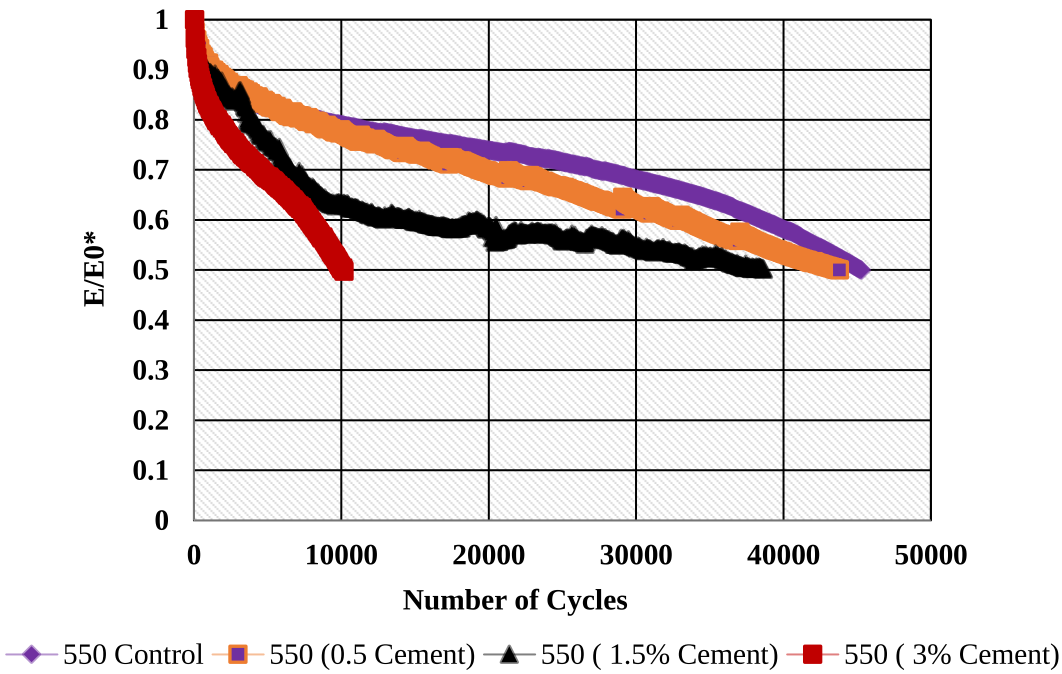

Figure 4.30 E/E0* versus Nf50% at 550 µm/m For M2*

Table 4.2 Fatigue test results for all beams (M1 & M2)

Portland Cement%	**Control Mix 0% Portland Cement**		**0.5% Portland Cement**		**1.5% Portland Cement**		**3% Portland Cement**	
Strain Level	M1 (Average) Number of cycles)	M2 (Average) Number of cycles)	M1 (Average Number of cycles)	M2 (Average) Number of cycles)	M1 (Average) Number of cycles)	M2 (Average) Number of cycles)	M1 (Average) Number of cycles)	M2 (Average) Number of cycles)
200		1,000,000						
250	-	238,997.5	-	221,047	-	591,193	60,000	1,000,000
300	1,000,000		-	-	120,000	113,000	-	-
350	-	110,898	684,689	91,549	56,248.5	62,349	22,899	53,749
400	450,000	-	200,000	-	-	-	-	-
450	161,747	80,000	94,698	67,000	20,299.5	-	5,949.5	30,000
500	-	-	-	-	-	-	-	-
550	70,000	45,299	-	43,849	-	38,699	-	10,200
600	41,349	-	17,849	-	10,699.5	-	4,300	-

For M1 mix, at 600 µm/m (a high strain range) the number of cycles to failure for (0%, 0.5%, 1.5% and 3%) Portland Cement additions were 41349, 17849, 10699 and 4300 cycles, respectively. It is clearly shown that as the percentage of Portland Cement increased above 0.5%, the fatigue life decreased. It is noticeable that the fatigue data for the beams containing 0% and 0.5% Portland Cement fall into a compact band in the life region between 41349 and 1000000 cycles, as shown in Figure (4.31). This band is parallel to, with greater fatigue lives, the band for the samples that contained 1.5% and 3% Portland Cement. The discrepancy can be attributed to different factors. As the Portland Cement increases, the material tends to be more brittle, which will decrease fatigue life at high strains. This can be attributed to the cementation effect that increases the bond between the mixture and the skeleton resulting in a decreased ductility that reduces the fatigue strength at high strain ranges. It is worth mentioning that at low strain levels, the fatigue life also decreased. This may be because the four-point bending test is not a homogenous test, and another factor is that the material used is 100% recycled material, which has a wide range of variation in its composition. Furthermore, since the test was conducted at 5℃, the emulsion is relatively stiff, which results in an increase in the stiffness of the mixture leading to a reduction in the fatigue life. It is shown in Figure (4.31) that adding Portland Cement to the mixture does not improve the fatigue life at either high or low strain ranges. It is noticeable, however, that adding 0.5% Portland Cement to the mixture leads to a small reduction in the fatigue life. It is worthy of mention that adding 1.5% and 3% of Portland Cement results in a significant reduction in fatigue life at high strain ranges. It is possible that the testing temperature of 5℃ played a role in favoring the fatigue life for the 0.5% Portland Cement addition over the 1.5% and 3% Portland Cement additions. This is because when adding 0.5% of Portland Cement, the cementitious material is less than when adding 1.5% and 3% Portland Cement and thus, the mixture tends to be less stiff. Furthermore, as the temperature decreases, the ductility of the mixture decreases, and the stiffness of the mixture increases, resulting in a decreased fatigue life of the mixture.

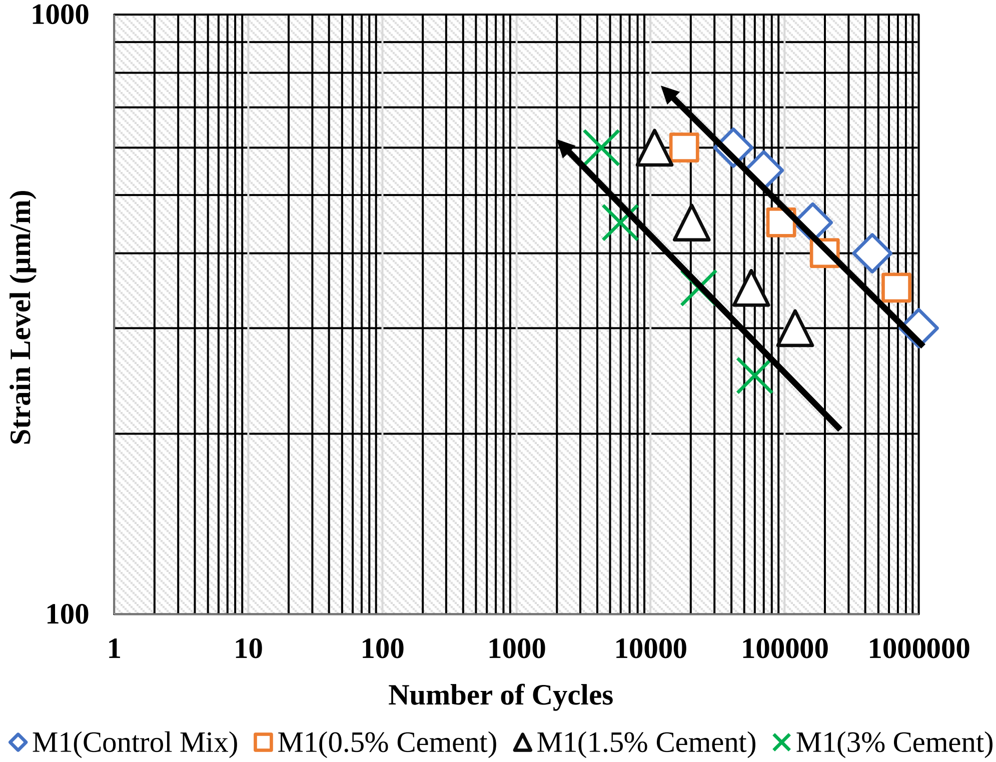

Figure 4.31 Fatigue Life for M1

For M2 mix, the fatigue life also did not improve with the addition of Portland Cement. In fact, there was a significant decrease in the fatigue life for a 3% Portland Cement addition. For M2 mix, the number of cycles to failure at a high strain level (550 µm/m) was 45299, 43849, 38699 and 10200 cycles for 0%, 0.5%, 1.5% and 3%, Portland Cement additions, respectively. This is because as the amount of Portland Cement increased, the material tended to be more brittle and also, the effect of test temperature (5°C) made the role of cementitious material more effective than it was at a higher temperature. Figure (4.32) shows that fatigue data for the beams containing 0% and 0.5%, 1.5% Portland Cement fall into a compact band in the life region between 70,000 and 1000,000 cycles. The fatigue lives at high strain levels are more than four times as long. However, at a low strain level, the fatigue lives are almost the same for all the groups (0%, 0.5%, 1.5% and 3%).

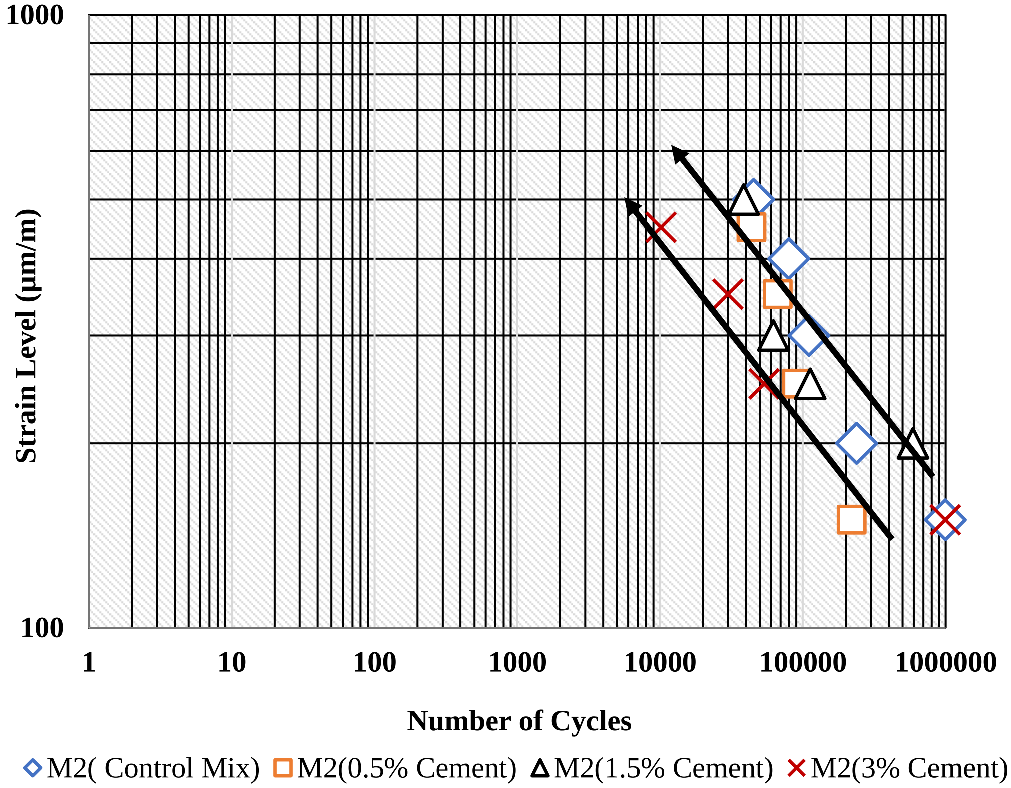

Figure 4.32 Fatigue Life for M2

The phase angle (δ) versus the number of cycles Nf50% is plotted in Figures (4.33 & 4.34) for M1 and M2 mixes, respectively (only one set of data is displayed). When the stiffness increases, the phase angle generally decreases as the material behaviour becomes more elastic. As mentioned earlier, as the percentage of Portland Cement is increased, the material tends to more elastic, and has an increased stiffness. It is visible that the control mix has a higher phase angle. However, the mixes that contain 0.5%, 1.5%, and 3%, respectively, have a lower phase angle because they tended to be more elastic due to the cementitious material.

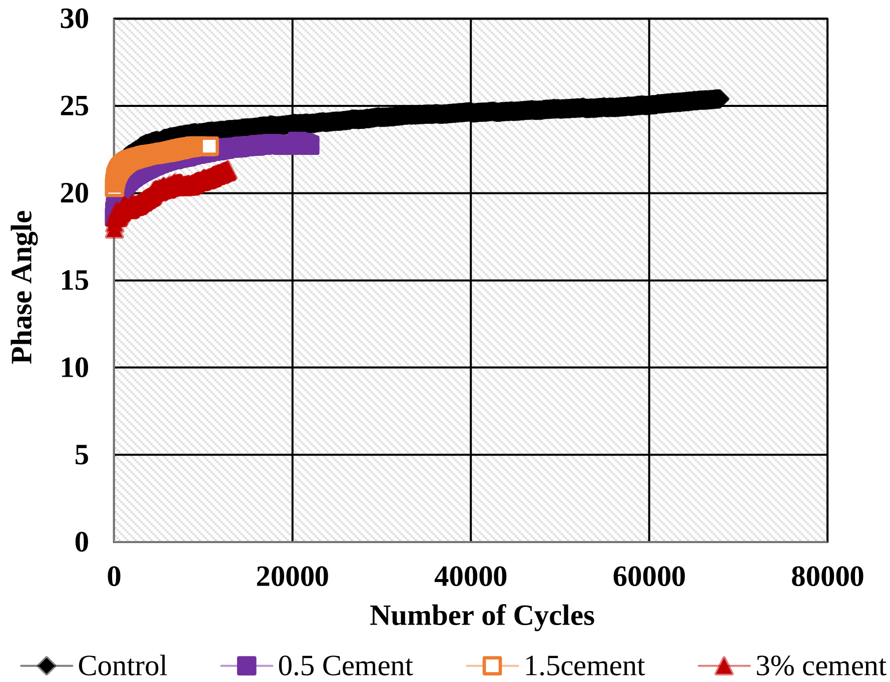

*Figure 4.33 Phase Angle **δ** (°) Versus Nf50% at 600 µm/m For M1*

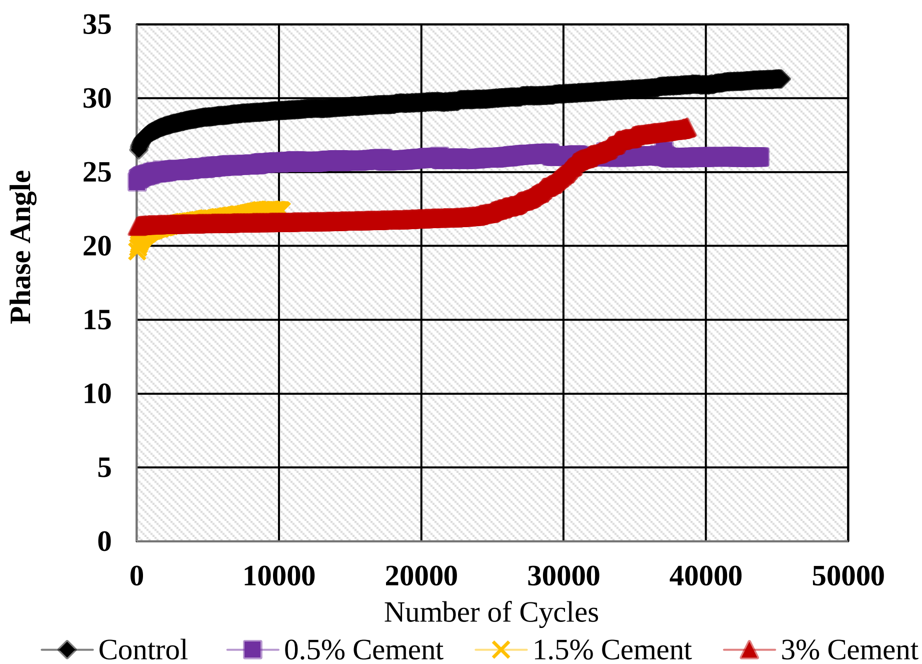

*Figure 4.34 Phase Angle **δ** (°) Versus Nf50% at 550 µm/m For M2*

The fatigue lives of the tested beams of M3 and M4 mixtures are presented in Table (4.3). For both mixes, the strain ranges used in the tests varied from 200 μm/m to 550 μm/m in 50 μm/m. increments. Figures (4.35 & 4.36) show the results for the M3 and M4 mixtures beam tests plotted on logarithmic axes of the number of cycles to failure versus the strain levels. It is shown in the Figures that as the amount of Portland Cement increases, the fatigue life decreases in a roughly linear manner on the logarithmic scales used in the graphs. For the M3 mix, the number of cycles to failure at a strain range of 550 μm/m was 12250, 11100, 4950 and 1300 cycles for additions of Portland Cement of 0%, 0.5%, 1.5% and 3%, respectively. Adding amounts of Portland Cement of 0.5% and 1.5% does not have a negative impact on the fatigue life, as shown in Figure (4.35). Also, similar to M1and M2 mixes, the fatigue lives for these Portland Cement additions fall into a compact band around a single curve between 1228187 and 1300 cycles. However, adding 3%, Portland Cement decreased the fatigue life by a factor of five. The fatigue life curve for this percentage addition is parallel to, but at fatigue lives less by a factor of five than the curve for specimens containing 0%, 0.5% and 1.5% Portland Cement. The fatigue life for the M4 mix was not changed by adding Portland Cement in the amounts of 0.5%, 1.5%, and 3 %, as shown in Figure (4.36), and all the results fall into a single band.

Table 4.3 Fatigue test Results for all Beams (M3 & M4)

Portland Cement%	**Control Mix 0% Portland Cement**		**0.5% Portland Cement**		**1.5% Portland Cement**		**3% Portland Cement**	
Strain Level (μm/m)	M3 (Average) Number of cycles	M4 (Average) Number of cycles	M3 (Average) Number of cycles	M4 (Average) Number of cycles	M3 (Average) Number of cycles	M4 (Average) Number of cycles	M3 (Average) Number of cycles	M4 (Average) Number of cycles
200	-	336,145	-	574,691	-	-	-	1,000,000
250	1,228,187	-	812,690	-	397,995	-	105,149	-
300	133,398	20,600	96,499	1,100	38,599	189,297	3,650	102,000
350	68,049	41,549	22,600	5,200	17,150	4,650	15,400	80,000
400	-	850	-	112,148	-	223,647	-	60,000
450	23,599	-	14,100	-	12,350	-	7,500	10,000
500	-	-	-	44,249	-	2,250	-	5,300
550	12,250	-	11,100	-	4,950	-	1,300	13,300

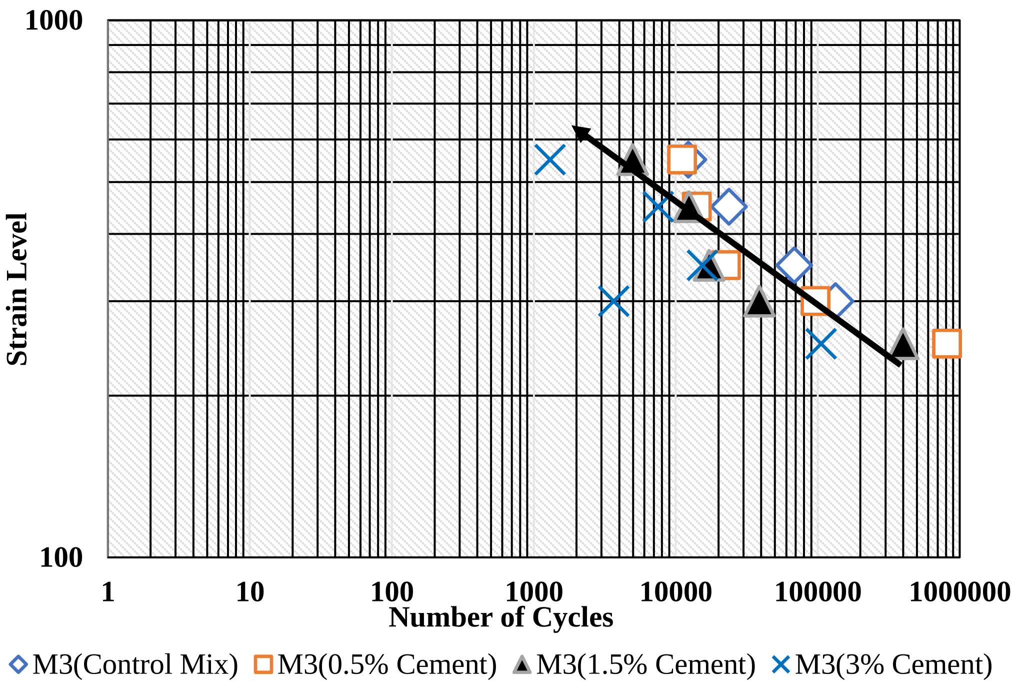

Figure 4.35 Fatigue life for M3

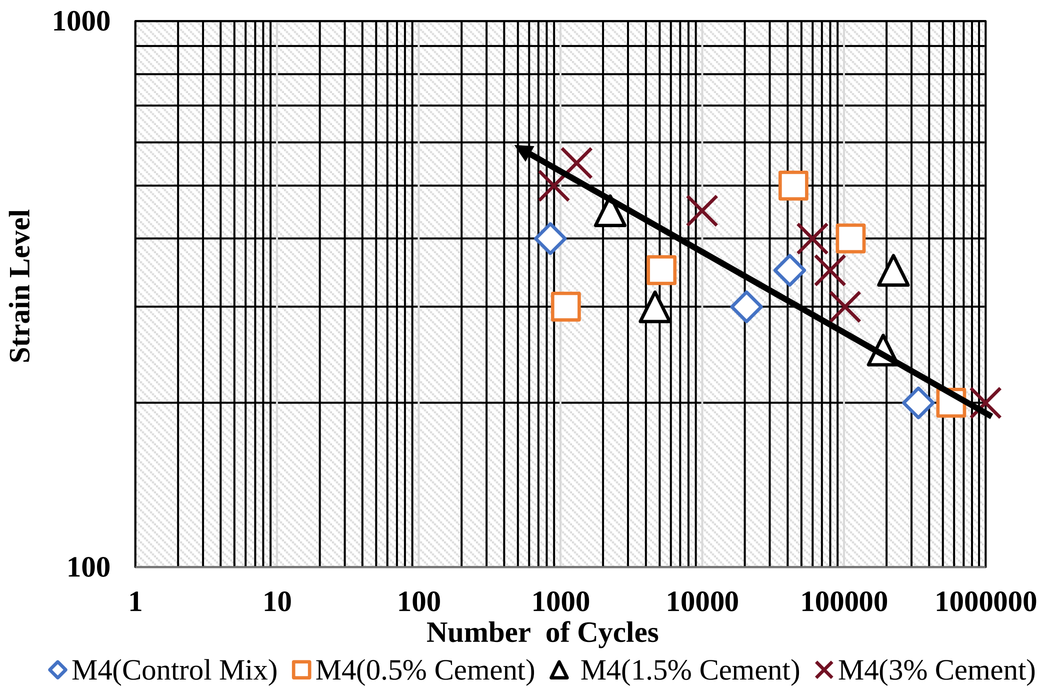

Figure 4.36 Fatigue life for M4

4.4 Thermal Test Results

Table (4.4) reports the test results for all mixtures in terms of the maximum stress at which the specimens failed (fracture stress) together with the corresponding fracture temperature. The table provides the average and standard deviation for all the tested samples. The first mix (M1) used a Cationic Slow Setting Emulsion (CSS-1H) mixed with a pulverized HL8 RAP; for the second mix (M2), an Anionic High Float Emulsion (HF-150) was mixed with the pulverized HL8 RAP. However, for the third mix (M3), a Cationic Slow Setting Emulsion (CSS-1H) was mixed with a pulverized HL3 RAP, and for the fourth mix (M4), the Anionic High Float Emulsion (HF-150) was mixed with the HL3 RAP. Figure (4.37, a, b, c, and d) shows stress versus temperature curves for each of the mixes with additions of 0%, 0.5%,1.5% and 3% Portland Cement, respectively. For all the mixtures and Portland Cement additions, stress versus temperature curves shows the same trends as those reported by (Marasteanu et al., 2007), which are shown in Figure 3.21 of Chapter 3. As the temperature decreases, the tensile stress increases at a continually increasing rate until it reaches the transition temperature or fails. If failure does not occur before the transition temperature, the rate of change of stress with temperature becomes constant, and the stress versus temperature curve becomes linear until the failure of the specimen. For the mixes without a Portland Cement addition, M2 and M3 mixes exhibit similar fracture temperatures, while M1 and M4 mixes have higher fracture temperatures than M2 and M3 mixes.

After 0.5% Portland Cement addition, all four mixes' temperature versus stress fall close to each other, with M1, M2 and M3 mixes failing at about the same fracture temperatures and fracture stresses. These fracture temperatures were lower, and the fracture stresses were higher than the values for a zero Portland Cement addition. The M4 mixture failed at a higher temperature and lower fracture stress than the other mixes. Further increasing the Portland Cement additions to the mixes to 1.5% and 3% moves the temperature versus stress curves to lower fracture stresses. The fracture stresses of all mixes are increased with an addition of o.5% Portland cement. However, they are progressively reduced with increasing Portland cement beyond 0.5%. This may be due to the fact, that as the Portland cement content increases, the tensile stresses and shrinkage cracks increase leading to specimens’ failure at higher temperatures and lower stresses. It was observed that the M1 mix exhibits a small increase in fracture temperature for both the 1.5% and 3% Portland Cement additions. M1 mix showed significant increases in fracture temperature with successive Portland Cement increases.

Table 4.4 Fracture Temperature and Fracture Stress for all the Tested Mixes

Mixture	M1							
Cement%	0		0.5		1.5		3	
TSRST Test	Fracture Temperature (°C)	Fracture Stress (MPa)	Fracture Temperature (°C)	Fracture Stress (MPa)	Fracture Temperature (°C)	Fracture Stress (MPa)	Fracture Temperature (°C)	Fracture Stress (MPa)
specimen 1	-24.0	0.67	-26.5	0.85	-26.5	0.33	-18.0	0.30
specimen 2	-21.0	0.45	-27.5	0.75	-22.5	0.67	-23.0	0.21
specimen 3	-15.7	0.38	-30.0	0.66	-20.0	0.50	-25.5	0.13
Ave	-20.2	0.5	-28.0	0.8	-23.0	0.50	-22.2	0.21
Std	4.2	0.15	1.8	0.10	3.3	0.2	3.8	0.1
Mixture	M2							
Cement%	0		0.5		1.5		3	
TSRST Test	Fracture Temperature (°C)	Fracture Stress (MPa)	Fracture Temperature (°C)	Fracture Stress (MPa)	Fracture Temperature (°C)	Fracture Stress (MPa)	Fracture Temperature (°C)	Fracture Stress (MPa)
specimen 1	-27.0	0.45	-27.0	0.79	-27.0	0.49	-29.0	0.23
specimen 2	-25.0	0.29	-23.5	0.61	-23.0	0.34	-25.5	0.09
specimen 3	-20.0	0.25	-28.0	0.57	-28.5	0.390	-26.5	0.12
Ave	-24.0	0.33	-26.2	0.66	-26.2	0.41	-27.0	0.15
Std	3.61	0.11	2.4	0.12	2.8	0.08	1.80	0.07
Mixture	M3							
Cement%	0		0.5		1.5		3	
TSRST Test	Fracture Temperature (°C)	Fracture Stress (MPa)	Fracture Temperature (°C)	Fracture Stress (MPa)	Fracture Temperature (°C)	Fracture Stress (MPa)	Fracture Temperature (°C)	Fracture Stress (MPa)
specimen 1	-28.5	0.35	-29.5	0.92	-30.0	0.63	-25.0	0.44
specimen 2	-22.0	0.18	-28.5	0.80	-26.5	0.38	-28.5	0.29
specimen 3	-24.5	0.20	-23.0	0.54	-27.5	0.35	-28.0	0.30
Ave	-25.0	0.24	-27.0	0.75	-28.0	0.45	-27.2	0.34
Std	3.28	0.09	3.50	0.19	1.80	0.15	1.89	0.08
Mixture	M4							
Cement%	0		0.5		1.5		3	
TSRST Test	Fracture Temperature (°C)	Fracture Stress (MPa)	Fracture Temperature (°C)	Fracture Stress (MPa)	Fracture Temperature (°C)	Fracture Stress (MPa)	Fracture Temperature (°C)	Fracture Stress (MPa)
specimen 1	-23.5	0.15	23.5	0.63	-12.5	0.18	-10.5	0.08
specimen 2	-16.5	0.18	--21.0	0.35	-18.5	0.21	-9.0	0.08
specimen 3	-17.0	0.07	-24.5	0.41	-20.0	0.32	-7.0	0.03
Ave	-19.0	0.13	-23.0	0.46	-17.0	0.24	-8.8	0.06
Std	3.91	0.06	1.80	0.15	3.97	0.07	1.76	0.029

The aim of this test series is to determine the combination of mix type and Portland cement addition that gives the lowest fracture temperature. Figures (4.38) and (4.39) present curves of fracture temperature and fracture stress versus Portland Cement content for each of the four mixes tested. Mix M4 has higher fracture temperatures (and lower fracture stresses) for all Portland Cement contents than the other mixes making it the least desirable mix. As mentioned previously, all the other mixes have good almost identical fracture temperatures accompanied by the highest almost identical fracture stresses of the test series. Although the fracture stress decreases for all mixes with increasing Portland Cement content above 0.5%, the stress at a given temperature also decreases. The result of these two trends is that the fracture temperatures for the M2 and M3 mixes remain almost constant for Portland Cement additions above 0.5%. The fracture temperature of the M1 mix increases somewhat with increasing Portland Cement content, while that of the M4 mix increases substantially faster.

To better understand whether both Portland content and emulsion type have significant effects on the fracture temperatures of the CIR mixtures or not, a two-way ANOVA analysis was conducted on both mixes M1(Slow Setting + pulverized HL8) and M2 (High Float pulverized HL8) with three replicates of each Portland Cement Percentage (0%,0.5%,1.5% and 3%). The test was carried out at a confidence interval of 95%. The main studied parameters are the amount of Portland Cement added (0%, 0.5%,1.5% and 3%) and type of emulsion used (Slow Setting and High Float Emulsions). The ANOVA test result is presented in Table (4.5). The results show that there is no significant effect of either the type of emulsion used or the variation in the amount of Portland Cement added to the mixtures on the fracture temperatures as F-actual is less than F-critical. That is clear in Figure (4.37, a, b, c & d) where the additions of Portland Cement content beyond 0.5% resulted in a small decrease in the fracture temperature. Furthermore, the interaction between the amount of Portland Cement added and the type of emulsion used was insignificant as F-actual is less than F-critical and P-value is greater than 0.05, which means that the type of emulsion acts independently of the amount of Portland Cement added.

Table 4.5 Statistical Analysis: Fracture Temperature for M1 AND M2 (ANOVA)

ANOVA						
Source of Variation	**SS**	**df**	**MS**	**F**	**P-value**	**F crit**
Emulsion	37.00167	1	37.00167	3.88656	0.066222	4.493998
Portland Cement	74.005	3	24.66833	2.591098	0.088796	3.238872
Interaction	39.405	3	13.135	1.379667	0.28493	3.238872
Within	152.3267	16	9.520417			
Total	302.7383	23				

Moreover, to investigate the effect of the type of emulsion (Slow setting and High Float), and the variation of the amount of Portland Cement added to the mixtures containing pulverized HL3RAP materials (M3 &M4) on low temperature resistance, a two-way ANOVA analysis was conducted, and the results are presented in Table (4.6). The result show that the effect of both the amount of Portland Cement added, and type of emulsion used on the fracture temperature were statistically significant, as the F-actual is greater than F-critical and P value is less than 0.05. Also, the interaction between the amount of Portland Cement added and the type of emulsion used was statistically significant because F-actual is greater than F-critical, and the P value is less than 0.05. That is evident in Figures (4.37, a, b, c & d). As can be seen, the fracture temperature was affected by the variation of the amount of Portland Cement added into the mixtures (M3&M4), especially when the addition of Portland Cement exceeded 0.5%.

Table 4.6 Statistical Analysis: Fracture Temperature for M1 AND M2 (ANOVA)

ANOVA						
Source of Variation	**SS**	**df**	**MS**	**F**	**P-value**	**F crit**
Emulsion	580.1667	1	580.1667	69.10174	3.36E-07	4.493998
Portland Cement	151.125	3	50.375	6	0.006119	3.238872
Interaction	183.5	3	61.16667	7.28536	0.002685	3.238872
Within	134.3333	16	8.395833			
Total	1049.125	23				

In summary mixes M1, M2 and M3 give low fracture temperatures (-28, -26 and -27, respectively) with a 0.5% Portland Cement addition. Mixes M2 and M3 give similarly low fracture temperatures for larger Portland Cement additions. These are -26℃ and -28℃ for M2 and M3 mixes, respectively, at 1.5% Portland Cement and -27℃ for both M2 and M3 mixes at 3% Portland Cement. From a designer’s point of view, any M1, M2 or M3 mixes with an addition of 0.5% Portland Cement achieved the lowest fracture temperature of the material, and Portland Cement combination tested. Further addition of Portland Cement content beyond 0.5% maintained the low fracture temperature for M2 and M3 mixes but offered no significant improvement.

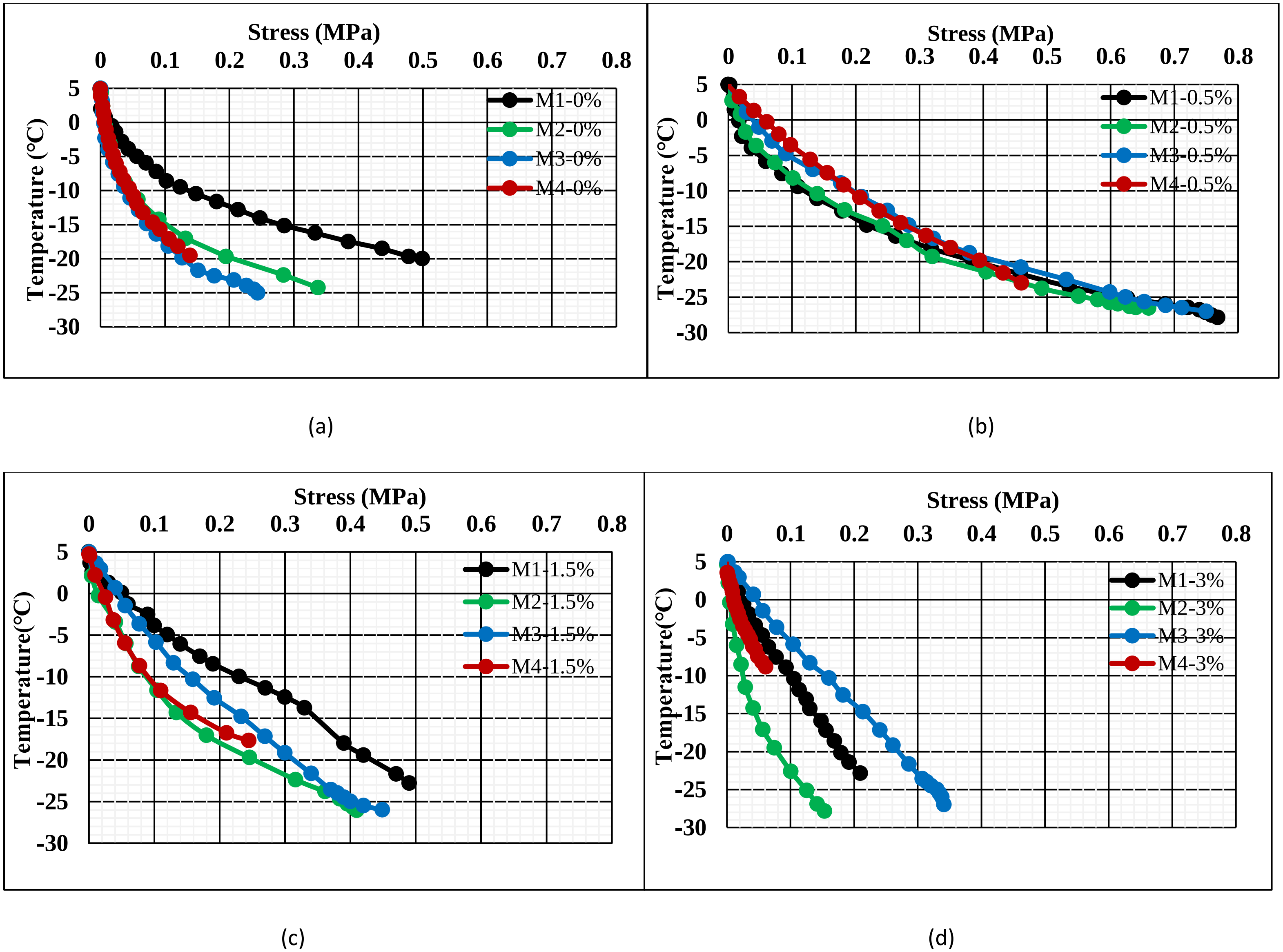

Figure 4.37 Thermal Cracking Stress versus Temperature for all mixtures at (a) 0%, (b) 0.5%, (c)1.5% and (d) 3% Cement Content

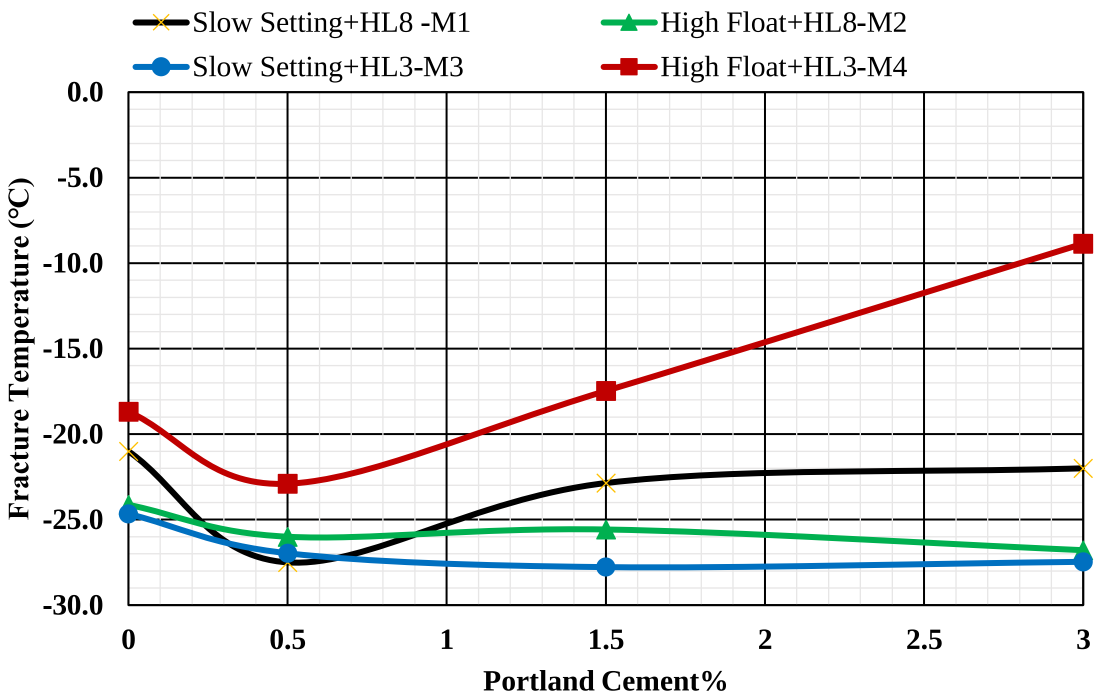

Figure 4.38 Variation of Fracture Temperature with Cement Content for the Four Mixes Tested

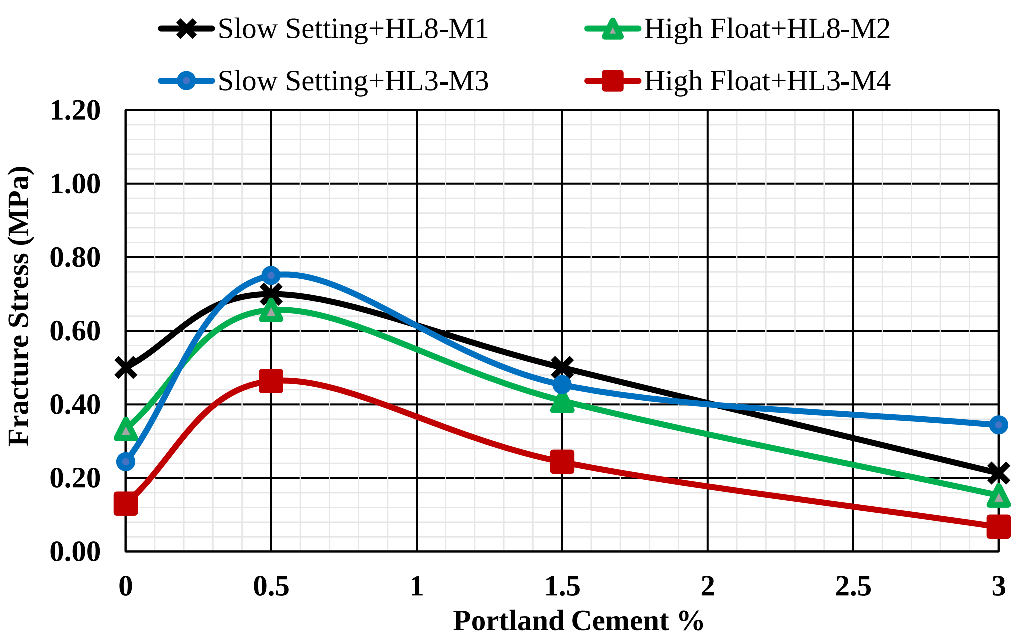

Figure 4.39 Variation of Fracture Stress with Cement Content for the Four Mixes Tested

4.5 The Effect of Gradation and Emulsion Type on Stiffness and Fatigue Strength

Since the main goal of this study was to improve the fatigue life without unduly compromising the stiffness, Figure (4.40) to Figure (4.44) are introduced to help us better understand the effect of gradation and emulsion type on stiffness and fatigue strength and their variation with Portland Cement content.

4.5.1 M1-A Slow Setting Emulsion (CSS-1H) and (Pulverized HL8) RAP

The data of Figure (4.40) are for similar temperatures (4℃ for stiffness and 5℃ for fatigue strength). The Figure gives a plot of stiffness and fatigue strength versus Portland Cement content for a Slow Setting Emulsion (CSS-1H) and pulverized HL8 RAP (M1). As shown in the Figure as the percentage of Portland Cement increases, the stiffness increases. Adding 0.5% and 1.5% Portland Cement significantly increases the stiffness compared to that of the control mix. However, adding 3% Portland Cement did not contribute to a further increase in stiffness. The Fatigue strength, on the other hand, decreases as the amount of Portland Cement increases. Adding 0.5%, 1.5% and 3% Portland Cement, caused a reduction in fatigue strength of 18%, 37% and 55%, respectively. The maximum fatigue strength is obtained at a 0% Portland Cement addition. However, the maximum stiffness is obtained by adding 1.5% or more Portland Cement. Between 0% and 1.5% Portland Cement, there is a tradeoff between fatigue strength and stiffness.

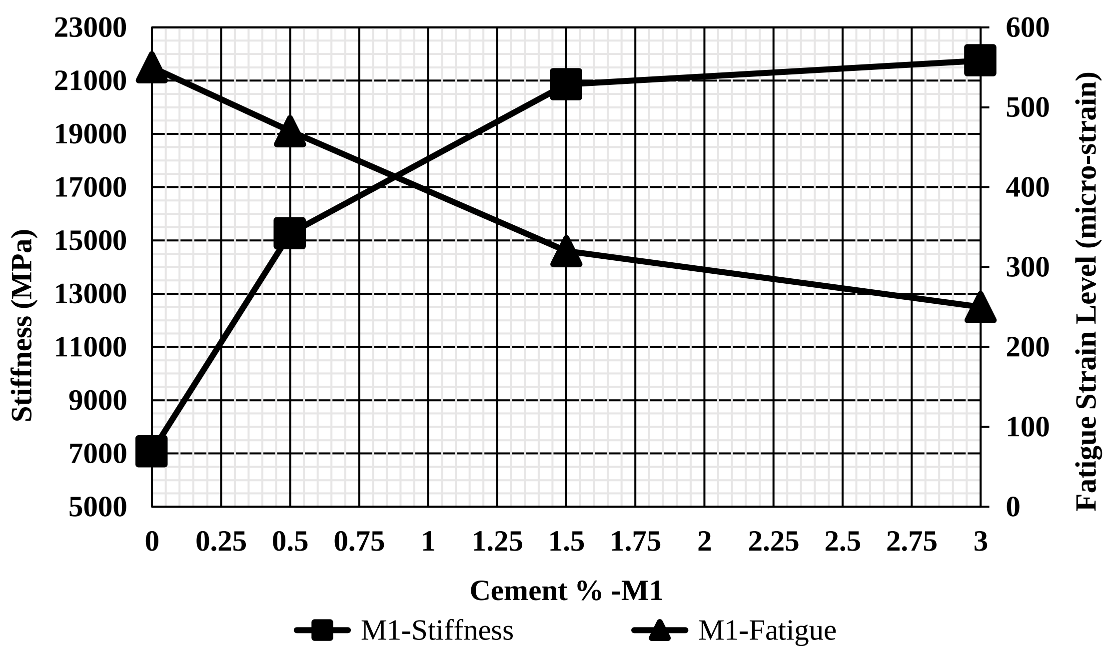

Figure 4.40 Fatigue Strength and Stiffness vs Cement% for M1

4.5.2 M2-An Anionic High Float Emulsion (HF-150) and (Pulverized HL8) RAP

Figure (4.41) gives a plot of stiffness and fatigue strength versus Portland Cement content for an Anionic High Float Emulsion (HF-150) and pulverized HL8 RAP (M2). As the amount of Portland Cement increases, the fatigue resistance decreases. When 0.5%, 1.5% and 3% Portland Cement was added, there was a continuous reduction in fatigue strength of 13%, 25% and 38%, respectively. There was an increase of about 60% in the stiffness when 0.5% of Portland Cement was added. However, further additions to 1.5% and 3% Portland Cement did not result in significant stiffness increases. The fatigue strength decreases by about 17% with an addition of 0.5% of Portland Cement. There is little change in fatigue strength with further additions of Portland Cement. The optimum fatigue strength is obtained at 0% Portland Cement, and the optimum stiffness remains at a maximum value for Portland Cement contents greater than 0.5%. There is a tradeoff between stiffness and fatigue strength between additions of 0% and 0.5% of Portland Cement.

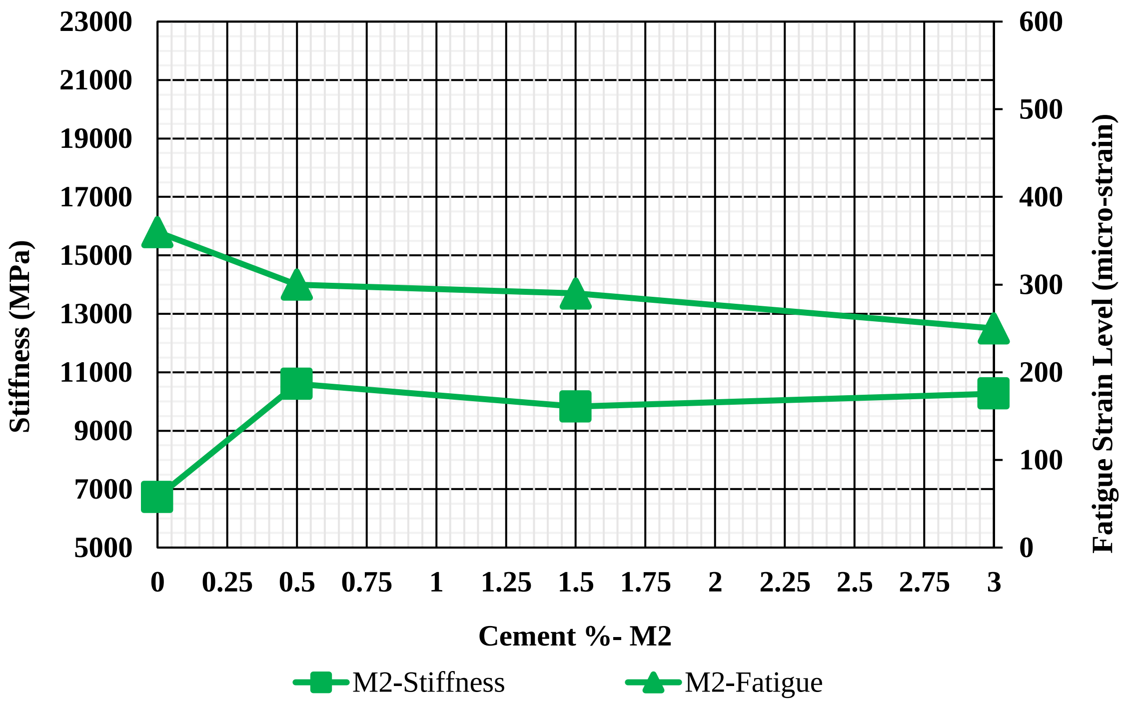

Figure 4.41 Fatigue and Stiffness vs Cement% for M2

4.5.3 M3- A Slow Setting Emulsion (CSS-1H) and (Pulverized HL3) RAP

Figure (4.42) gives a plot of stiffness and fatigue strength versus Portland Cement content for a Slow Setting Emulsion (CSS-1H) and pulverized HL3 RAP materials (M3) at 4℃ and 5℃, respectively. Adding Portland Cement to the mixture did not have any effect on the fatigue life. However, adding Portland Cement in the amounts of 0.5%, 1.5% and 3% increased the stiffness of the mixture, with the maximum stiffness occurring at a 3% Portland Cement addition. Although there is no tradeoff between fatigue strength and stiffness when adding 3% Portland Cement, it is not recommended to add Portland Cement beyond 1.5% due to the associated shrinkage cracks and cost.

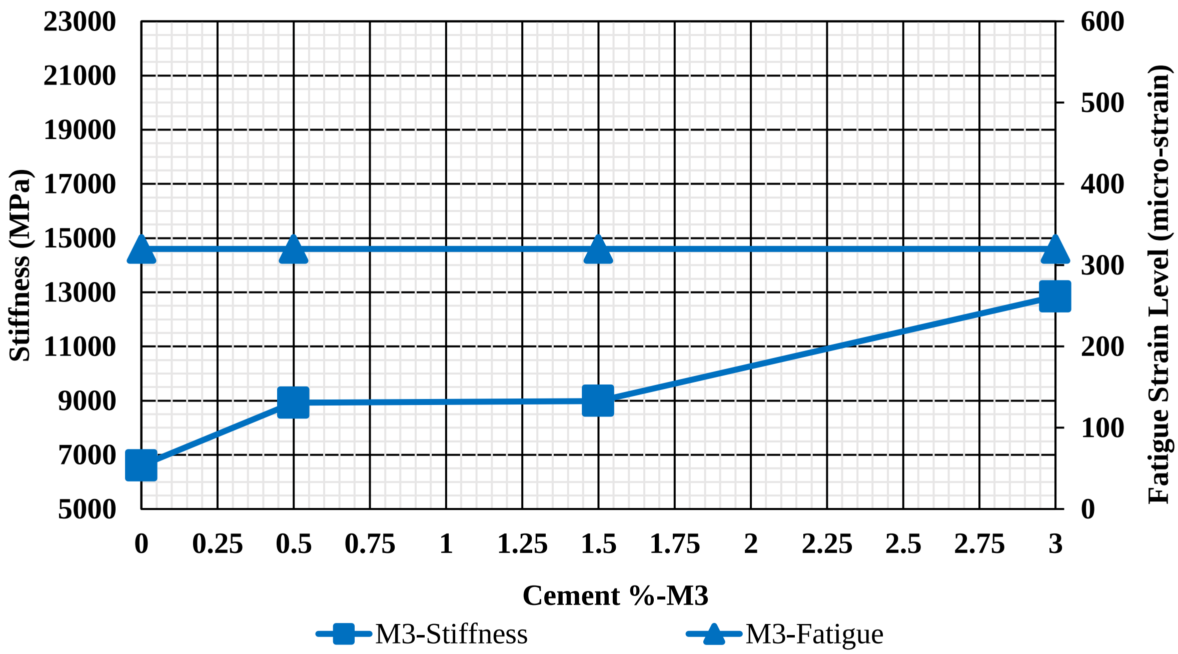

Figure 4.42 Fatigue and Stiffness vs Cement% for M3

4.5.4 M4- An Anionic High Float Emulsion (HF-150) and (Pulverized HL3) RAP

Figure (4.43) gives a plot of stiffness and fatigue strength versus Portland Cement content for an Anionic High Float Emulsion (HF-150) and HL3 RAP materials (M4) at 4℃ and 5℃, respectively. As the percentage of Portland Cement increases from 0% to 1.5%, the stiffness increases. However, adding Portland Cement in an amount greater than 1.5% did not further improve the stiffness of the mixture. The fatigue strength was not affected by the amounts of

Portland Cement added to the mixture. The designer can optimize both fatigue strength and stiffness by adding 1.5% Portland Cement.

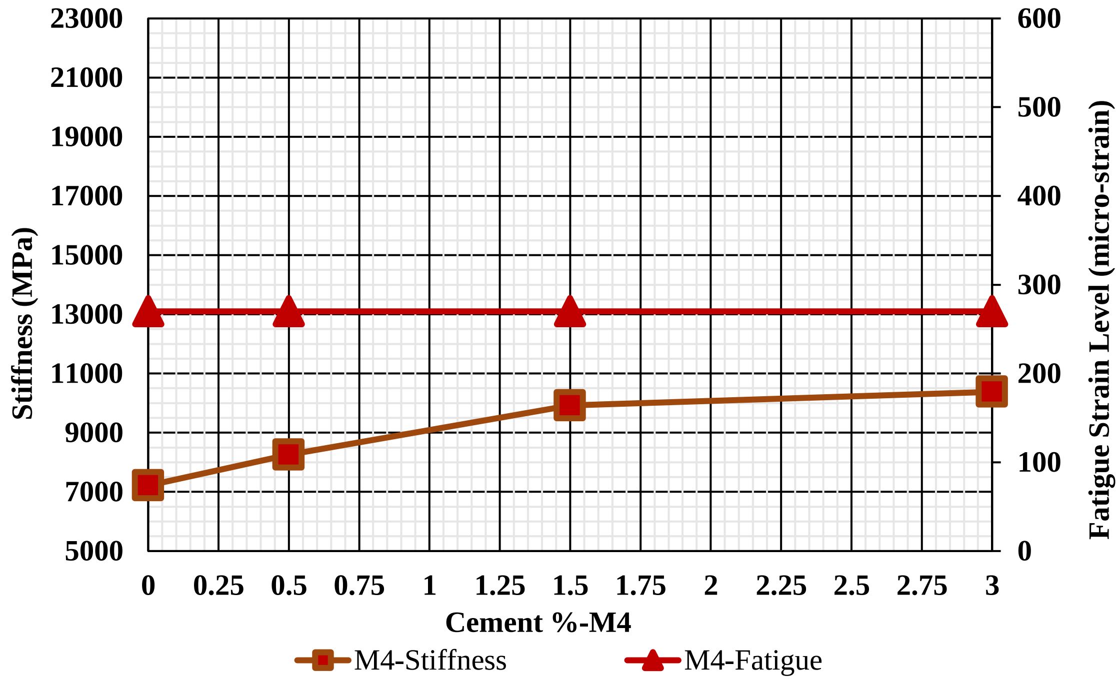

Figure 4.43 Fatigue and Stiffness vs Cement% for M4

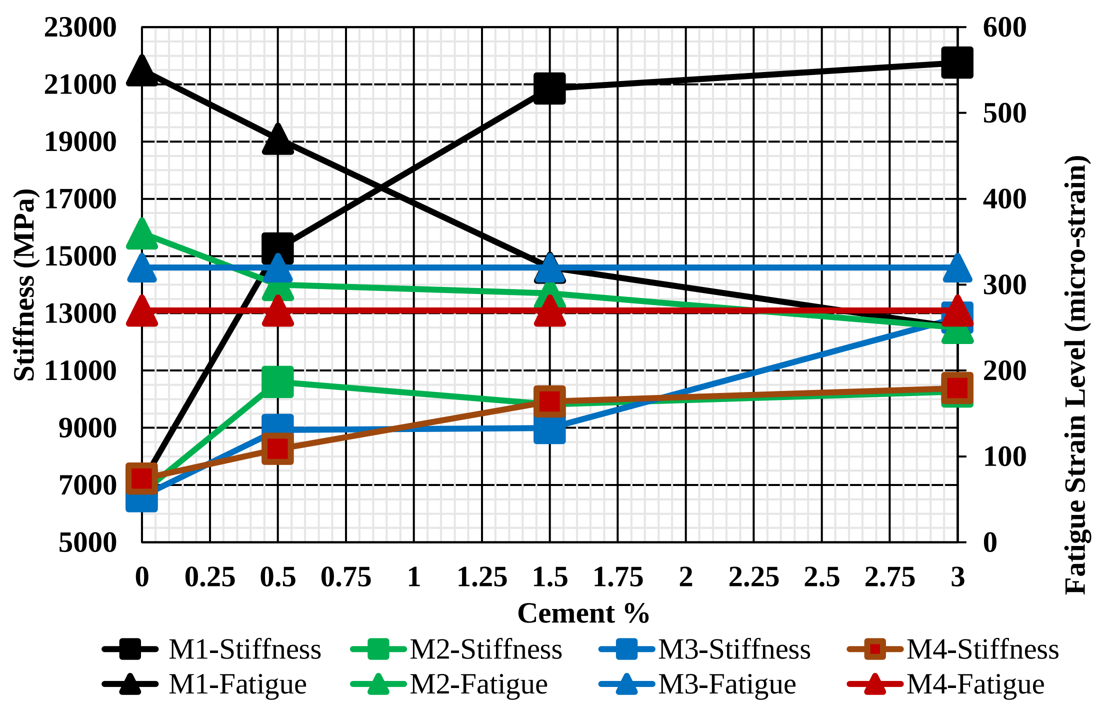

Figure 4.44 Stiffness and Fatigue Strength for M1,M2,M3&M4 Vs Portland Cement Percentages

Finally, Figure (4.44) shows the trend of both the stiffness and fatigue strength versus the amount of Portland Cement for all mixes. The Slow Setting Emulsion with the pulverized HL8 RAP, which is (M1), at 0% Portland Cement addition gives the highest fatigue strength, and at a 3% Portland Cement addition gives the highest stiffness of any of the mixtures. Between a 0% and a 1.5% Portland Cement addition, there is a tradeoff between the stiffness and fatigue strength, but over this range, this mixture has a higher stiffness and fatigue strength than any of the other mixtures. A Slow Setting Emulsion (CSS-1H) and pulverized HL3 RAP (M3) give the second-best fatigue strength and stiffness of all the mixes at a 3% Portland Cement addition. However, adding Portland Cement beyond 1.5% will increase both shrinkage cracks and cost. The third best choice in terms of stiffness and fatigue strength is the Anionic High Float Emulsion (HF-150) and pulverized HL8 RAP (M2) with a 0.5% Portland Cement addition. The last choice in terms of both stiffness and fatigue strength is the Anionic High Float Emulsion (HF-150) and pulverized HL3 RAP (M4) with a 1.5% Portland Cement addition to avoid shrinkage cracks. This gives both an increased cost and poorer performance than the other mixtures.

From a designer's point of view, the combination of slow setting emulsion and a pulverized HL8 RAP at cement contents between 0% and 1.5% offers the only noticeably superior performances in fatigue strength and stiffness among the material combinations. Fatigue strength is the greatest at a 0% cement addition, and the stiffness is the greatest at additions of cement above 1.5%. Between 0 % and 1.5% cement addition, there is a tradeoff between fatigue strength and stiffness. All of the other combinations have similar fatigue strength and stiffness values for cement contents above 0.5%. An outlying result is the stiffness of the combination of slow setting emulsion and pulverized HL3 RAP at a 3% Portland Cement addition. Additions of Portland Cement up to 3% increase the stiffness for all mixtures (combination of emulsion and aggregate) but reduce the fatigue strength for the slow setting emulsion and a pulverized HL8 RAP and for a high float emulsion with the pulverized HL8 RAP (trade-off relationship for M1 and M2). Furthermore, additions of Portland Cement content beyond 0.5% resulted in a small decrease in the fracture temperature but also a significant decrease in fracture stresses for the M2 and M3 mixes. Thus, the addition of a Portland Cement content between 0.5% and 1.5% is recommended to improve the stiffness and avoid shrinkage cracks, tensile stresses, and a reduction of fatigue strength.

4.6 Pavement design and performance prediction

For Ontario highways, several Key Performance Indices (KPIs), such as the Pavement Condition Index (PCI), the Distress Manifestation Index (DMI), the International Roughness Index (IRI) and the Riding Comfort Index (RCI), are used by management in making decisions. The Pavement Condition Index (PCI) provides a numerical rating for the condition of road segments within the road network, where 0 is the worst possible condition, and 100 is the best condition (Jannat and Tighe,2015).

In this study, it was assumed that CIR technology was chosen to rehabilitate an aged two-way minor arterial road, which was designed to be used for 20 years. The aging road was assumed to have an average daily truck traffic (AADTT) of 400 with an annual growth rate of 3%. The properties of the granular base, granular sub-base and wearing course asphalt concrete recommended by the Ministry of Transportation of Ontario (MTO,2019) were used to design the pavement structures. The designed pavement structure is shown in Table (4.7). The PCI of the CIR pavement designs was computed using the pavement distress data forecasted by AASHTOWare Pavement ME over a period of 12 years. The PCI calculations were conducted using the formula given in MTO's Pavement Design and Rehabilitation Manual (MTO,2013), which are given by Equation (4.1) and Equation (4.2)

$$PCI = Max\,(0, Min\,(100, 13.75 + 9 \times DMI - 7.5 \times IRI) \tag{4.1}$$

$$DMI = 10\,\frac{(208 - \sum_{K}^{N} S_k + D_K)W_k}{208} \tag{4.2}$$

Where:
DMI = distress manifestation index
N = number of distresses related to a given pavement type Sk = severity rate of distress k
Dk = density rate of distress k
Wk = weighting factor of distress k

Table (4.8) presents the predicted performance of M1, M2, M3 and M4. An example of pavement distress predicted by AASHTOWare Pavement ME for M2 is shown in Appendix-III.

Table 4.7 Designed Pavement Structure for the Rehabilitated Pavement

Layer Type	Material type	Thickness (mm)
Surface layer	Ontario SP 12.5	50
Binder layer	CIR mixtures	100
Base layer	Ontario Granular A	150
Sub-base layer	Ontario Granular B	400

Using PCI as the key pavement performance indicator, performance deterioration curves were plotted for all the mixtures (M1, M2, M3 and M4). Figures (4.45, a, b, c, and d) present the PCI versus pavement age for M1, M2, M3 and M4, respectively. As shown in the Figures, the performance deterioration trends of the pavements are not affected by the addition of Portland Cement.

It was reported in section (4.4) that the addition of 0.5% Portland Cement achieved the lowest fracture temperatures and highest fracture stresses and stresses, as shown in both Figures (4.38 & 4.39). Also, the stiffness is enhanced with a small compromise in fatigue life, as is reported in section (4.5.4) and shown in Figure (4.44). Therefore, Figure (4.46) is used to show PCI performance versus pavement age for all mixtures at the addition of 0.5% Portland Cement. As can be seen, the performance deterioration curves exhibit the same behaviour over a period of 12 years regardless of the type of emulsions (Slow Setting or High Float) added or type of gradation used (pulverized HL8 or HL3).

Table 4.8 Predicted Performance of CIR Mixtures M1, M2, M3 & M4

Distress Type	Reliability	Target	Predicted			
			M1-0%	M1-0.5%	M1-1.5%	M1-3%
Terminal IRI (m/km)	75	2.7	1.8	1.86	1.87	1.74
Permanent deformation - total	75	17	7.9	7.69	7.72	7.52
AC total fatigue cracking: bottom up	75	35	0.76	0.76	0.76	0.76
AC total transverse cracking	75	190	21.65	21.65	21.65	21.65
Permanent deformation – AC only	75	6	0.45	0.43	0.43	0.45

Distress Type	Reliability	Target	Predicted			
			M2-0%	M2-0.5%	M2-1.5%	M2-3%
Terminal IRI (m/km)	75	2.7	1.76	1.74	1.74	1.75
Permanent deformation - total	75	17	8.05	7.62	7.69	7.81
AC total fatigue cracking: bottom up	75	35	0.76	0.76	0.76	0.76
AC total transverse cracking	75	190	21.65	21.65	21.65	21.65
Permanent deformation – AC only	75	6	0.49	0.43	0.43	0.44

Distress Type	Reliability	Target	Predicted			
			M3-0%	M3-0.5%	M3-1.5%	M3-3%
Terminal IRI (m/km)	75	2.7	1.88	1.75	1.78	1.82
Permanent deformation - total	75	17	8.06	7.85	7.79	7.81
AC total fatigue cracking: bottom up	75	35	0.76	0.76	0.76	0.76
AC total transverse cracking	75	190	21.65	21.65	21.65	21.65
Permanent deformation – AC only	75	6	0.48	0.44	0.43	0.44

Distress Type	Reliability	Target	Predicted			
			M4-0%	M4-0.5%	M1-4.5%	M4-3%
Terminal IRI (m/km)	75	2.7	1.81	1.81	1.82	1.82
Permanent deformation - total	75	17	8.0	8.0	7.81	7.81
AC total fatigue cracking: bottom up	75	35	0.76	0.76	0.76	0.76
AC total transverse cracking	75	190	21.65	21.65	21.65	21.65
Permanent deformation – AC only	75	6	0.48	0.48	0.44	0.44

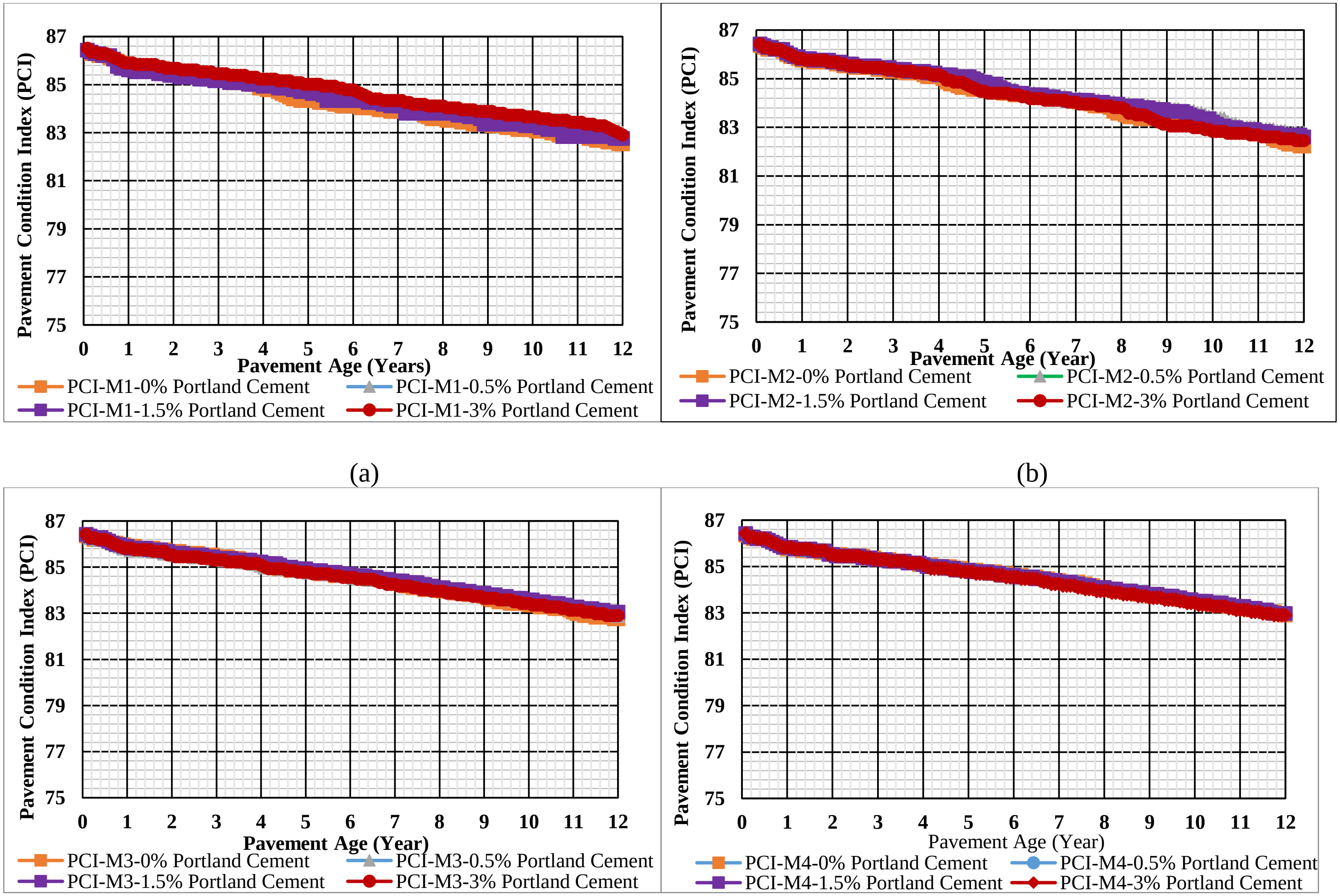

(a) (b)

(C) (d)

Figure 4.45 PCI VS Pavement age for all mixes(M1,M2,M3&M4)

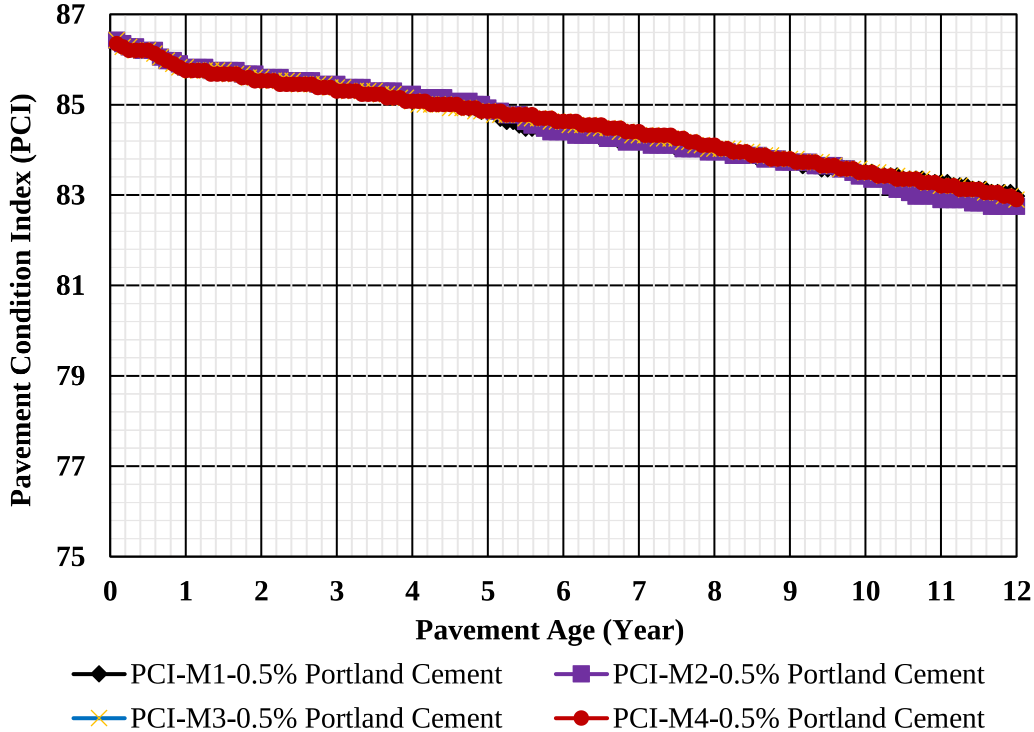

Figure 4.46 PCI VS Pavement age for M1, M2, M3 and M4 at 0.5% Portland Cement Content

5 Classic Maxwell Model for the Stress-Strain Behaviour of Cold In Place Recycled Asphalt

5.1 Viscoelasticity

Viscosity can be defined as the resistance of a fluid to flow, which means that a large force is needed to generate a specific flow if the material viscosity is high. Viscoelastic material displays both elastic and viscous behaviour, and it is time and temperature dependent. When a load is applied, viscous materials deform at a constant rate under constant stress; (as a result, they exhibit time-dependent behaviour). There is a delay in time for the material to respond to the stress, which leads to a loss of energy inside the material. Materials may exhibit a viscous or elastic behaviour or a combination of both (Franck et al.,1993) primarily.

A number of rheological models have been proposed to describe the viscoelastic behaviour of materials. These models consist of a combination of two components, which are a time-independent spring and a time-dependent dashpot. The spring element simulates time-independent behaviour (elastic characteristics), and the dashpot element simulates time-dependent behaviour (viscous characteristics) as explained by Equation (5.1).

$$\dot{\varepsilon} = \frac{\sigma}{\eta} \tag{5.1}$$

Where: $\dot{\varepsilon}$ is the strain rate, σ is the applied stress, and η is the viscosity.

Various assemblies of springs and dashpots have been used to create different viscoelastic models. For instance, the simplest viscoelastic model, the classic Maxwell model, consists of a spring and dashpot connected in series. These models have been used to predict a relationship between stress-strain and time for materials.

5.1.1 Dissipated Energy Approach

The energy that is being input into a material is usually represented by the area under the stress-strain curve when a material is exposed to monotonic external loading. For cyclic loading, the energy dissipated during a loading cycle is taken to be equal to the area inside the stress-strain hysteresis loop.

A study was conducted by Shivakumar (1987) to evaluate the dissipated energy in an elastic-plastic material associated with crack propagation. It was concluded that crack propagation was associated with dissipation of energy. Furthermore, it was concluded that the dissipated energy is comprised of three phases: the first phase is the energy required to separate the faces of a crack, the second phase is the plastic dissipated energy, and the third stage involves the residual strain energy. When the propagation and growth of the cracks occur, the residual strain energy will change (Turner and Kolednik, 1994). Moreover, another study was conducted by Manfredi (2001) to evaluate the dissipated energy,concluding that a low amplitude plastic stress-strain cycle does not cause damage. As a result, when considering the total damage, the energy dissipated during these cycles should be eliminated. Another study was conducted on dissipated energy evaluation by Sucuoğlu and Erberik (2004), and they concluded that the dissipated energy per load cycle decreased as the number of cycles increased.

In viscoelastic materials, energy can be both dissipated and stored. When viscoelastic materials are exposed to external loading, part of the dissipated energy can be transformed through the dashpot to thermal energy; as a result, decreasing the material damage per cycle (Hilton, 1992). Usually, the fatigue life curve (stress vs the number of cycles) is divided into three phases: In the first phase, heating plays an important role in reducing the recoverable stiffness. In constructing an equivalent constant temperature model of stiffness versus cycles, the stiffness in this region will be represented by a linear extension of phase II of Figure (5.1) to the first cycle. In phase II, the reduction of the stiffness is primarily controlled by fatigue, and the small effect of heating can be ignored. Finally, phase III is considered the failure phase, in which the reduction of the stiffness exceeds 50% of the initial stiffness. It is worthwhile to mention that the dissipated energy per cycle decreases when a test is conducted under strain control. However, the dissipated energy per cycle increases for testing under stress control, as shown in Figures (5.2 & 5.3).

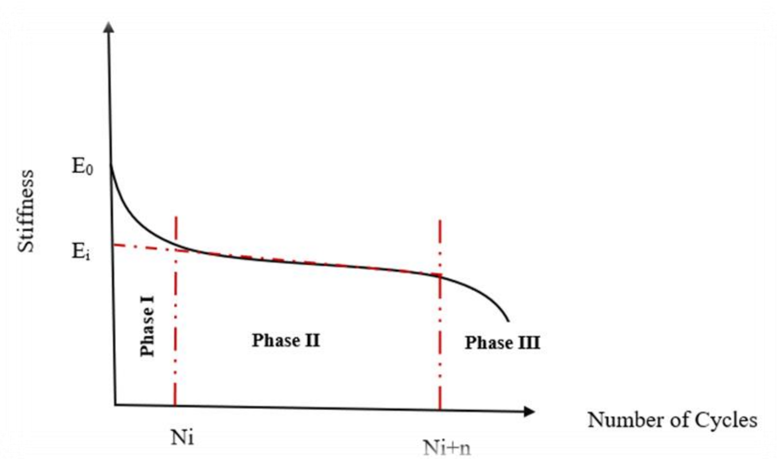

Figure 5.1 Failure Phases Stiffness vs Number of cycles(Baaj et al., 2005)

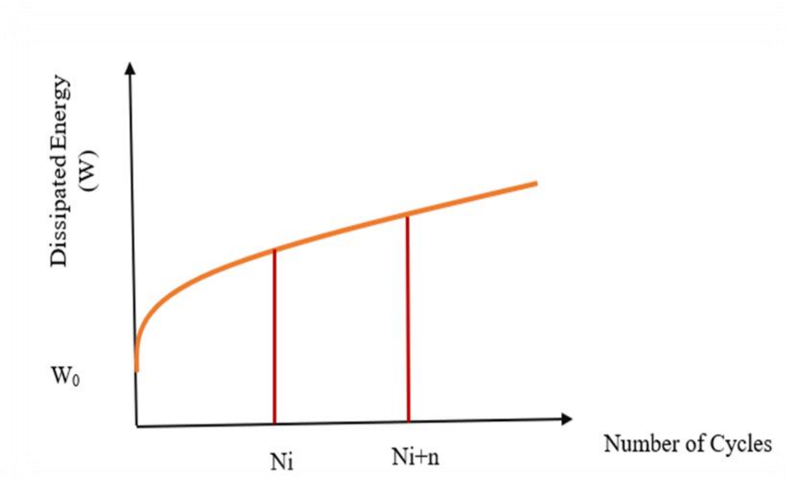

Figure 5.2 Dissipated Energy Vs Number of Cycles (Stress Control) (Baaj et al., 2005)

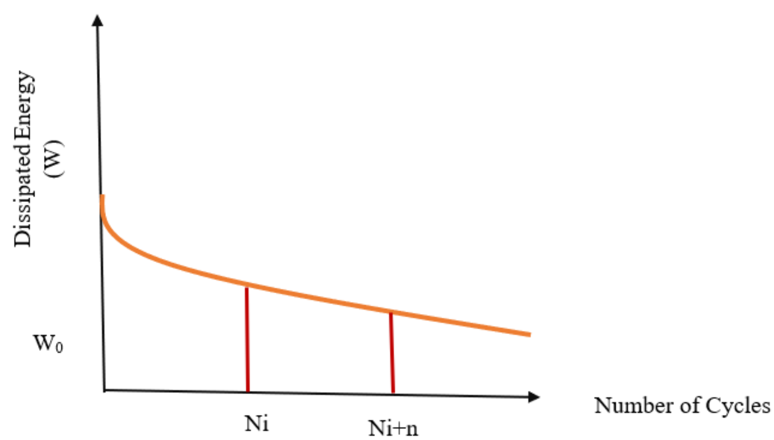

Figure 5.3 Dissipated Energy Vs Number of Cycles (Strain Control)(Baaj et al., 2005)

To understand the stress-strain behaviour during cyclic loading on a reversal-by-reversal basis, an accurate simulation of the hysteresis-loop shape is needed. The assumption that the classic Maxwell model consisting of a spring and dashpot in series will provide a reasonable model of the mechanical behaviour of the asphalt material will be examined.

After a spring and frictional slider, a model was introduced by Martin et al. (1971) to simulate the shape of a material elastic-plastic hysteresis-loop and the Masing (1926) memory of a material to the previous deformation. Jhansale and Topper (1971) used the same Masing kinematic hardening rule and memory model to simulate the moment-curvature behaviour of a beam under bending. They concluded that the moment-curvature of the beam could be modelled by the same rheological model as the material. Williams, Lind, Conle, Topper and Leis (1977) showed both theoretically and experimentally that for a geometrically linear, physically nonlinear structure, the characteristics of deformation response are conserved in the translation from material to structure. Later Williams and Topper (1981) provided further evidence that for Masing materials, the rheological model could be used as a general model of cyclic plasticity in any set of force deformation relationships for reversed plasticity of simply connected structures. Therefore, in the light of these studies, it is assumed that the classic Maxwell model representing a rheological model of a material can be applied to simulate either the stress-strain behaviour of our material or the force-deformation relationship of our test specimen.

The aim of this chapter is to experimentally determine the applicability of the Classic Maxwell Model to simulating the viscous-elastic deformation behaviour exhibited by our test specimen when subjected to cyclic loading.

5.2 Classic Maxwell Model

This Maxwell Model is used to simulate the stable cyclic stress-strain behaviour displayed by viscous-elastic materials and structural systems subjected to proportional constant staining. The model is used here to represent the relationship between applied forces and displacements or stress and strain. The classic Maxwell model consists of a spring and dashpot connected in series shown in Figure (5.4).

Figure 5.4 Classic Maxwell Model (Zaoutsos et al., 2011)

The behaviour of the stress relaxation phenomena under constant strain can be described by the classic Maxwell model as is given by the following Equations (5.2, 5.3,5.4 and 5.5) and shown in Figure (5.5):

$$\sigma(t) = \sigma_0 \, exp\,(-\frac{Et}{\eta}) = E\varepsilon_0 \, exp\,(-\frac{Et}{\eta}) \quad (5.2)$$

Where: (ε0) is the initial strain at t=0, the time just after the application of the strain, σ is the stress (MPa), (E) is the spring stiffness coefficient, and (η) is the dashpot coefficient.

The rate of change in stress is given by the following Equation (5.3)

$$\frac{d\sigma}{dt} = -\frac{\sigma_0 E}{\eta} \, exp\,(-\frac{Et}{\eta}) \tag{5.3}$$

The initial rate of change in stress at t=0 would be given by Equation (5.4)

$$\frac{d\sigma}{dt} = -\frac{\sigma_0 E}{\eta} \tag{5.4}$$

Finally, if the stresses were to decrease continuously at the initial rate, the relaxation behaviour can be described by the classic Maxwell model as given by Equation (5.5)

$$\sigma = \sigma_0 - (\sigma_0 \frac{\mathrm{Et}}{\eta}) \tag{5.5}$$

This equation can be used for successive small increments of time to describe the stress versus time behaviour of a material.

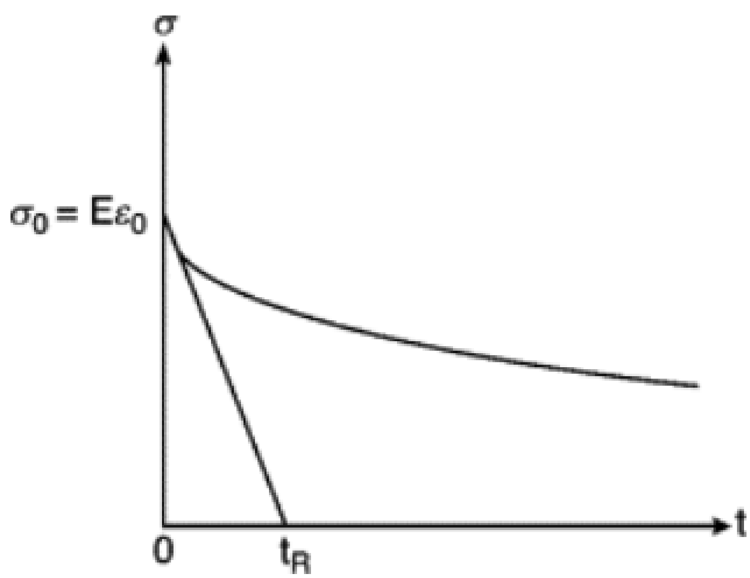

Figure 5.5 Relaxation Response by Maxwell Model (Zaoutsos et al., 2011)

In this project, four mixes were prepared and tested under cyclic loading. However, since there was not enough fatigue data (there was not sufficient data to draw the hysteresis loops) for mixes M1, M2 and M3, only mix four (M4) that contained 3% Portland Cement was used to calibrate the spring stiffness and dashpot coefficients. Figure (5.6) shows stress-strain hysteresis loops for M4-3% Portland Cement cycled at a 400-strain range for load cycles 200 to1000. The reason for excluding the first 200 cycles is to eliminate the effect of heating and the initial increases in the machine strain cycle (the controlled strain built up over a number of cycles). The test was conducted at 5°C and a test frequency of 5Hz. As can be seen in the Figure, the mean stress in each cycle has decreased during initial strain cycling until an equilibrium state is reached in which the tension stress peak equals the compression stress peak. Figure (5.7) shows the stress range versus time (number of cycles) for the experimental data of this test. The range of stress decreases as the number of cycles (and time) increases, leading to a reduction in the material stiffness, which is defined here as the ratio of the stress range to the strain range as the number of cycles increases and can be seen that the mean stress reduces as cycling continues.

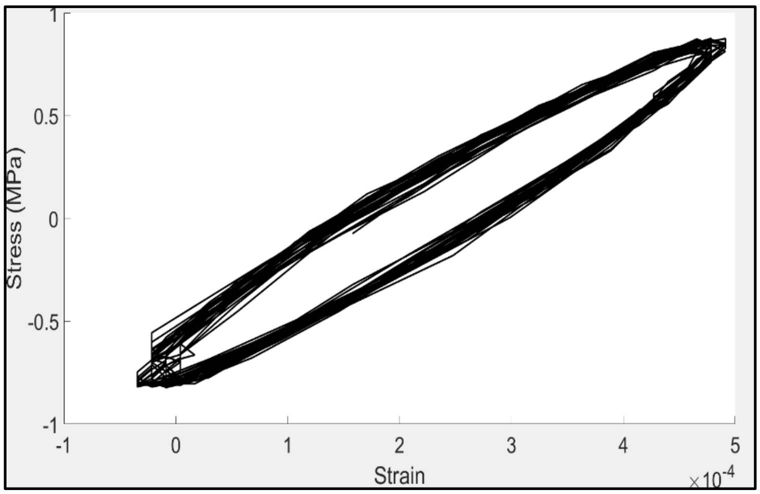

Figure 5.6 Hysteresis Loops of the Experimental Data

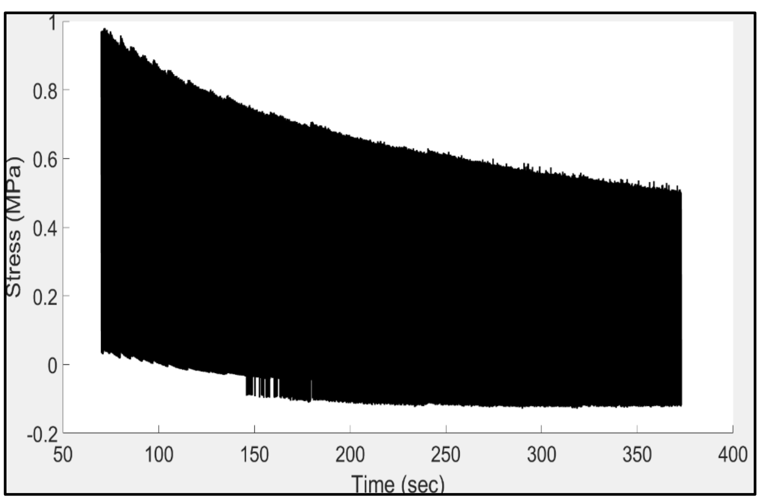

Figure 5.7 Stress Range vs Time for the Experimental Data

5.2.1 Calibration Procedure:

5.2.1.1 Loading Phase

1-Divide the time per half cycle into 100 increments ($\Delta t = (1/2f) * (1/100)$.

2-Divide the strain per half cycle into 100 increments ($\delta\varepsilon = \varepsilon/100$).

3-Calculate σ_0 ($\sigma_0 = \delta\varepsilon * E$) for an assumed value of E shown in Figure (5.8).

4- During the strain increment δ E, the stress relaxes from σ_0 to σ_1 ($\sigma_1 = \sigma_0 - \sigma_0 * E * t_1 / \eta$), a value of (η) is assumed and stress relaxation behaviour as shown in Figure (5.9).

5-Calculating σ_2 ($\sigma_2 = \sigma_1 + \sigma_0$) as shown in Figure (5.9).

6- Repeat this calculation until the end of the half-cycle at the one-hundredth element.

Where: σ_0 is the initial stress, (E) is the spring coefficient, and (η) is the dashpot coefficient

5.2.1.2 Unloading Phase

Repeat the steps for the loading procedure phase, except when calculating σ_2 ($\sigma_2 = \sigma_1 - \sigma_0$). MATLAB software was used to run the code.

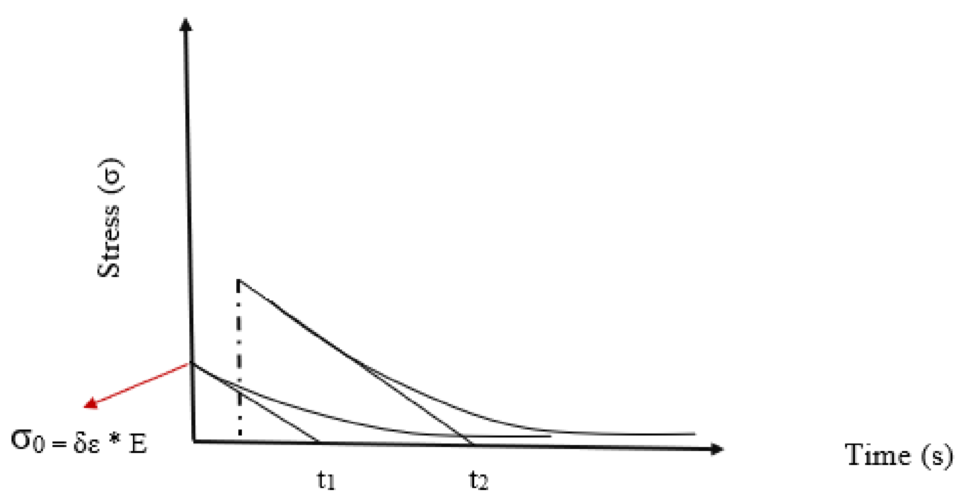

Figure 5.8 Stress Relaxation

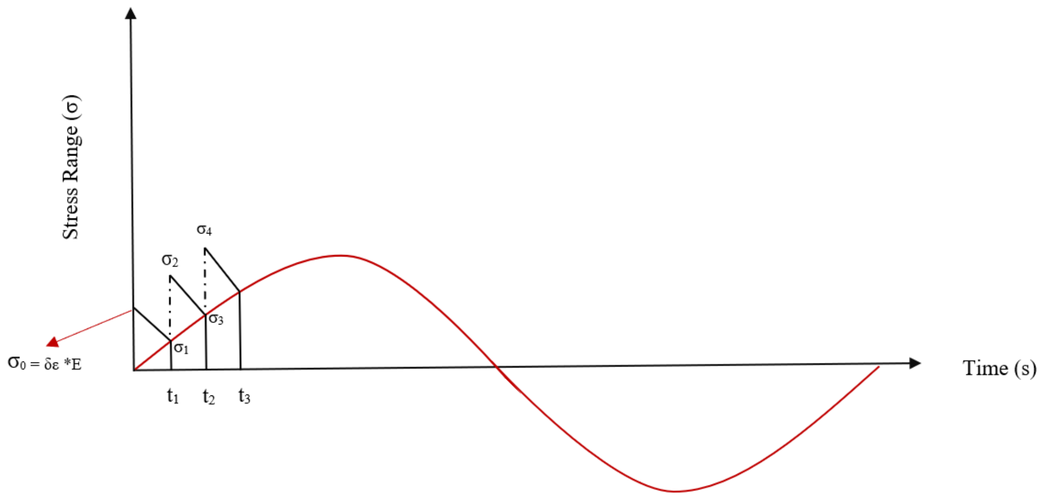

Figure 5.9 Calculated Stress vs Time

5.2.2 Fitting the Experimental Data to the Classic Maxwell Model:

Figures (5.10 and 5.11) plot experimental data in terms of stress range and normalized stress range versus accumulated cyclic strain for strain ranges of 400, 350 and 300 micro-strains. In Figure (5.10), the curves are extrapolated to the first cycle to obtain a sigma zero, a value of the stress range that does not include initial effects (buildup of the control strain cycle and heating). In Figure (5.11), where the stress ranges are normalized in terms of the value of sigma zero for each test, the stress range versus accumulated strain data falls into a compact linear band. This suggests that if the coefficients of a Maxwell model are described in terms of accumulated strain, the model should describe the material behaviour for all strain ranges.

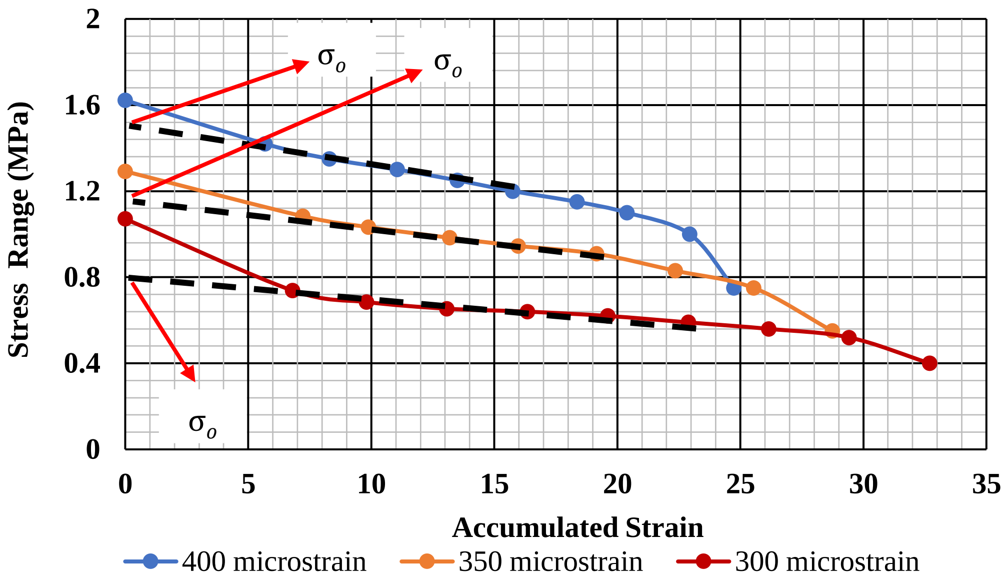

Figure 5.10 Stress Range vs accumulated Strain

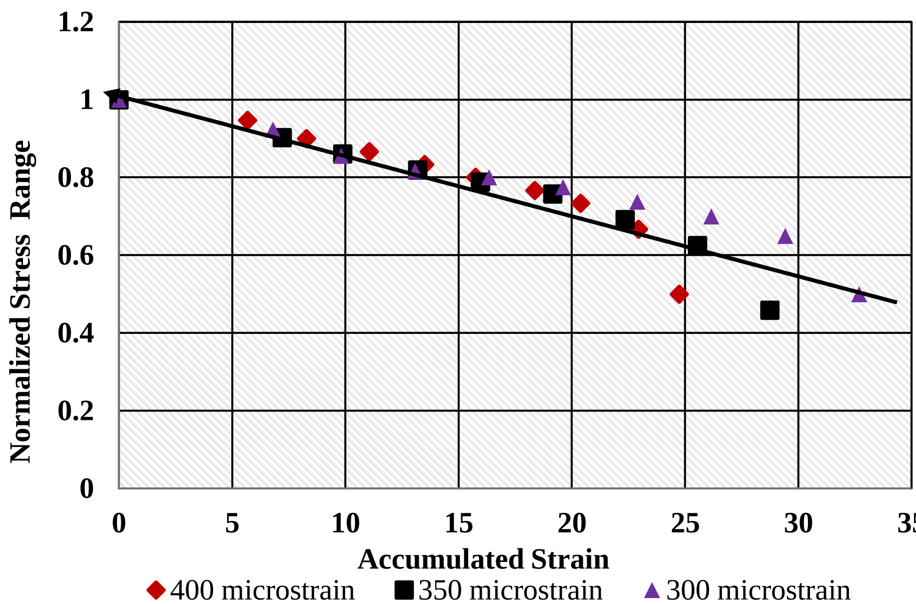

Figure 5.11 Normalized Stress Range vs accumulated Strain

For the highest strain range of 600 micro-strain, the stiffness and dashpot constants were fitted by trial and error to match the stress-strain response of the Maxwell model to the observed data at accumulated strain levels of $10 * 10^0$, $15 * 10^0$ and $20 * 10^0$. The best fit values of the model are shown together with the corresponding experimental data for the stress-strain loops in Figure (5.12).

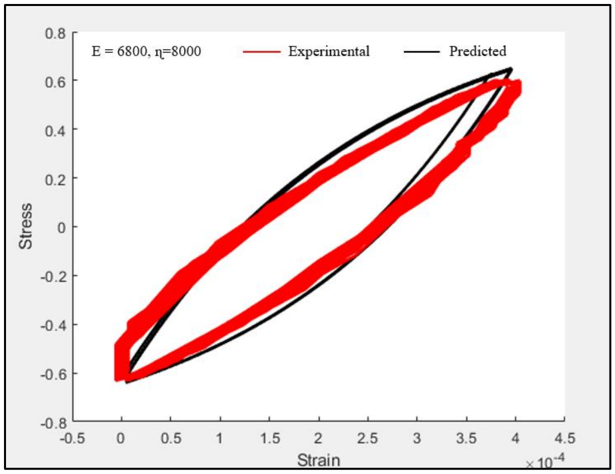

(a)

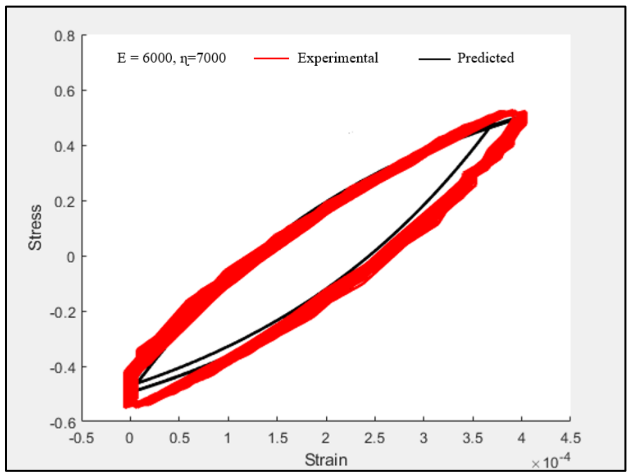

(b)

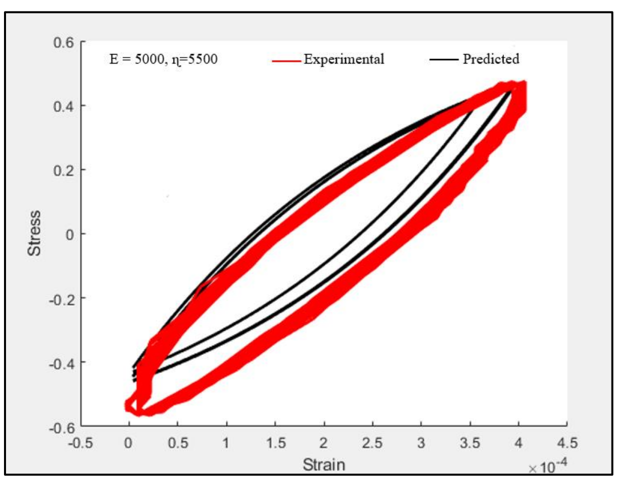

(c)

Figure 5.12 Stress Range vs Strain Hysteresis Loops at a Strain Range of 400 micro-strain $a, \Sigma\varepsilon = 10 * 10^0$), (b, $\Sigma\varepsilon$ =15* 10^0) (c) and (c, $\Sigma\varepsilon$ = 20* 10^0

The spring and dashpot coefficients versus the accumulated strain predicted by the calibrated model were plotted together with measured values for these three levels, which are ($10 * 10^0$), (15* 10^0) and ($20 * 10^0$) in Figure (5.13) together with a linear curve fitted to the model predictions. The model coefficients used in making the predictions are given by Equations (5.6 & 5.7) below:

$$E = E_0\ (1 - \alpha_1\ \Sigma\varepsilon/E_0) \tag{5.6}$$

$$\eta = \eta_0\ (1 - \alpha_2\ \Sigma\varepsilon/\eta_0) \tag{5.7}$$

where:

(E_0) is the initial spring stiffness at the first cycle which is (E_0 =8633.3),
(α_1) is the slope associated with the spring coefficient ($\alpha_1 = 180$)
(η_0) is the dashpot coefficient at the first cycle which is (η_0 =10583)
(α_2) is the slope associated with the dashpot coefficient ($\alpha_2 = 250$), and (Σε) is the accumulated strain

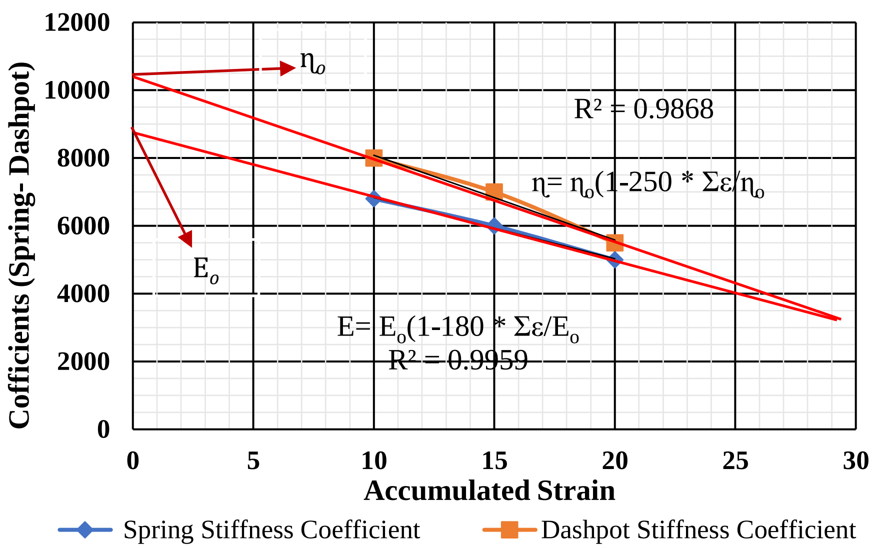

Figure 5.13 Stiffness and Dashpot Coefficients vs Accumulated Strain for a 400 micro-strain Strain Range Test

The values of the E_0 and η_0 at the first cycle were found by extrapolation of the E and n versus accumulated strain curves. The linear curves are a reasonably good fit to the data, and their slopes are taken as being representative of the relationship between these parameters and accumulated strain for this material. Therefore, the model with appropriately fitted constants for E, η_0, (α_1) and (α_2) was used to calculate stress-strain loops for the other two strain ranges (350 and 300 micro-strain) at the same accumulated strains used for fitting the 400 micro-strain range data and are shown together with the corresponding test data in Figures (5.14 & 5.15), respectively. The model predictions fall close to the data but with sharper loop tips; the reason for this difference is that in order to simplify loop shape calculations, the sine wave control signal of the test machine was approximated by a triangle wave in the calculations.

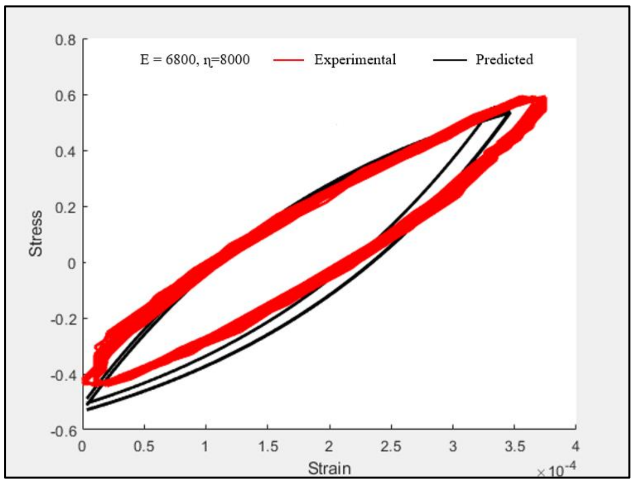

(a)

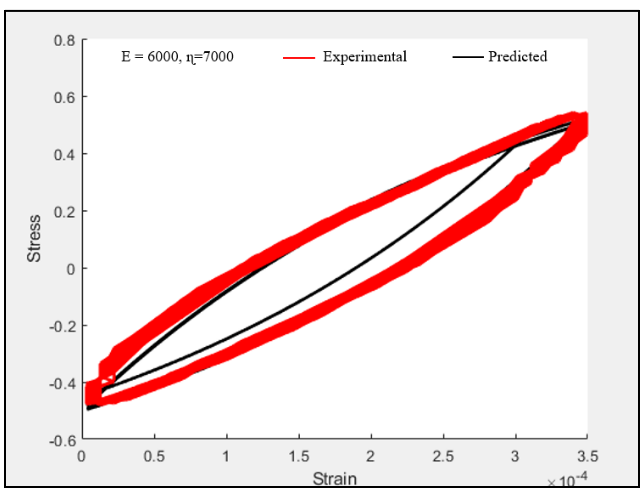

(b)

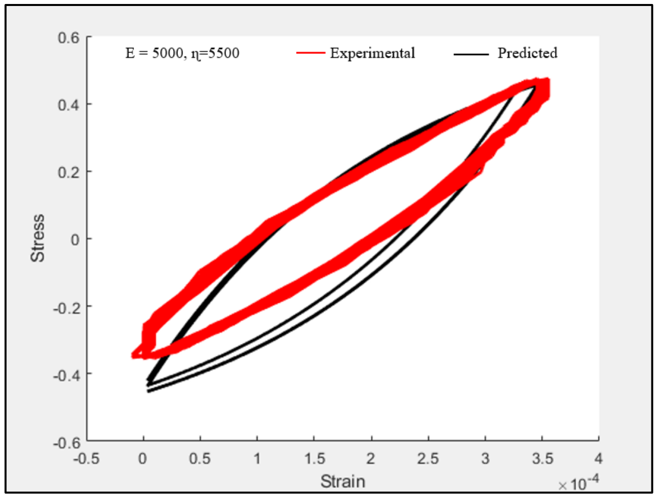

(c)

Figure 5.14 Stress Range vs Strain Hysteresis Loops at a Strain Range of 350micro-strain (a, $\Sigma\varepsilon = 10 * 10^0$***), (b,*** $\Sigma\varepsilon$ ***=15**** 10^0***) & (c) and (c,*** $\Sigma\varepsilon$ ***= 20**** 10^0 ***)***

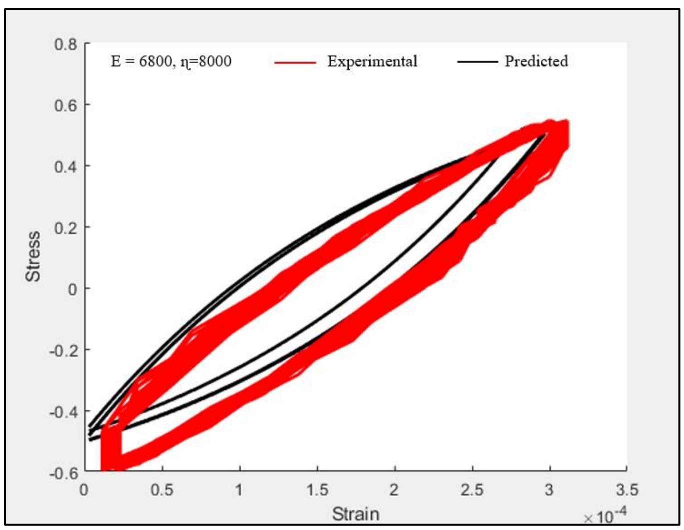

(a)

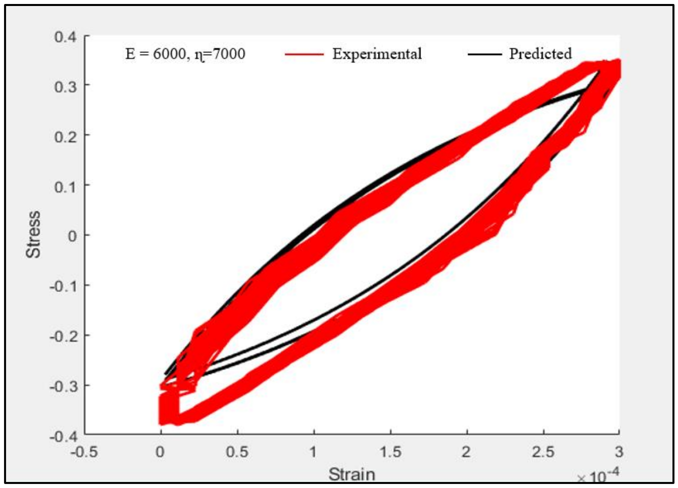

(b)

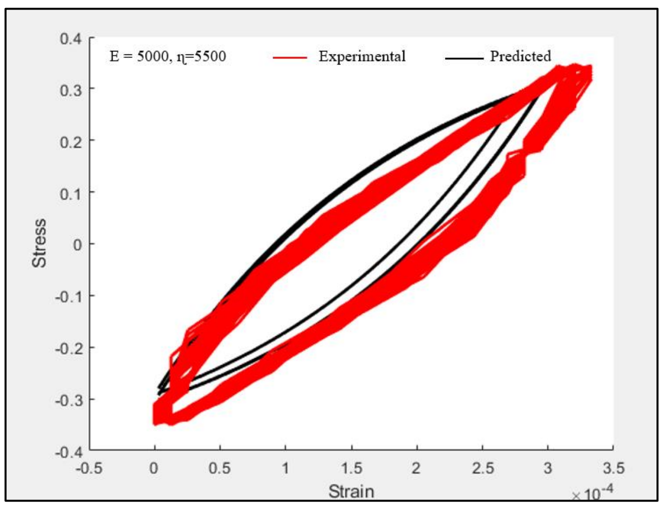

(c)

Figure 5.15 Stress Range vs Strain Hysteresis Loops at a Strain Range of 300micro-strain(a,** $\Sigma\varepsilon = 10 * 10^0$**), (b,** $\Sigma\varepsilon$ **=15 10^0**) & (c) & (c,** $\Sigma\varepsilon$ **= 20*** 10^0 **)***

Figure (5.16) shows the stress versus strain history for the first few cycles of a test predicted by our calibrated model. The model was run at a constant strain range of 400 micro-strain. It shows that the mean stress decreases as cycling proceeds. Figure (5.17) shows the triangle wave stress versus time history given by the Maxwell model predictions for the 400 micro-strain range tests. The mean stress in the cycles decreases to zero as cycling progresses. This behaviour is similar to the test specimen behaviour shown in Figure (5.7).

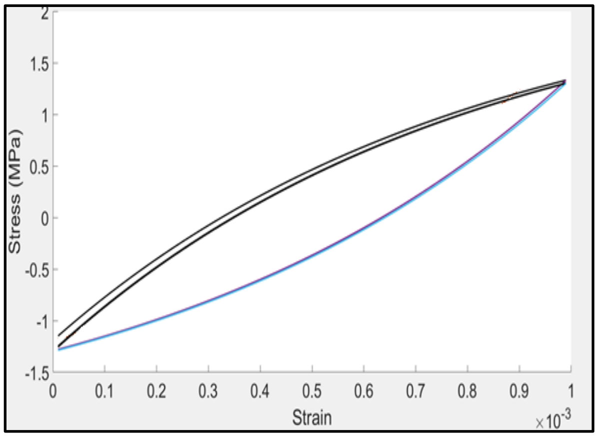

Figure 5.16 Stress Range versus Strain of Bending specimen Predicted by Classic Maxwell Model

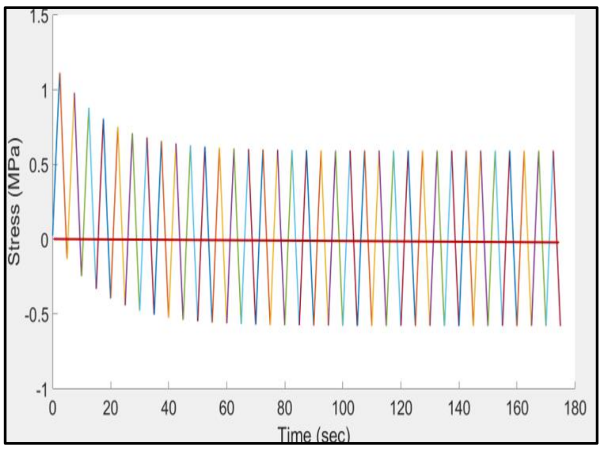

Figure 5.17 Prediction of Stress vs Time for the Classic Maxwell Model (Triangle Wave)

5.2.3 Classic Maxwell Model and the Prediction of Fatigue Life

The classic Maxwell Model was used to predict the fatigue life of mixture-4 (M4), which contained 3% Portland Cement for the tested strain ranges. The failure criterion was that failure occurs when the stiffness of the beam reaches to a value of 50% of its initial stiffness. The calibrated Classic Maxwell Model was used to predict the fatigue life of M4 at 400, 350 and 300 micro-strains as follows:

The initial values of (E_0)and (ɳ0) for M4 shown in Figure (5.13) were used to predict the fatigue lives. These initial values for (E_0) and (ɳ0) were (8633.33) and (10583), respectively. The model was run in strain control at each of the three strain ranges, and the stress range values were recorded. Failure according to our criterion occurred when the stress range reached 50% of its initial value (since the strain range was constant, this corresponds to a 50% reduction in stiffness). Figures (5.18, 5.19 and 5.20) show the stress-strain loops at failure for the three strain levels (400, 350 and 300 micro-strain), respectively.

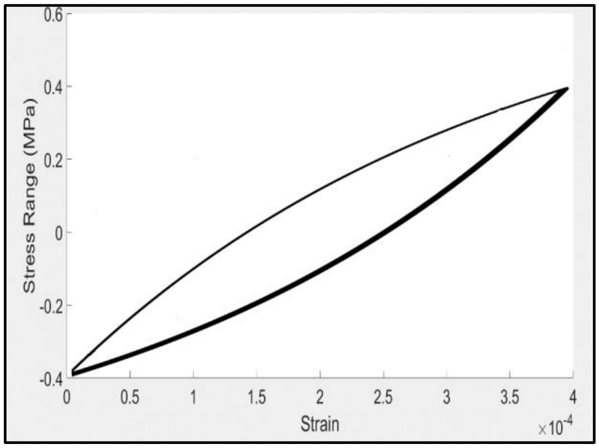

Figure 5.18 The Hysteresis Loop Prediction at for 400 micro-strain

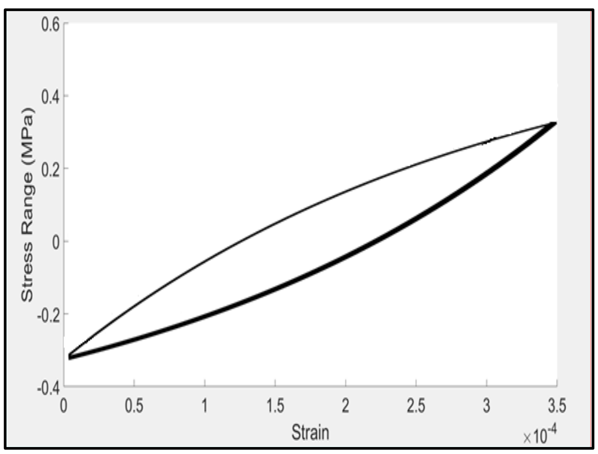

Figure 5.19 The Hysteresis Loop Prediction at for 350 micro-strain

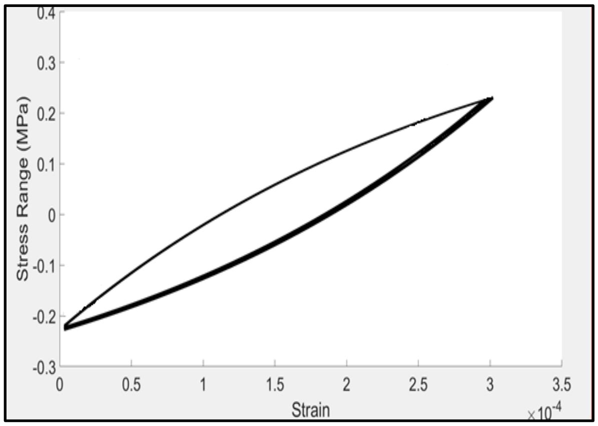

Figure 5.20 The Hysteresis Loop Prediction at for 300 micro-strain

The predicted and experimental fatigue lives are plotted together via strain range versus cycles to failure (at 50% of the initial stiffness) in Figure (5.21).

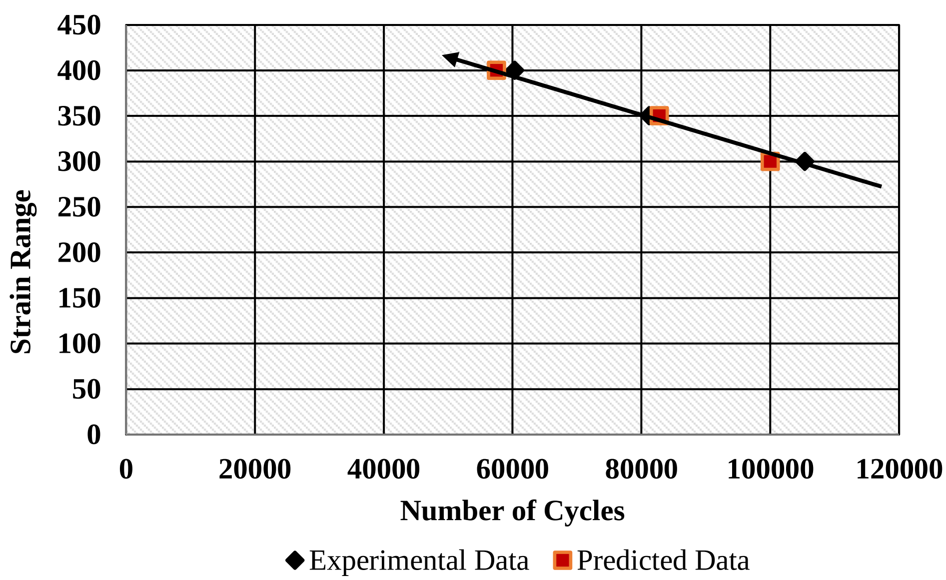

Figure 5.21 Experimental and predicted Fatigue Lives

5.3 Summary

The classic Maxwell Model comprised of a spring and dashpot connected in series was fitted to the asphalt stress-strain hysteresis loops obtained during cyclic straining. The model can be used to predict the behaviour of the asphalt mixtures either in terms of the stress-strain behaviour of our material or the load-displacement relationship of our test specimen. The model was used to predict the stress-time and stress-strain histories of the M4 specimens that contain 3% Portland Cement. Data for a strain range of 400 micro-strain was used to calibrate the model by calculating the Spring stiffness coefficient (E) and dashpot coefficient (η). Calibrations were made at three accumulated strains (Σε) values, and a relationship between the spring and dashpot coefficients and the accumulated strain was obtained. The relationships between the spring and dashpot coefficients and accumulated strain are linear. The coefficients of the spring and dashpot were found by fitting the highest strain 400 micro-strain to match the stress-strain hysteresis loops of the Maxwell model to the experimental data at three levels of accumulated strain, which are (Σε) $= 10 * 10^0$, (Σε) = 15* $10^0$and $(\Sigma\varepsilon) = 20 * 10^0$. Then these coefficients were used to predict the hysteresis loops for 350 and 300 micro-strains. Furthermore, the calibrated maxwell model was used to predict the variation of mean stress with cyclic straining. Also, the model was used the predict the stress and stress-strain histories for our strain-controlled tests. It successfully predicted stress-strain loops for the two tests not used in its calibration (specimens tested under 300 and 350 micro-strain range), the cyclic mean stress relaxation at the beginning of a test and the decrease of stress range with cycling during a test. The latter was used to determine the fatigue life of the specimens based on the criterion that failure occurred when the specimen stiffness had decreased to one-half of its initial value. The predicted lives fell close to the experimental values.

6 Contributions

6.1 Contributions

This research provides a significant number of contributions. The main contribution is to provide a better understanding of the short- and long-term performance and characterization of CIR mixtures that are stabilized with different percentages of Portland Cement. Particularly, the findings will have significant applications in selecting the optimum content of Portland Cement that contributes significantly to the durability of asphalt pavement. Generally, this study is a step towards the enhancement of green roads, in Canada, especially in Ontario, that will be constructed to a level of sustainability that is higher than that of current common practice and provides environmental, economic and social benefits. In addition, it will also provide for technology transfer to promote the goals of sustainable pavements in developing countries of the world. Although the study investigates the performance of CIR and CIREAM in Ontario, other provinces in Canada can potentially benefit from the findings.

6.2 Benefit to Canada

This research will provide significant positive economic and environmental impacts for Canada. Determining the optimum cement content will help increase the load-carrying capacity of the pavement structure by providing early strength, increasing the rutting resistance and reducing the sensitivity of the mixture to moisture. This project will benefit Canada in many aspects, such as:

1- Conservation of non-renewable natural resources through salvaging and reusing both-aggregates and asphalt in existing pavements. For example, in 2003, the cost-saving by MTO in the project trial of CIR and CIREAM versus mill and hot mix asphalt overlay was $20,000 per km over 50 years of predicted LCC.

2- Providing sustainable pavement.

3- Reducing or eliminating the disposal of old distressed pavement materials that are inherent in conventional rehabilitation methods,

4- Full use of the materials in the existing pavement and a zero-waste approach to pavement repair since the entire existing asphalt concrete layer is processed and reused in place without the need for off-site transportation of waste materials. For that reason, haulage is drastically reduced or totally eliminated, and as a result, the overall energy consumption is significantly reduced because of the elimination of greenhouse emissions and the damaging effect of haulage vehicles to roadways in the vicinity of the project site and traffic delays resulting from this increase in construction traffic.

5- Consumes less energy due to the use of in-place construction activities compared to other rehabilitation treatments. The global CO_2 emissions of the asphalt industry will be significantly reduced. The preservation of non-renewable raw materials such as high-quality aggregates is also a very important environmental benefit. Aggregates are used in all the layers of the road structure in addition to their use in several other construction applications. The demand for aggregates increases continuously, and using recycled material to replace natural aggregates is very beneficial.

7 Conclusions and Recommendations

7.1 Conclusions

A total of 96, 32 , 146 and 48 specimens were prepared for indirect tensile strength, Dynamic Modulus, Fatigue and Thermal cracking tests, respectively. The 96 specimens were divided in four groups - M1- M2 - M3 and M4, each of which contained 24 specimens. Then these 24 specimens were split into four groups that contained different Portland Cement Percentages of 0%, 0.5%, 1.5%, and 3% of the total weight of the mixture. For the Dynamic Modulus, the 32 specimens were divided into four groups, M1- M2- M3 and M4, and each group contained amounts of Portland Cement in different percentages of 0%, 0.5%, 1.5%, and 3% of the total weight of the mixture.The 146 fatigue specimens were tested under a four-point bending test setup, and these specimens were split into four groups, M1- M2-M3 and M4 and all of which contained different percentages of Portland Cement 0%, 0.5%, 1.5%, and 3% of the total weight of the mixture. Finally, the 48 thermal cracking beam spcimens were tested to evaluate the thermal behavoiur of the CIR mixtures. The specimens were divided into four groups as well , M1- M2-M3 and M4 and all of them contained different percentages of Portland Cement 0%, 0.5%, 1.5%, and 3% of the total weight of the mixture. The specimens were prepared using pulverized recycled material (HL8 and HL3) that was mixed with the Cationic Slow Setting Emulsion (CSS-1H) and Anionic High Float Emulsion (HF-150). It is concluded that the stiffness of the CIR mixes is strongly affected by the additions of Portland Cement when mixed with (CSS-1H) or (HF-150), and the pulverized aggregate (HL8). However, the higher percentages of Portland Cement (3%) resulted in a noticeable reduction in fatigue life. Fatigue life is negatively impacted by increasing the percentage of Portland Cement due to the development of tensile stresses and shrinkage cracks in the CIR mixtures. Moreover, at 0.5 % to 1.5% Portland Cement additions, there was a noticeable increase in the stiffness with only a small reduction in fatigue life (trade-off relationship). The stiffness of CIR mixtures improved with increasing percentages of Portland Cement content, while the fatigue life is independent of the Portland Cement Content % for the CIR mixtures that were produced by mixing pulverized (Hl3) with (CSS-1H) or (HF-150) as in the mixtures (M3 &M4).

In addition, there was a significant enhancement in the indirect tensile strength, and moisture susceptibility resistance as the % of Portland Cement content increased. However, that had a negative impact on low fracture temperature, as the mixtures tended be more brittle and more likely to develop shrinkage cracks and tensile stress leading to the failure of the mixtures at higher temperatures and lower fracture stresses. Also, all mixtures containing 0.5% Portland Cement fractured at higher stresses than those containing 0%, 1.5%, and 3% Portland Cement. Finally, a classic Maxwell model, a rheological model, which consisted of a spring and dashpot connected in series, was utilized to simulate the stress-strain behaviour of a test specimen. The model, when calibrated, accurately described stress-strain behaviour, including the stress-strain hysteresis loop shape and gave good estimates of the accumulated plastic strain and the number of cycles required for the stiffness and stress range to decrease to one half their initial values, the criterion for failure used in this investigation.

7.2 Recommendations For Future Work

The following future studies to increase our knowledge of the fatigue and stiffness properties of CIR mixture are suggested:

1- Field trial testing should be conducted and compared to laboratory results.

2- Collecting a large set of data (stiffness, fatigue strength and rutting) from different regions of Ontario can also help compare the field performance under different climate regimes.

3- Field testing should be performed for Resilient Modulus, ITS and rutting to examine the stiffness strength, mix deformation and long-term performance.

4- Other cementitious additives such as limestone should be used with CIR and their performance compared with that of Portland Cement.

5- It is recommended that the amount of Portland Cement added to the CIR mixtures should not exceed the amount of the asphalt emulsion added.

6- The addition of Portland Cement content of up to 1.5% increases stiffness strength and improves fracture temperatures with a slight compromise in the fatigue life.

7- It is recommended that the effect of cementitious additives on CIREAM mixes be studied, and the results compared with CIR mixes.

8- It is recommended that curing time be varied to determine its effect on the mechanical behaviour of the CIR mixture.

9- It is recommended to calibrate to model at a variety of temperatures and combinations of materials (Portland Cement fractions)

References

AASHTO. (1993). Standard Test Method for Thermal Stress Restrained Specimen Tensile Strength; AASHTO TP 10-93. Washington DC.

AASHTO. (2007). Standard Method of Test for Determining the Fatigue Life of Compacted Hot-Mix Asphalt (HMA) Subjected to Repeated Flexural Bending; AASHTO T321-07. Washington DC.

AASHTO. (2009). Standard Practice for Developing Dynamic Modulus Master Curves for Hot Mix Asphalt (HMA), AASHTO TP 62-09. Washington DC.

Abiodun, S. (2014). Cold In-Place Recycling with Expanded Asphalt Mix (CIREAM).

Alkins, A., Lane, B., & Komorowska, T. (2008). Sustainable Pavements: Environmental, Economic, and Social Benefits of In Situ Pavement Recycling. Transportation Research Record: Journal of the Transportation Research Board, (2084), 100-103.

Ann Myers, L., Roque, R., & Brisson, B. (2001). Propagation Mechanisms for Surface-Initiated Longitudinal Wheel Path Cracks. Transportation Research Record: Journal of the Transportation Research Board, (1778), 113-122.

ASTM, C. (2006). Standard test method for sieve analysis of fine and coarse aggregates. ASTM C136-06.

ASTM. (2012). Standard Test Method for Indirect Tensile (IDT) Strength of Bituminous Mixtures (2012); ASTM D6931-12. West Conshohocken, PA

ASTM, A. (2015). D6927-15 Standard Test Method for Marshall Stability and Flow of Asphalt Mixtures. ASTM International: West Conshohocken, PA, USA.

ARRA. Full Depth Reclamation [Internet]. Asphalt Recycling and Reclaiming Association; [cited 2017 Jan 25]. Available from: http://www.mdt.mt.gov/publications/docs/brochures/research/toolbox/ARRA/arrafull.pdf

Baaj, H., Di Benedetto, H., & Chaverot, P. (2005). Effect of binder characteristics on fatigue of asphalt pavement using an intrinsic damage approach. Road Materials and Pavement Design, 6(2), 147-174.

Bhavsar, J. (2015). Comparing Cold In-Place Recycling (CIR) and Cold In-Place Recycling with Expanded Asphalt Mixture (CIREAM).

Brayton, T. E., Lee, K. W., Harington, J., & Kearney, E. J. (2001). Characterization of Cold In-Place Recycling Asphalt Mixtures. In Construction and Materials Issues 2001 (pp. 193-205).

Chan, S., Eng, P., Engineer, P. D., Lane, B., Raymond, C., Engineer, S. P. D., & Kazmierowski, T. (2009). Five Year Performance Review of Cold In-Place Recycling and Cold In-place Recycling with Expanded Asphalt Mix on Highway 7, Perth, Ontario. In Annual Conference and Exhibition of the Transportation Association of Canada-Transportation in a Climate of Change (pp. 1-16).

Chesnee, W., Stein, C., Justus, H., Kearney, E., & Cross, S. (2011). Evaluation of Factors Affecting Long-term Performance of Cold in-Place Recycled Pavements in New York State. Transportation Research Record: Journal of the Transportation Research Board, (2227), 13-22.

Clyne, T. R., Li, X., Amratian, M. O., and Skok, E. L. (2003). "Dynamic and resilient modulus of Mn/DOT asphalt mixtures.

Davidson, J. K., Eng, P., & Eng, J. M. C. P. (2003) Best Practices In Cold In-Pace Recycling.

De Larrard, F., & Hu, C. (1993). Conception d'un rhéomètre pour bétons fluides. Bulletin de Liaison des Laboratoires des Ponts et Chaussées, (186).

Franck, A., & Germany, T. I. (1993). Viscoelasticity and dynamic mechanical testing. TA Instruments, New Castle, DE, USA AN004

Goh, S. W., & You, Z. (2011). Moisture Damage and Fatigue Cracking of Foamed Warm Mix Asphalt Using a Simple Laboratory Setup. In Transportation and Development Institute Congress 2011: Integrated Transportation and Development for a Better Tomorrow (pp. 762-771).

Hilton, M. R., & Fleischauer, P. D. (1992). Applications of solid lubricant films in spacecraft. Surface and Coatings Technology, 54, 435-441

International Organization for Standardization, (2008). Buildings and Constructed Assets, Service-life planning Part 5: Life-cycle Costing (ISO 15686-5), Geneva, Switzerland: International Organization for Standardization.

Jannat, G. E., & Tighe, S. L. (2015). Performance based evaluation of overall pavement condition indices for Ontario highway systems. In TAC 2015: Getting You There Safely-2015 Conference and Exhibition of the Transportation Association of Canada//ATC: Destination sÃ© curitÃ© routiÃ¨ re-2015 CongrÃ¨ s et Exposition de l'Association des transports du Canada.

Jhansale, H. R., & Topper, T. H. (1971). Cyclic Deformation and Fatigue Behaviour of Axial and Flexural Members-A Method of Simulation and Correlation.

Jitareekul, P., & BEng, M. (2009). An Investigation into Cold In-Place Recycling of Asphalt Pavements.

Johnson, A. M. (2000). Best practices handbook on asphalt pavement maintenance (No. MN/RC-2000-04).

Kavussi, A., & Modarres, A. (2010). Laboratory Fatigue Models for Recycled Mixes with Bitumen Emulsion and Cement. Construction and Building Materials, 24(10), 1920-1927.

Kavussi, A., & Modarres, A. (2010). A Model for Resilient Modulus Determination of Recycled Mixes with Bitumen Emulsion and Cement from ITS Testing Results. Construction and Building Materials, 24(11), 2252-2259.

Kazmierowski, T., Marks, P., & Lee, S. (1999). Ten-year Performance Review of In-Situ Hot-Mix Recycling in Ontario. Transportation Research Record: Journal of the Transportation Research Board, (1684), 194-202.

Kearney, E., & Huffman, J. (1999). Full-depth Reclamation Process. Transportation Research Record: Journal of the Transportation Research Board, (1684), 203-209.

Kelly, P. (2014). Solid mechanics part I. I: An Introduction to Solid Mechanics.

Lane, B., & Kazmierowski, T. (2005). Guidelines for the Use of Life Cycle Cost Analysis on MTO Freeway Projects. Ministry of Transportation, Engineering Standards Branch, Materials Engineering & Research Office.

Lane, B., & Kazmierowski, T. (2005). Implementation of Cold In-Place Recycling with Expanded Asphalt Technology in Canada. Transportation Research Record: Journal of the Transportation Research Board, (1905), 17-24.

Lane, B., & Lee, W. (2014). Comparing 10 Year Performance of Cold In-Place Recycling (CIR) with Emulsion versus CIR with Expanded Asphalt on Highway 7, Perth, Ontario. Transportation Association of Canada.

Lewis, A. J. N., & Collings, D. C. (1999). Cold In-Place Recycling: A Relevant Process for Road Rehabilitation and Upgrading. In CAPSA 99, 7 th Conference on Asphalt Pavements for Southern Africa (pp. 1-11).

Mallick, R., Kandhal, P., & Bradbury, R. (2008). Using Warm-Mix Asphalt Technology to Incorporate High Percentage of Reclaimed Asphalt Pavement Material in Asphalt Mixtures. Transportation Research Record: Journal of the Transportation Research Board, (2051), 71-79.

Mallick, R., Bonner, D., Bradbury, R., Andrews, J., Kandhal, P., & Kearney, E. (2002). Evaluation of Performance of Full-depth Reclamation Mixes. Transportation Research Record: Journal of the Transportation Research Board, (1809), 199-208.

Mallick, R., Teto, M., Kandhal, P., Ray Brown, E., Bradbury, R., & Kearney, E. (2002). Laboratory Study of Full-depth Reclamation Mixes. Transportation Research Record: Journal of the Transportation Research Board, (1813), 103-110.

Manfredi, G. (2001). Evaluation of seismic energy demand. Earthquake engineering & structural dynamics, 30(4), 485-499.

Marasteanu, M. O., Clyne, T. R., Li, X., & Skok, E. L. (2003). Dynamic and Resilient Modulus of Mn/DOT Asphalt Mixtures.

Marasteanu, M. O., Li, X., Clyne, T. R., Voller, V., Timm, D. H., & Newcomb, D. (2004). Low Temperature Cracking of Asphalt Concrete Pavement.

Marasteanu, M., Zofka, A., Turos, M., Li, X., Velasquez, R., Li, X., ... & McGraw, J. (2007). Investigation of low temperature cracking in asphalt pavements national pooled fund study 776.

Martin, J.F., Topper, T.H. and Sinclair, G.M., (1971). "Computer Bused Simulation of Cyclic Stress-Strain Behaviour with Applications to fatigue, " Materials Research and Standards, MTRSA,Vol, 11, N0 2, p,23

Masing, G. (1926). Eigenspannumyen und verfeshungung beim messing. In Proc. Inter. Congress for Applied Mechanics (pp. 332-335)

Mo, L., Li, X., Fang, X., Huurman, M., & Wu, S. (2012). Laboratory Investigation of Compaction Characteristics and Performance of Warm mix Asphalt Containing Chemical Additives. Construction and Building Materials, 37, 239-247.

Modarres, A., Nejad, F. M., Kavussi, A., Hassani, A., & Shabanzadeh, E. (2011). A Parametric Study on the Laboratory Fatigue Characteristics of Recycled Mixes. Construction and Building Materials, 25(4), 2085-2093.

Moore, K. D. (2004). Foamed Asphalt Gains New Attention in Cold In-Place Recycling. Better Roads, 74(7).

MTO-LS. (1996). Preparation of Marshall Specimens for Cold In-Place Recycled Mixtures; MTO LS-300.Ontario.

MTO-LS. (1999). Bulk Relative Density of Compacted Bituminous Mixes; MTO LS-262. Ontario

MTO-LS. (2009). Quantitative Extraction of Asphalt Cement and Analysis of Extracted Aggregate from Bituminous Paving Mixtures; MTO LS-282. Ontario.

MTO-LS. (2012). Theoretical Maximum Relative Density of Bituminous Paving Mixtures; MTO LS-264. Ontario.

Ministry of Transportation of Ontario. Pavement Design and Rehabilitation Manual. Second Ed. Ontario, Canada: Materials Engineering and Research Office, Ministry of Transportation of Ontario; 2013.

Ministry of Transportation of Ontario. Ontario’s Default Parameters for AASHTOWare Pavement ME Design-Interim Report 2019.pdf [Internet]. 2019 [cited 2019 Sep 11]. Available from: https://www.raqsb.mto.gov.on.ca/login/raqs.nsf/f7655a6959db3dd785256c1d0073eb7b/4365876106ab3bea85258411006bf14a/$FILE/ATTVSW69/Ontario's%20Default%20Parameters%20for%20AASHTOWare%20Pavement%20ME%20Design-Interim%20Report%202019.pdf

Muhit, I. B., Raihan, M. T., & Nuruzzaman, M. D. (2014). Determination of mortar strength using stone dust as a partially replaced material for cement and sand. Advances in concrete construction, 2(4), 249.

Mun, S., Guddati, M., & Richard Kim, Y. (2004). Fatigue Cracking Mechanisms in Asphalt Pavements with Viscoelastic Continuum Damage Finite-Element Program. Transportation Research Record: Journal of the Transportation Research Board, (1896), 96-106.

Niazi, Y., & Jalili, M. (2009). Effect of Portland Cement and Lime Additives on Properties of Cold In-Place Recycled Mixtures with Asphalt Emulsion. Construction and Building Materials, 23(3), 1338-1343.

Ontario Provincial Standard Specification (OPSS 331), (2007), No author given, “Construction Specification for Cold In-place Recycling,” Ministry of Transportation Ontario.

Ontario Provincial Standard Specification (OPSS 333), (2007), No author given, “Construction Specification for Cold In-place Recycling,” Ministry of Transportation Ontario.

Onyango, M. A. (2009). "Verification of mechanistic prediction models for permanent deformation in asphalt mixes using accelerated pavement testing."

Read, J., & Whiteoak, D. (2003). The Shell Bitumen Handbook. Thomas Telford.

Recycling, A., Reclaiming Association, & Dunn, L. (2001). Basic asphalt recycling manual. Asphalt Recycling and Reclaiming Association.

Romanoschi, S. A., Hossain, M., Heitzman, M., & Gisi, A. J. (2003, August). Foamed Asphalt Stabilized Reclaimed Asphalt Pavement: A promising technology for Mid-western roads. In Proceedings of the 2003 Mid-Continent Transportation Research Symposium, Ames, IA.

Salomon, A., & Newcomb, D. E. (2000). Cold In-Place Recycling Literature Review and Preliminary Mixture Design Procedure (No. MN/RC-2000-21).

Shaheen, M. (2016). Evaluation of X-Ray Computed Tomography and Finite Element Models for Fatigue Experimental Hot Mix Asphalt Characterization (Doctoral dissertation, University of Waterloo).

Shivakumar, K. N., & Crews Jr, J. H. (1987). Energy dissipation associated with crack extension in an elastic-plastic material. Engineering fracture mechanics, 28(3), 319-330.

Sucuoglu, H., & Erberik, M. A. (2004, September). Evaluation of inelastic displacements in deteriorating systems using an energy-based approach. In Proceedings of the international workshop Bled, Slovenia, PEER report (No. 2004/05, pp. 421-433).

Tighe, S.(2001). Guidelines for Probabilistic Pavement Life Cycle Cost Analysis. Transportation Research Record: Journal of the Transportation Research Board, (1769), 28-38.

Transportation Association of Canada [TAC] (2013), Pavement Design and Management Guide ,Ottawa, Ontario, 2013.

Turner, C. E., & Kolednik, O. (1994). Application of energy dissipation rate arguments to stable crack growth. Fatigue & Fracture of Engineering Materials & Structures, 17(10), 1109-1127.

Williams, D. P., Lind, N. C., Conle, A., Topper, T. H., & Leis, B. N. (1977). Structural cyclic deformation response modelling. Mechanics in engineering, 291-311.Williams, D. P., & Topper, T. H. (1981). A generalized model of structural reversed plasticity. Experimental Mechanics, 21(4), 145-154.

Wirtgen. (2004). Wirtgen Cold Recycling Manual (2nd).Windhagen, Germany: Wirtgen Group.

Wirtgen. (2012). Wirtgen Cold Recycling Manual (2nd).Windhagen, Germany: Wirtgen Group.

Witczak, M. W. (2005). Simple Performance Tests: Summary of Recommended Methods and Database (Vol. 46). Transportation Research Board.

Wirtgen. Cold Recycling: Wirtgen Cold Recycling Technology [Internet]. 3rd ed. Germany: Wirtgen GmbH; 2010 [cited 2017 Jan 25]. Available from: http://media.wirtgengroup.com/media/02_wirtgen/infomaterial_1/kaltrecycler/kaltrecycling_technologie/kaltrec cycling handbuch/Kaltrecycling_Handbuch_EN.pdf

Zaoutsos, S. P., & Papanicolaou, G. C. (2011). Viscoelastic constitutive modeling of creep and stress relaxation in polymer and polymer matrix composites. Creep and fatigue in polymer matrix composites, Woodhead publishing in Materials, Pennsylvania, 1-45.

Appendices

Appendix-I

Data Sheet

PRODUCT DATA SHEET

PDS 03.02.20 P

CSS-1H

CATIONIC SLOW-SETTING HARD-PENETRATION ASPHALT EMULSION

PRODUCT DESCRIPTION

CSS-1H is a slow-setting cationic asphalt emulsion that is designed for various paving and industrial uses.

Asphalt emulsions are classified according to the electric charge that surrounds the emulsion's asphalt particles (i.e. whether it is a cationic or an anionic emulsion) and how quickly the suspended asphalt particles separate from the surrounding water ("breaking"). A slow-setting emulsion is designed to maximize the mixing time with aggregates. Longer workability times ensure a good coating on dense-graded aggregates with a high fines content. The setting speed of any emulsion is relative to atmospheric conditions at the time of construction.

RECOMMENDED USE

CSS-1H can be used for tack coats, fog seals, and as a dust suppressant. Long workability times make it ideal for dense-graded emulsion base mixes and base stabilization. Other uses include the mulch treatment of soil that has been seeded and fertilized.

TEMPERATURE VISCOSITY CHART

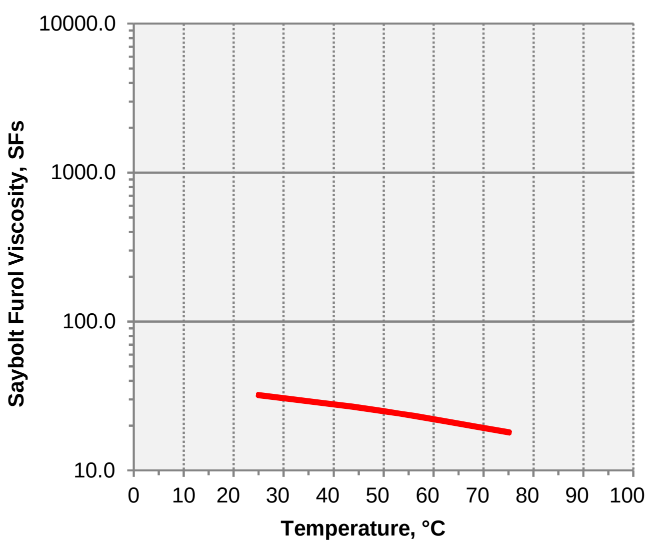

SPECIFICATIONS AND TYPICAL RESULTS

TEST	TYPICAL DATA	SPEC. Min	SPEC. Max
Tests on Emulsion			
SF Viscosity, 25°C, SFs	**28**	20	100
Sieve Test, 850 µm, %	**0.04**	-	0.1
Settlement, 5 days, %	**1.3**	-	5.0
Distillation Residue, 260°C, %	**60.8**	57	-
Oil Portion of Distillation, %	**trace**	-	5
Particle Charge	**(+)**	(+)	
Tests on Residue			
Penetration, 25°C, dmm	**65**	40	125
Solubility in TCE, %	**99.55**	97.5	-
Ductility, 25°C, cm	**64.5**	40	-

PACKAGING, STORAGE AND HANDLING

- **CSS-1H** should be stored in bulk tanks, ideally vertical to minimize surface area.
- Do not allow **CSS-1H** to either freeze or boil: it will break. Safe storage temperatures range from 10°C (50°F) to 85°C (185°F).
- In bulk storage, mix the **CSS-1H** every 1 to 2 weeks (more frequently in cold weather). Mixing may be done by paddle agitator (slow), loose gear pump, slow centrifugal pump, or other suitable low shear pump.
- Do not bubble air through **CSS-1H** to agitate it: this creates excessive foam and may cause the **CSS-1H** to break.
- Always use clean storage containers. Make sure prior contents are compatible with **CSS-1H** or the emulsion may break.
- Only use approved and sealed containers for sampling the emulsion.

PRODUCT DATA SHEET

PDS 03.02.20 P

CSS-1H

CATIONIC SLOW-SETTING HARD-PENETRATION ASPHALT EMULSION

APPLICATION GUIDELINES

- May be further diluted with potable water up to a maximum of 50%
- Do not dilute product with any cutter stock.
- Do not apply **CSS-1H** if precipitation is anticipated.
- Contact your local ***MCA*** **Marketing** representative for application temperature guidelines.

TACK COATS

CSS-1H applied to an existing pavement surface will eliminate slippage planes and provide a bond with the new asphalt lift. It will deliver a strong bond and it will not track under construction traffic. Spray rates range from 0.25 to 0.70 L/m^2 (0.05 to 0.15 gal/yd^2).

FOG SEALS

CSS-1H is applied to an existing asphalt surface that has become oxidized with age in order to renew it and to seal narrow cracks and surface voids. Because of its quick cure and non-tracking properties, conventional sand blotting is often not required. Spray rates range from 0.45 to 0.70 L/m^2 (0.10 to 0.15 gal/yd^2) depending on the surface texture and degree of cracking.

DUST CONTROL

CSS-1H is ideal for spraying on low volume, unpaved roads as a means of dust control. This emulsion is usually diluted with water to further decrease its viscosity in order to enhance its penetration into the existing surface. The diluted **CSS-1H** is sprayed in repeated light applications at a rate of 0.45 to 2.25 L/m^2 (0.1 to 0.5 gal/yd^2) depending on the condition of the existing surface.

DENSE-GRADED EMULSION MIXES

Dense-graded emulsion mixes are produced at a central plant or in-place by mixing **CSS-1H** using dense-graded aggregates with a relatively high fines content. **CSS-1H** provides a mix that is workable on the job site immediately after mixing or when the mix is produced at a plant and trucked to the site. Application rates will vary depending on aggregate type and gradation. A mix design is highly recommended.

BASE STABILIZATION

Base stabilization is an in situ rehabilitation process for pavements composed of asphalt concrete over a granular base. The process involves the pulverization of asphalt concrete and mixing it with the base course. This is followed by the stabilization of the resulting granular material with **CSS-1H**. A mix design is highly recommended to determine the appropriate asphalt emulsion content.

CERTIFICATION OF QUALITY

McAsphalt Industries Limited is accredited to the quality management standard **ISO 9001**, the environmental management standard **ISO 14001,** and the occupational health and safety standard **ISO 45001**.

Each lot of **CSS-1H** is produced using the strictest quality, safety, and environmental guidelines. Each production lot is tested to ensure it meets or exceeds all performance requirements and is delivered with a Certificate of Analysis.

PRODUCT SUPPORT

With the ***MCA*** **Advantage**, you get a partner and advisor who will consult with you about designs, specifications, technical services, processes, and material selection. By developing innovative, custom-designed products that offer additional benefits such as peak performance in unique conditions, improved field performance, and greater environmental and health benefits, the ***MCA*** **Advantage** provides significant long-term cost savings, resulting in lower total cost of ownership.

PRODUCT DATA SHEET

PDS 03.02.20 P

HF-150S

ANIONIC HIGH-FLOAT SPRAY-GRADE ASPHALT EMULSION

PRODUCT DESCRIPTION

HF-150S is a high-float, spray-grade asphalt emulsion that is designed to be used in surface treatments.

Asphalt emulsions are classified according to the electric charge that surrounds the emulsion's asphalt particles (i.e. whether it is a cationic or an anionic emulsion) and how quickly the suspended asphalt particles separate from the surrounding water ("breaking"). **HF-150S** is designed to allow some mixing and aggregate wetting time but also to break and cure faster than a slow-setting emulsion.

A high-float (HF) emulsion creates a gel-like structure in the asphalt residue after the water evaporates. This permits a thicker asphalt film on the aggregate without the danger of runoff, resulting in better aggregate coating and lower moisture susceptibility. The thicker asphalt film will create mixes and surface treatments with higher durability and longer lifespans. High-float emulsions also confer a reduced temperature susceptibility (i.e. better resistance to rutting and cracking).

GENERAL PRODUCT FEATURES

- "High-float" gel structure allows for the spraying of thicker emulsion films without the risk of runoff.
- Allows the usage of graded aggregate for surface treatments, meaning inexpensive but high performing surfacing
- Allows the use of anti-stripping agents to improve moisture resistance and improve bonds with difficult aggregates
- Thicker asphalt films on aggregate surfaces means more durable mixes and better resistance to long-term aging.
- Produces adequate wetting and good contact with fine aggregates while providing good adhesion to substrates, whether they are asphalt or granular

RECOMMENDED USE

HF-150S emulsions are ideal for use in surface treatments using graded aggregate. Their high wetting power and gel structure combined with the relatively quick cure allows for a good bond to substrate as well as a strong but flexible grip on the cover aggregate. **HF-150S** emulsion is ideal for surface treatments using graded aggregate or aggregate with high fines content. It is less well suited for clean or washed chip.

SPECIFICATIONS AND TYPICAL RESULTS

TEST	TYPICAL DATA	SPEC. Min	SPEC. Max
Tests on Emulsion			
SF Viscosity, 50°C, SFs	**85**	35	150
Sieve Test, 850 µm, %	**0.01**	-	0.1
Storage Stability, 24 h, %	**0.6**	-	1.5
Distillation Residue, 260°C, %	**65**	62	-
Oil Portion of Distillation, %	**1.5**	0.5	4
Demulsibility, 50 ml 0.1 N $CaCl_2$, %	**85**	75	-
Particle Charge	**(-)**	(-)	
Tests on Residue			
Penetration, 25°C, dmm	**185**	150	250
Apparent Viscosity, 60°C, Pa.s	**175**	Function of pen.	
Float, 60°C, sec	**1200+**	1200	-
Solubility in TCE, %	**99.75**	97.5	-

TEMPERATURE VISCOSITY CHART

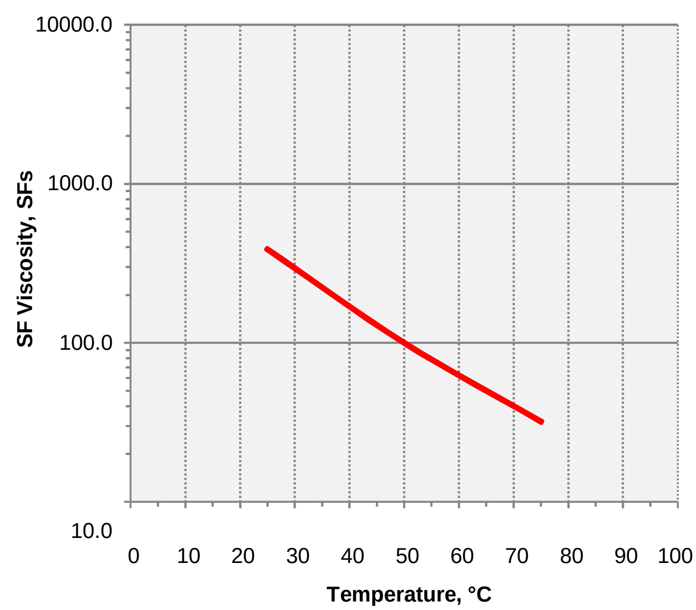

PRODUCT DATA SHEET

PDS 03.02.20 P

HF-150S

ANIONIC HIGH-FLOAT SPRAY-GRADE ASPHALT EMULSION

APPLICATION GUIDELINES

- Do not apply if precipitation is anticipated.
- Do not dilute product with any cutter stock or water.

DESIGN GUIDELINES

Mix designs should be formulated prior to initial construction and each time aggregate sources are changed. Testing of the final product is highly recommended to ensure a quality mix or seal. ***MCA*** **Technical Services** offer complete mix design service and product quality analysis.

CHIP SEALS/SURFACE TREATMENTS

HF-150S is ideally mixed with graded aggregate typically all passing the 16 mm (5/8 in) or 12.5 mm (½ in) sieve, with 60–70% passing the 4.75 mm (no. 4) sieve and preferably not more than 6% passing the 0.075 mm (no. 200) sieve. Graded aggregate is an alternative to the more expensive, single-sized cover stone chip.

PACKAGING, STORAGE AND HANDLING

- **HF-150S** should be stored in bulk tanks, ideally vertical to minimize surface area.
- Do not allow **HF-150S** to either freeze or boil: it will break. Safe storage temperatures range from 10°C (50°F) to 85°C (185°F).
- In bulk storage, mix the **HF-150S** every 1 to 2 weeks (more frequently in cold weather). Mixing may be done by paddle agitator (slow), loose gear pump, slow centrifugal pump, or other suitable low shear pump.
- Do not bubble air through **HF-150S** to agitate it: this creates excessive foam and may cause the **HF-150S** to break.
- Always use clean storage containers. Make sure prior contents are compatible with **HF-150S** or the emulsion may break.
- Only use approved and sealed containers for sampling the emulsion.

CERTIFICATION OF QUALITY

McAsphalt Industries Limited is accredited to the quality management standard **ISO 9001**, the environmental management standard **ISO 14001,** and the occupational health and safety standard **ISO 45001**.

Each lot of **HF-150S** is produced using the strictest quality, safety, and environmental guidelines. Each production lot is tested to ensure it meets or exceeds all performance requirements and is delivered with a Certificate of Analysis.

PRODUCT SUPPORT

With the ***MCA*** **Advantage**, you get a partner and advisor who will consult with you about designs, specifications, technical services, processes, and material selection. By developing innovative, custom-designed products that offer additional benefits such as peak performance in unique conditions, improved field performance, and greater environmental and health benefits, the ***MCA*** **Advantage** provides significant long-term cost savings, resulting in lower total cost of ownership.

Appendix-II

ANOVA Analysis

Regression Statistics	M1(Dry)				
Multiple R	0.96264356				
R Square	0.926682623				
Adjusted R Square	0.890023935				
Standard Error	0.438700483				
Observations	4				
ANOVA	df	SS	MS	F	Significance F
Regression	1	4.865083772	4.865083772	25.27866283	0.03735644
Residual	2	0.384916228	0.192458114		
Total	3	5.25			

Regression Statistics	M1(Wet)				
Multiple R	0.977939168				
R Square	0.956365016				
Adjusted R Square	0.934547524				
Standard Error	0.338440294				
Observations	4				
ANOVA	df	SS	MS	F	Significance F
Regression	1	5.020916335	5.020916335	43.83478261	0.022060832
Residual	2	0.229083665	0.114541833		
Total	3	5.25			

Regression Statistics	M2 (Dry				
Multiple R	0.968541				
R Square	0.938072				
Adjusted R Square	0.907108				
Standard Error	0.403189				
Observations	4				
ANOVA	df	SS	MS	F	Significance F
Regression	1	4.924878	4.924878	30.29557	0.031459
Residual	2	0.325122	0.162561		
Total	3	5.25			

Regression Statistics	M2(Wet)				
Multiple R	0.919589				
R Square	0.845645				
Adjusted R Square	0.768467				
Standard Error	0.63654				
Observations	4				
ANOVA	df	SS	MS	F	Significance F
Regression	1	4.439634	4.439634	10.95711	0.080411
Residual	2	0.810366	0.405183		
Total	3	5.25			

Regression Statistics	M3(Dry)				
Multiple R	0.995306				
R Square	0.990634				
Adjusted R Square	0.98595				
Standard Error	0.156801				
Observations	4				
ANOVA	df	SS	MS	F	Significance F
Regression	1	5.200827	5.200827	211.5305	0.004694
Residual	2	0.049173	0.024587		
Total	3	5.25			

Regression Statistics	M3(Wet)				
Multiple R	0.998498				
R Square	0.996999				
Adjusted R Square	0.995498				
Standard Error	0.088762				
Observations	4				
ANOVA	df	SS	MS	F	Significance F
Regression	1	5.234243	5.234243	664.3547	0.001502
Residual	2	0.015757	0.007879		
Total	3	5.25			

Regression Statistics	M4(Dry)				
Multiple R	0.905558				
R Square	0.820036				
Adjusted R Square	0.730053				
Standard Error	0.687319				
Observations	4				
ANOVA	df	SS	MS	F	Significance F
Regression	1	4.305186	4.305186	9.113304	0.094442
Residual	2	0.944814	0.472407		
Total	3	5.25			

Regression Statistics	M4(Wet)				
Multiple R	0.985567				
R Square	0.971341				
Adjusted R Square	0.957012				
Standard Error	0.274279				
Observations	4				
ANOVA	df	SS	MS	F	Significance F
Regression	1	5.099542	5.099542	67.78696	0.014433
Residual	2	0.150458	0.075229		
Total	3	5.25			

Appendix-III

Sample AASHTOWare Pavement ME Outputs

LVR_400AADT_CIR_0%-12 years December 2019

File Name: C:\Users\admin\Desktop\Taha M2\LVR_400AADT_CIR_0%-12 years December 2019.dgpx

Design Inputs

Design Life: 12 years

Design Type: FLEXIBLE

Base construction: May, 2020

Pavement construction: June, 2021

Traffic opening: September, 2021

Climate Data Sources (Lat/Lon): 44, -78.75

Design Structure

Layer type	Material Type	Thickness(mm)
Flexible	Default asphalt concrete	50.0
Flexible	Default asphalt concrete	100.0
NonStabilized	A-1-a	150.0
NonStabilized	A-1-b	400.0
Subgrade	A-6	Semi-infinite

Volumetric at Construction:	
Effective binder content (%)	11.8
Air voids (%)	7.0

Traffic

Age (year)	Heavy Trucks (cumulative)
2021 (initial)	400
2027 (6 years)	424,055
2033 (12 years)	919,115

Design Outputs

Distress Prediction Summary

Distress Type	Distress @ Specified Reliability		Reliability (%)		Criterion Satisfied?
	Target	Predicted	Target	Achieved	
Terminal IRI (m/km)	2.70	1.76	75.00	99.83	Pass
Permanent deformation - total pavement (mm)	17.00	8.05	75.00	100.00	Pass
AC bottom-up fatigue cracking (percent)	35.00	0.76	75.00	100.00	Pass
AC thermal cracking (m/km)	190.00	21.65	75.00	100.00	Pass
AC top-down fatigue cracking (m/km)	380.00	243.19	75.00	86.47	Pass
Permanent deformation - AC only (mm)	6.00	0.49	75.00	100.00	Pass

Distress Charts

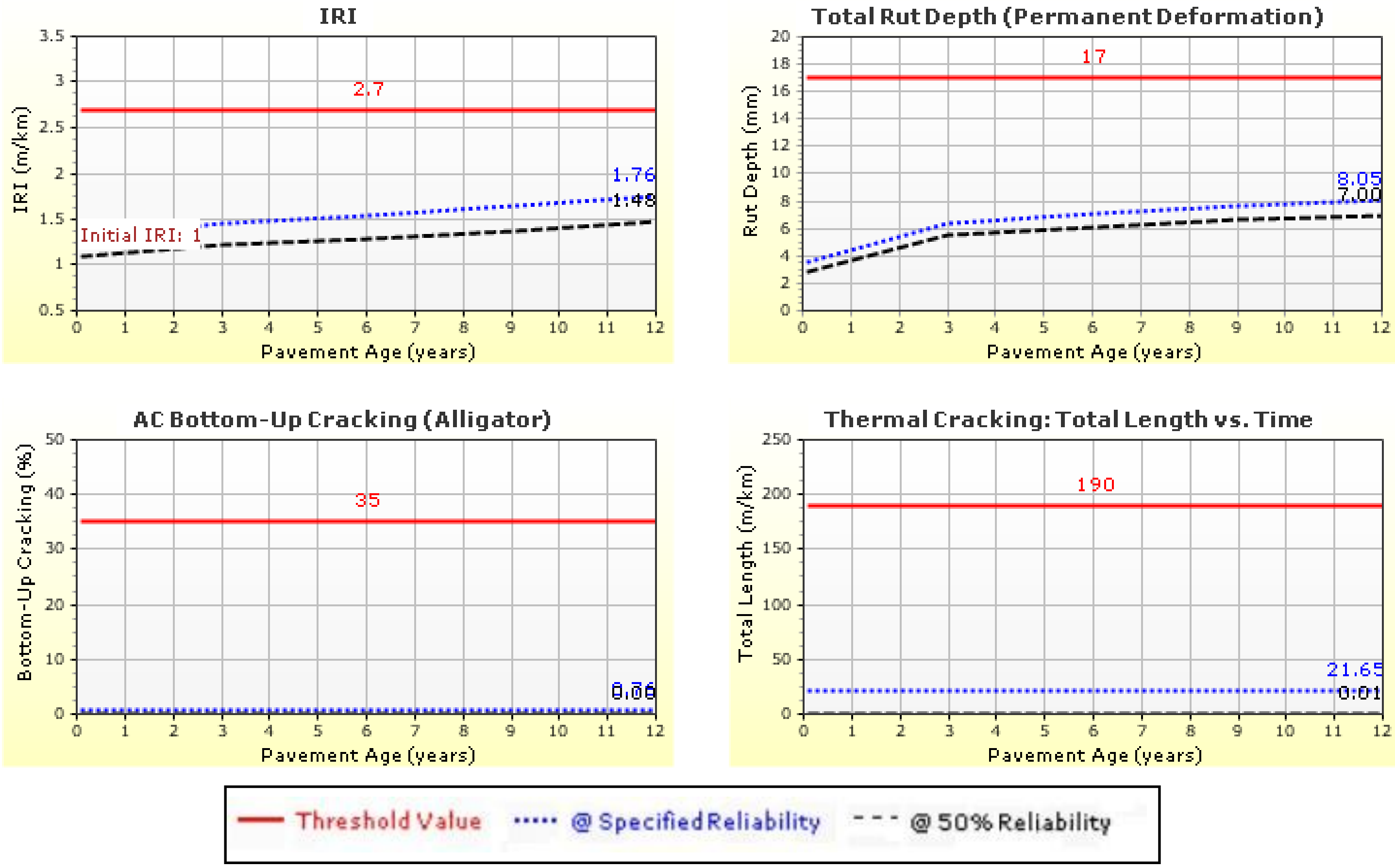

LVR_400AADT_CIR_0%-12 years December 2019

File Name: C:\Users\admin\Desktop\Taha M2\LVR_400AADT_CIR_0%-12 years December 2019.dgpx

Traffic Inputs

Graphical Representation of Traffic Inputs

Initial two-way AADTT:	400	Percent of trucks in design direction (%):	50.0
Number of lanes in design direction:	2	Percent of trucks in design lane (%):	90.0
		Operational speed (kph)	80.0

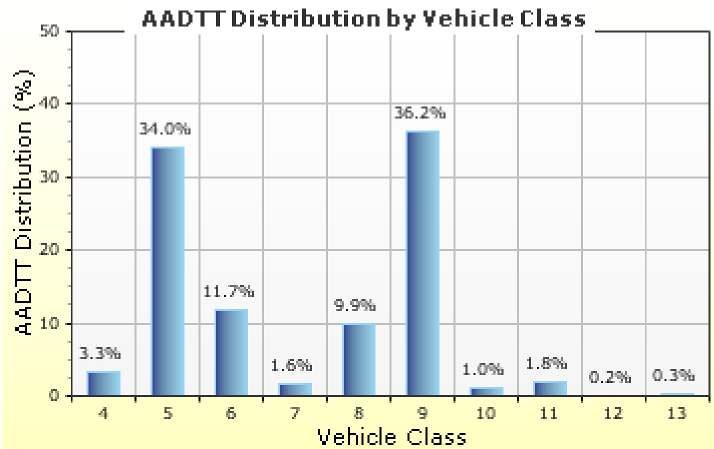

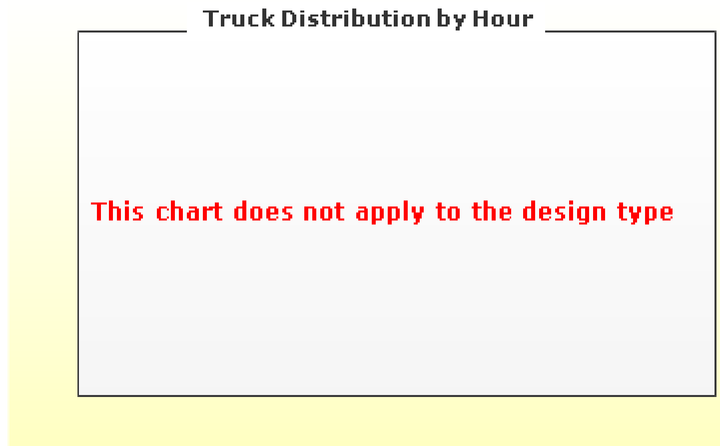

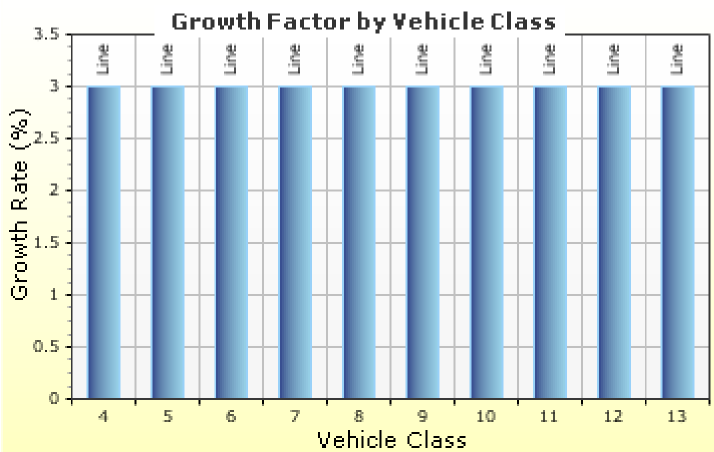

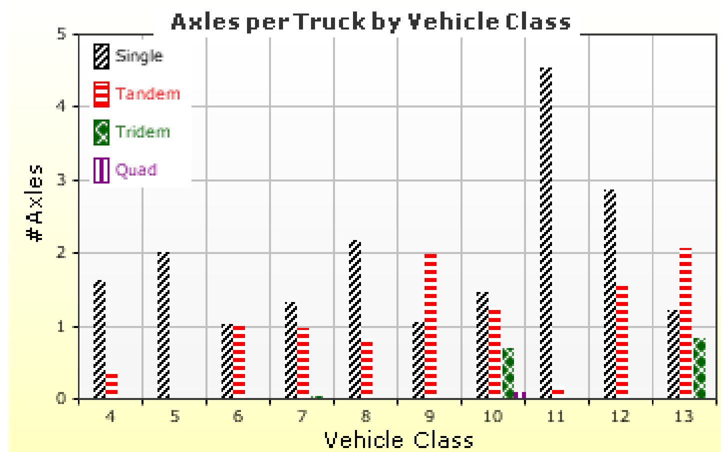

Traffic Volume Monthly Adjustment Factors

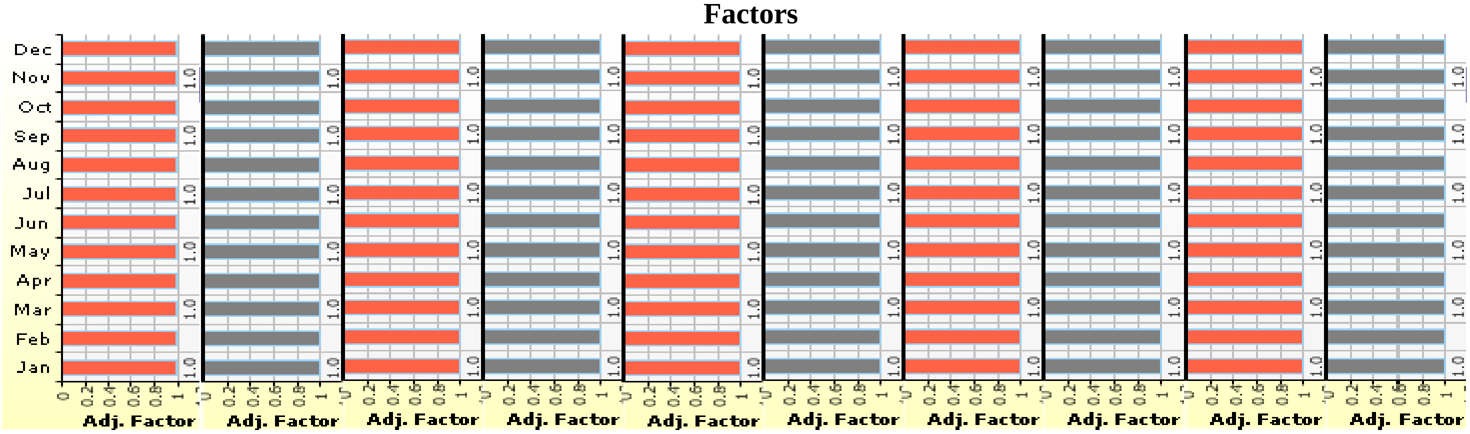

Tabular Representation of Traffic Inputs

Volume Monthly Adjustment Factors

evel 3: Default MAF

Month	Vehicle Class									
	4	5	6	7	8	9	10	11	12	13
January	1.0	1.0	1.0	1.0	1.0	1.0	1.0	1.0	1.0	1.0
February	1.0	1.0	1.0	1.0	1.0	1.0	1.0	1.0	1.0	1.0
March	1.0	1.0	1.0	1.0	1.0	1.0	1.0	1.0	1.0	1.0
April	1.0	1.0	1.0	1.0	1.0	1.0	1.0	1.0	1.0	1.0
May	1.0	1.0	1.0	1.0	1.0	1.0	1.0	1.0	1.0	1.0
June	1.0	1.0	1.0	1.0	1.0	1.0	1.0	1.0	1.0	1.0
July	1.0	1.0	1.0	1.0	1.0	1.0	1.0	1.0	1.0	1.0
August	1.0	1.0	1.0	1.0	1.0	1.0	1.0	1.0	1.0	1.0
September	1.0	1.0	1.0	1.0	1.0	1.0	1.0	1.0	1.0	1.0
October	1.0	1.0	1.0	1.0	1.0	1.0	1.0	1.0	1.0	1.0
November	1.0	1.0	1.0	1.0	1.0	1.0	1.0	1.0	1.0	1.0
December	1.0	1.0	1.0	1.0	1.0	1.0	1.0	1.0	1.0	1.0

Distributions by Vehicle Class

Truck Distribution by Hour does not apply

Vehicle Class	AADTT Distribution (%)(Level 3)	Growth Factor	
		Rate (%)	Function
Class 4	3.3%	3%	Linear
Class 5	34%	3%	Linear
Class 6	11.7%	3%	Linear
Class 7	1.6%	3%	Linear
Class 8	9.9%	3%	Linear
Class 9	36.2%	3%	Linear
Class 10	1%	3%	Linear
Class 11	1.8%	3%	Linear
Class 12	0.2%	3%	Linear
Class 13	0.3%	3%	Linear

Vehicle Class	Single Axle	Tandem Axle	Tridem Axle	Quad Axle
Class 4	1.62	0.39	0	0
Class 5	2	0	0	0
Class 6	1.01	0.993	0	0
Class 7	1.314	0.989	0.03	0
Class 8	2.163	0.845	0	0
Class 9	1.055	1.968	0.003	0
Class 10	1.446	1.234	0.7	0.088
Class 11	4.546	0.168	0	0
Class 12	2.857	1.526	0	0
Class 13	1.201	2.058	0.848	0.024

Average Axle Spacing	
Tandem axle spacing (m)	[illegible]
Tridem axle spacing (m)	1.7
Quad axle spacing (m)	1.3

Wheelbase does not apply

Traffic Wander	
Mean wheel location (mm)	460.0
Traffic wander standard deviation (mm)	254.0
Design lane width (m)	3.7

Axle Configuration	
Average axle width (m)	2.6
Dual tire spacing (mm)	305.0
Tire pressure (kPa)	827.4

AADTT (Average Annual Daily Truck Traffic) Growth

*** Traffic cap is not enforced**

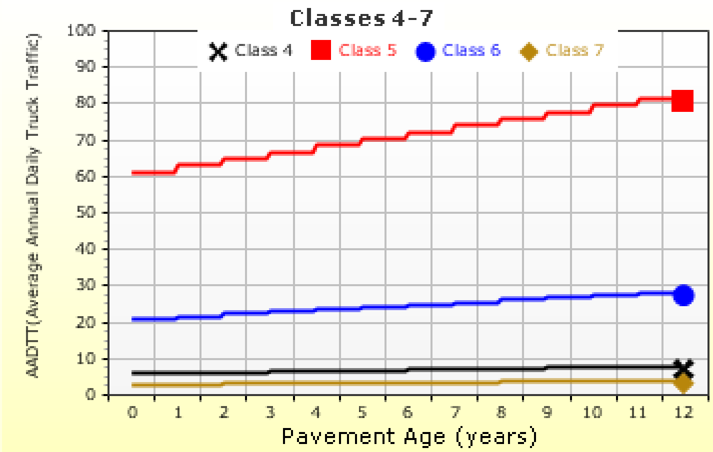

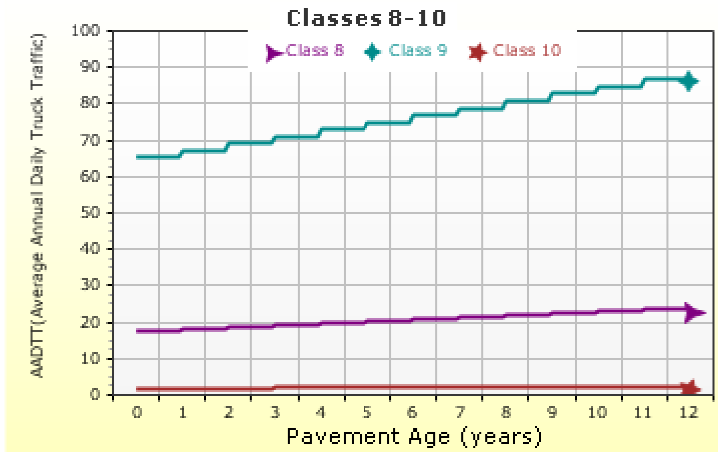

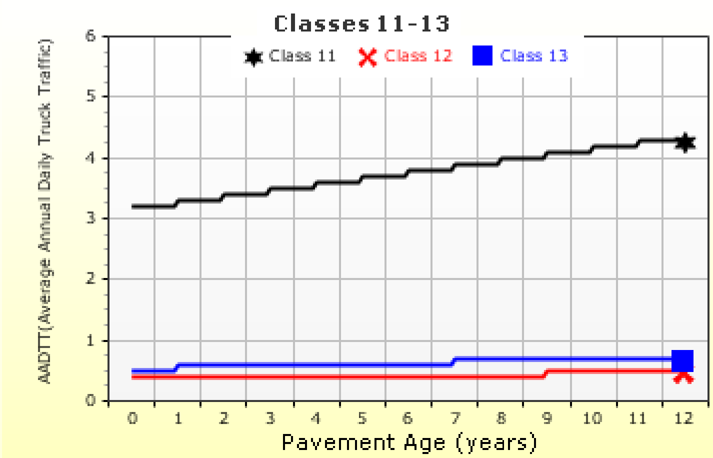

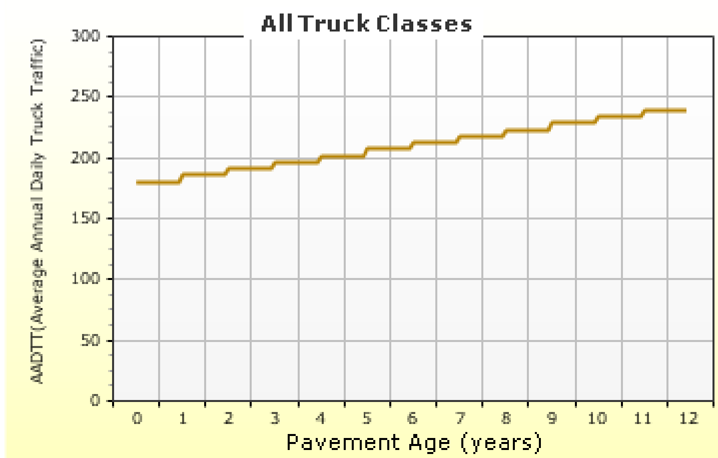

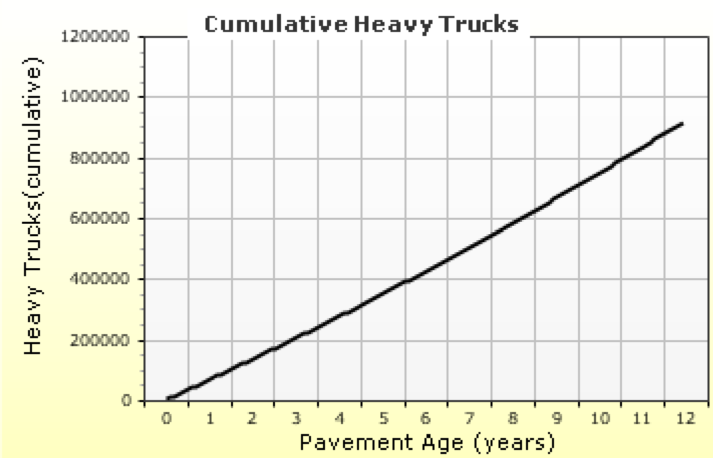

LVR_400AADT_CIR_0%-12 years December 2019

File Name: C:\Users\admin\Desktop\Taha M2\LVR_400AADT_CIR_0%-12 years December 2019.dgpx

Climate Inputs

Climate Data Sources:

Climate Station Cities:	Location (lat lon elevation(m))
CA, ON	44.00000 -78.75000 193

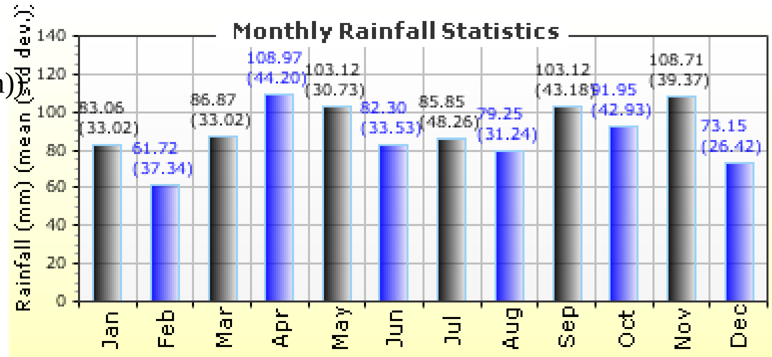

Annual Statistics:

Mean annual air temperature (ºC)	7.62
Mean annual precipitation (mm)	1068.32
Freezing index (ºC - days)	573.75
Average annual number of freeze/thaw cycles:	77.00

Water table depth (m)	10.00

Monthly Climate Summary:

LVR_400AADT_CIR_0%-12 years December 2019

File Name: C:\Users\admin\Desktop\Taha M2\LVR_400AADT_CIR_0%-12 years December 2019.dgpx

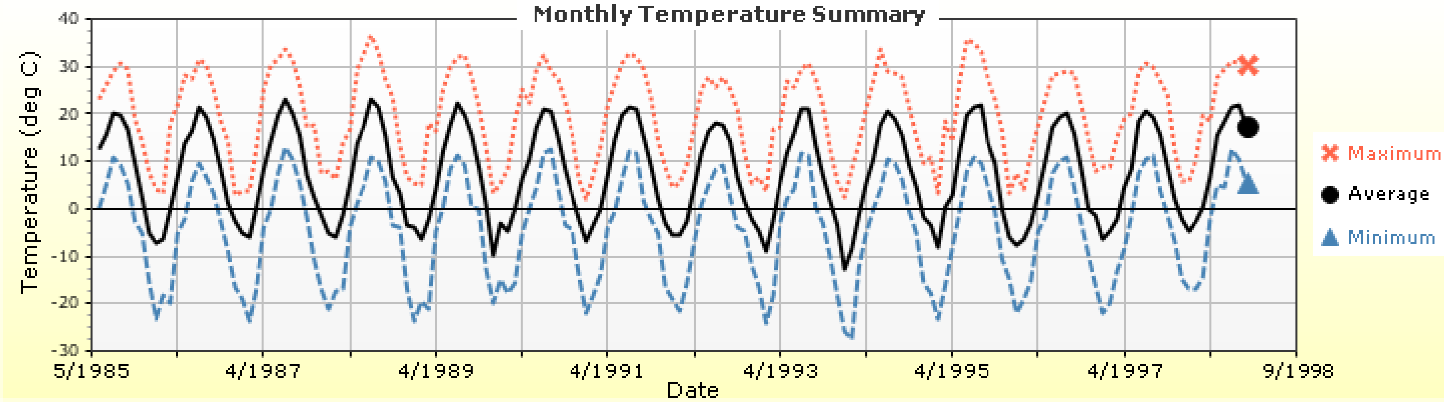

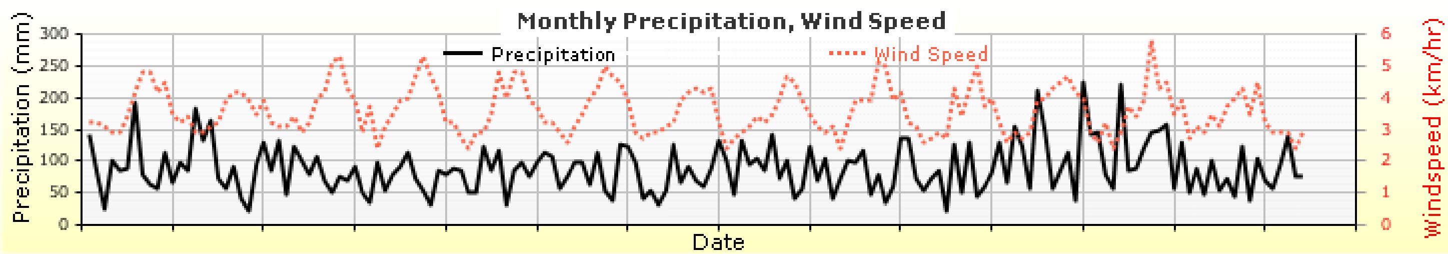

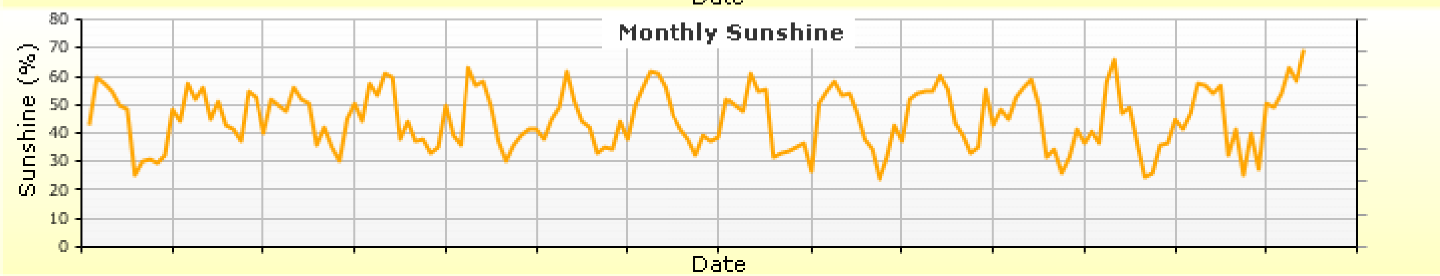

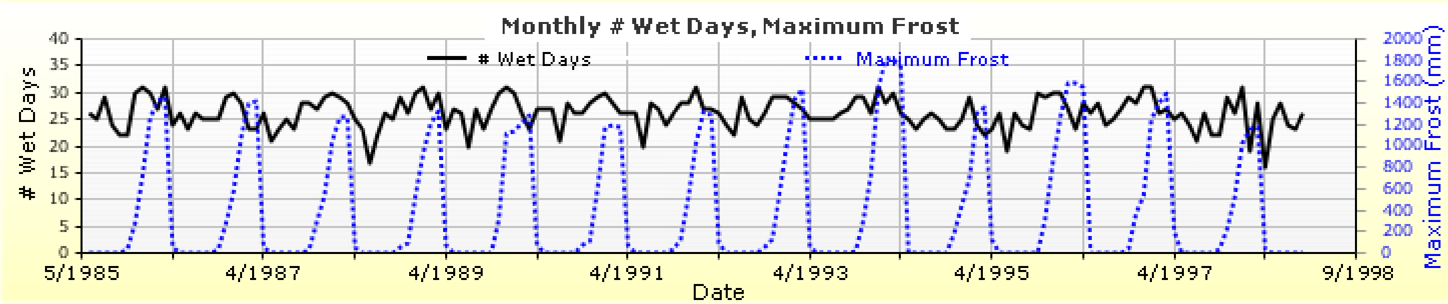

LVR_400AADT_CIR_0%-12 years December 2019

File Name: C:\Users\admin\Desktop\Taha M2\LVR_400AADT_CIR_0%-12 years December 2019.dgpx

Hourly Air Temperature Distribution by Month:

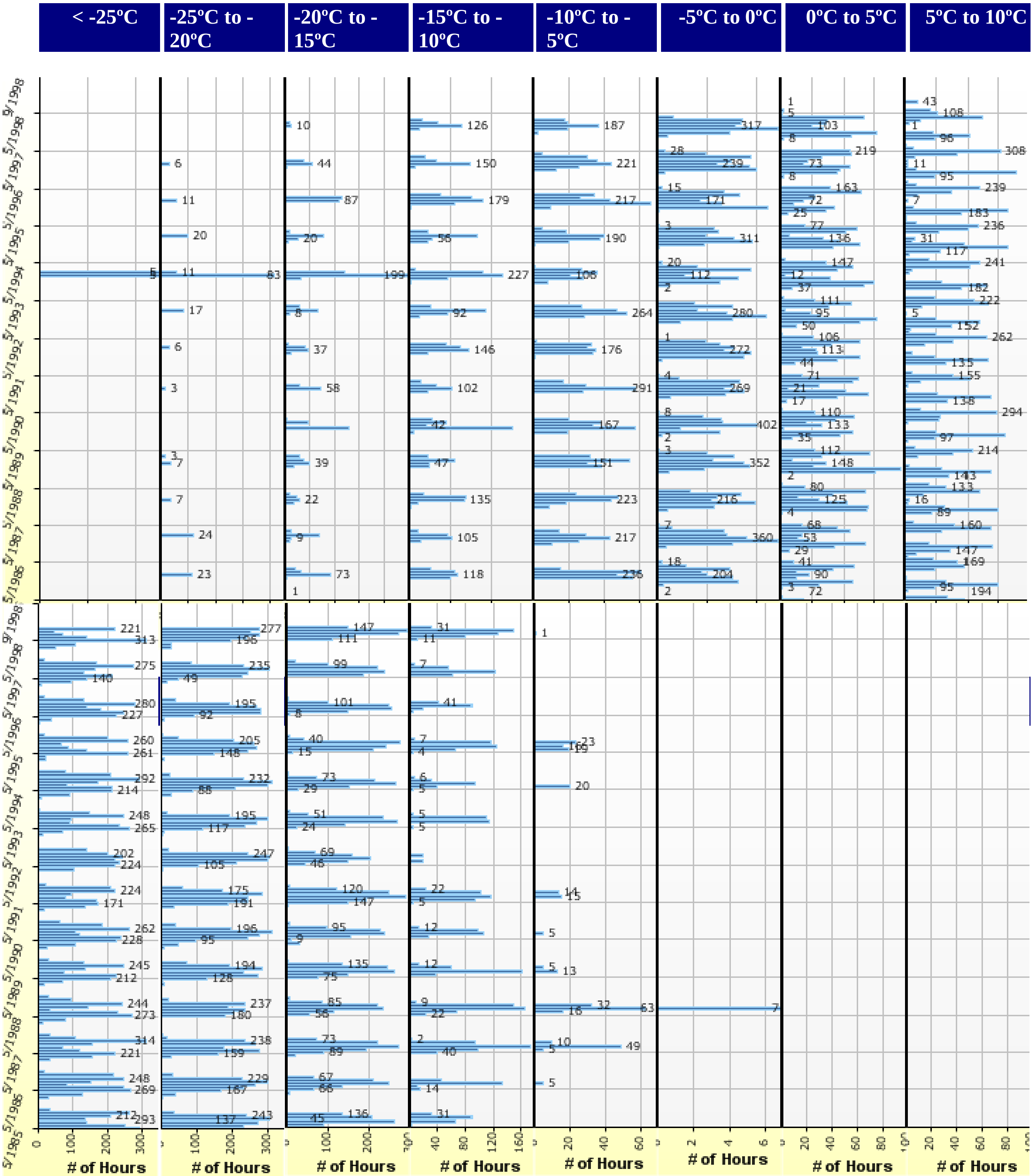

Design Properties

HMA Design Properties

Use Multilayer Rutting Model	False
Using G* based model (not nationally calibrated)	False
Is NCHRP 1-37A HMA Rutting Model Coefficients	True
Endurance Limit	-
Use Reflective Cracking	True

Structure - ICM Properties	
AC surface shortwave absorptivity	0.85

Layer Name	Layer Type	Interface Friction
Layer 1 Flexible : Default asphalt concrete	Flexible (1)	1.00
Layer 2 Flexible : Default asphalt concrete	Flexible (1)	1.00
Layer 3 Non-stabilized Base : A-1 -a	Non-stabilized Base (4)	1.00
Layer 4 Non-stabilized Base : A-1 -b	Non-stabilized Base (4)	1.00
Layer 5 Subgrade : A-6	Subgrade (5)	-

Thermal Cracking

Thermal Contraction	
Is thermal contraction calculated?	True
Mix coefficient of thermal contraction (mm/mm/ºC)	-
Aggregate coefficient of thermal contraction (mm/mm/ºC)	9.0e-006
Voids in Mineral Aggregate (%)	18.8

Indirect Tensile Strength (Input Level: 3)	
Test Temperature (ºC)	Indirect Tensilte Strength (Mpa)
-10.0	2.79

Creep Compliance (1/GPa) (Input Level: 3)			
Loading time (sec)	-20 ºC	-10 ºC	0 ºC
1	5.57e-002	8.57e-002	1.16e-001
2	6.17e-002	1.01e-001	1.51e-001
5	7.07e-002	1.25e-001	2.15e-001
10	7.83e-002	1.48e-001	2.80e-001
20	8.68e-002	1.74e-001	3.65e-001
50	9.94e-002	2.16e-001	5.19e-001
100	1.10e-001	2.55e-001	6.77e-001

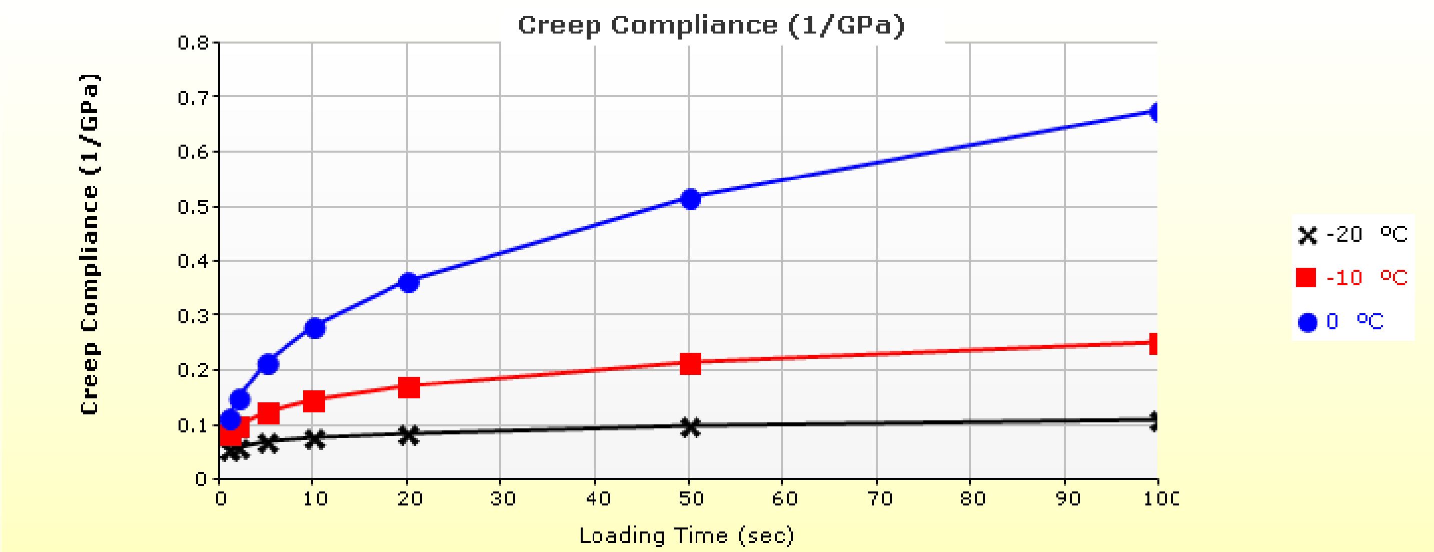

LVR_400AADT_CIR_0%-12 years December 2019

File Name: C:\Users\admin\Desktop\Taha M2\LVR_400AADT_CIR_0%-12 years December 2019.dgpx

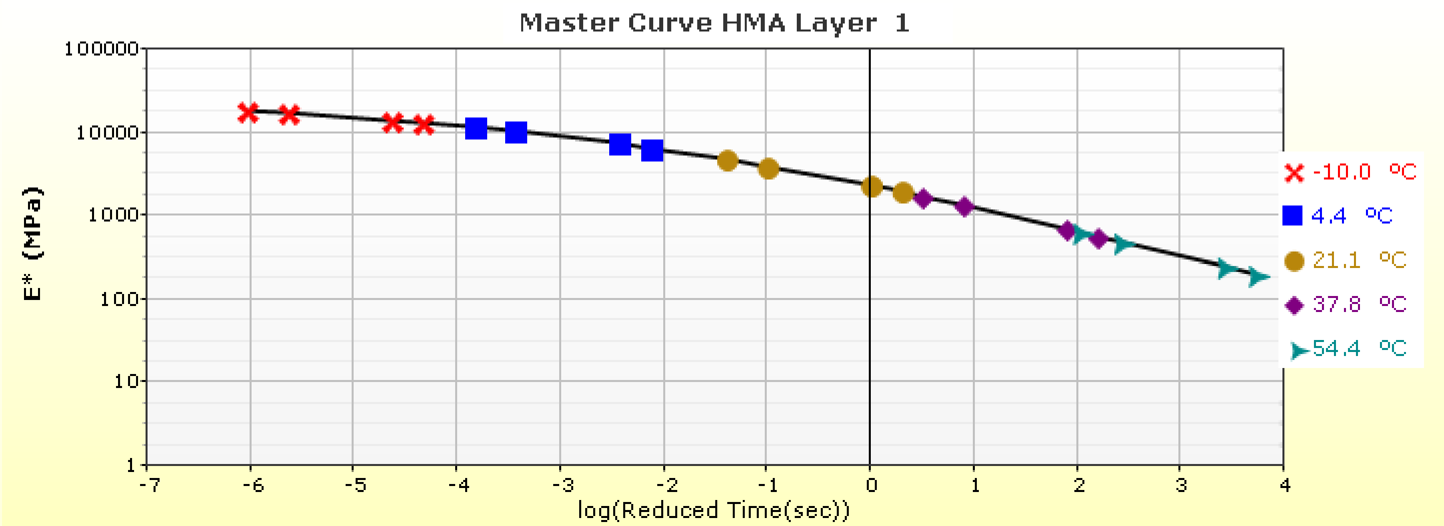

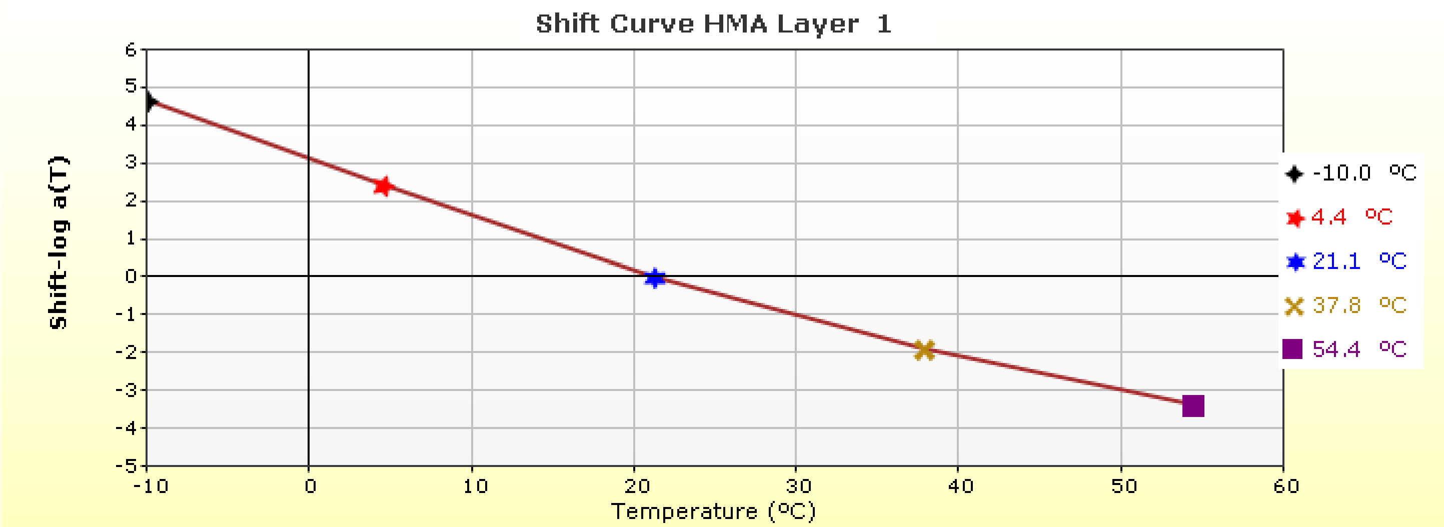

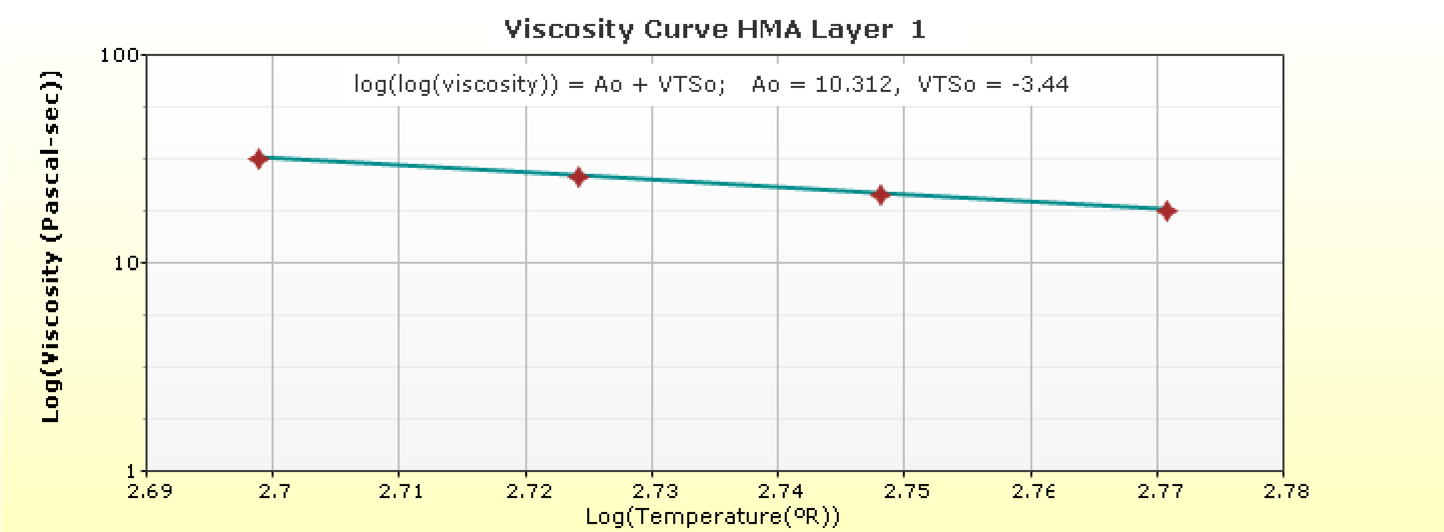

HMA Layer 2: Layer 2 Flexible : Default asphalt concrete

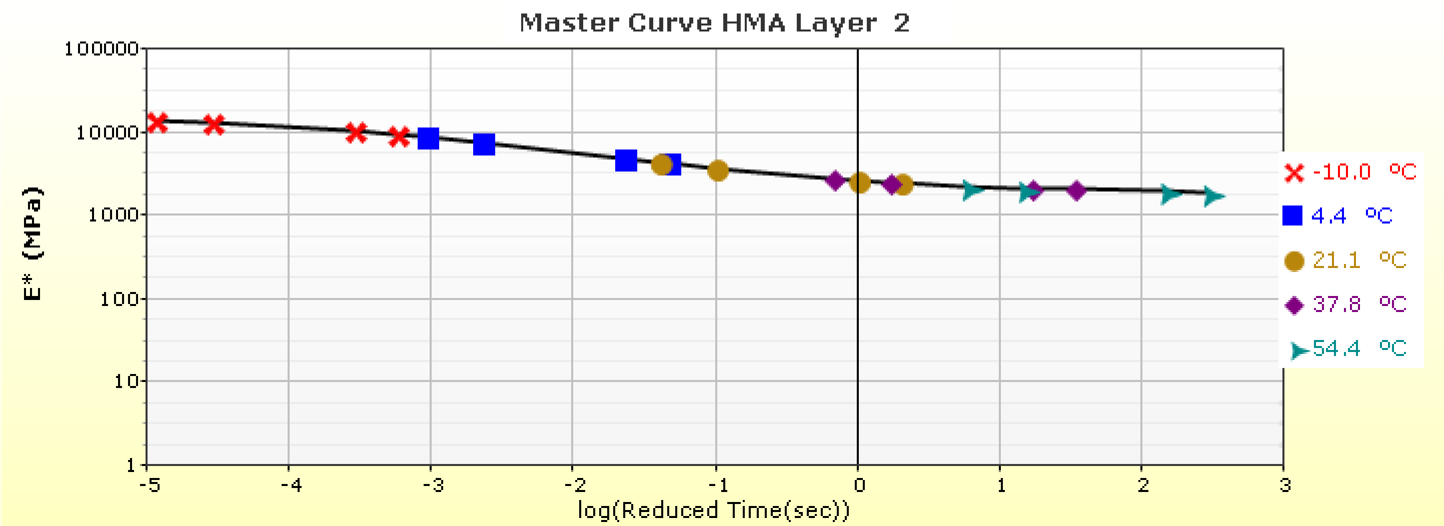

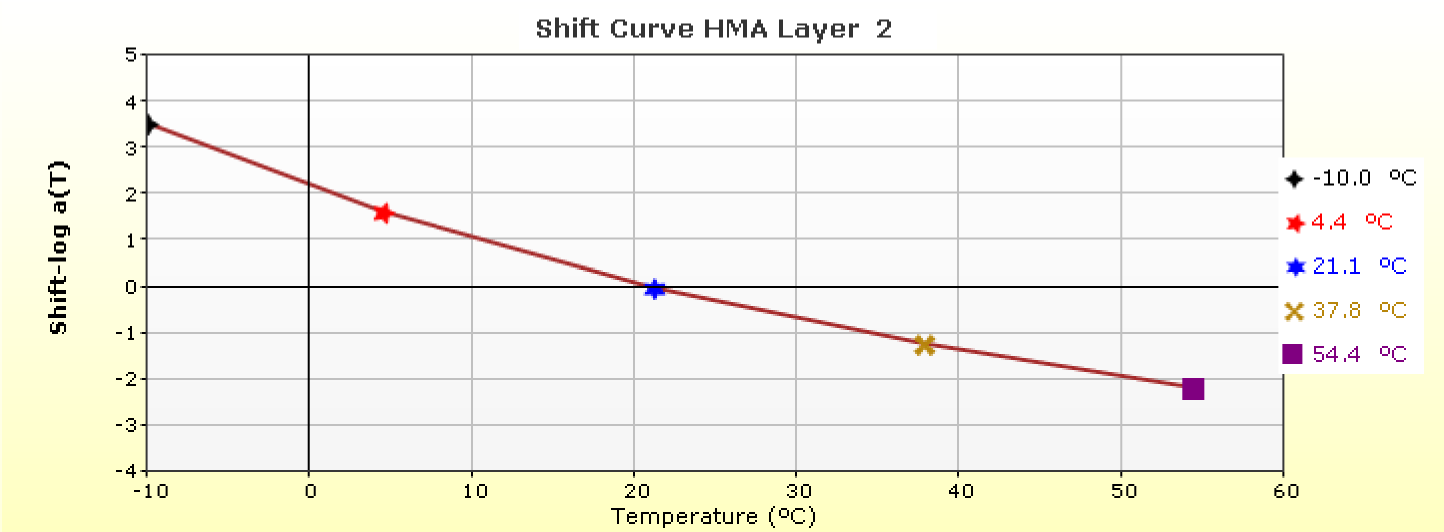

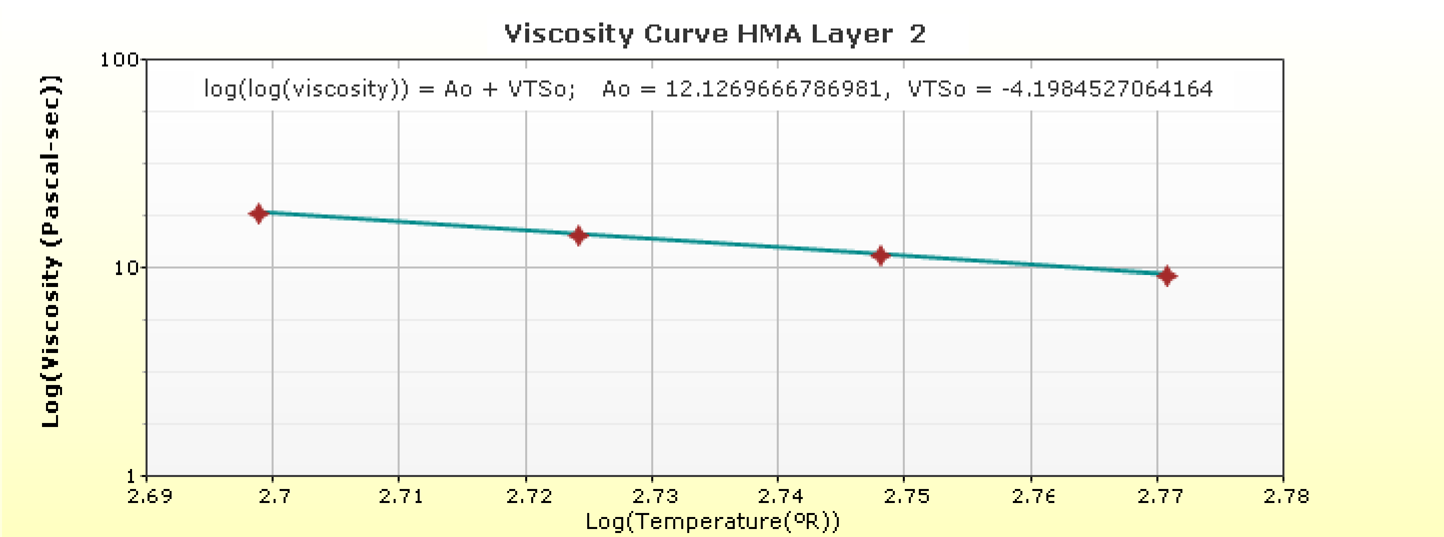

LVR_400AADT_CIR_0%-12 years December 2019

File Name: C:\Users\admin\Desktop\Taha M2\LVR_400AADT_CIR_0%-12 years December 2019.dgpx

Analysis Output Charts

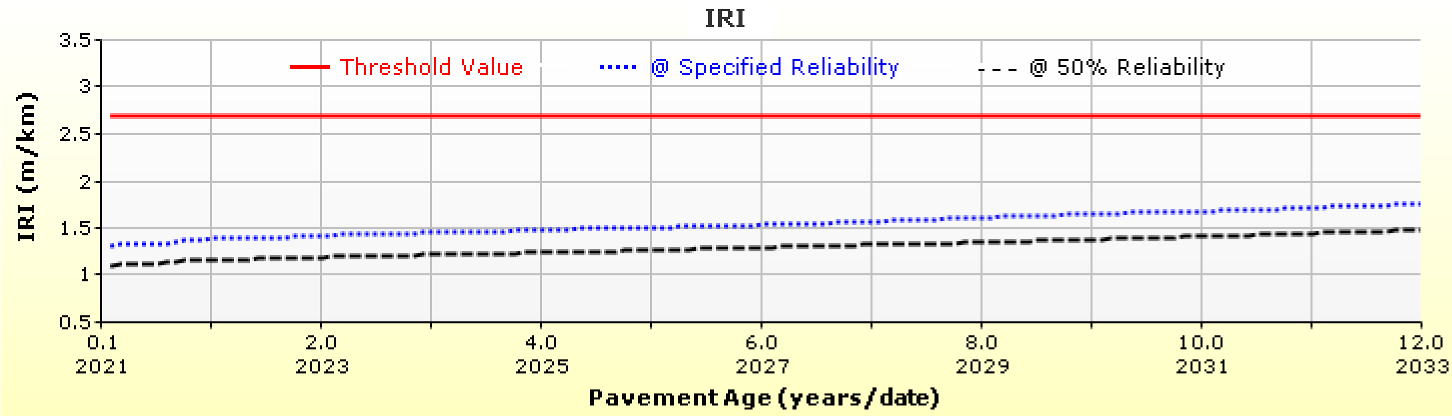

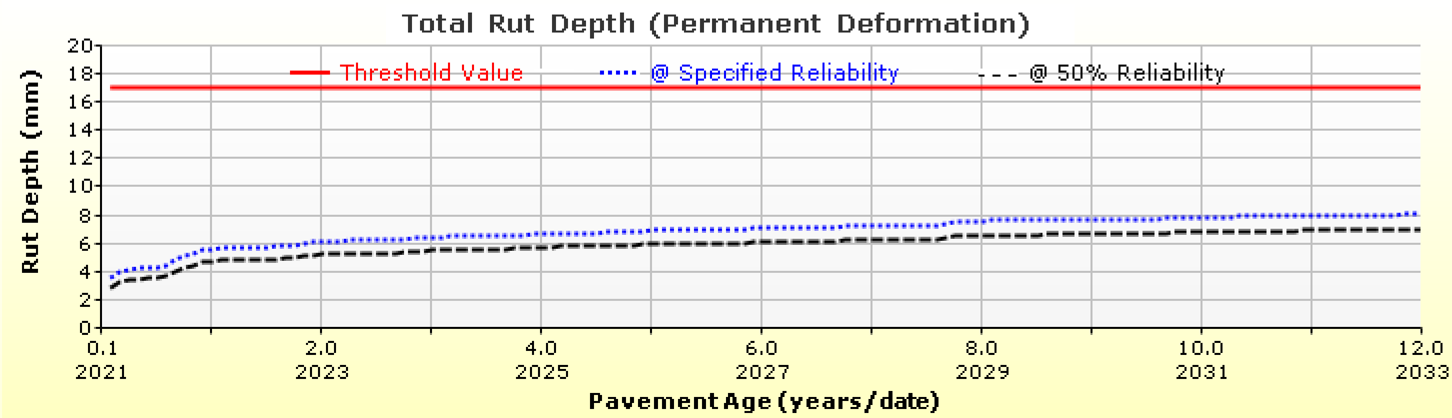

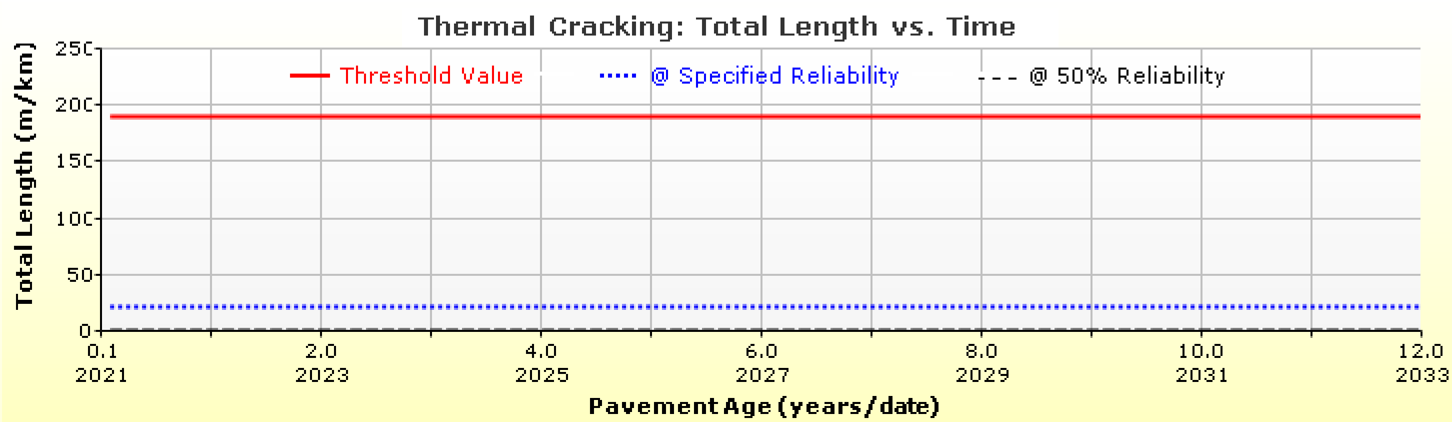

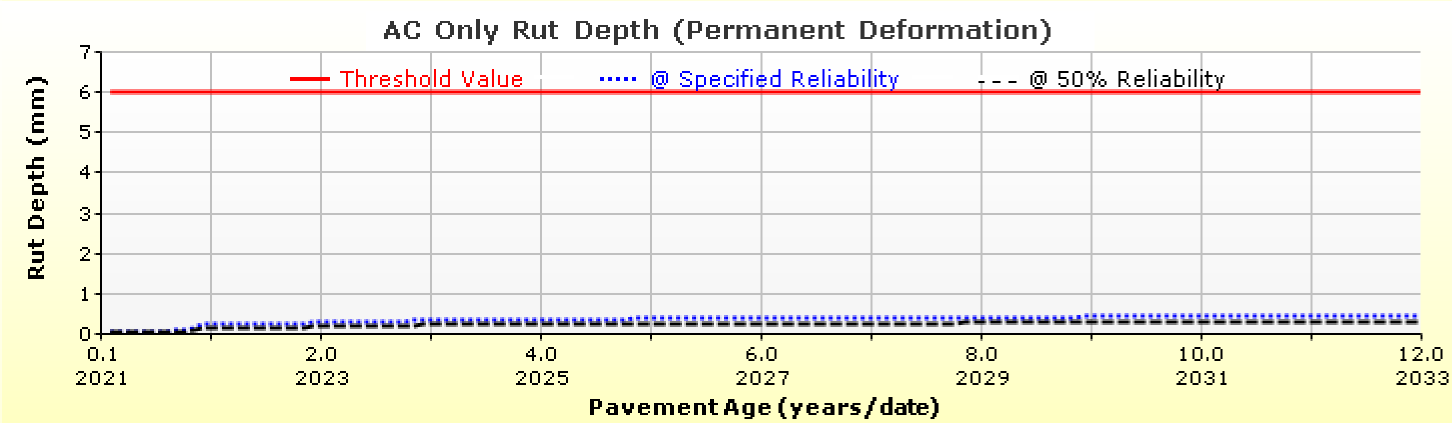

LVR_400AADT_CIR_0%-12 years December 2019

File Name: C:\Users\admin\Desktop\Taha M2\LVR_400AADT_CIR_0%-12 years December 2019.dgpx

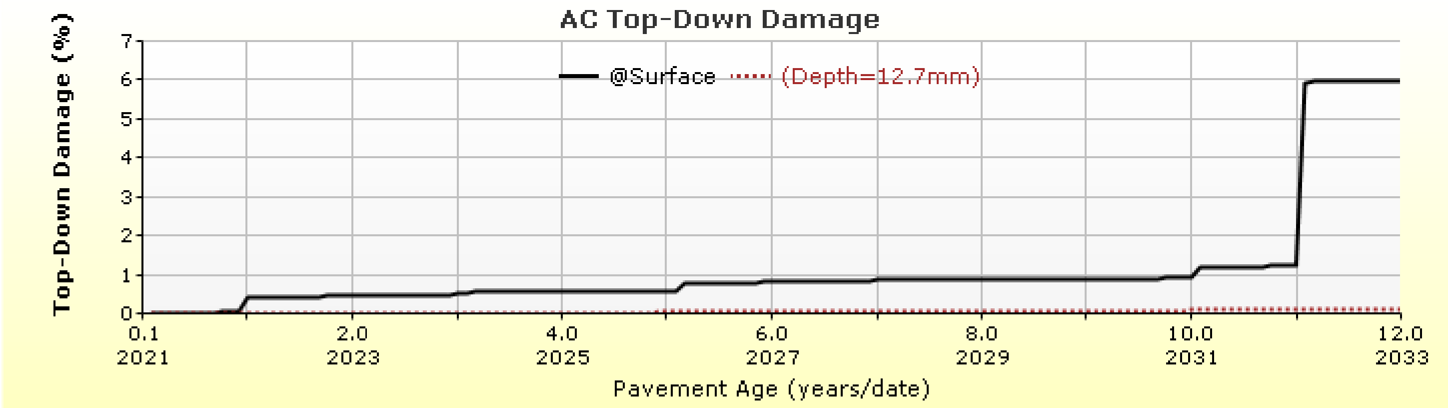

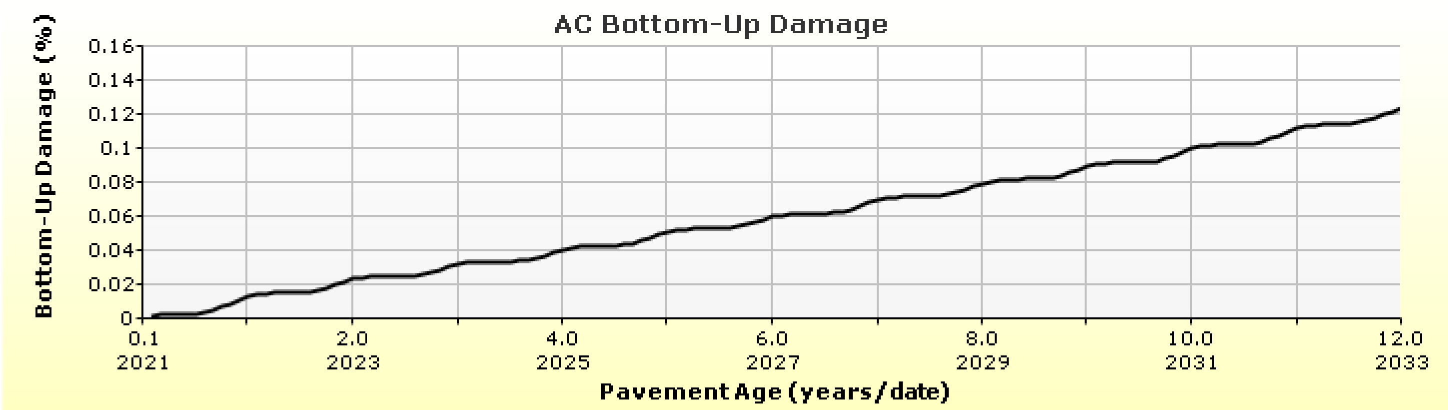

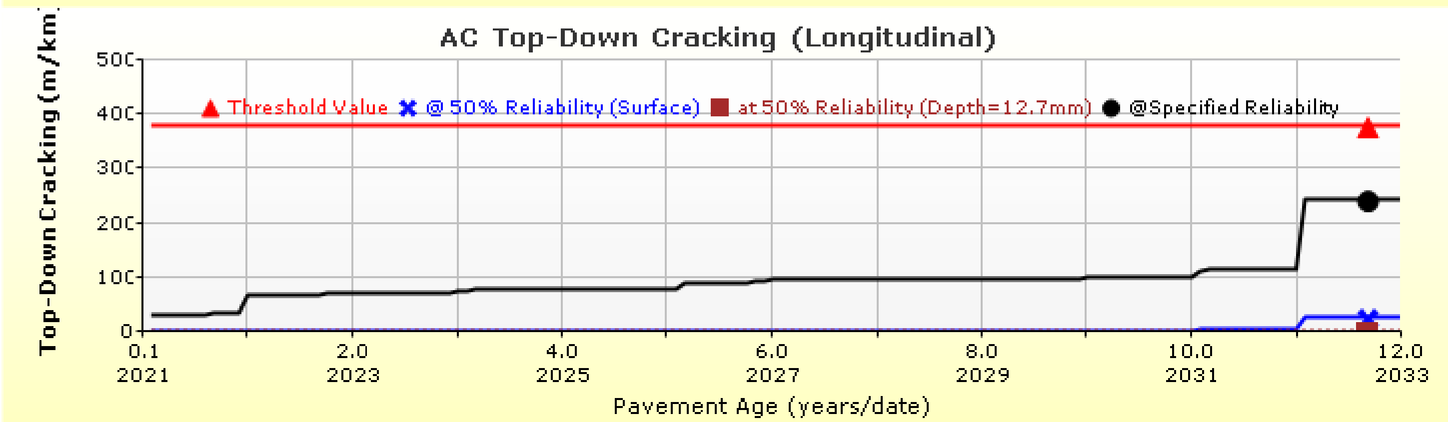

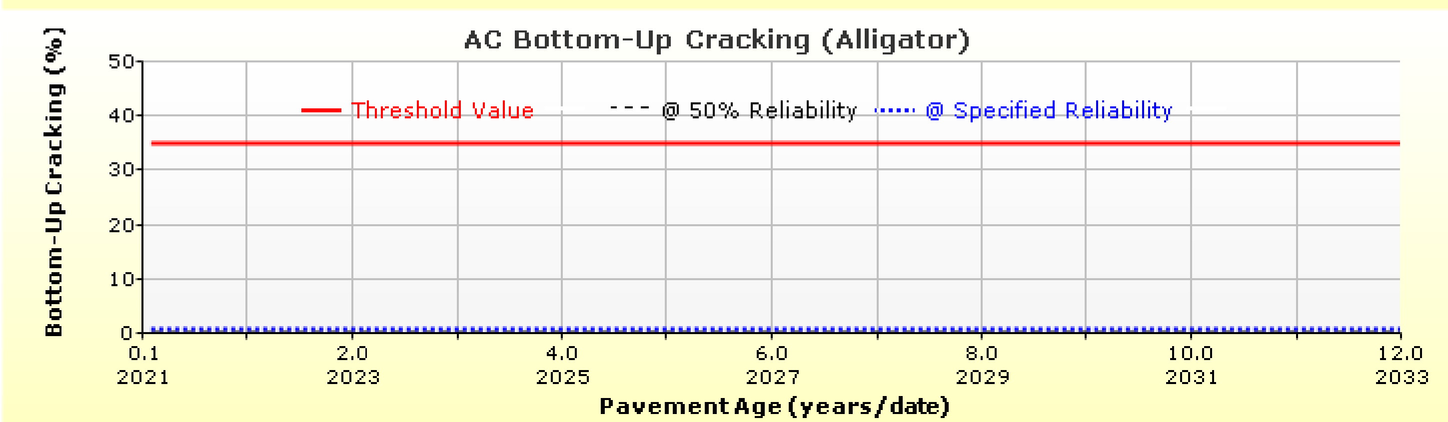

LVR_400AADT_CIR_0%-12 years December 2019

File Name: C:\Users\admin\Desktop\Taha M2\LVR_400AADT_CIR_0%-12 years December 2019.dgpx

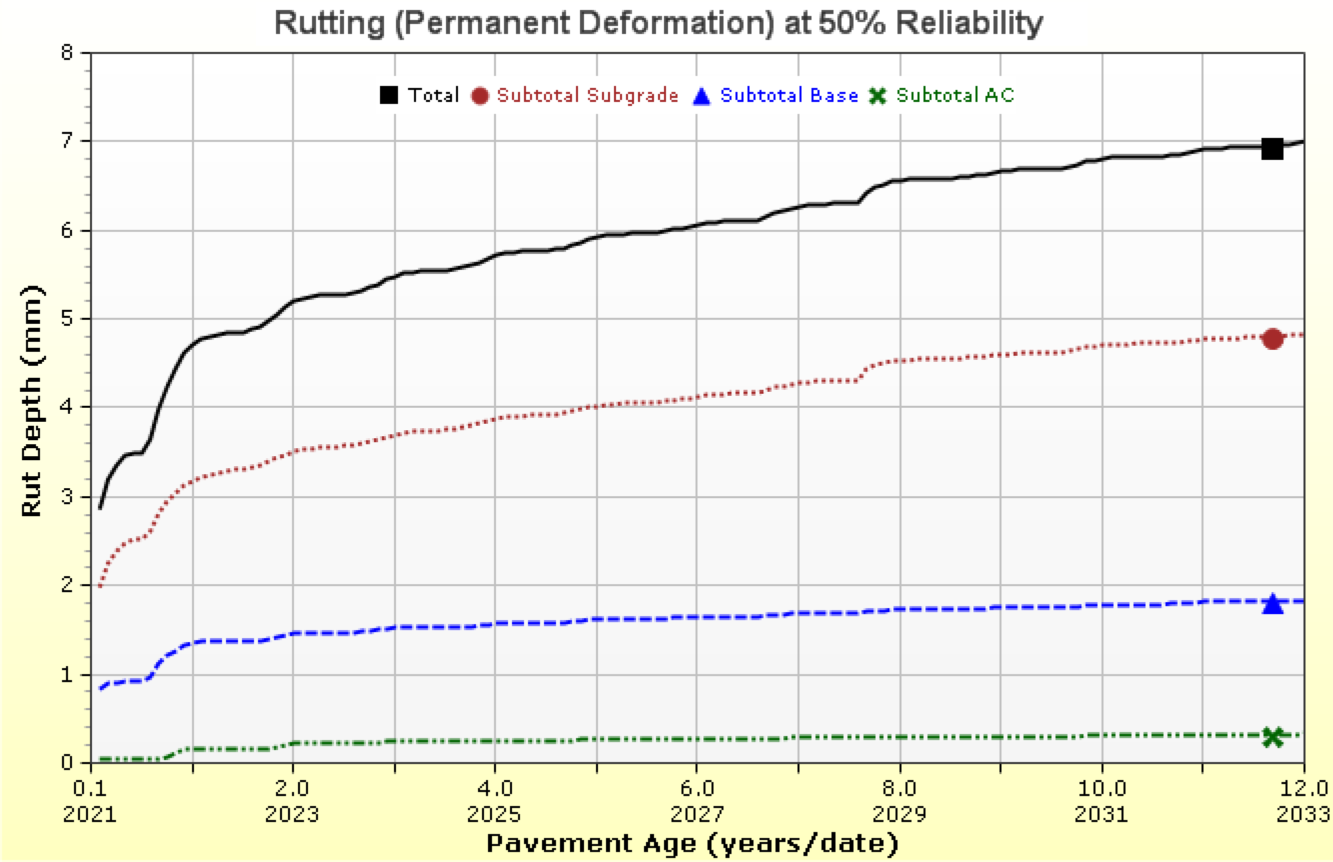

LVR_400AADT_CIR_0%-12 years December 2019

File Name: C:\Users\admin\Desktop\Taha M2\LVR_400AADT_CIR_0%-12 years December 2019.dgpx

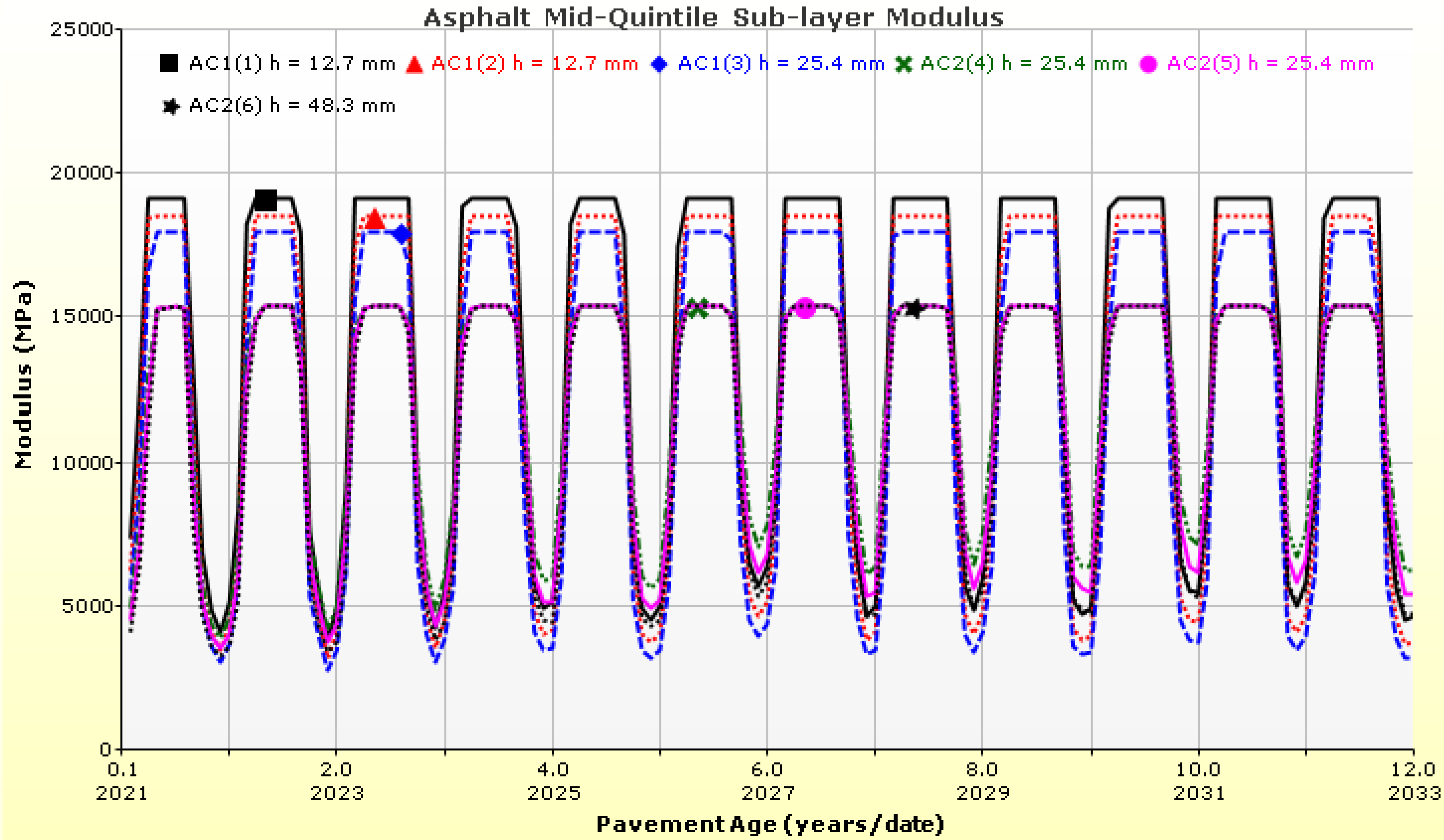

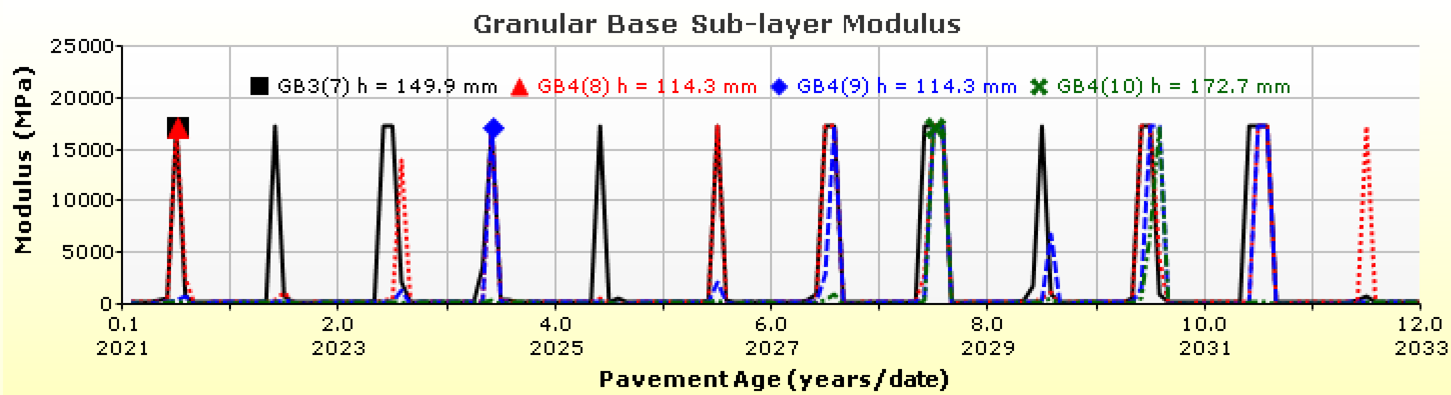

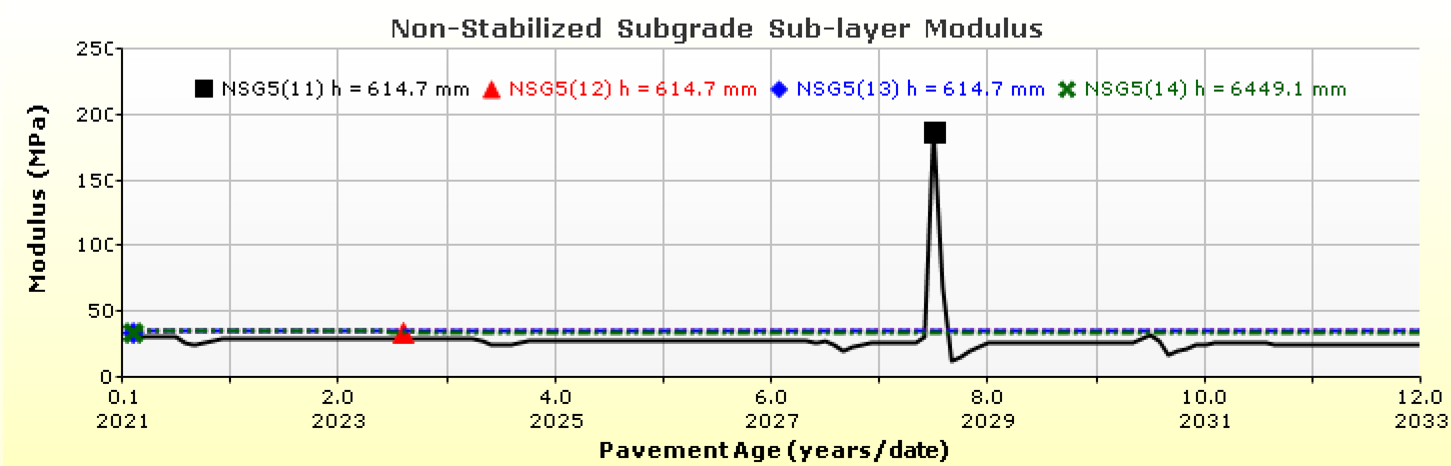

Layer Information

Layer 1 Flexible : Default asphalt concrete

Asphalt		
Thickness (mm)	50.0	
Unit weight (kgf/m^3)	2460.0	
Poisson's ratio	Is Calculated?	False
	Ratio	0.35
	Parameter A	-
	Parameter B	-

Asphalt Dynamic Modulus (Input Level: 3)

Gradation	Percent Passing
19 mm sieve	100
9.5 mm sieve	83.2
4.75 mm sieve	54
0.075mm sieve	4

Asphalt Binder

Parameter	Value
Grade	Superpave Performance Grade
Binder Type	64-28
A	10.312
VTS	-3.44

General Info

Name	Value
Reference temperature (ºC)	21.1
Effective binder content (%)	11.8
Air voids (%)	7
Thermal conductivity (watt/meter-kelvin)	1.16
Heat capacity (joule/kg-kelvin)	963

Identifiers

Field	Value
Display name/identifier	Default asphalt concrete
Description of object	
Author	
Date Created	9/16/2010 1:00:00 AM
Approver	
Date approved	9/16/2010 1:00:00 AM
State	
District	
County	
Highway	
Direction of Travel	
From station (km)	
To station (km)	
Province	
User defined field 1	
User defined field 2	
User defined field 3	
Revision Number	0

Layer 2 Flexible : Default asphalt concrete

Asphalt		
Thickness (mm)	100.0	
Unit weight (kgf/m^3)	2460.0	
Poisson's ratio	Is Calculated?	False
	Ratio	0.35
	Parameter A	-
	Parameter B	-

Asphalt Dynamic Modulus (Input Level: 1)

T (ºC)	0.1 Hz	0.5 Hz	1 Hz	5 Hz	10 Hz	25 Hz
-10	8149.928	9446.637	10308.08	11842.91	12627.55	13546.20
4	3810.748	4767.692	5352.709	6726.761	7443.048	8234.681
21	1268.153	1770.179	2001.670	2883.784	3375.964	3924.223
57	1268.153	1770.179	2001.670	2883.784	3375.964	3924.223

Asphalt Binder

Temperature (ºC)	Binder Gstar (Pa)	Phase angle (deg)
4.4	5494.5	57
12.8	1919	59.3
21.1	490.2	61.6
29.4	161.2	62.4
37.8	39.9	62.7
46.1	15.2	62.7

General Info

Name	Value
Reference temperature (ºC)	21.1
Effective binder content (%)	11.2
Air voids (%)	7
Thermal conductivity (watt/meter-kelvin)	1.16
Heat capacity (joule/kg-kelvin)	963

Identifiers

Field	Value
Display name/identifier	Default asphalt concrete
Description of object	
Author	
Date Created	9/16/2010 1:00:00 AM
Approver	
Date approved	9/16/2010 1:00:00 AM
State	
District	
County	
Highway	
Direction of Travel	
From station (km)	
To station (km)	
Province	
User defined field 1	
User defined field 2	
User defined field 3	
Revision Number	0

Layer 3 Non-stabilized Base : A-1-a

Unbound	
Layer thickness (mm)	150.0
Poisson's ratio	0.35
Coefficient of lateral earth pressure (k0)	0.5

Modulus (Input Level: 3)

Analysis Type:	Modify input values by temperature/moisture
Method:	Resilient Modulus (MPa)

Resilient Modulus (MPa)
250.0

Use Correction factor for NDT modulus?	-
NDT Correction Factor:	-

Identifiers

Field	Value
Display name/identifier	A-1-a
Description of object	Default material
Author	AASHTO
Date Created	1/1/2011 12:00:00 AM
Approver	
Date approved	1/1/2011 12:00:00 AM
State	
District	
County	
Highway	
Direction of Travel	
From station (km)	
To station (km)	
Province	
User defined field 1	
User defined field 2	
User defined field 3	
Revision Number	0

Sieve

Liquid Limit	6.0
Plasticity Index	0.0
Is layer compacted?	False

	Is User Defined?	Value
Maximum dry unit weight (kgf/m^3)	False	2038.2
Saturated hydraulic conductivity (m/hr)	False	2.376e-02
Specific gravity of solids	False	2.7
Water Content (%)	False	5.7

User-defined Soil Water Characteristic Curve (SWCC)	
Is User Defined?	False
af	3.0201
bf	2.5984
cf	0.7539
hr	100.0000

Sieve Size	% Passing
0.001mm	
0.002mm	
0.020mm	
0.075mm	5.0
0.150mm	
0.180mm	
0.250mm	
0.300mm	13.5
0.425mm	
0.600mm	
0.850mm	
1.18mm	27.5
2.0mm	
2.36mm	
4.75mm	45.0
9.5mm	61.5
12.5mm	77.5
19.0mm	92.5
25.0mm	100.0
37.5mm	
50.0mm	
63.0mm	
75.0mm	
90.0mm	

Layer 4 Non-stabilized Base : A-1-b

Unbound	
Layer thickness (mm)	400.0
Poisson's ratio	0.35
Coefficient of lateral earth pressure (k0)	0.5

Modulus (Input Level: 3)

Analysis Type:	Modify input values by temperature/moisture
Method:	Resilient Modulus (MPa)

Resilient Modulus (MPa)
150.0

Use Correction factor for NDT modulus?	-
NDT Correction Factor:	-

Identifiers

Field	Value
Display name/identifier	A-1-b
Description of object	Default material
Author	AASHTO
Date Created	1/1/2011 12:00:00 AM
Approver	
Date approved	1/1/2011 12:00:00 AM
State	
District	
County	
Highway	
Direction of Travel	
From station (km)	
To station (km)	
Province	
User defined field 1	
User defined field 2	
User defined field 3	
Revision Number	0

Sieve

Liquid Limit	11.0
Plasticity Index	0.0
Is layer compacted?	False

	Is User Defined?	Value
Maximum dry unit weight (kgf/m^3)	False	1981.7
Saturated hydraulic conductivity (m/hr)	False	7.17e-03
Specific gravity of solids	False	2.7
Water Content (%)	False	7.9

User-defined Soil Water Characteristic Curve (SWCC)	
Is User Defined?	False
af	5.0954
bf	2.5384
cf	0.8464
hr	100.0000

Sieve Size	% Passing
0.001mm	
0.002mm	
0.020mm	
0.075mm	4.0
0.150mm	
0.180mm	
0.250mm	
0.300mm	33.5
0.425mm	
0.600mm	
0.850mm	
1.18mm	55.0
2.0mm	
2.36mm	
4.75mm	60.0
9.5mm	
12.5mm	
19.0mm	
25.0mm	75.0
37.5mm	
50.0mm	
63.0mm	
75.0mm	
90.0mm	

Layer 5 Subgrade : A-6

Unbound	
Layer thickness (mm)	Semi-infinite
Poisson's ratio	0.3
Coefficient of lateral earth pressure (k0)	0.5

Modulus (Input Level: 3)

Analysis Type:	Modify input values by temperature/moisture
Method:	Resilient Modulus (MPa)

Resilient Modulus (MPa)
35.0

Use Correction factor for NDT modulus?	-
NDT Correction Factor:	-

Identifiers

Field	**Value**
Display name/identifier	A-6
Description of object	Default material
Author	AASHTO
Date Created	1/1/2011 12:00:00 AM
Approver	
Date approved	1/1/2011 12:00:00 AM
State	
District	
County	
Highway	
Direction of Travel	
From station (km)	
To station (km)	
Province	
User defined field 1	
User defined field 2	
User defined field 3	
Revision Number	0

Sieve

Liquid Limit	18.0
Plasticity Index	4.0
Is layer compacted?	False

	Is User Defined?	**Value**
Maximum dry unit weight (kgf/m^3)	False	1992.5
Saturated hydraulic conductivity (m/hr)	False	1.095e-06
Specific gravity of solids	False	2.7
Water Content (%)	False	8.8

User-defined Soil Water Characteristic Curve (SWCC)	
Is User Defined?	False
af	26.3898
bf	1.0483
cf	0.8553
hr	332.0000

Sieve Size	**% Passing**
0.001mm	
0.002mm	8.0
0.020mm	
0.075mm	29.0
0.150mm	
0.180mm	58.0
0.250mm	
0.300mm	
0.425mm	72.0
0.600mm	
0.850mm	
1.18mm	
2.0mm	84.0
2.36mm	
4.75mm	90.0
9.5mm	94.0
12.5mm	97.0
19.0mm	98.0
25.0mm	100.0
37.5mm	
50.0mm	
63.0mm	
75.0mm	
90.0mm	

Calibration Coefficients

AC Fatigue

$$N_f = 0.00432 * C * \beta_{f1} k_1 \left(\frac{1}{\varepsilon_1}\right)^{k_2\beta_{f2}} \left(\frac{1}{E}\right)^{k_3\beta_{f3}}$$

$$C = 10^M$$

$$M = 4.84\left(\frac{V_b}{V_a + V_b} - 0.69\right)$$

k1: 3.75
k2: 2.87
k3: 1.46
Bf1: (5.014 * Pow(hac,-3.416)) * 1 + 0
Bf2: 1.38
Bf3: 0.88

AC Rutting

$$\frac{\varepsilon_p}{\varepsilon_r} = k_z \beta_{r1} 10^{k_1} T^{k_2\beta_{r2}} N^{k_3\beta_{r3}}$$

$$k_z = (C_1 + C_2 * depth) * 0.328196^{depth}$$

$$C_1 = -0.1039 * H_\alpha^2 + 2.4868 * H_\alpha - 17.342$$

$$C_2 = 0.0172 * H_\alpha^2 - 1.7331 * H_\alpha + 27.428$$

Where:

H_{ac} = total AC thickness(in)

ε_p = plastic strain(in/in)
ε_r = resilient strain(in/in)
T = layer temperature(°F)
N = number of load repetitions

AC Rutting Standard Deviation	0.24 * Pow(RUT,0.8026) + 0.001	
AC Layer 1	K1:-2.45 K2:3.01 K3:0.22	Br1:0.128 Br2:0.52 Br3:1.36
AC Layer 2	K1:-2.45 K2:3.01 K3:0.22	Br1:0.4 Br2:0.52 Br3:1.36

Thermal Fracture

$$C_f = 400 * N\left(\frac{\log C / h_{ac}}{\sigma}\right)$$

$$\Delta C = (k * \beta t)^{n+1} * A * \Delta K^n$$

$$A = 10^{(4.389 - 2.52 * \log(E * \sigma_m * n))}$$

C_f = observed amount of thermal cracking(ft/500ft)
k = refression coefficient determined through field calibration
$N()$ = standard normal distribution evaluated at()
σ = standard deviation of the log of the depth of cracks in the pavments
C = crack depth(in)
h_{ac} = thickness of asphalt layer(in)
ΔC = Change in the crack depth due to a cooling cycle
ΔK = Change in the stress intensity factor due to a cooling cycle
A, n = Fracture parameters for the asphalt mixture
E = mixture stiffness
σ_M = Undamaged mixture tensile strength
β_t = Calibration parameter

Level 1 K: ((3 * Pow(10,-7)) * Pow(MAAT,4.0319)) * 1 + 0	Level 1 Standard Deviation: 0.14 * THERMAL + 168
Level 2 K: ((3 * Pow(10,-7)) * Pow(MAAT,4.0319)) * 1 + 0	Level 2 Standard Deviation: 0.20 * THERMAL + 168
Level 3 K: ((3 * Pow(10,-7)) * Pow(MAAT,4.0319)) * 1 + 0	Level 3 Standard Deviation: 0.289 * THERMAL + 168

CSM Fatigue

$$N_f = 10^{\left(\frac{k_1 \beta_{c1}\left(\frac{\sigma_s}{M_r}\right)}{k_2 \beta_{c2}}\right)}$$

N_f = number of repetitions to fatigue cracking
σ_s = Tensile stress(psi)
M_r = modulus of rupture(psi)

k1: 0.972	k2: 0.0825	Bc1: 1	Bc2:1

Unbound Layer Rutting

$$\delta_a(N) = \beta_{s_1} k_1 \varepsilon_v h \left(\frac{\varepsilon_0}{\varepsilon_r}\right) \left| e^{-\left(\frac{\rho}{N}\right)^{\beta}} \right|$$

δ_a = permanent deformation for the layer
N = number of repetitions
ε_v = average veritcal strain(in/in)
$\varepsilon_0, \beta, \rho$ = material properties
ε_r = resilient strain(in/in)

Base Rutting		Subgrade Rutting	
k1: 0.965	Bs1: 1	k1: 0.675	Bs1: 1
Standard Deviation (BASERUT) 0.1477 * Pow(BASERUT,0.6711) + 0.001		Standard Deviation (BASERUT) 0.1235 * Pow(SUBRUT,0.5012) + 0.001	

AC Cracking

AC Top Down Cracking

$$FC_{top} = \left(\frac{C_4}{1 + e^{(C_1 - C_2 * log_{10}(Damage))}}\right) * 10.56$$

c1: 7	c2: 3.5	c3: 0	c4: 1000

AC Bottom Up Cracking

$$FC = \left(\frac{6000}{1 + e^{\left(C_1 * C_1' + C_2 * C_2' log_{10}(D * 100)\right)}}\right) * \left(\frac{1}{60}\right)$$

$$C_2' = -2.40874 - 39.748 * (1 + h_{ac})^{-2.856}$$

$$C_1' = -2 * C_2'$$

c1: 1.31	c2: (0.867 + 0.2583 * hac) * 1 + 0	c3: 6000

Top down AC Cracking Standard Deviation	Bottom up AC Cracking Standard Deviation
200 + 2300/(1+exp(1.072-2.1654*LOG10(TOP+0.0001)))	1.13 + 13/(1+exp(7.57-15.5*LOG10(BOTTOM+0.0001)))

CSM Cracking

$$FC_{ctb} = C_1 + \frac{C_2}{1 + e^{C_3 - C_4 * log_{10}(Damage)}}$$

C1: 0	C2: 75	C3: 2	C4: 2

CSM Standard Deviation

CTB*1

IRI Flexible Pavements

C1 - Rutting
C2 - Fatigue Crack
C3 - Transverse Crack
C4 - Site Factors

C1: 55	C2: 0.4	C3: 0.008	C4: 0.015

LVR_400AADT_CIR_0.5%-12 years December 2019

File Name: C:\Users\admin\Desktop\Taha M2\LVR_400AADT_CIR_0.5%-12 years December 2019.dgpx

Design Inputs

Design Life: 12 years

Design Type: FLEXIBLE

Base construction: May, 2020

Pavement construction: June, 2021

Traffic opening: September, 2021

Climate Data Sources (Lat/Lon): 44, -78.75

Design Structure

Layer type	Material Type	Thickness(mm)
Flexible	Default asphalt concrete	50.0
Flexible	Default asphalt concrete	100.0
NonStabilized	A-1-a	150.0
NonStabilized	A-1-b	400.0
Subgrade	A-6	Semi-infinite

Volumetric at Construction:	
Effective binder content (%)	11.8
Air voids (%)	7.0

Traffic

Age (year)	Heavy Trucks (cumulative)
2021 (initial)	400
2027 (6 years)	424,055
2033 (12 years)	919,115

Design Outputs

Distress Prediction Summary

Distress Type	Distress @ Specified Reliability		Reliability (%)		Criterion Satisfied?
	Target	Predicted	Target	Achieved	
Terminal IRI (m/km)	2.70	1.74	75.00	99.86	Pass
Permanent deformation - total pavement (mm)	17.00	7.62	75.00	100.00	Pass
AC bottom-up fatigue cracking (percent)	35.00	0.76	75.00	100.00	Pass
AC thermal cracking (m/km)	190.00	21.65	75.00	100.00	Pass
AC top-down fatigue cracking (m/km)	380.00	63.83	75.00	100.00	Pass
Permanent deformation - AC only (mm)	6.00	0.43	75.00	100.00	Pass

Distress Charts

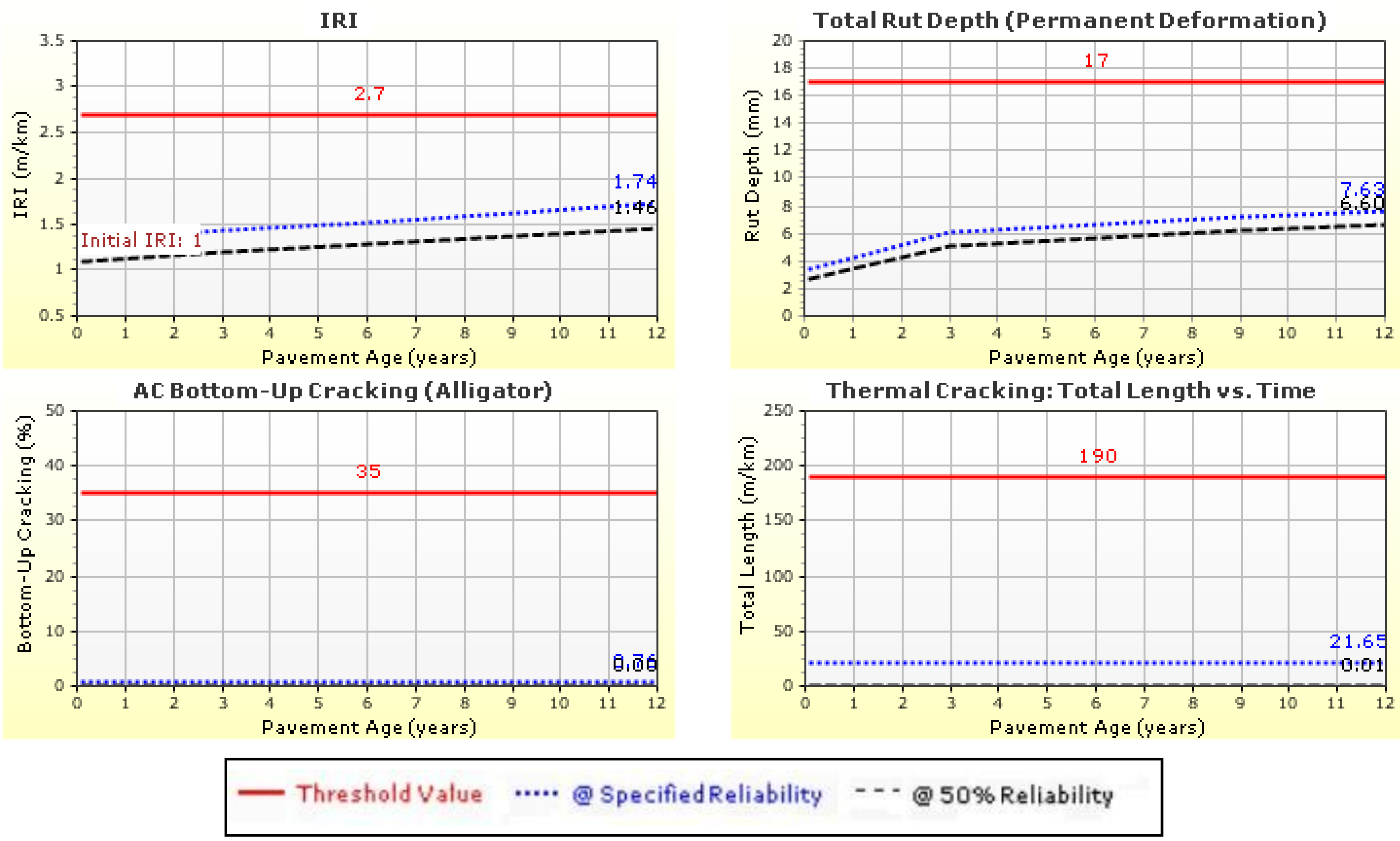

LVR_400AADT_CIR_0.5%-12 years December 2019

File Name: C:\Users\admin\Desktop\Taha M2\LVR_400AADT_CIR_0.5%-12 years December 2019.dgpx

Traffic Inputs

Graphical Representation of Traffic Inputs

Initial two-way AADTT:	400	Percent of trucks in design direction (%):	50.0
Number of lanes in design direction:	2	Percent of trucks in design lane (%):	90.0
		Operational speed (kph)	80.0

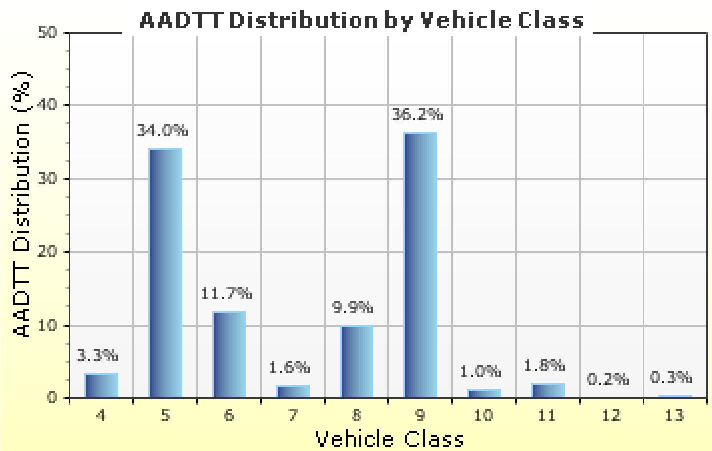

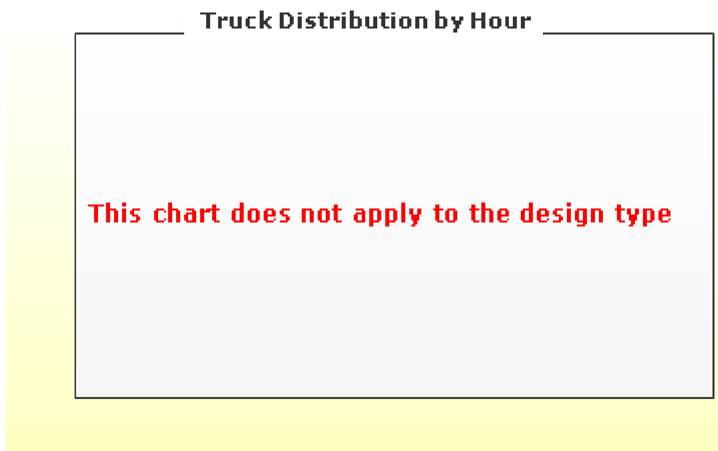

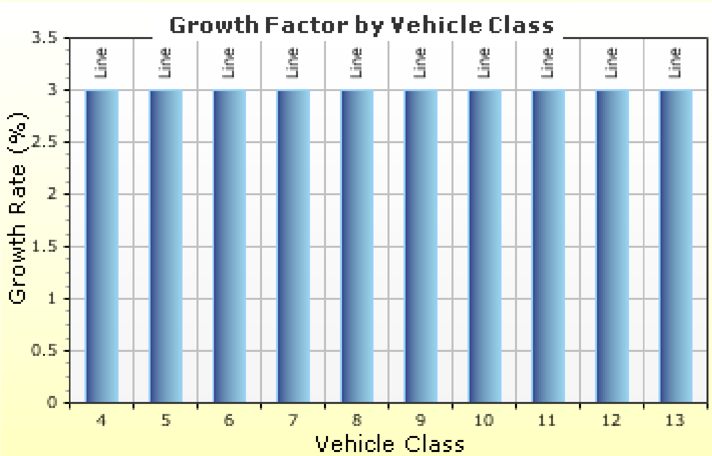

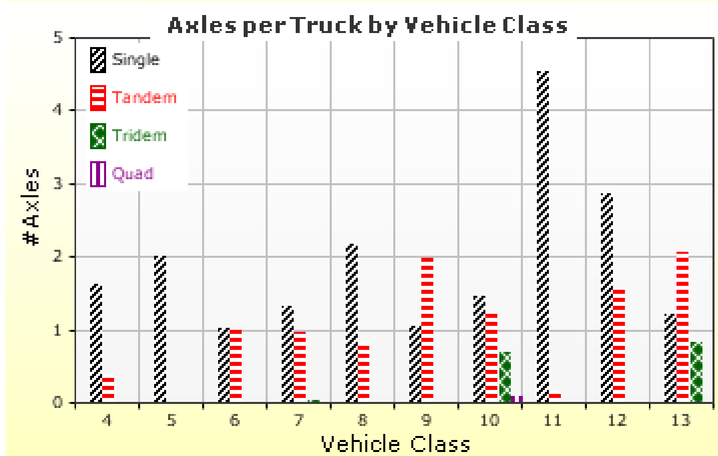

Traffic Volume Monthly Adjustment Factors

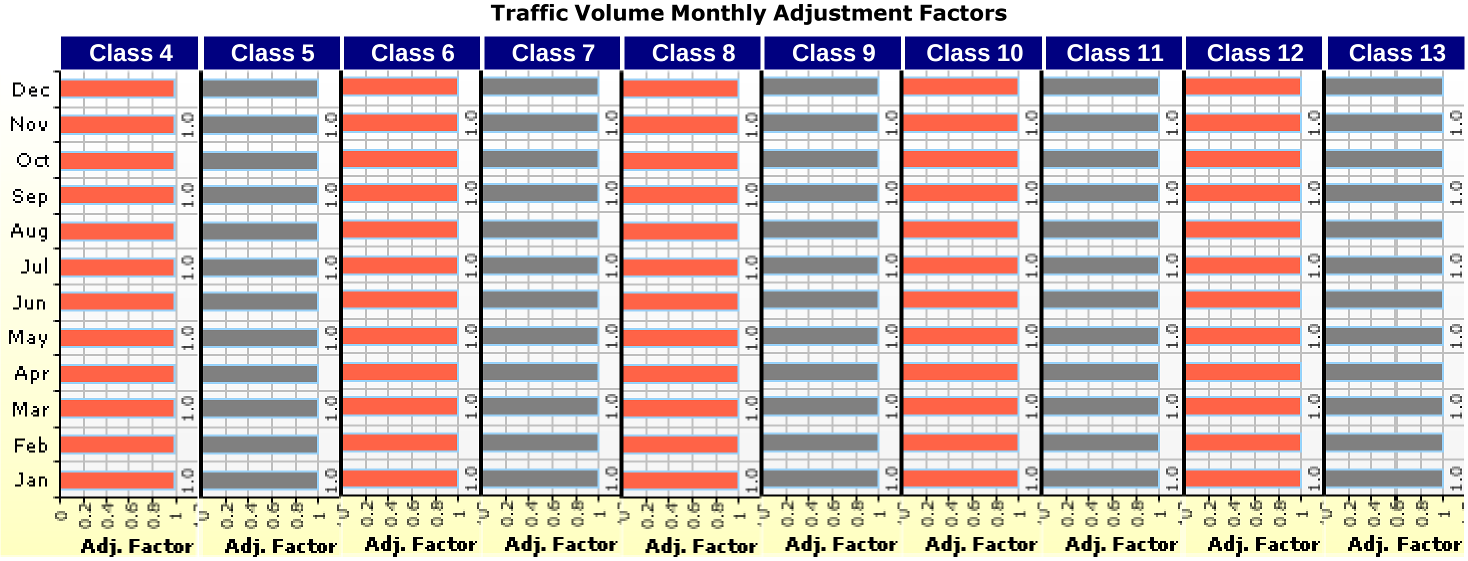

LVR_400AADT_CIR_0.5%-12 years December 2019

File Name: C:\Users\admin\Desktop\Taha M2\LVR_400AADT_CIR_0.5%-12 years December 2019.dgpx

Tabular Representation of Traffic Inputs

Volume Monthly Adjustment Factors

Level 3: Default MAF

Month	Vehicle Class 4	5	6	7	8	9	10	11	12	13
January	1.0	1.0	1.0	1.0	1.0	1.0	1.0	1.0	1.0	1.0
February	1.0	1.0	1.0	1.0	1.0	1.0	1.0	1.0	1.0	1.0
March	1.0	1.0	1.0	1.0	1.0	1.0	1.0	1.0	1.0	1.0
April	1.0	1.0	1.0	1.0	1.0	1.0	1.0	1.0	1.0	1.0
May	1.0	1.0	1.0	1.0	1.0	1.0	1.0	1.0	1.0	1.0
June	1.0	1.0	1.0	1.0	1.0	1.0	1.0	1.0	1.0	1.0
July	1.0	1.0	1.0	1.0	1.0	1.0	1.0	1.0	1.0	1.0
August	1.0	1.0	1.0	1.0	1.0	1.0	1.0	1.0	1.0	1.0
September	1.0	1.0	1.0	1.0	1.0	1.0	1.0	1.0	1.0	1.0
October	1.0	1.0	1.0	1.0	1.0	1.0	1.0	1.0	1.0	1.0
November	1.0	1.0	1.0	1.0	1.0	1.0	1.0	1.0	1.0	1.0
December	1.0	1.0	1.0	1.0	1.0	1.0	1.0	1.0	1.0	1.0

Distributions by Vehicle Class

Vehicle Class	AADTT Distribution (%) (Level 3)	Growth Factor Rate (%)	Growth Factor Function
Class 4	3.3%	3%	Linear
Class 5	34%	3%	Linear
Class 6	11.7%	3%	Linear
Class 7	1.6%	3%	Linear
Class 8	9.9%	3%	Linear
Class 9	36.2%	3%	Linear
Class 10	1%	3%	Linear
Class 11	1.8%	3%	Linear
Class 12	0.2%	3%	Linear
Class 13	0.3%	3%	Linear

Truck Distribution by Hour does not apply

Axle Configuration

Traffic Wander	
Mean wheel location (mm)	460.0
Traffic wander standard deviation (mm)	254.0
Design lane width (m)	3.7

Axle Configuration	
Average axle width (m)	2.6
Dual tire spacing (mm)	305.0
Tire pressure (kPa)	827.4

Average Axle Spacing	
Tandem axle spacing (m)	1.5
Tridem axle spacing (m)	1.7
Quad axle spacing (m)	1.3

Wheelbase does not apply

Number of Axles per Truck

Vehicle Class	Single Axle	Tandem Axle	Tridem Axle	Quad Axle
Class 4	1.62	0.39	0	0
Class 5	2	0	0	0
Class 6	1.01	0.993	0	0
Class 7	1.314	0.989	0.03	0
Class 8	2.163	0.845	0	0
Class 9	1.055	1.968	0.003	0
Class 10	1.446	1.234	0.7	0.088
Class 11	4.546	0.168	0	0
Class 12	2.857	1.526	0	0
Class 13	1.201	2.058	0.848	0.024

AADTT (Average Annual Daily Truck Traffic) Growth

*** Traffic cap is not enforced**

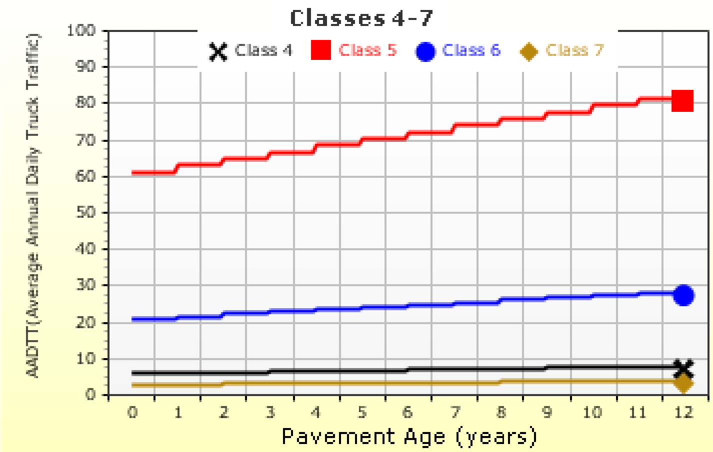

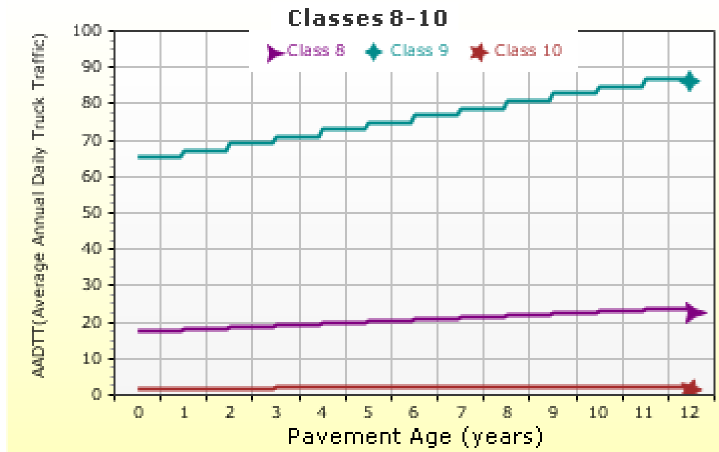

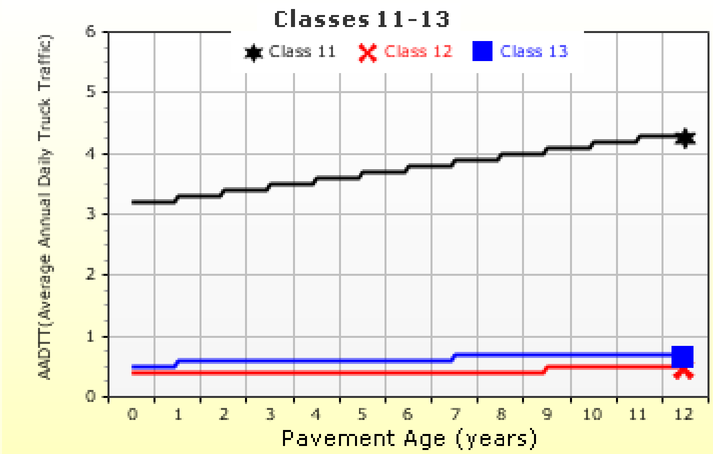

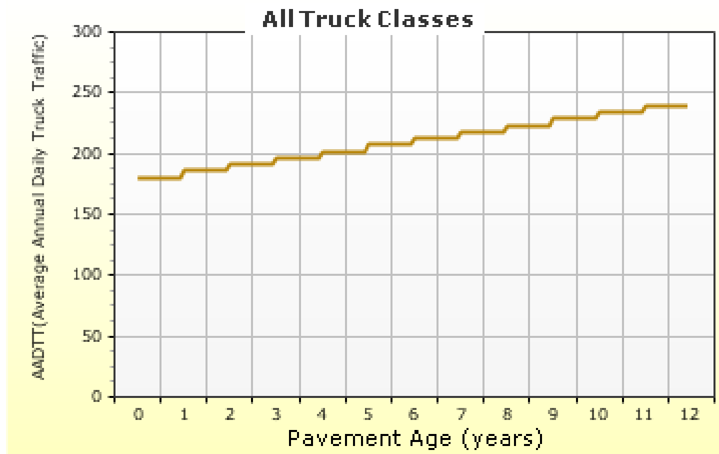

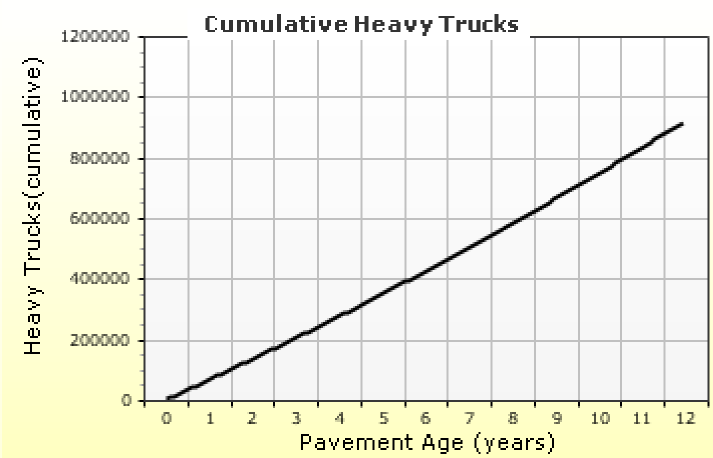

Climate Inputs

Climate Data Sources:

Climate Station Cities:	Location (lat lon elevation(m))
CA, ON	44.00000 -78.75000 193

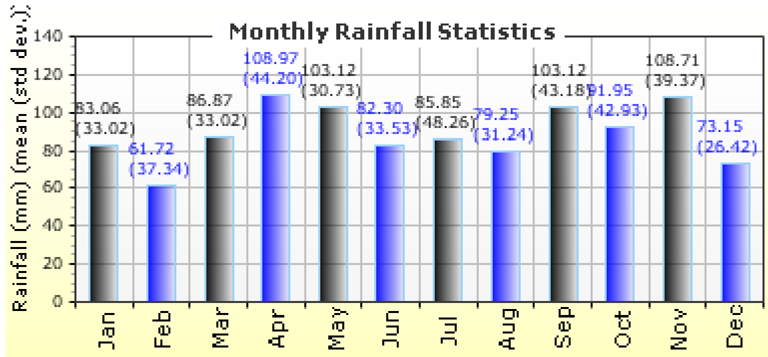

Annual Statistics:

Mean annual air temperature (ºC)	7.62
Mean annual precipitation (mm)	1068.32
Freezing index (ºC - days)	573.75
Average annual number of freeze/thaw cycles:	77.00

Water table depth (m) 10.00

Monthly Climate Summary:

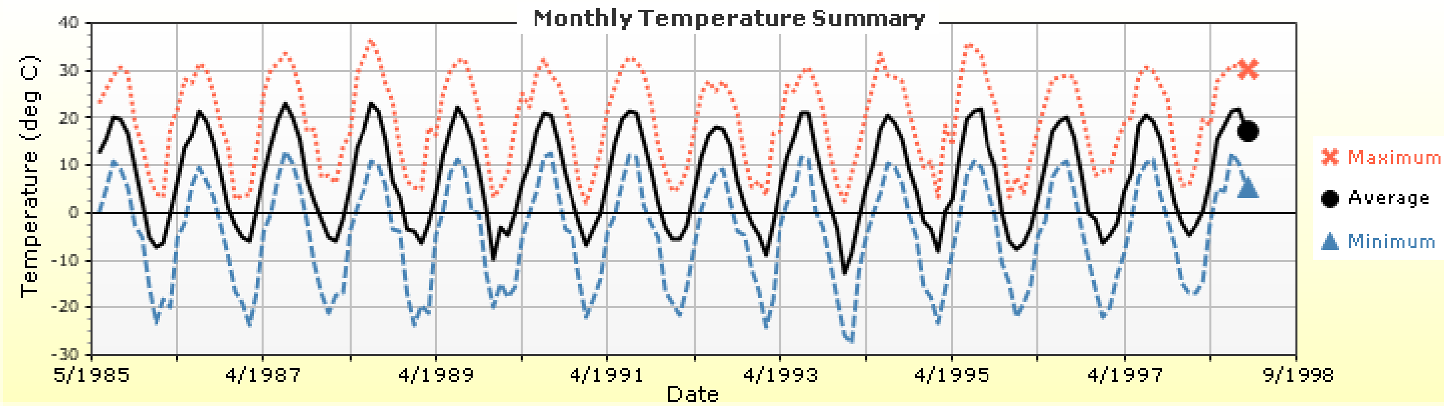

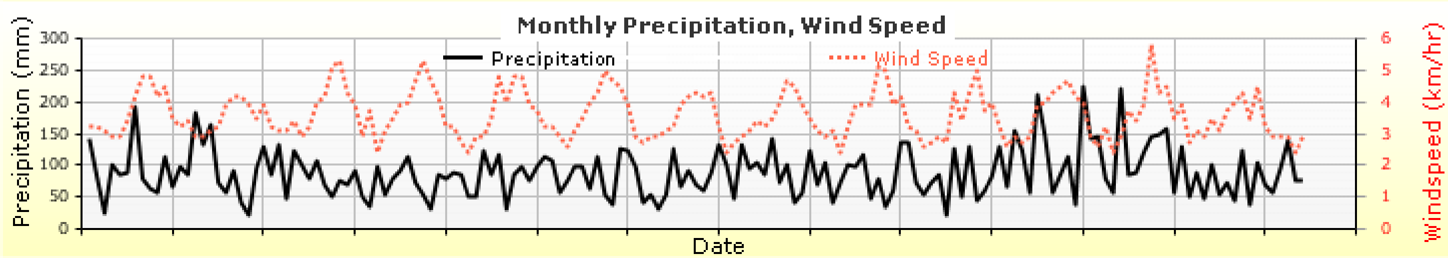

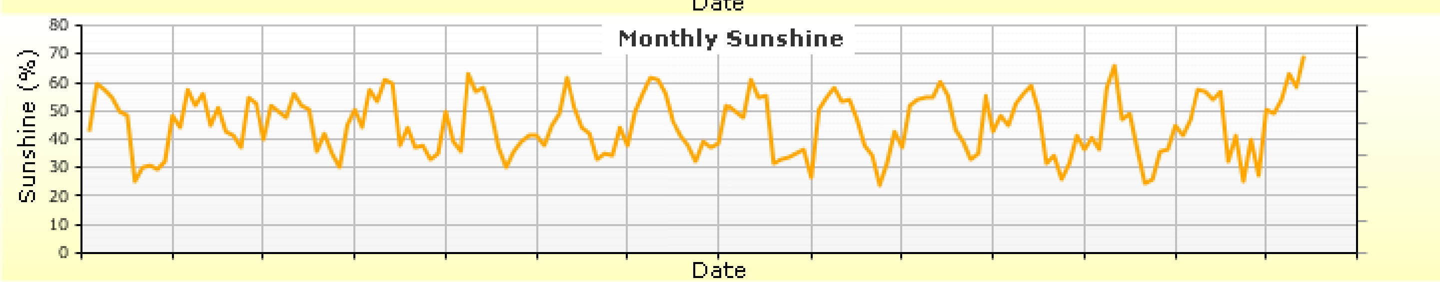

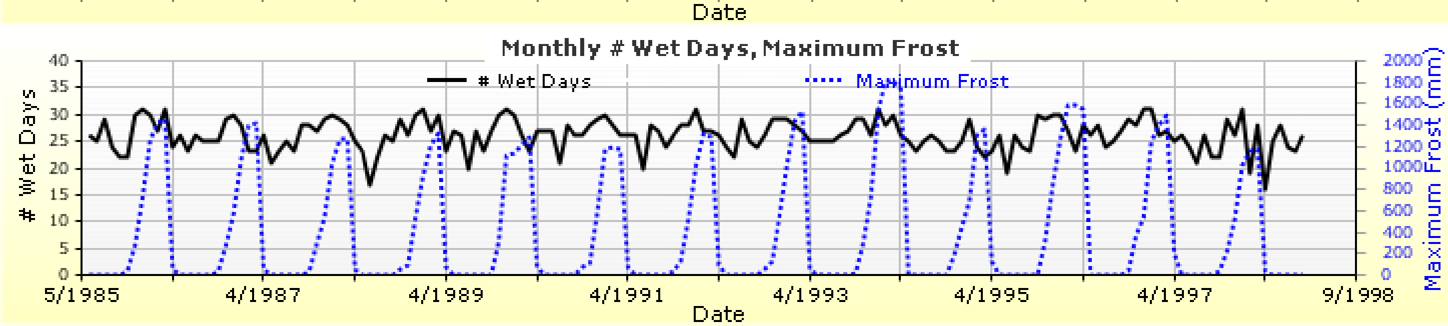

LVR_400AADT_CIR_0.5%-12 years December 2019

File Name: C:\Users\admin\Desktop\Taha M2\LVR_400AADT_CIR_0.5%-12 years December 2019.dgpx

Hourly Air Temperature Distribution by Month:

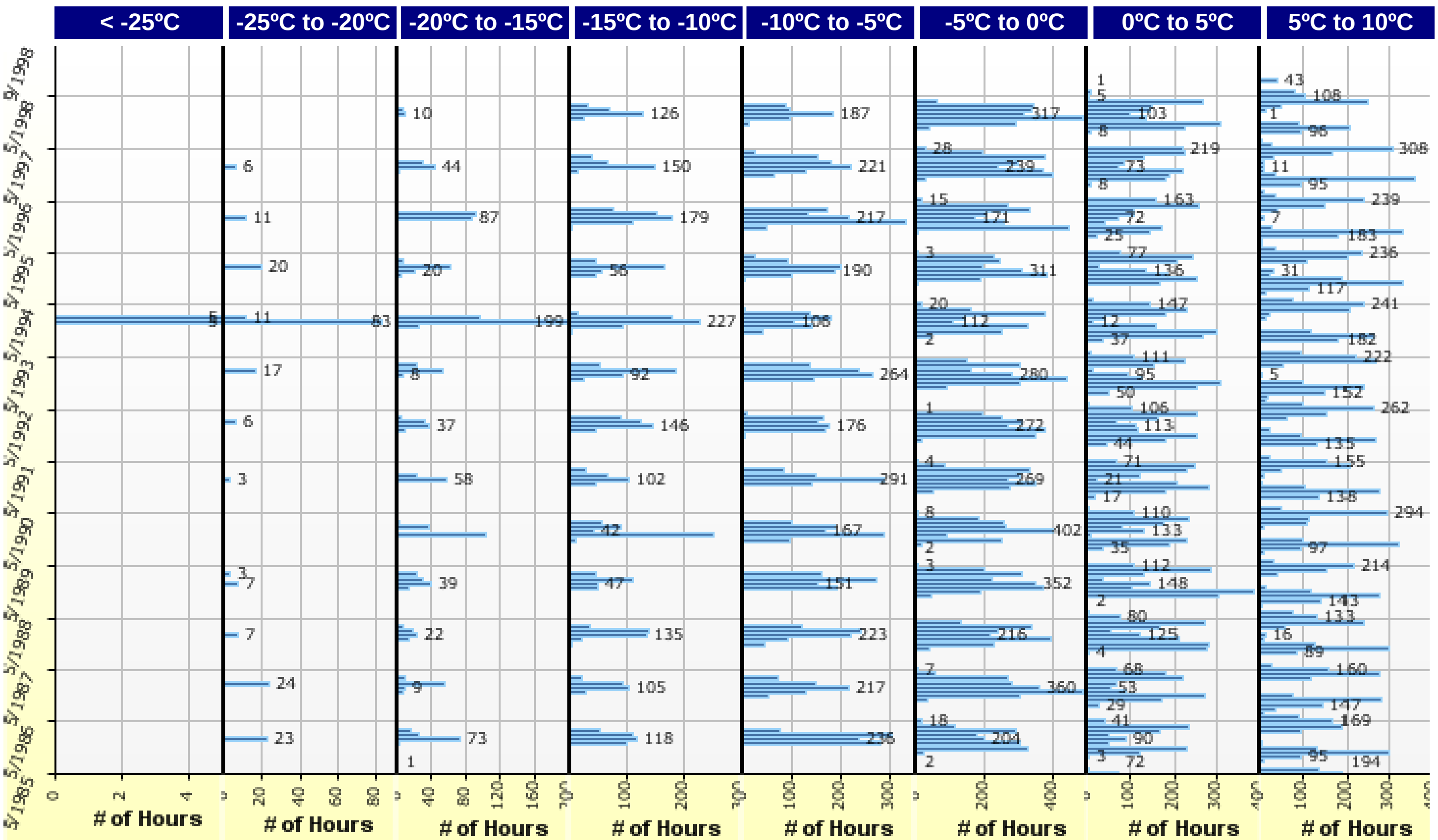

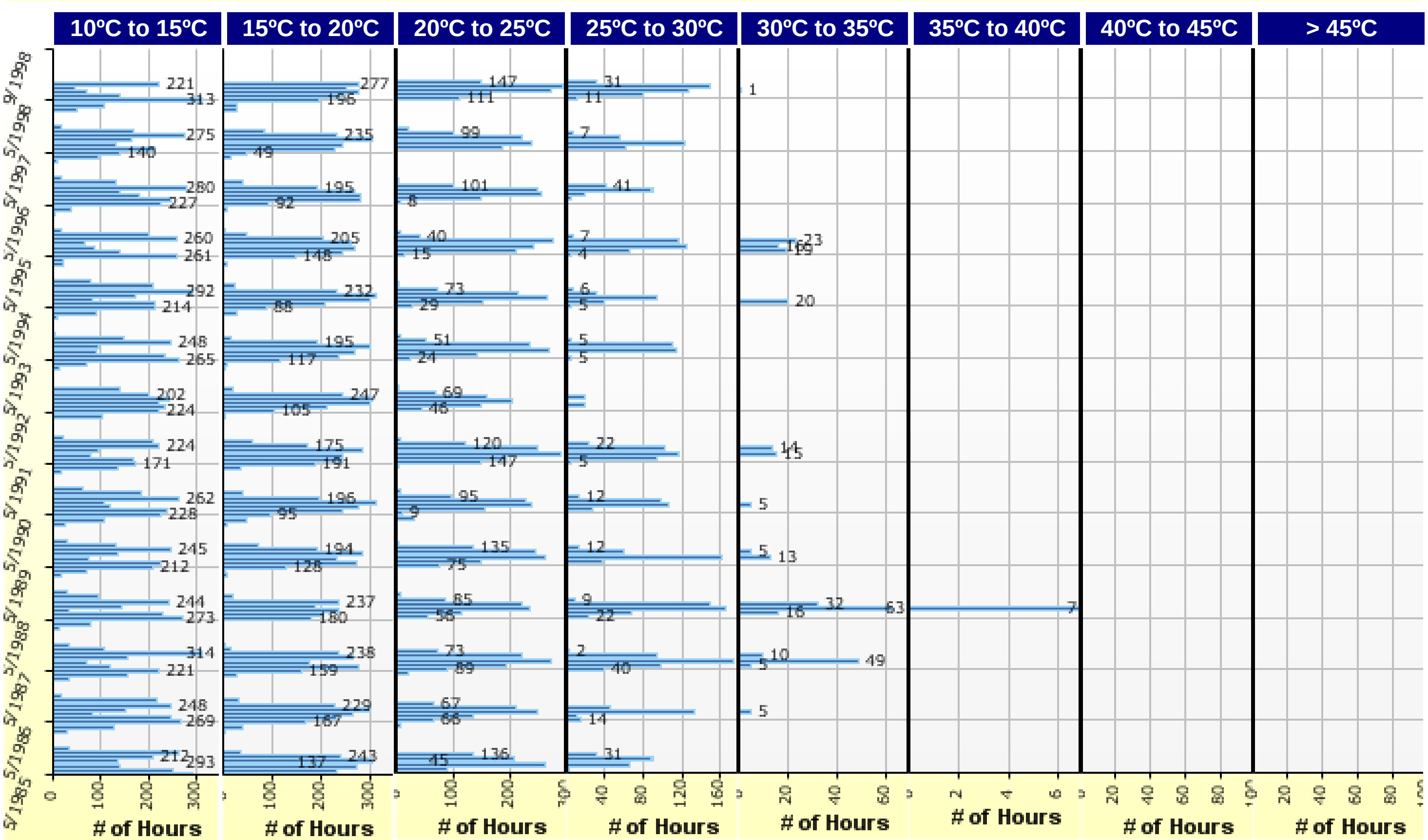

Design Properties

HMA Design Properties

Use Multilayer Rutting Model	False
Using G* based model (not nationally calibrated)	False
Is NCHRP 1-37A HMA Rutting Model Coefficients	True
Endurance Limit	-
Use Reflective Cracking	True

Structure - ICM Properties	
AC surface shortwave absorptivity	0.85

Layer Name	Layer Type	Interface Friction
Layer 1 Flexible : Default asphalt concrete	Flexible (1)	1.00
Layer 2 Flexible : Default asphalt concrete	Flexible (1)	1.00
Layer 3 Non-stabilized Base : A-1 -a	Non-stabilized Base (4)	1.00
Layer 4 Non-stabilized Base : A-1 -b	Non-stabilized Base (4)	1.00
Layer 5 Subgrade : A-6	Subgrade (5)	-

Thermal Cracking

Thermal Contraction	
Is thermal contraction calculated?	True
Mix coefficient of thermal contraction (mm/mm/ºC)	-
Aggregate coefficient of thermal contraction (mm/mm/ºC)	9.0e-006
Voids in Mineral Aggregate (%)	18.8

Indirect Tensile Strength (Input Level: 3)	
Test Temperature (ºC)	Indirect Tensilte Strength (Mpa)
-10.0	2.79

Creep Compliance (1/GPa) (Input Level: 3)			
Loading time (sec)	-20 ºC	-10 ºC	0 ºC
1	5.57e-002	8.57e-002	1.16e-001
2	6.17e-002	1.01e-001	1.51e-001
5	7.07e-002	1.25e-001	2.15e-001
10	7.83e-002	1.48e-001	2.80e-001
20	8.68e-002	1.74e-001	3.65e-001
50	9.94e-002	2.16e-001	5.19e-001
100	1.10e-001	2.55e-001	6.77e-001

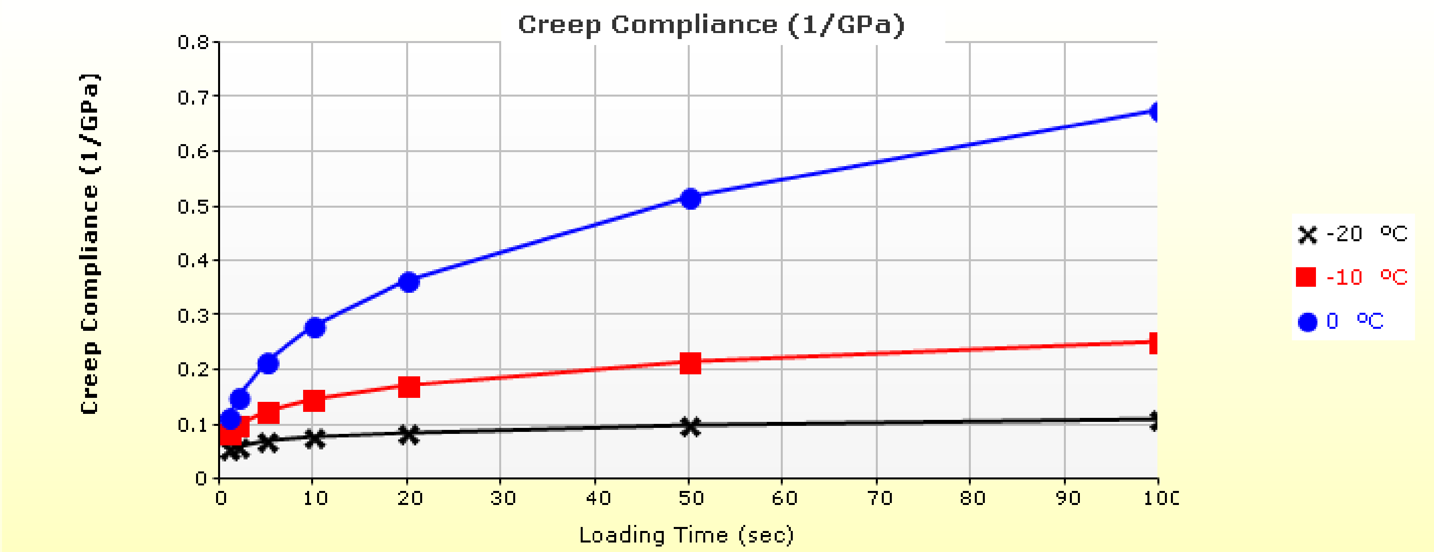

LVR_400AADT_CIR_0.5%-12 years December 2019

File Name: C:\Users\admin\Desktop\Taha M2\LVR_400AADT_CIR_0.5%-12 years December 2019.dgpx

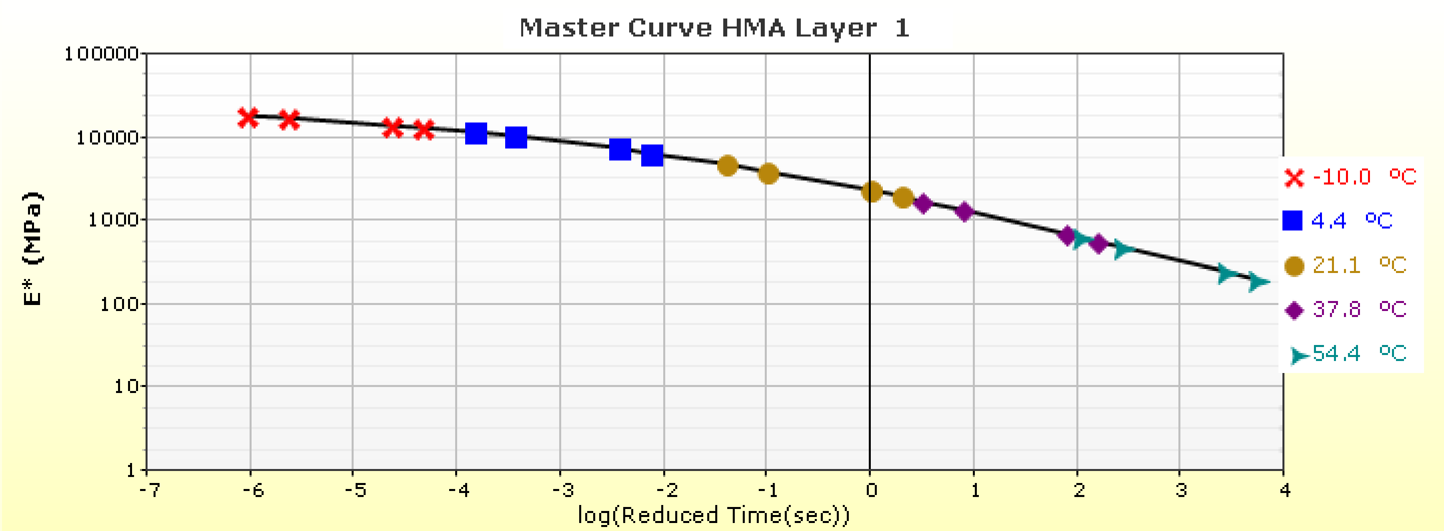

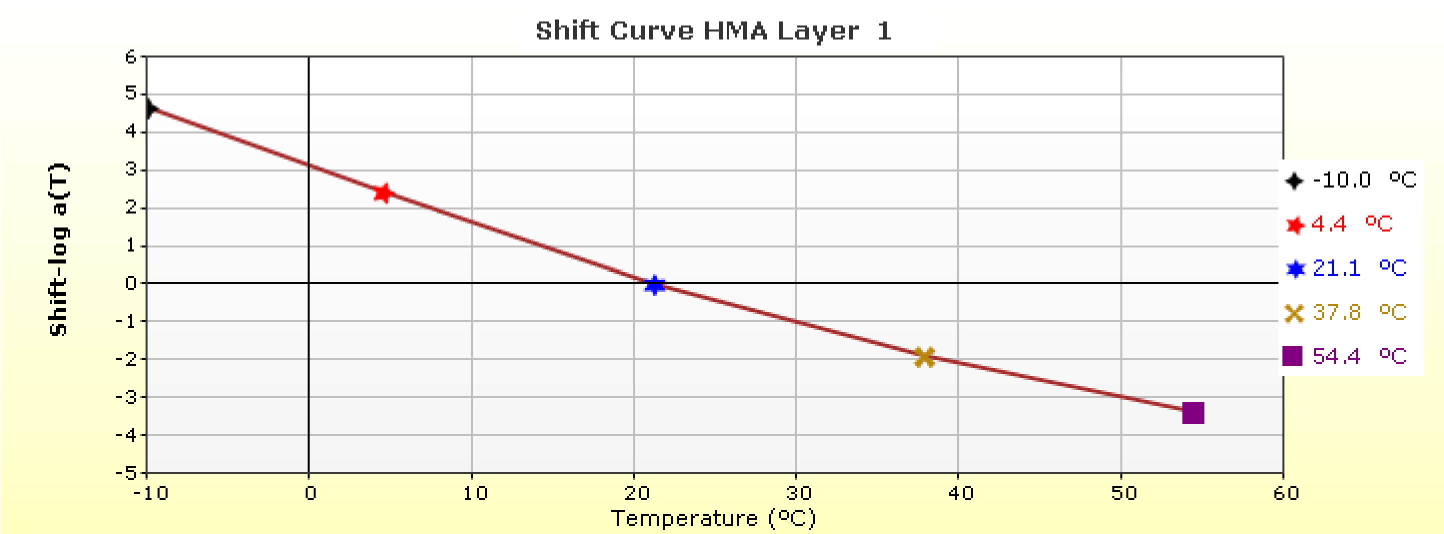

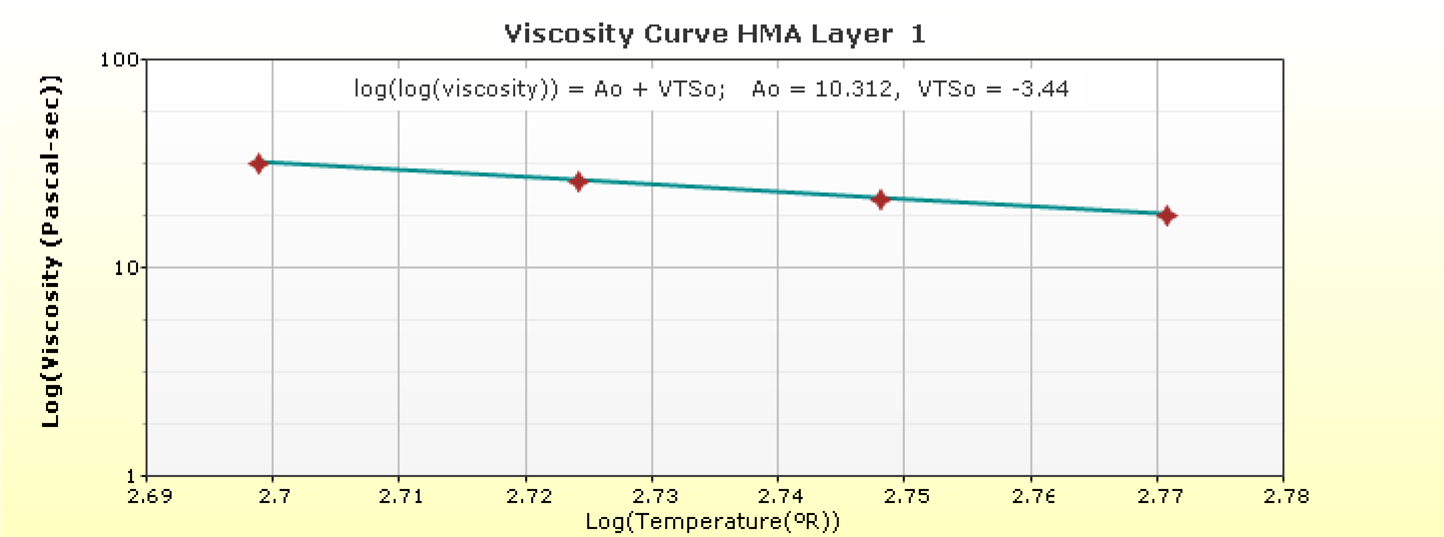

LVR_400AADT_CIR_0.5%-12 years December 2019

File Name: C:\Users\admin\Desktop\Taha M2\LVR_400AADT_CIR_0.5%-12 years December 2019.dgpx

HMA Layer 2: Layer 2 Flexible : Default asphalt concrete

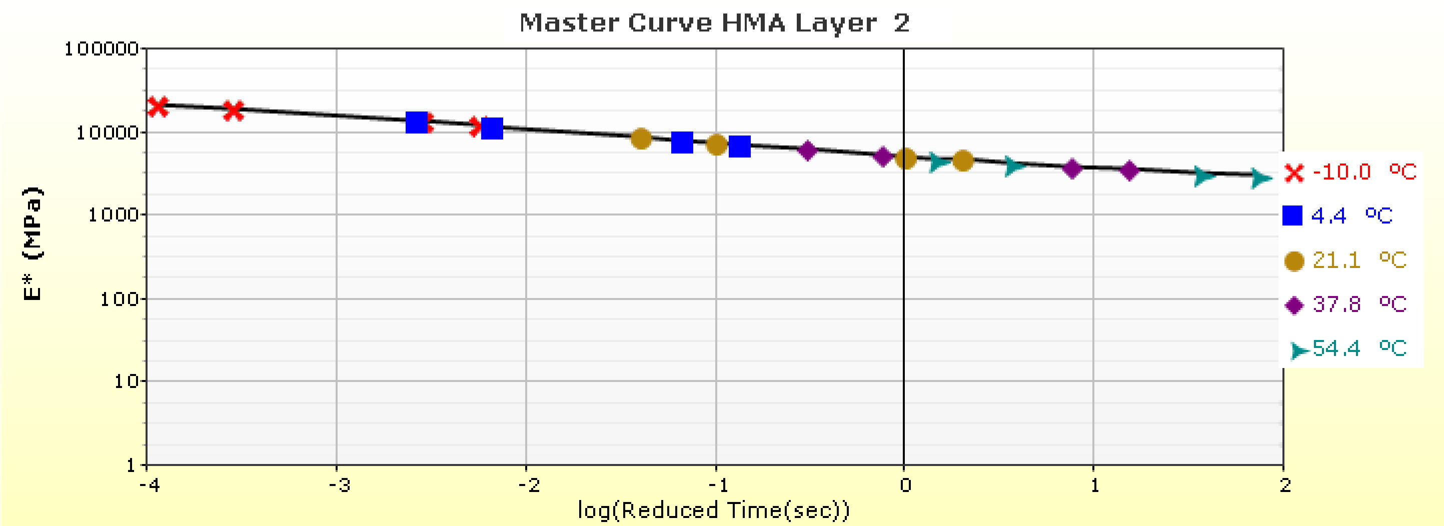

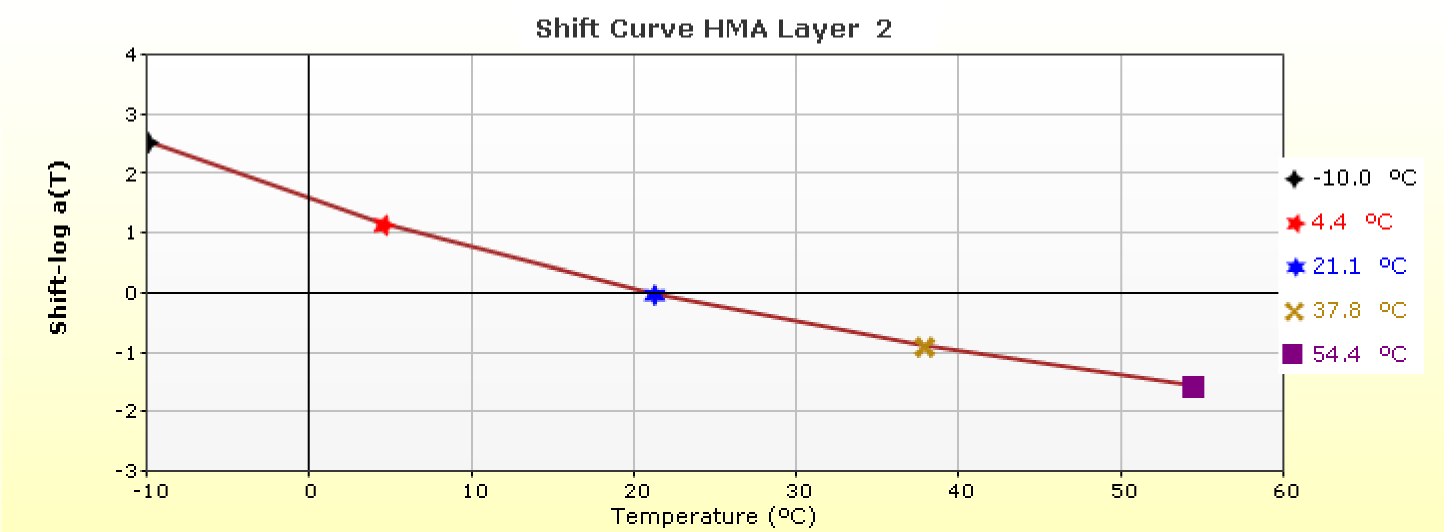

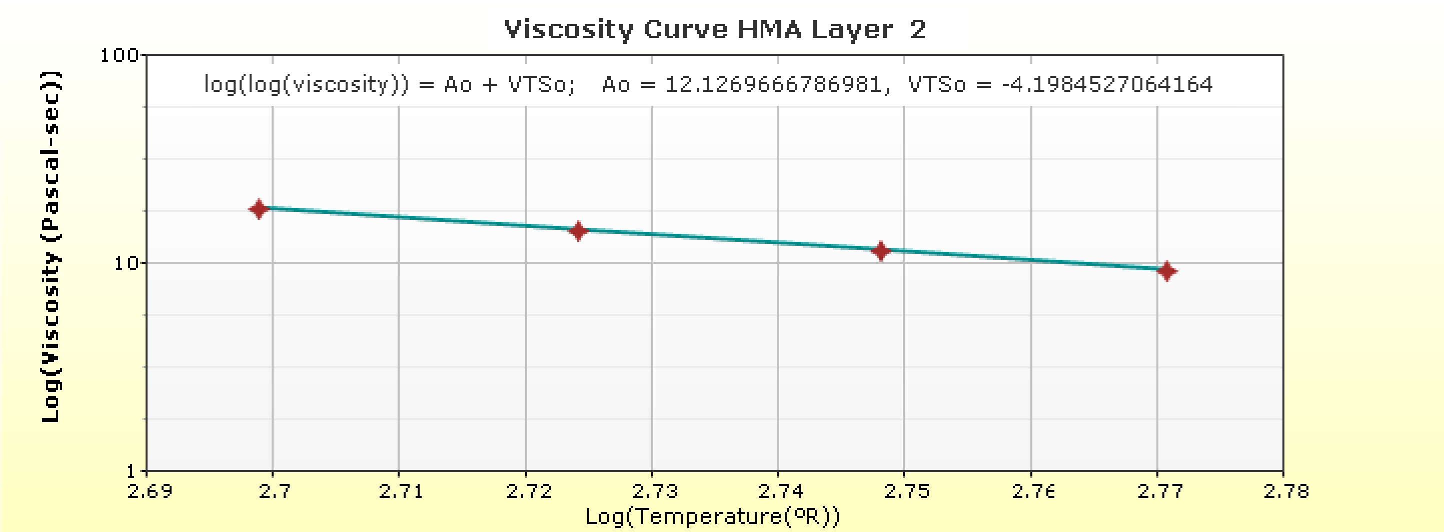

Analysis Output Charts

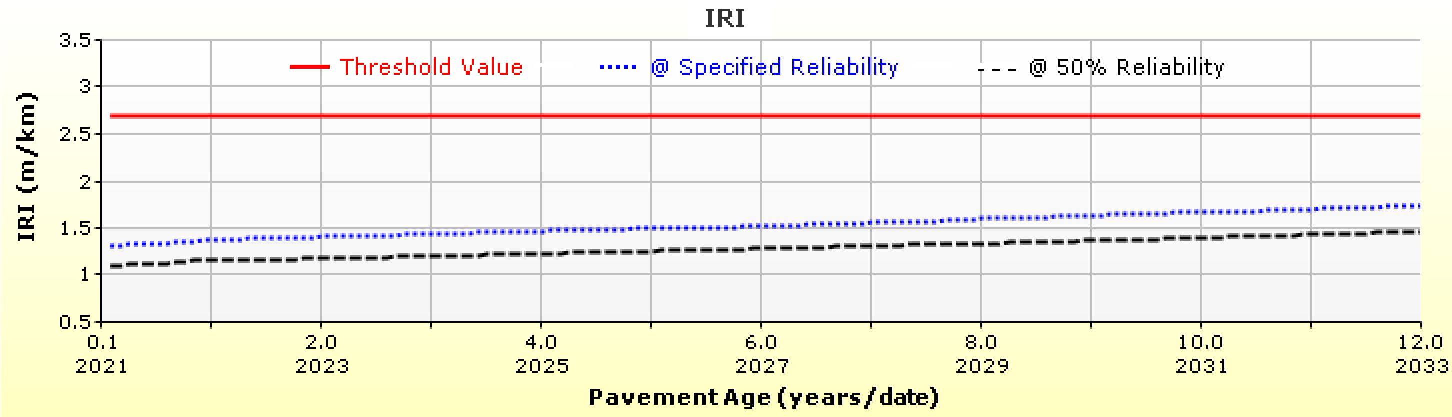

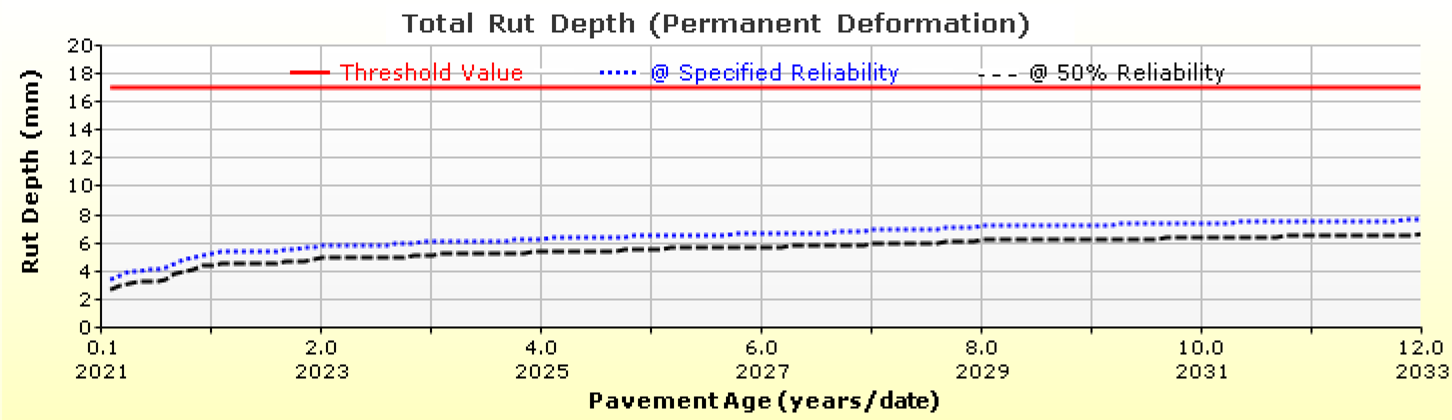

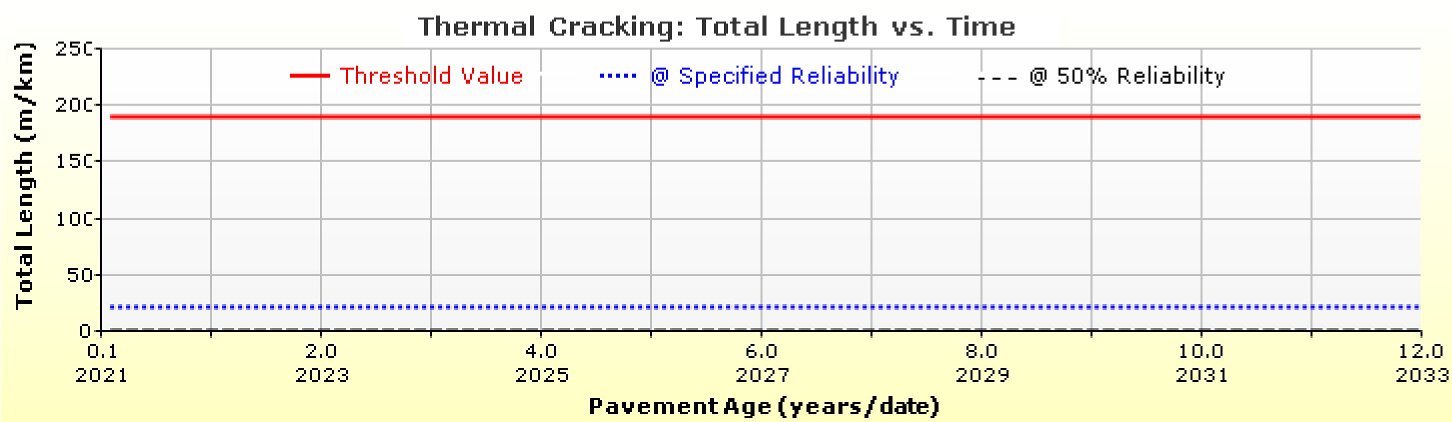

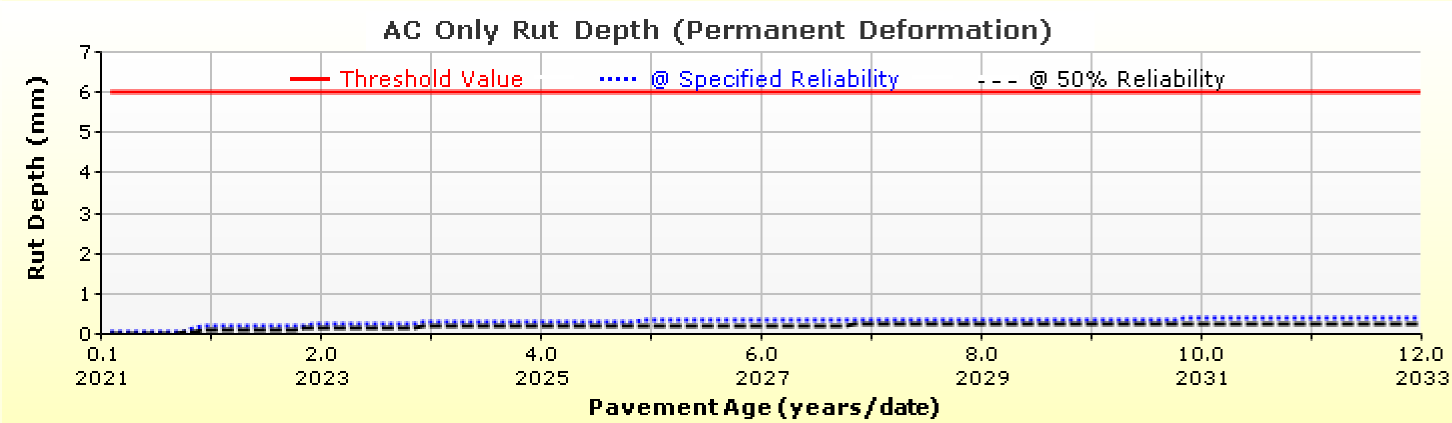

LVR_400AADT_CIR_0.5%-12 years December 2019

File Name: C:\Users\admin\Desktop\Taha M2\LVR_400AADT_CIR_0.5%-12 years December 2019.dgpx

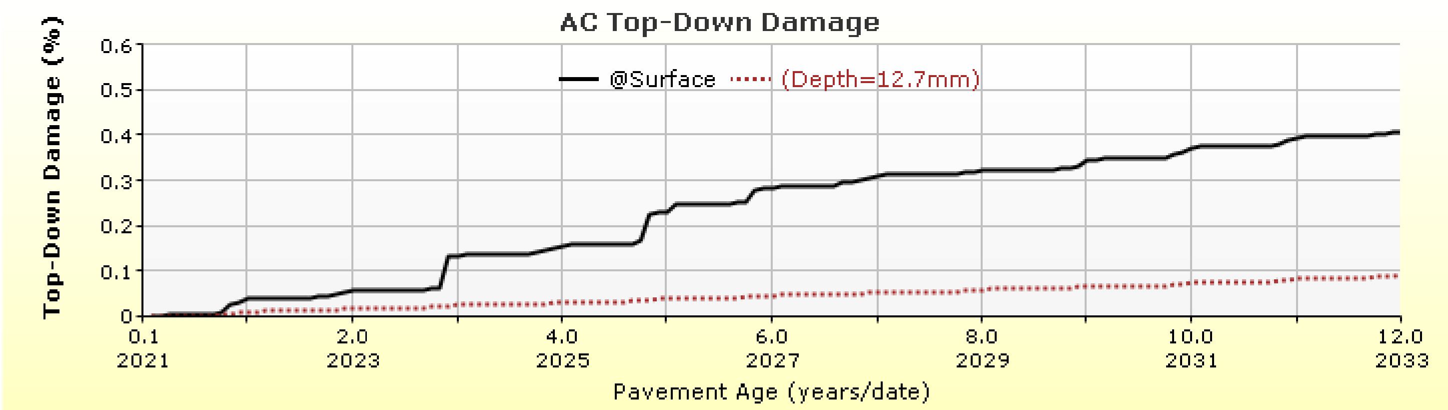

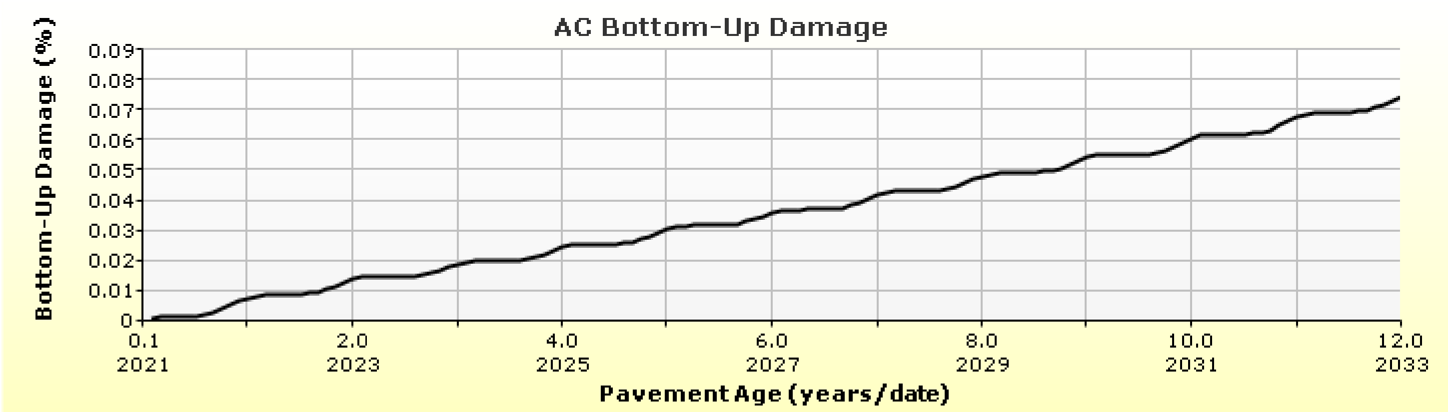

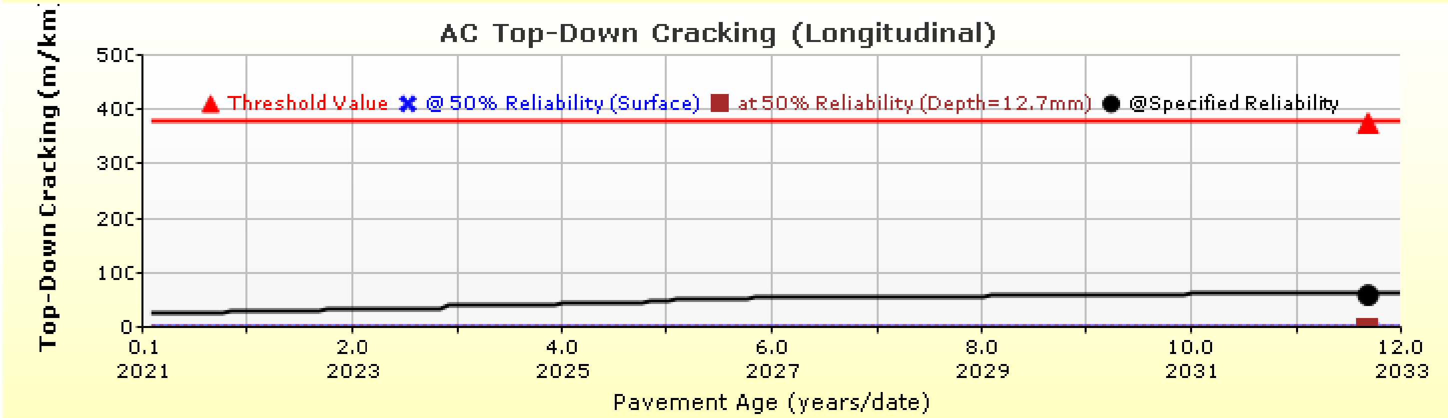

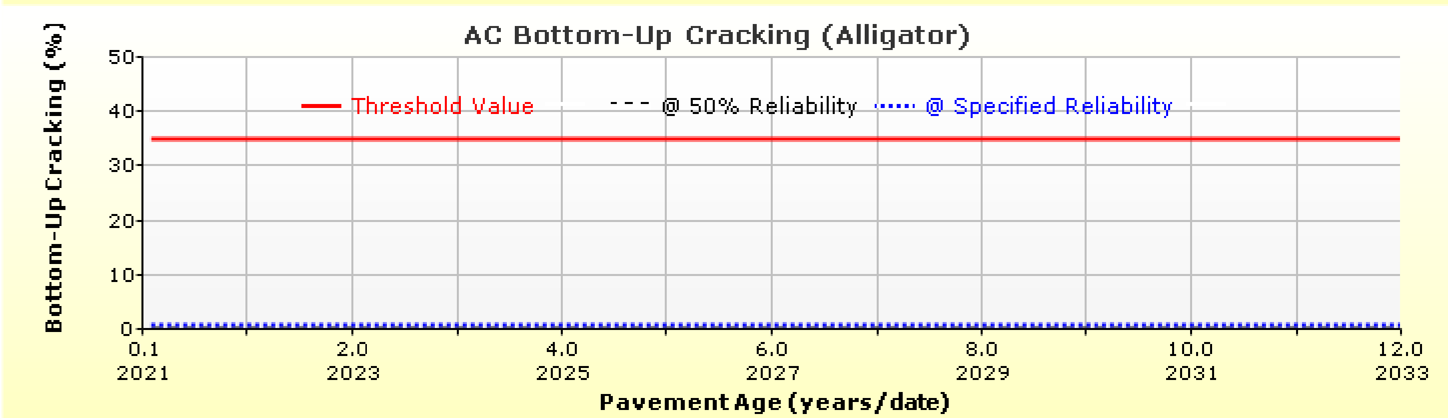

LVR_400AADT_CIR_0.5%-12 years December 2019

File Name: C:\Users\admin\Desktop\Taha M2\LVR_400AADT_CIR_0.5%-12 years December 2019.dgpx

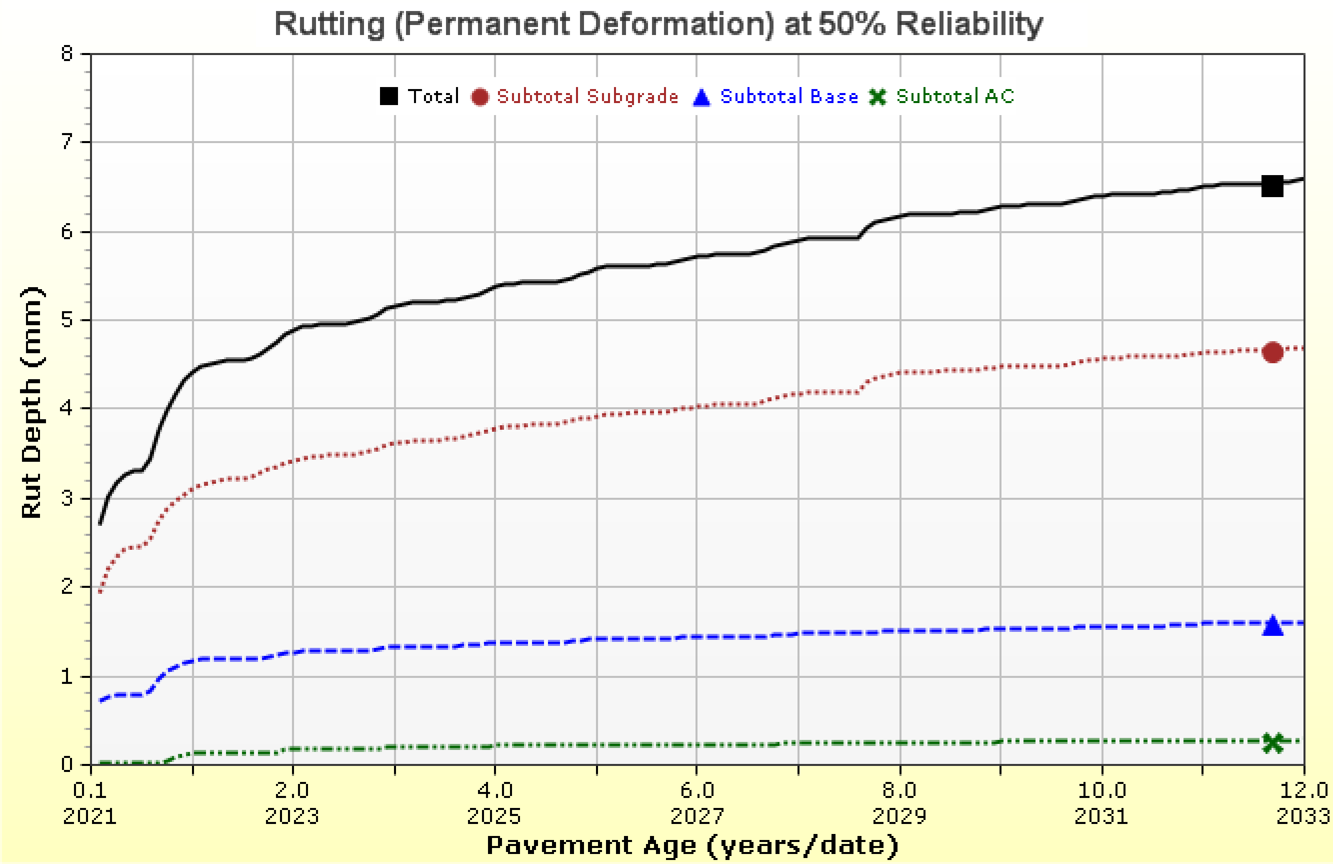

LVR_400AADT_CIR_0.5%-12 years December 2019

File Name: C:\Users\admin\Desktop\Taha M2\LVR_400AADT_CIR_0.5%-12 years December 2019.dgpx

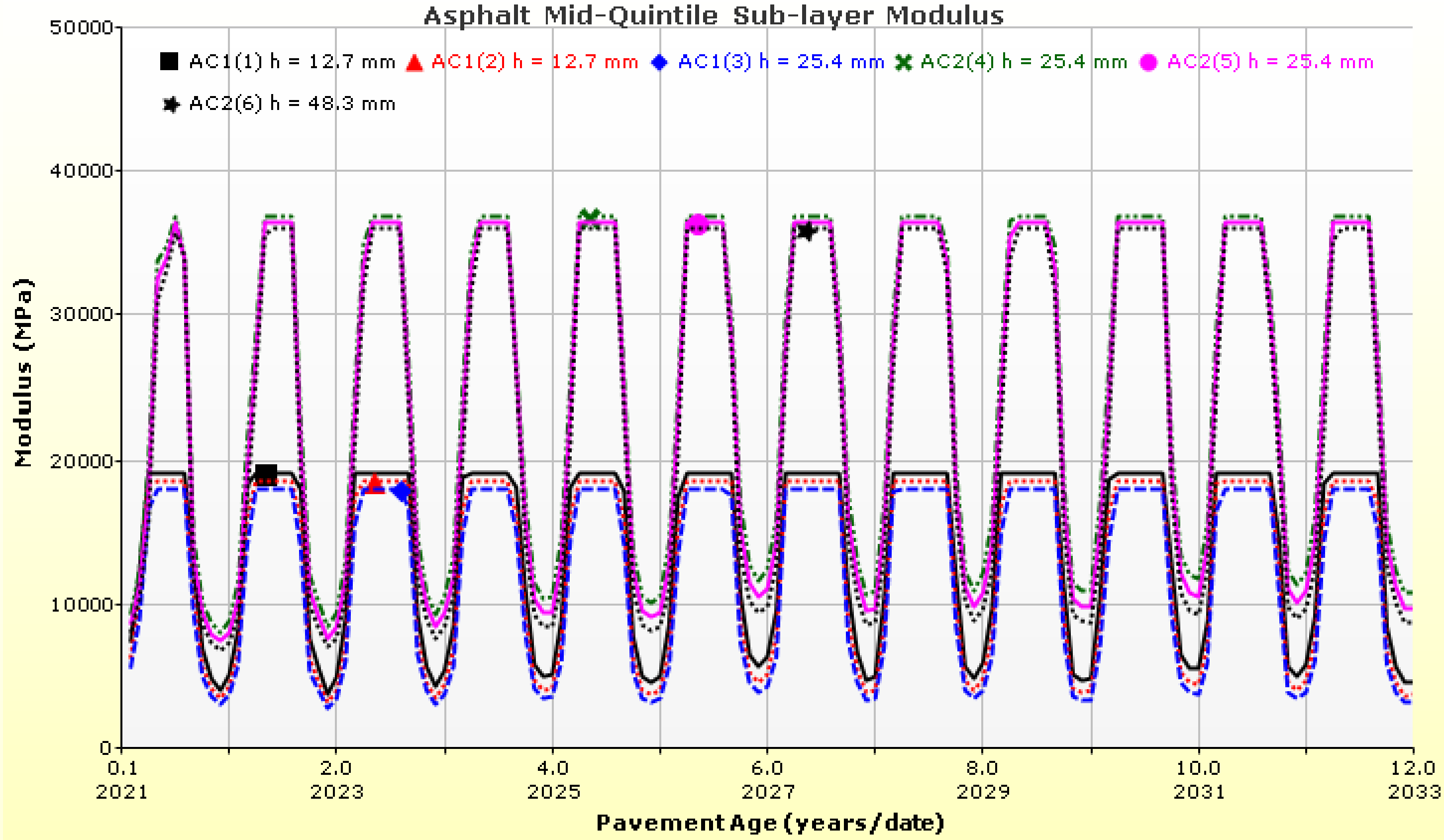

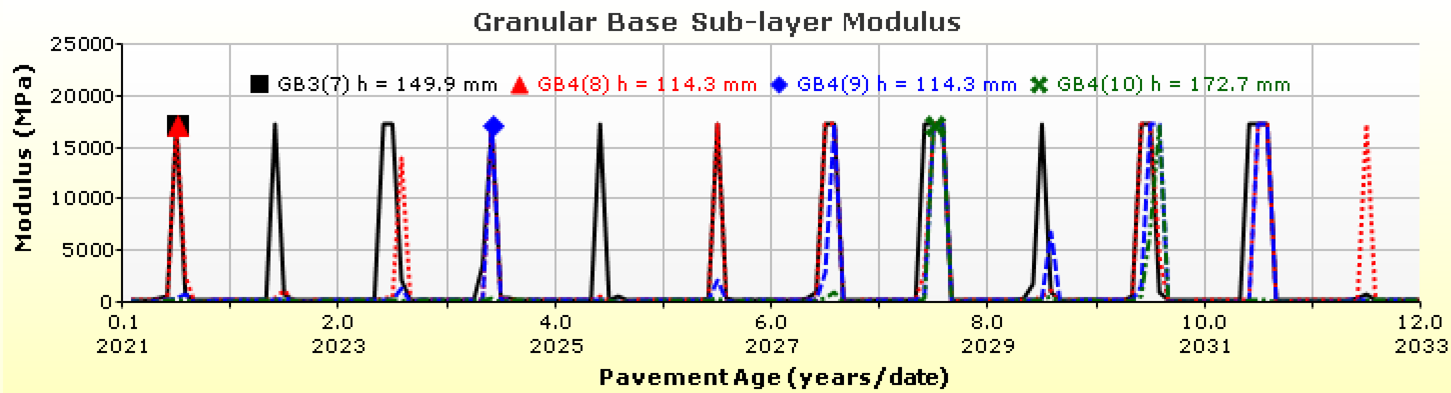

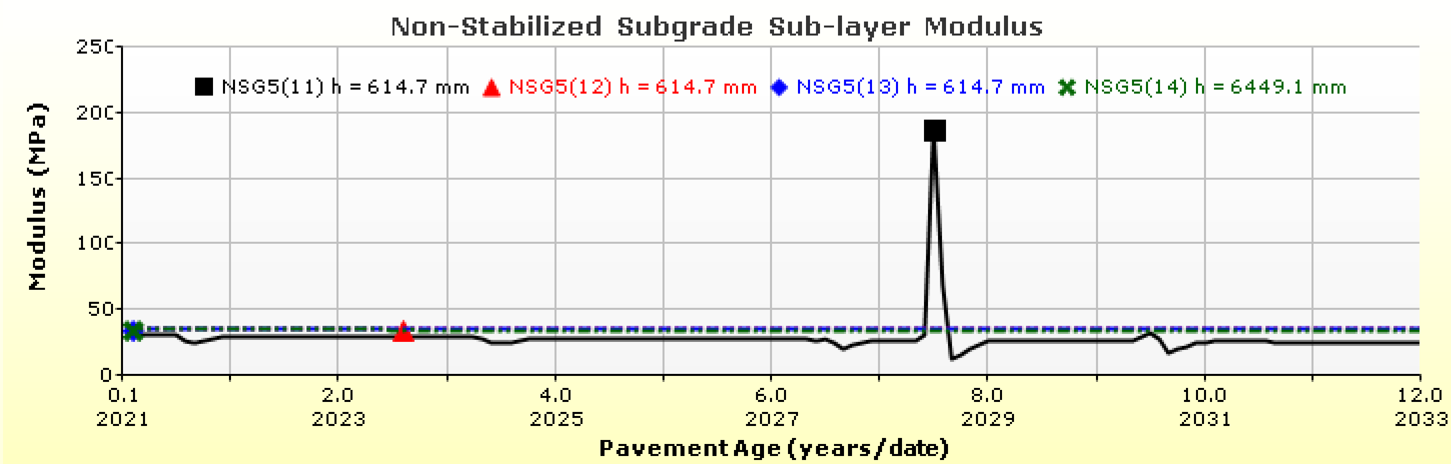

Layer Information

Layer 1 Flexible : Default asphalt concrete

Asphalt		
Thickness (mm)	50.0	
Unit weight (kgf/m^3)	2460.0	
Poisson's ratio	Is Calculated?	False
	Ratio	0.35
	Parameter A	-
	Parameter B	-

Asphalt Dynamic Modulus (Input Level: 3)

Gradation	Percent Passing
19 mm sieve	100
9.5 mm sieve	83.2
4.75 mm sieve	54
0.075mm sieve	4

Asphalt Binder

Parameter	Value
Grade	Superpave Performance Grade
Binder Type	64-28
A	10.312
VTS	-3.44

General Info

Name	Value
Reference temperature (ºC)	21.1
Effective binder content (%)	11.8
Air voids (%)	7
Thermal conductivity (watt/meter-kelvin)	1.16
Heat capacity (joule/kg-kelvin)	963

Identifiers

Field	Value
Display name/identifier	Default asphalt concrete
Description of object	
Author	
Date Created	9/16/2010 1:00:00 AM
Approver	
Date approved	9/16/2010 1:00:00 AM
State	
District	
County	
Highway	
Direction of Travel	
From station (km)	
To station (km)	
Province	
User defined field 1	
User defined field 2	
User defined field 3	
Revision Number	0

Layer 2 Flexible : Default asphalt concrete

Asphalt		
Thickness (mm)	100.0	
Unit weight (kgf/m^3)	2460.0	
Poisson's ratio	Is Calculated?	False
	Ratio	0.35
	Parameter A	-
	Parameter B	-

Asphalt Dynamic Modulus (Input Level: 1)

T (ºC)	0.1 Hz	0.5 Hz	1 Hz	5 Hz	10 Hz	25 Hz
-10	11583.54	13515.76	14697.46	16879.86	17896.52	20328.18
4	6732.273	7422.616	9453.853	10601.15	11678.20	12895.28
21	2259.515	3371.524	3773.661	5181.153	5923.615	6749.267
57	2259.515	3371.524	3773.661	5181.153	5923.615	6749.267

Asphalt Binder

Temperature (ºC)	Binder Gstar (Pa)	Phase angle (deg)
4.4	5494.5	57
12.8	1919	59.3
21.1	490.2	61.6
29.4	161.2	62.4
37.8	39.9	62.7
46.1	15.2	62.7

General Info

Name	Value
Reference temperature (ºC)	21.1
Effective binder content (%)	11.2
Air voids (%)	7
Thermal conductivity (watt/meter-kelvin)	1.16
Heat capacity (joule/kg-kelvin)	963

Identifiers

Field	Value
Display name/identifier	Default asphalt concrete
Description of object	
Author	
Date Created	9/16/2010 1:00:00 AM
Approver	
Date approved	9/16/2010 1:00:00 AM
State	
District	
County	
Highway	
Direction of Travel	
From station (km)	
To station (km)	
Province	
User defined field 1	
User defined field 2	
User defined field 3	
Revision Number	0

Layer 3 Non-stabilized Base : A-1-a

Unbound	
Layer thickness (mm)	150.0
Poisson's ratio	0.35
Coefficient of lateral earth pressure (k0)	0.5

Modulus (Input Level: 3)

Analysis Type:	Modify input values by temperature/moisture
Method:	Resilient Modulus (MPa)

Resilient Modulus (MPa)
250.0

Use Correction factor for NDT modulus?	-
NDT Correction Factor:	-

Identifiers

Field	Value
Display name/identifier	A-1-a
Description of object	Default material
Author	AASHTO
Date Created	1/1/2011 12:00:00 AM
Approver	
Date approved	1/1/2011 12:00:00 AM
State	
District	
County	
Highway	
Direction of Travel	
From station (km)	
To station (km)	
Province	
User defined field 1	
User defined field 2	
User defined field 3	
Revision Number	0

Sieve

Liquid Limit	6.0
Plasticity Index	0.0
Is layer compacted?	False

	Is User Defined?	Value
Maximum dry unit weight (kgf/m^3)	False	2038.2
Saturated hydraulic conductivity (m/hr)	False	2.376e-02
Specific gravity of solids	False	2.7
Water Content (%)	False	5.7

User-defined Soil Water Characteristic Curve (SWCC)	
Is User Defined?	False
af	3.0201
bf	2.5984
cf	0.7539
hr	100.0000

Sieve Size	% Passing
0.001mm	
0.002mm	
0.020mm	
0.075mm	5.0
0.150mm	
0.180mm	
0.250mm	
0.300mm	13.5
0.425mm	
0.600mm	
0.850mm	
1.18mm	27.5
2.0mm	
2.36mm	
4.75mm	45.0
9.5mm	61.5
12.5mm	77.5
19.0mm	92.5
25.0mm	100.0
37.5mm	
50.0mm	
63.0mm	
75.0mm	
90.0mm	

Layer 4 Non-stabilized Base : A-1-b

Unbound	
Layer thickness (mm)	400.0
Poisson's ratio	0.35
Coefficient of lateral earth pressure (k0)	0.5

Modulus (Input Level: 3)

Analysis Type:	Modify input values by temperature/moisture
Method:	Resilient Modulus (MPa)

Resilient Modulus (MPa)
150.0

Use Correction factor for NDT modulus?	-
NDT Correction Factor:	-

Identifiers

Field	Value
Display name/identifier	A-1-b
Description of object	Default material
Author	AASHTO
Date Created	1/1/2011 12:00:00 AM
Approver	
Date approved	1/1/2011 12:00:00 AM
State	
District	
County	
Highway	
Direction of Travel	
From station (km)	
To station (km)	
Province	
User defined field 1	
User defined field 2	
User defined field 3	
Revision Number	0

Sieve

Liquid Limit	11.0
Plasticity Index	0.0
Is layer compacted?	False

	Is User Defined?	Value
Maximum dry unit weight (kgf/m^3)	False	1981.7
Saturated hydraulic conductivity (m/hr)	False	7.17e-03
Specific gravity of solids	False	2.7
Water Content (%)	False	7.9

User-defined Soil Water Characteristic Curve (SWCC)	
Is User Defined?	False
af	5.0954
bf	2.5384
cf	0.8464
hr	100.0000

Sieve Size	% Passing
0.001mm	
0.002mm	
0.020mm	
0.075mm	4.0
0.150mm	
0.180mm	
0.250mm	
0.300mm	33.5
0.425mm	
0.600mm	
0.850mm	
1.18mm	55.0
2.0mm	
2.36mm	
4.75mm	60.0
9.5mm	
12.5mm	
19.0mm	
25.0mm	75.0
37.5mm	
50.0mm	
63.0mm	
75.0mm	
90.0mm	

Layer 5 Subgrade : A-6

Unbound	
Layer thickness (mm)	Semi-infinite
Poisson's ratio	0.3
Coefficient of lateral earth pressure (k0)	0.5

Modulus (Input Level: 3)

Analysis Type:	Modify input values by temperature/moisture
Method:	Resilient Modulus (MPa)

Resilient Modulus (MPa)
35.0

Use Correction factor for NDT modulus?	-
NDT Correction Factor:	-

Identifiers

Field	Value
Display name/identifier	A-6
Description of object	Default material
Author	AASHTO
Date Created	1/1/2011 12:00:00 AM
Approver	
Date approved	1/1/2011 12:00:00 AM
State	
District	
County	
Highway	
Direction of Travel	
From station (km)	
To station (km)	
Province	
User defined field 1	
User defined field 2	
User defined field 3	
Revision Number	0

Sieve

Liquid Limit	18.0
Plasticity Index	4.0
Is layer compacted?	False

	Is User Defined?	Value
Maximum dry unit weight (kgf/m^3)	False	1992.5
Saturated hydraulic conductivity (m/hr)	False	1.095e-06
Specific gravity of solids	False	2.7
Water Content (%)	False	8.8

User-defined Soil Water Characteristic Curve (SWCC)	
Is User Defined?	False
af	26.3898
bf	1.0483
cf	0.8553
hr	332.0000

Sieve Size	% Passing
0.001mm	
0.002mm	8.0
0.020mm	
0.075mm	29.0
0.150mm	
0.180mm	58.0
0.250mm	
0.300mm	
0.425mm	72.0
0.600mm	
0.850mm	
1.18mm	
2.0mm	84.0
2.36mm	
4.75mm	90.0
9.5mm	94.0
12.5mm	97.0
19.0mm	98.0
25.0mm	100.0
37.5mm	
50.0mm	
63.0mm	
75.0mm	
90.0mm	

Calibration Coefficients

AC Fatigue

$$N_f = 0.00432 * C * \beta_{f1} k_1 \left(\frac{1}{\varepsilon_1}\right)^{k_2 \beta_{f2}} \left(\frac{1}{E}\right)^{k_3 \beta_{f3}}$$

$$C = 10^M$$

$$M = 4.84\left(\frac{V_b}{V_a + V_b} - 0.69\right)$$

k1: 3.75	
k2: 2.87	
k3: 1.46	
Bf1: (5.014 * Pow(hac,-3.416)) * 1 + 0	
Bf2: 1.38	
Bf3: 0.88	

AC Rutting

$$\frac{\varepsilon_p}{\varepsilon_r} = k_z \beta_{r1} 10^{k_1} T^{k_2 \beta_{r2}} N^{k_3 \beta_{r3}}$$

$$k_z = (C_1 + C_2 * depth) * 0.328196^{depth}$$

$$C_1 = -0.1039 * H_\alpha^2 + 2.4868 * H_\alpha - 17.342$$

$$C_2 = 0.0172 * H_\alpha^2 - 1.7331 * H_\alpha + 27.428$$

Where:

H_{ac} = total AC thickness(in)

ε_p = plastic strain$\left(^{in}/_{in}\right)$
ε_r = resilient strain$\left(^{in}/_{in}\right)$
T = layer temperature$\left(^\circ F\right)$
N = number of load repetitions

AC Rutting Standard Deviation	0.24 * Pow(RUT,0.8026) + 0.001	
AC Layer 1	K1:-2.45 K2:3.01 K3:0.22	Br1:0.128 Br2:0.52 Br3:1.36
AC Layer 2	K1:-2.45 K2:3.01 K3:0.22	Br1:0.4 Br2:0.52 Br3:1.36

Thermal Fracture

$$C_f = 400 * N\left(\frac{\log C / h_{ac}}{\sigma}\right)$$

$$\Delta C = (k * \beta t)^{n+1} * A * \Delta K^n$$

$$A = 10^{(4.389 - 2.52 * \log(E * \sigma_m * n))}$$

C_f = observed amount of thermal cracking(ft/500ft)
k = refression coefficient determined through field calibration
$N()$ = standard normal distribution evaluated at()
σ = standard deviation of the log of the depth of cracks in the pavments
C = crack depth(in)
h_{ac} = thickness of asphalt layer(in)
ΔC = Change in the crack depth due to a cooling cycle
ΔK = Change in the stress intensity factor due to a cooling cycle
A, n = Fracture parameters for the asphalt mixture
E = mixture stiffness
σ_M = Undamaged mixture tensile strength
β_t = Calibration parameter

Level 1 K: ((3 * Pow(10,-7)) * Pow(MAAT,4.0319)) * 1 + 0	Level 1 Standard Deviation: 0.14 * THERMAL + 168
Level 2 K: ((3 * Pow(10,-7)) * Pow(MAAT,4.0319)) * 1 + 0	Level 2 Standard Deviation: 0.20 * THERMAL + 168
Level 3 K: ((3 * Pow(10,-7)) * Pow(MAAT,4.0319)) * 1 + 0	Level 3 Standard Deviation: 0.289 * THERMAL + 168

CSM Fatigue

$$N_f = 10^{\left(\frac{k_1 \beta_{c1}\left(\frac{\sigma_s}{M_r}\right)}{k_2 \beta_{c2}}\right)}$$

N_f = number of repetitions to fatigue cracking
σ_s = Tensile stress(psi)
M_r = modulus of rupture(psi)

k1: 0.972	k2: 0.0825	Bc1: 1	Bc2:1

Unbound Layer Rutting

$$\delta_a(N) = \beta_{s_1} k_1 \varepsilon_v h \left(\frac{\varepsilon_0}{\varepsilon_r}\right) \left| e^{-\left(\frac{\rho}{N}\right)^{\beta}} \right|$$

δ_a = permanent deformation for the layer
N = number of repetitions
ε_v = average veritcal strain(in/in)
$\varepsilon_0, \beta, \rho$ = material properties
ε_r = resilient strain(in/in)

Base Rutting		Subgrade Rutting	
k1: 0.965	Bs1: 1	k1: 0.675	Bs1: 1
Standard Deviation (BASERUT) 0.1477 * Pow(BASERUT,0.6711) + 0.001		Standard Deviation (BASERUT) 0.1235 * Pow(SUBRUT,0.5012) + 0.001	

AC Cracking

AC Top Down Cracking

$$FC_{top} = \left(\frac{C_4}{1 + e^{(C_1 - C_2 * log_{10}(Damage))}}\right) * 10.56$$

c1: 7	c2: 3.5	c3: 0	c4: 1000

AC Bottom Up Cracking

$$FC = \left(\frac{6000}{1 + e^{(C_1 * C_1' + C_2 * C_2' log_{10}(D*100))}}\right) * \left(\frac{1}{60}\right)$$

$$C_2' = -2.40874 - 39.748 * (1 + h_{ac})^{-2.856}$$

$$C_1' = -2 * C_2'$$

c1: 1.31	c2: (0.867 + 0.2583 * hac) * 1 + 0	c3: 6000

Top down AC Cracking Standard Deviation	Bottom up AC Cracking Standard Deviation
200 + 2300/(1+exp(1.072-2.1654*LOG10(TOP+0.0001)))	1.13 + 13/(1+exp(7.57-15.5*LOG10(BOTTOM+0.0001)))

CSM Cracking

$$FC_{ctb} = C_1 + \frac{C_2}{1 + e^{C_3 - C_4 * log_{10}(Damage)}}$$

C1: 0	C2: 75	C3: 2	C4: 2

CSM Standard Deviation
CTB*1

IRI Flexible Pavements

C1 - Rutting
C2 - Fatigue Crack
C3 - Transverse Crack
C4 - Site Factors

C1: 55	C2: 0.4	C3: 0.008	C4: 0.015

LVR_400AADT_CIR_1.5%-12 years December 2019

File Name: C:\Users\admin\Desktop\Taha M2\LVR_400AADT_CIR_1.5%-12 years December 2019.dgpx

Design Inputs

Design Life: 12 years

Design Type: FLEXIBLE

Base construction: May, 2020

Pavement construction: June, 2021

Traffic opening: September, 2021

Climate Data Sources (Lat/Lon): 44, -78.75

Design Structure

Layer type	Material Type	Thickness(mm)
Flexible	Default asphalt concrete	50.0
Flexible	Default asphalt concrete	100.0
NonStabilized	A-1-a	150.0
NonStabilized	A-1-b	400.0
Subgrade	A-6	Semi-infinite

Volumetric at Construction:	
Effective binder content (%)	11.8
Air voids (%)	7.0

Traffic

Age (year)	Heavy Trucks (cumulative)
2021 (initial)	400
2027 (6 years)	424,055
2033 (12 years)	919,115

Design Outputs

Distress Prediction Summary

Distress Type	Distress @ Specified Reliability		Reliability (%)		Criterion Satisfied?
	Target	Predicted	Target	Achieved	
Terminal IRI (m/km)	2.70	1.74	75.00	99.86	Pass
Permanent deformation - total pavement (mm)	17.00	7.69	75.00	100.00	Pass
AC bottom-up fatigue cracking (percent)	35.00	0.76	75.00	100.00	Pass
AC thermal cracking (m/km)	190.00	21.65	75.00	100.00	Pass
AC top-down fatigue cracking (m/km)	380.00	101.14	75.00	99.49	Pass
Permanent deformation - AC only (mm)	6.00	0.43	75.00	100.00	Pass

LVR_400AADT_CIR_1.5%-12 years December 2019

File Name: C:\Users\admin\Desktop\Taha M2\LVR_400AADT_CIR_1.5%-12 years December 2019.dgpx

Distress Charts

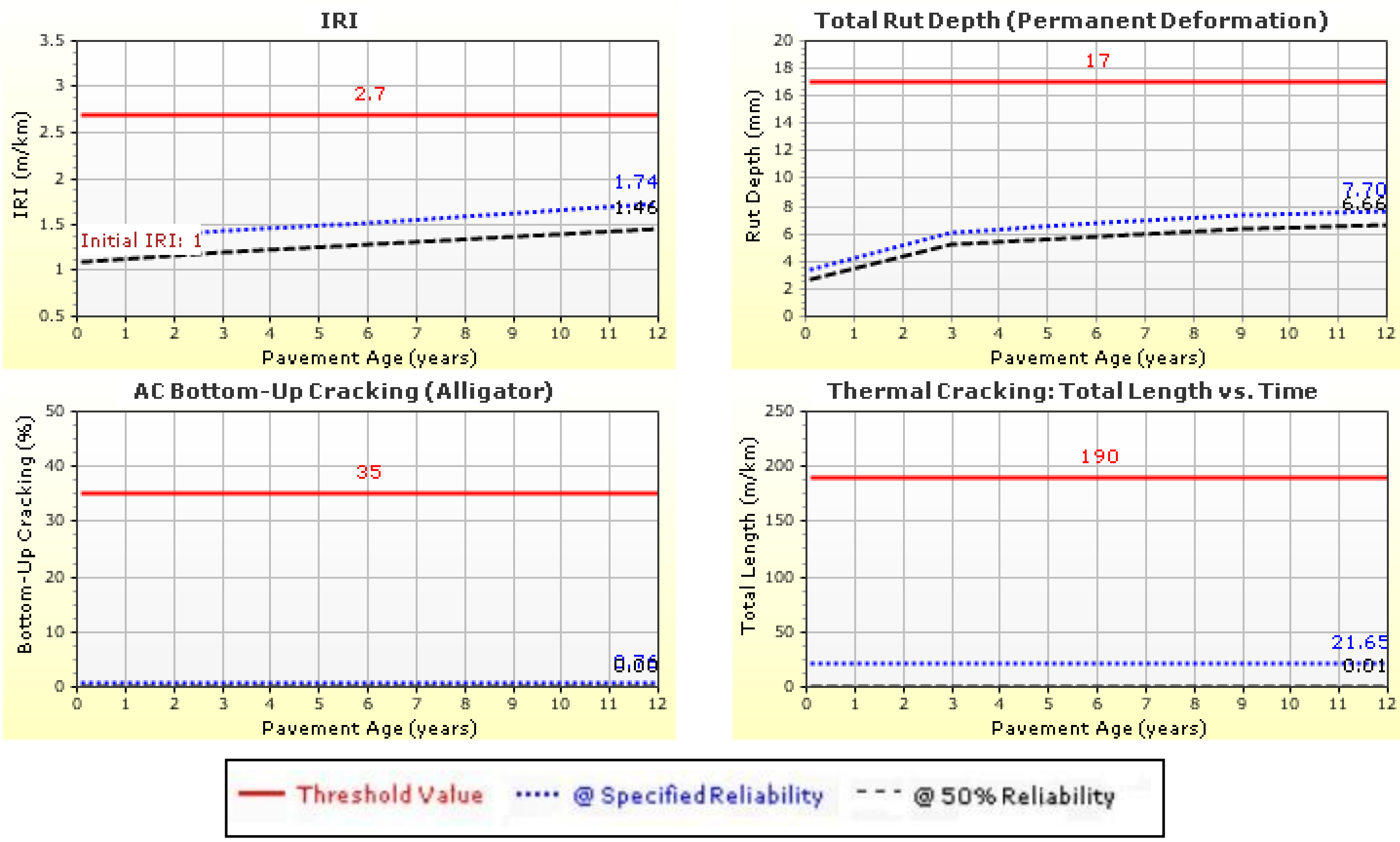

LVR_400AADT_CIR_1.5%-12 years December 2019

File Name: C:\Users\admin\Desktop\Taha M2\LVR_400AADT_CIR_1.5%-12 years December 2019.dgpx

Traffic Inputs

Graphical Representation of Traffic Inputs

Initial two-way AADTT:	400	Percent of trucks in design direction (%):	50.0
Number of lanes in design direction:	2	Percent of trucks in design lane (%):	90.0
		Operational speed (kph)	80.0

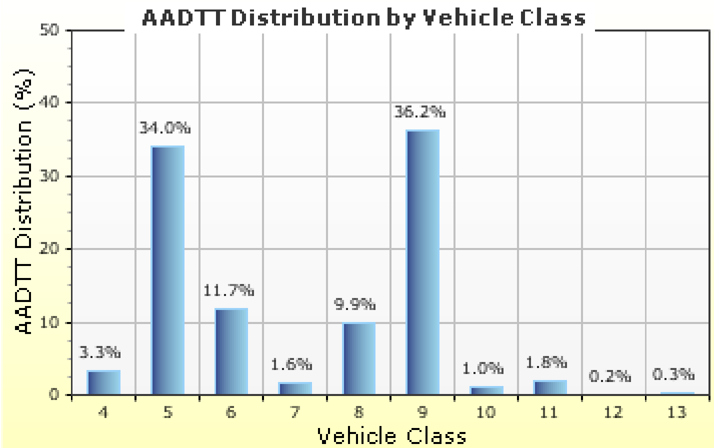

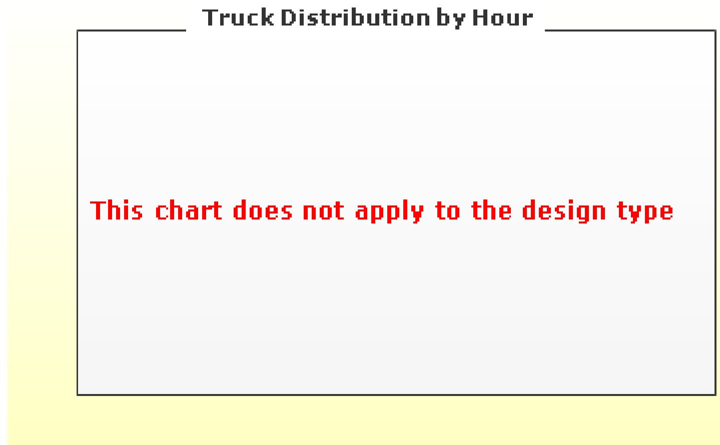

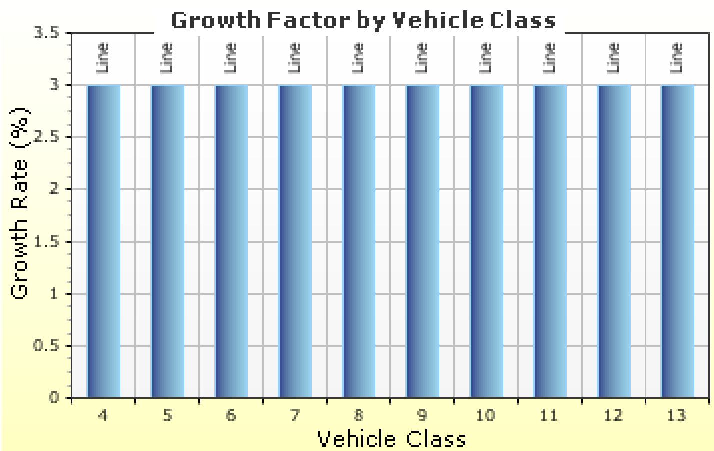

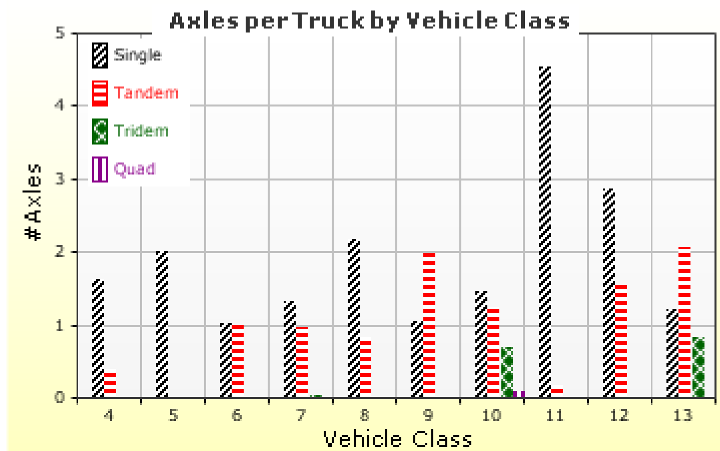

Traffic Volume Monthly Adjustment Factors

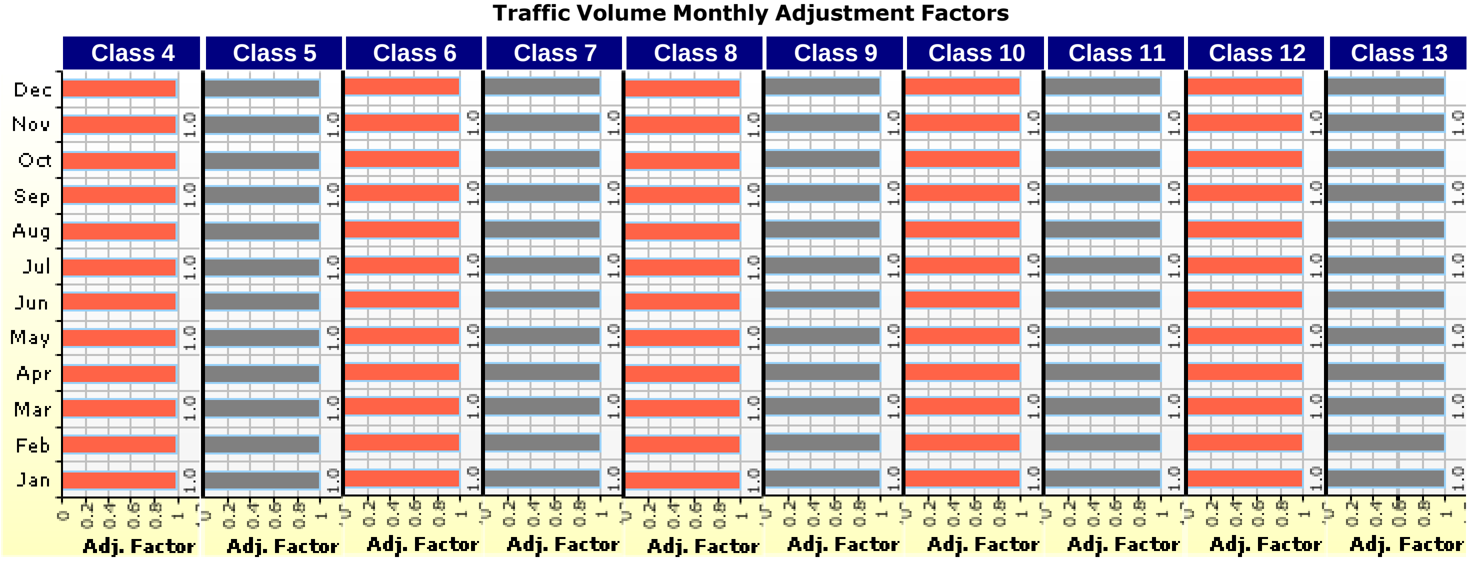

LVR_400AADT_CIR_1.5%-12 years December 2019

File Name: C:\Users\admin\Desktop\Taha M2\LVR_400AADT_CIR_1.5%-12 years December 2019.dgpx

Tabular Representation of Traffic Inputs

Volume Monthly Adjustment Factors

Level 3: Default MAF

Month	Vehicle Class									
	4	5	6	7	8	9	10	11	12	13
January	1.0	1.0	1.0	1.0	1.0	1.0	1.0	1.0	1.0	1.0
February	1.0	1.0	1.0	1.0	1.0	1.0	1.0	1.0	1.0	1.0
March	1.0	1.0	1.0	1.0	1.0	1.0	1.0	1.0	1.0	1.0
April	1.0	1.0	1.0	1.0	1.0	1.0	1.0	1.0	1.0	1.0
May	1.0	1.0	1.0	1.0	1.0	1.0	1.0	1.0	1.0	1.0
June	1.0	1.0	1.0	1.0	1.0	1.0	1.0	1.0	1.0	1.0
July	1.0	1.0	1.0	1.0	1.0	1.0	1.0	1.0	1.0	1.0
August	1.0	1.0	1.0	1.0	1.0	1.0	1.0	1.0	1.0	1.0
September	1.0	1.0	1.0	1.0	1.0	1.0	1.0	1.0	1.0	1.0
October	1.0	1.0	1.0	1.0	1.0	1.0	1.0	1.0	1.0	1.0
November	1.0	1.0	1.0	1.0	1.0	1.0	1.0	1.0	1.0	1.0
December	1.0	1.0	1.0	1.0	1.0	1.0	1.0	1.0	1.0	1.0

Distributions by Vehicle Class

Vehicle Class	AADTT Distribution (%) (Level 3)	Growth Factor	
		Rate (%)	Function
Class 4	3.3%	3%	Linear
Class 5	34%	3%	Linear
Class 6	11.7%	3%	Linear
Class 7	1.6%	3%	Linear
Class 8	9.9%	3%	Linear
Class 9	36.2%	3%	Linear
Class 10	1%	3%	Linear
Class 11	1.8%	3%	Linear
Class 12	0.2%	3%	Linear
Class 13	0.3%	3%	Linear

Truck Distribution by Hour does not apply

Axle Configuration

Traffic Wander	
Mean wheel location (mm)	460.0
Traffic wander standard deviation (mm)	254.0
Design lane width (m)	3.7

Axle Configuration	
Average axle width (m)	2.6
Dual tire spacing (mm)	305.0
Tire pressure (kPa)	827.4

Average Axle Spacing	
Tandem axle spacing (m)	1.5
Tridem axle spacing (m)	1.7
Quad axle spacing (m)	1.3

Wheelbase does not apply

Number of Axles per Truck

Vehicle Class	Single Axle	Tandem Axle	Tridem Axle	Quad Axle
Class 4	1.62	0.39	0	0
Class 5	2	0	0	0
Class 6	1.01	0.993	0	0
Class 7	1.314	0.989	0.03	0
Class 8	2.163	0.845	0	0
Class 9	1.055	1.968	0.003	0
Class 10	1.446	1.234	0.7	0.088
Class 11	4.546	0.168	0	0
Class 12	2.857	1.526	0	0
Class 13	1.201	2.058	0.848	0.024

AADTT (Average Annual Daily Truck Traffic) Growth

*** Traffic cap is not enforced**

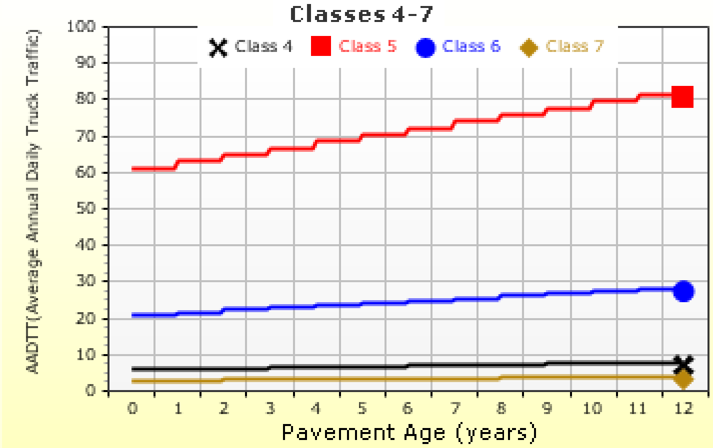

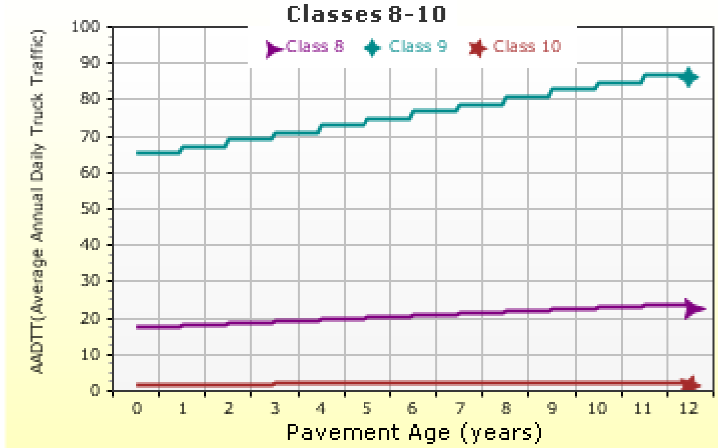

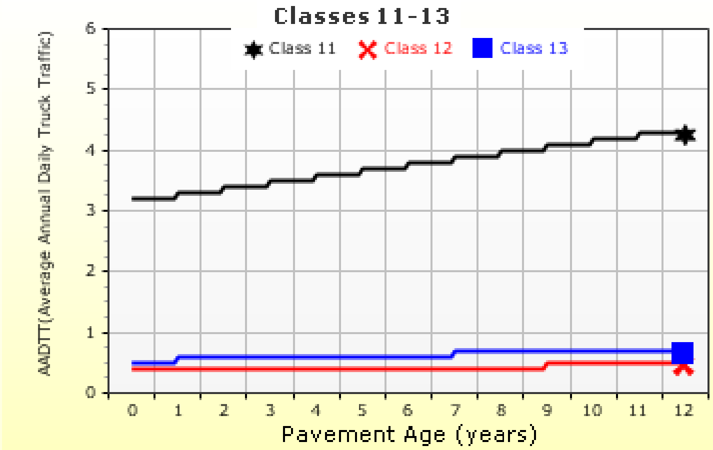

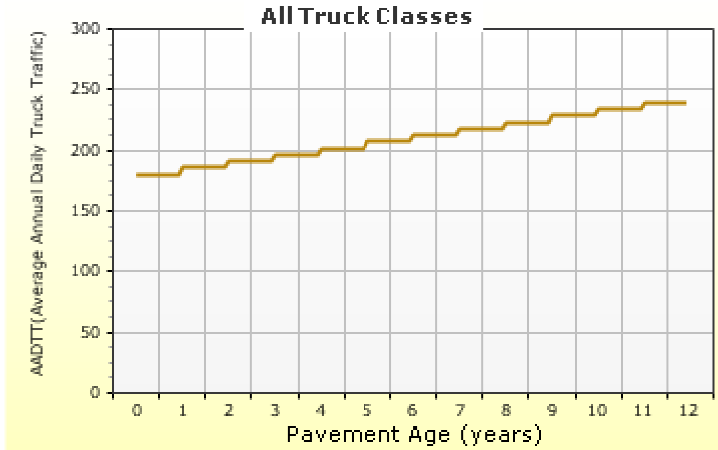

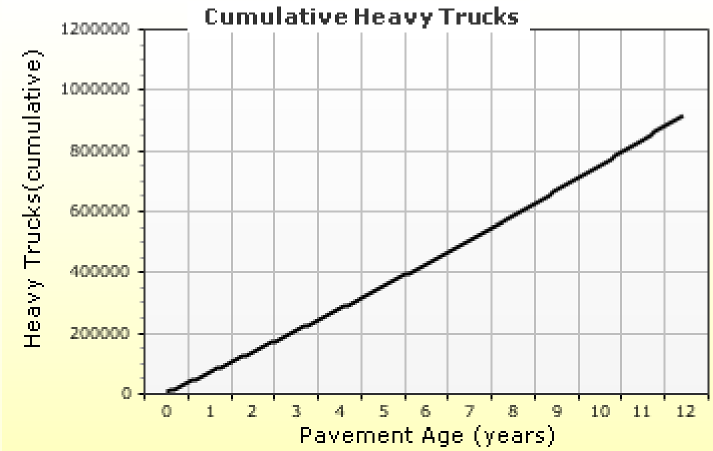

Climate Inputs

Climate Data Sources:

Climate Station Cities:	Location (lat lon elevation(m))
CA, ON	44.00000 -78.75000 193

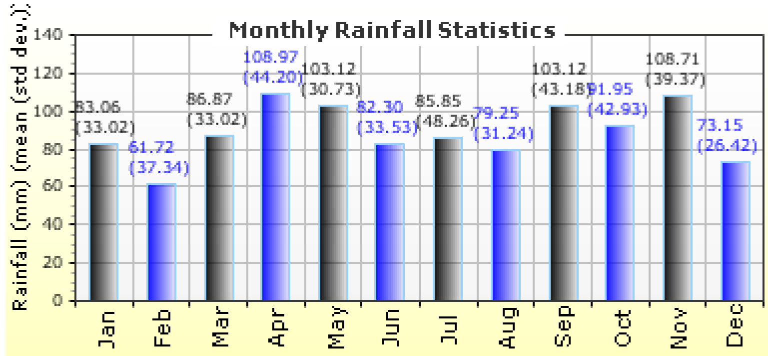

Annual Statistics:

Mean annual air temperature (ºC)	7.62
Mean annual precipitation (mm)	1068.32
Freezing index (ºC - days)	573.75
Average annual number of freeze/thaw cycles:	77.00
Water table depth (m)	10.00

Monthly Climate Summary:

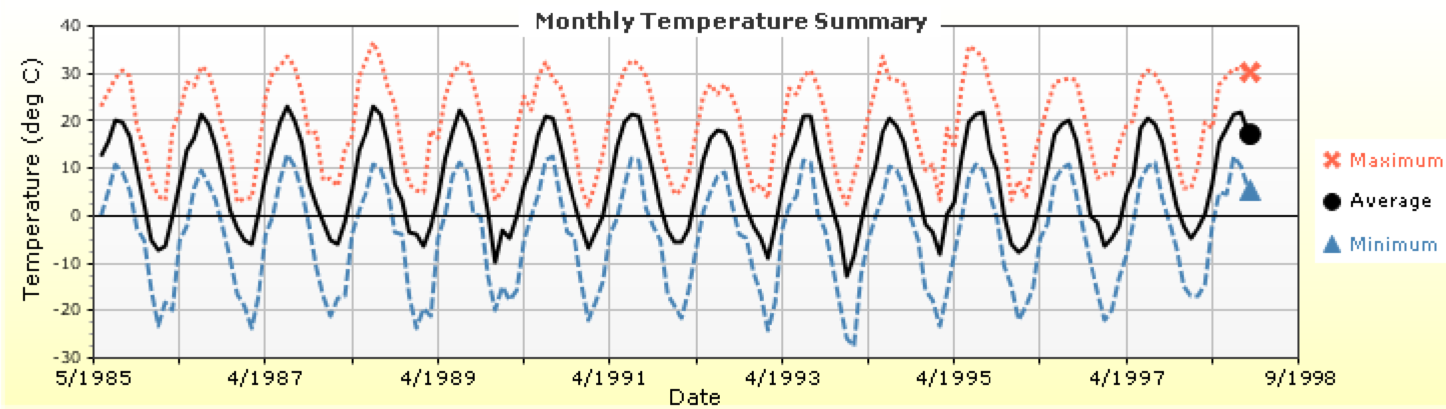

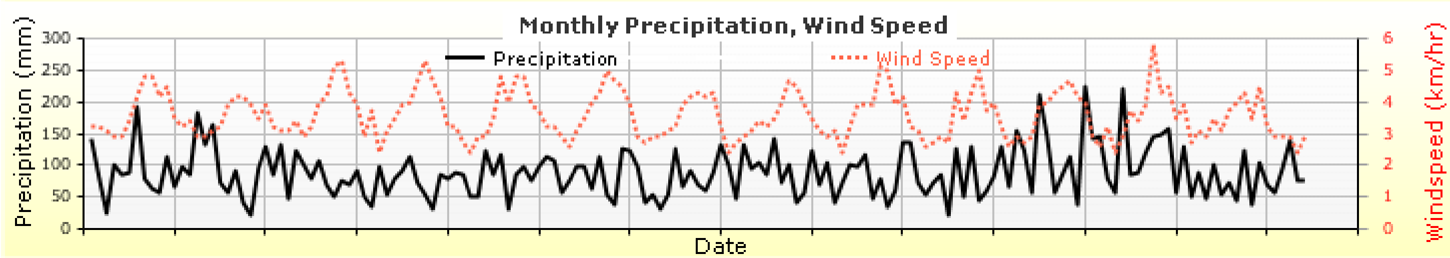

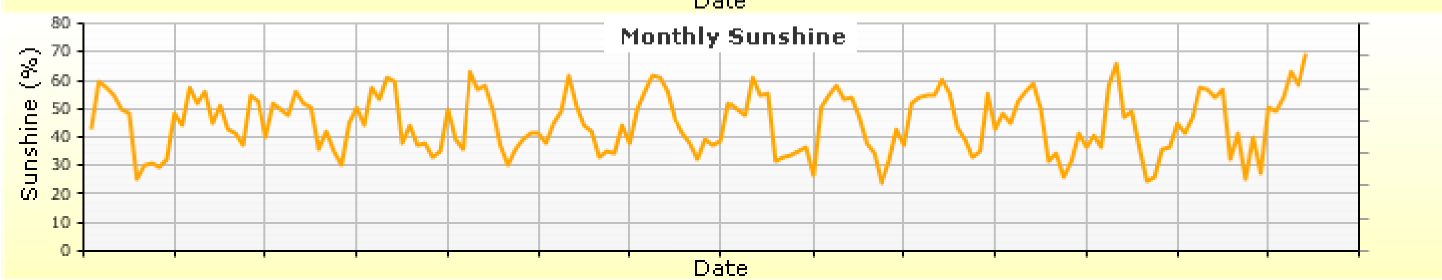

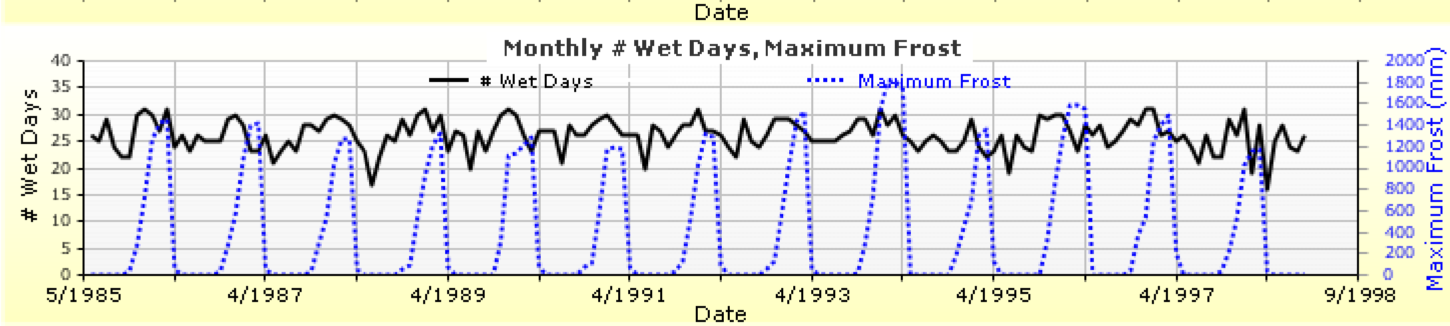

LVR_400AADT_CIR_1.5%-12 years December 2019

File Name: C:\Users\admin\Desktop\Taha M2\LVR_400AADT_CIR_1.5%-12 years December 2019.dgpx

Hourly Air Temperature Distribution by Month:

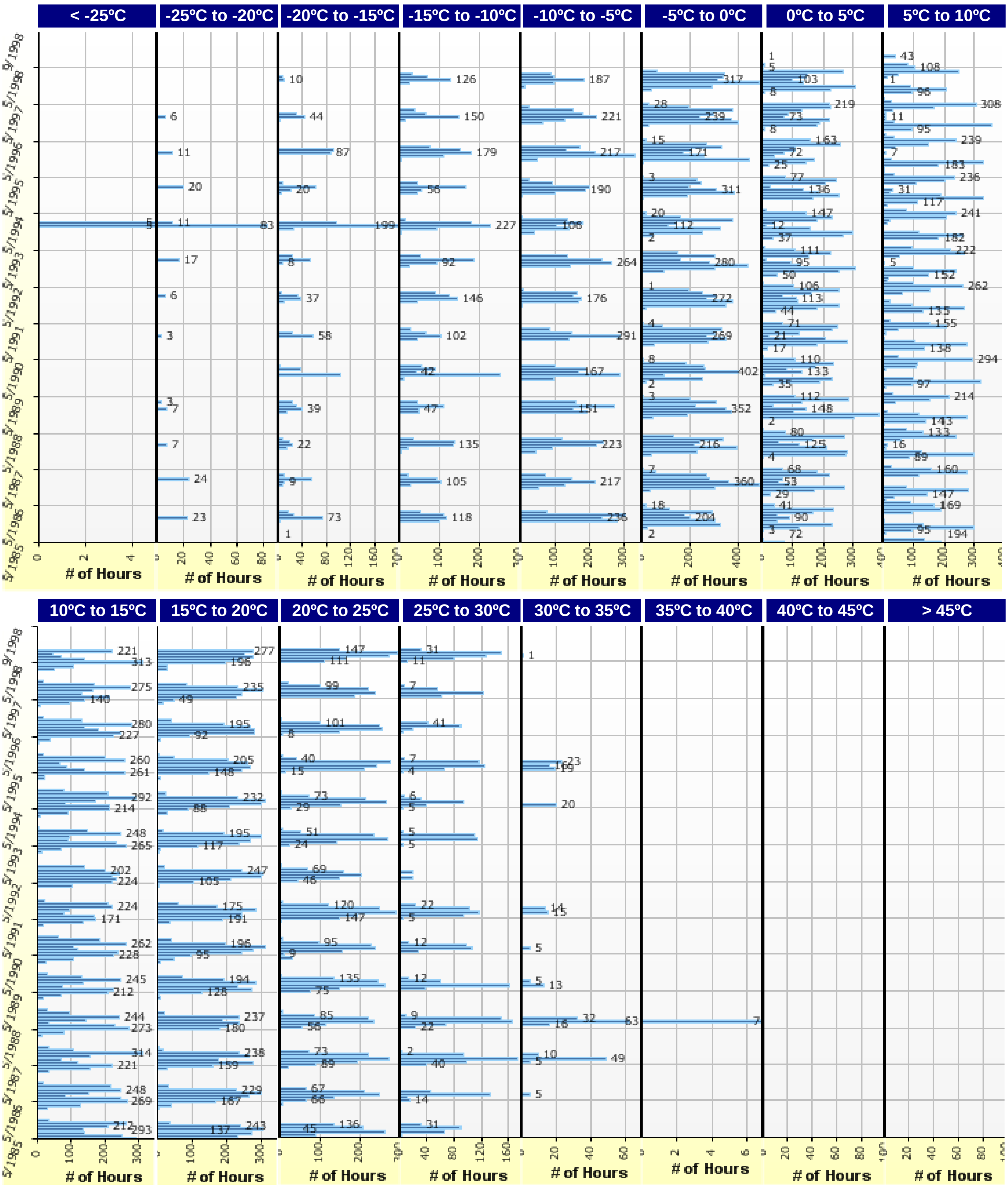

Design Properties

HMA Design Properties

Use Multilayer Rutting Model	False
Using G* based model (not nationally calibrated)	False
Is NCHRP 1-37A HMA Rutting Model Coefficients	True
Endurance Limit	-
Use Reflective Cracking	True

Structure - ICM Properties	
AC surface shortwave absorptivity	0.85

Layer Name	Layer Type	Interface Friction
Layer 1 Flexible : Default asphalt concrete	Flexible (1)	1.00
Layer 2 Flexible : Default asphalt concrete	Flexible (1)	1.00
Layer 3 Non-stabilized Base : A-1 -a	Non-stabilized Base (4)	1.00
Layer 4 Non-stabilized Base : A-1 -b	Non-stabilized Base (4)	1.00
Layer 5 Subgrade : A-6	Subgrade (5)	-

Thermal Cracking

Thermal Contraction	
Is thermal contraction calculated?	True
Mix coefficient of thermal contraction (mm/mm/ºC)	-
Aggregate coefficient of thermal contraction (mm/mm/ºC)	9.0e-006
Voids in Mineral Aggregate (%)	18.8

Indirect Tensile Strength (Input Level: 3)	
Test Temperature (ºC)	Indirect Tensilte Strength (Mpa)
-10.0	2.79

Creep Compliance (1/GPa) (Input Level: 3)			
Loading time (sec)	-20 ºC	-10 ºC	0 ºC
1	5.57e-002	8.57e-002	1.16e-001
2	6.17e-002	1.01e-001	1.51e-001
5	7.07e-002	1.25e-001	2.15e-001
10	7.83e-002	1.48e-001	2.80e-001
20	8.68e-002	1.74e-001	3.65e-001
50	9.94e-002	2.16e-001	5.19e-001
100	1.10e-001	2.55e-001	6.77e-001

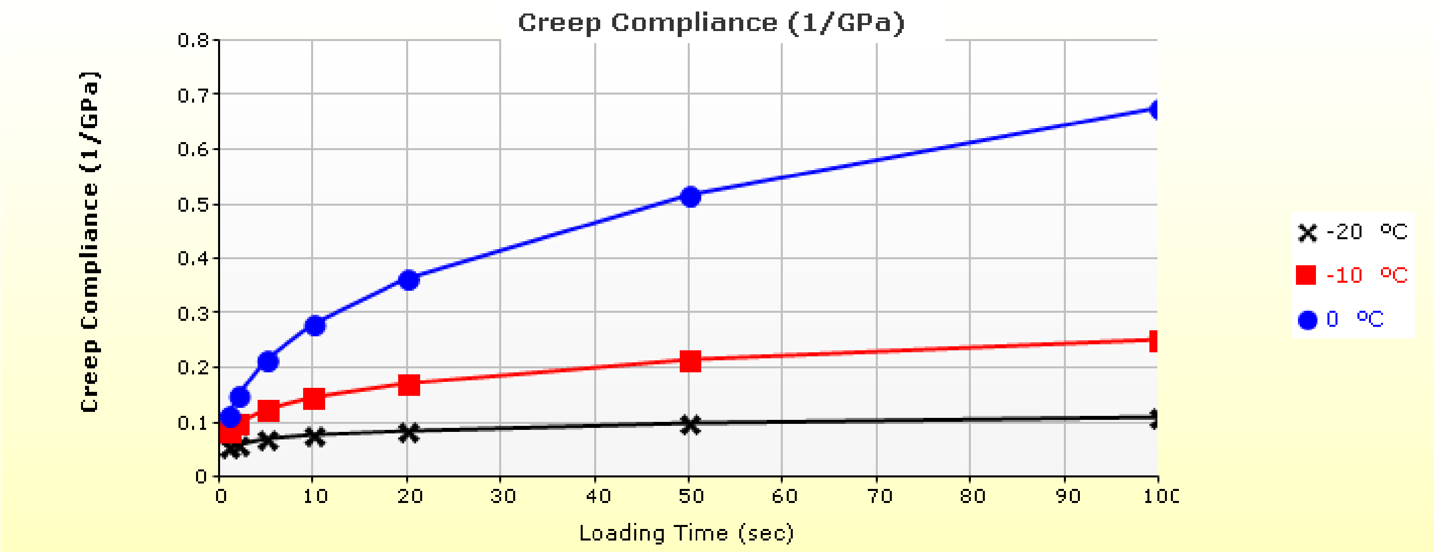

LVR_400AADT_CIR_1.5%-12 years December 2019

File Name: C:\Users\admin\Desktop\Taha M2\LVR_400AADT_CIR_1.5%-12 years December 2019.dgpx

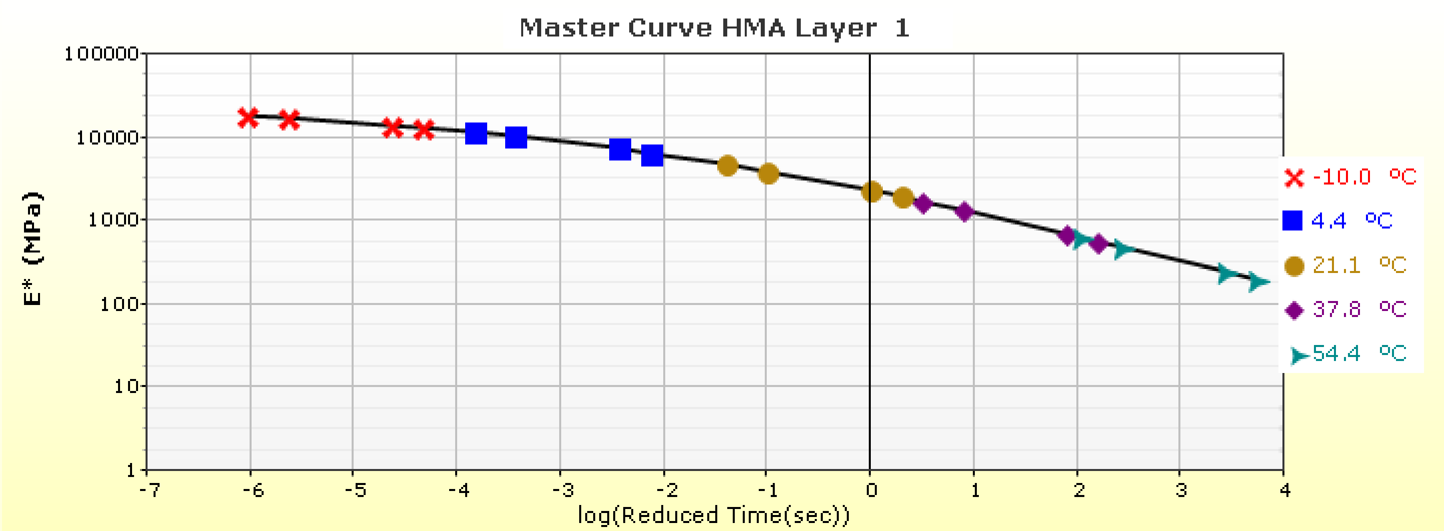

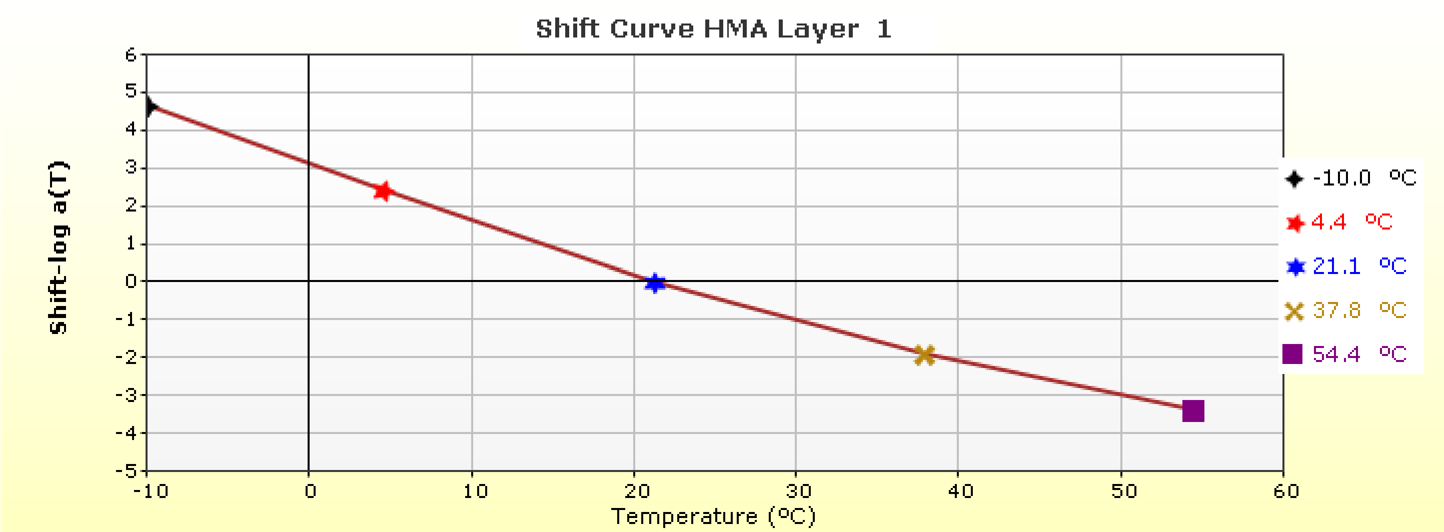

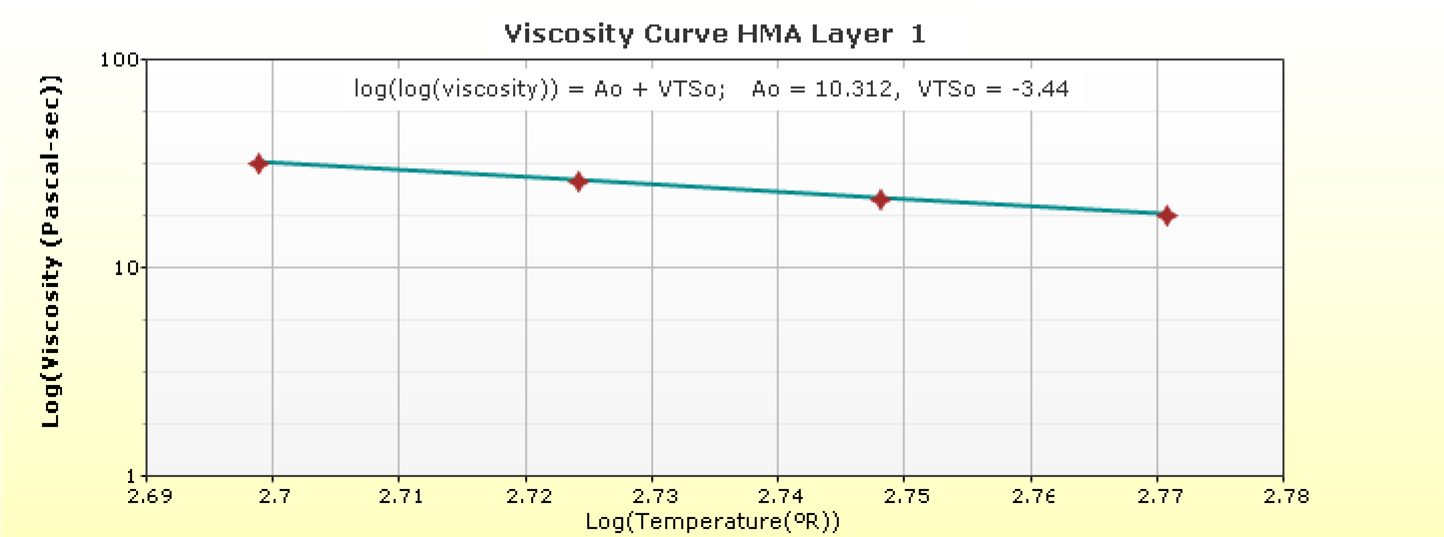

HMA Layer 2: Layer 2 Flexible : Default asphalt concrete

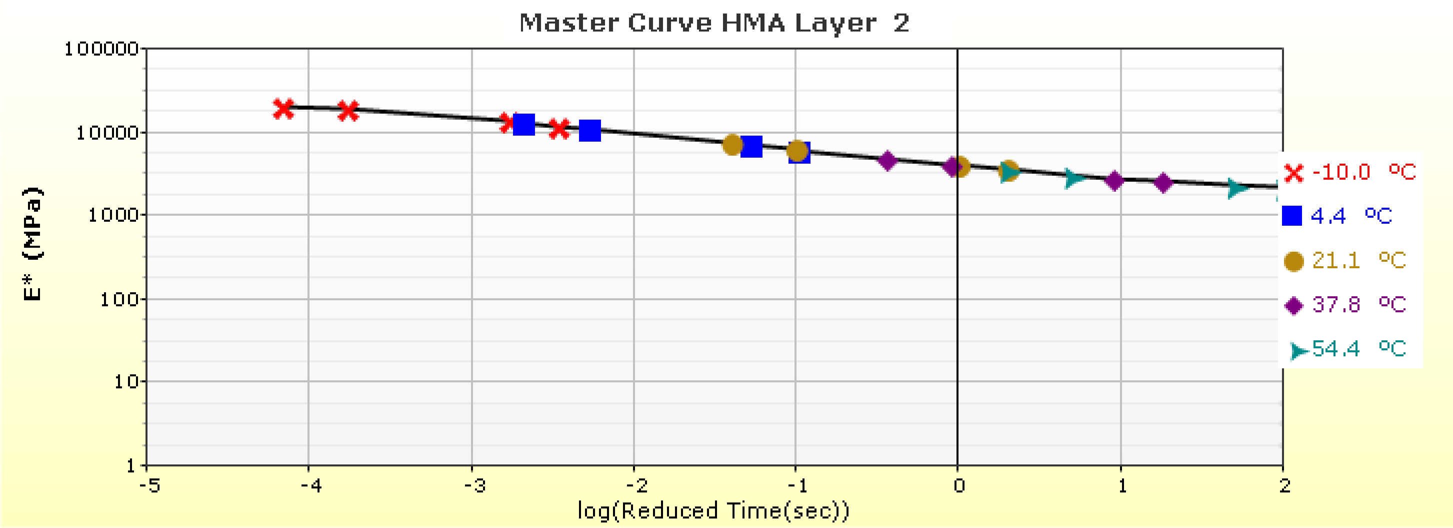

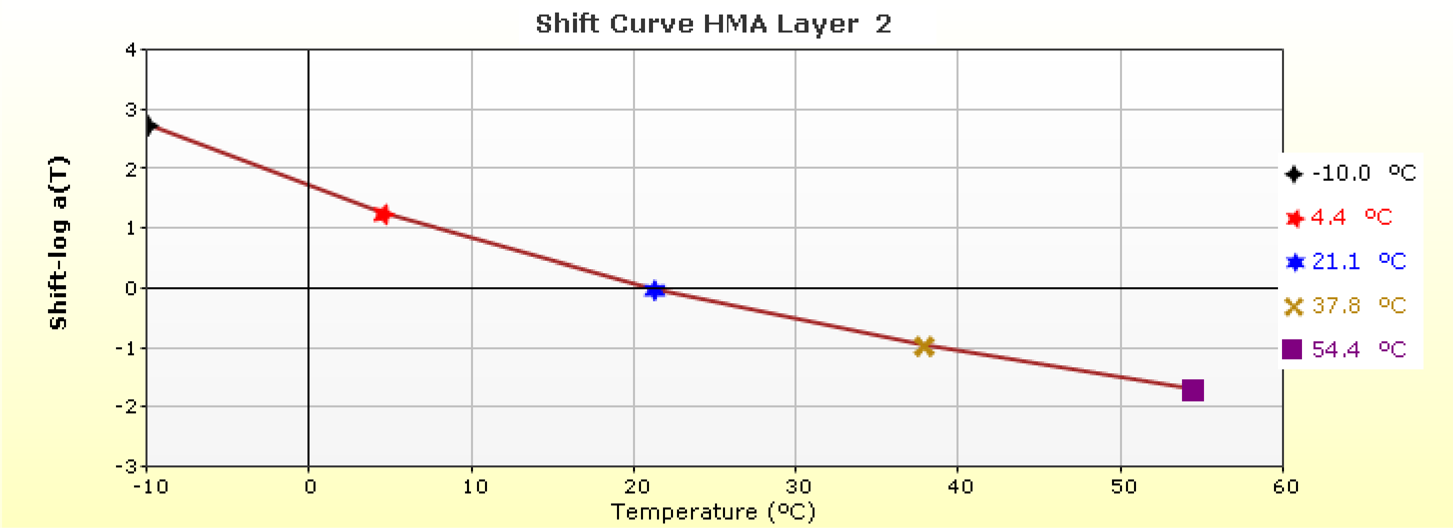

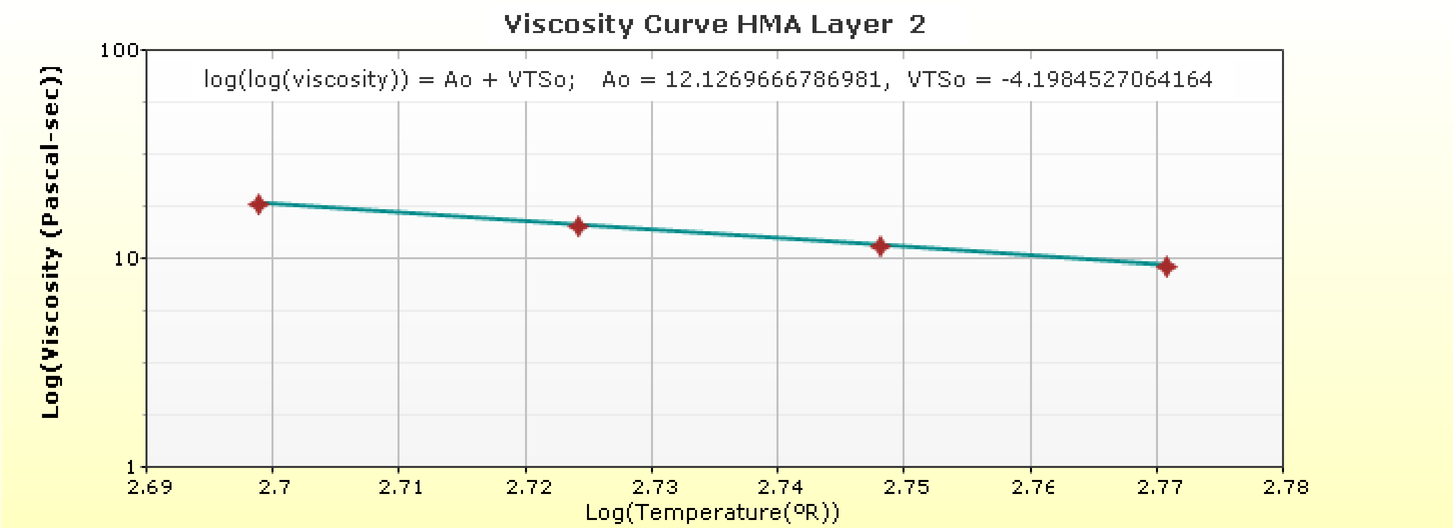

Analysis Output Charts

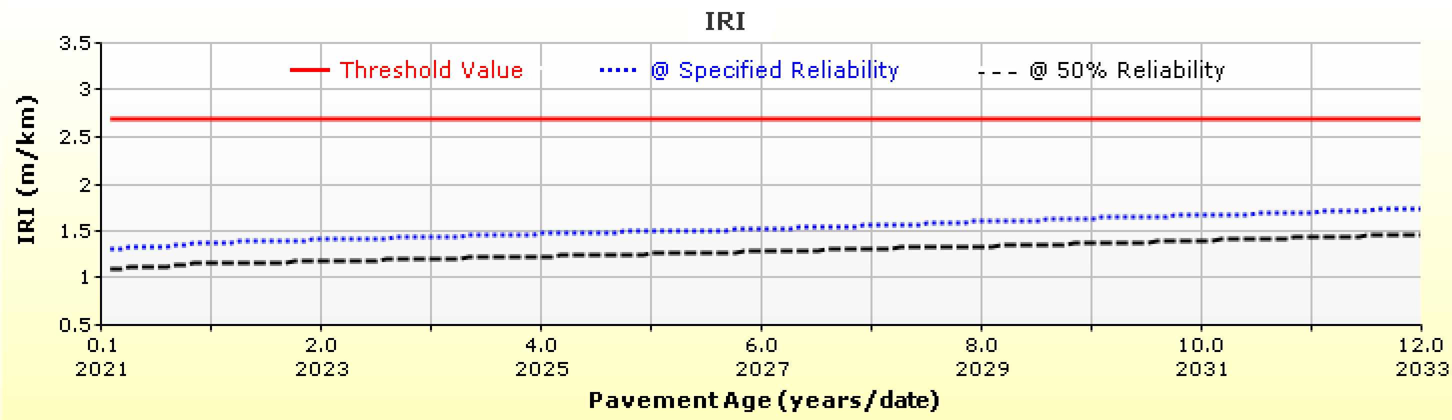

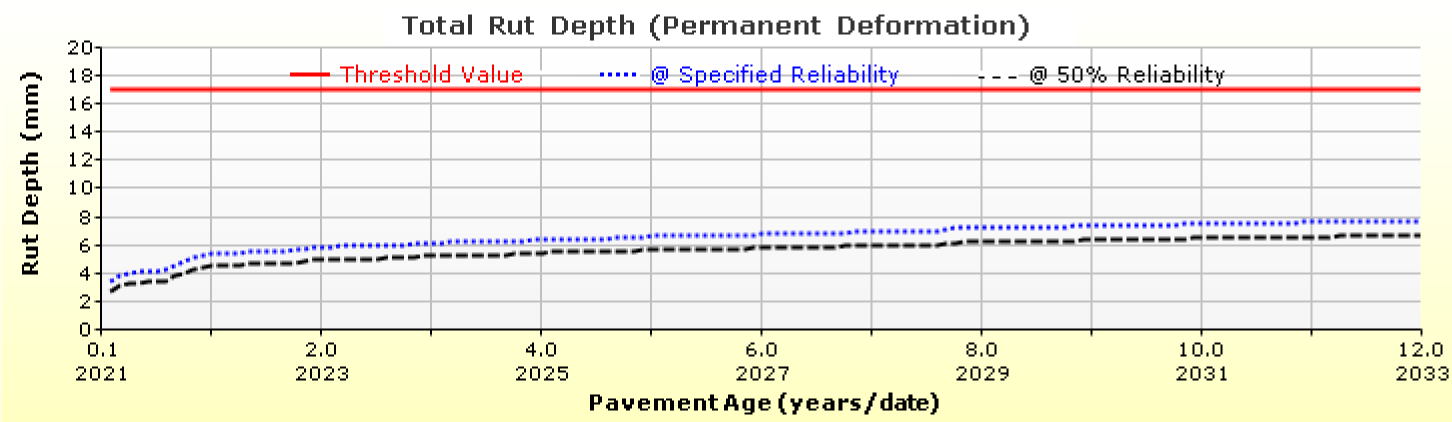

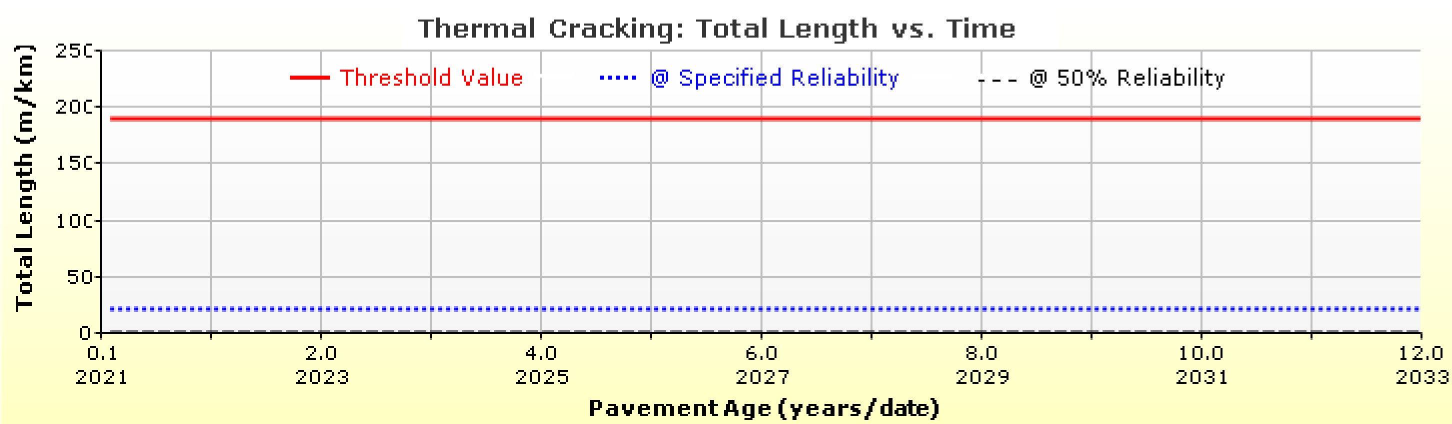

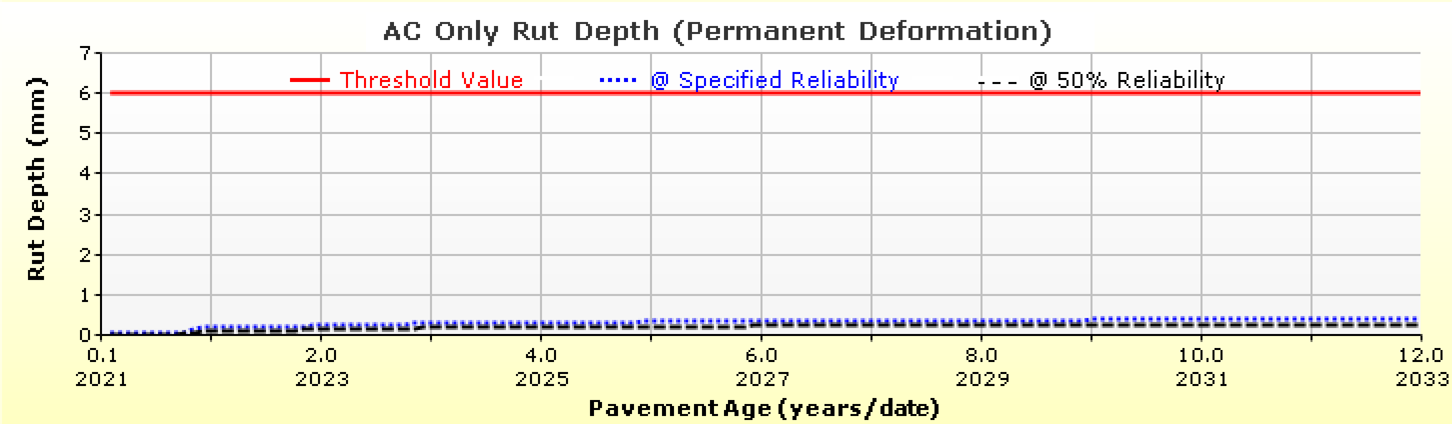

LVR_400AADT_CIR_1.5%-12 years December 2019

File Name: C:\Users\admin\Desktop\Taha M2\LVR_400AADT_CIR_1.5%-12 years December 2019.dgpx

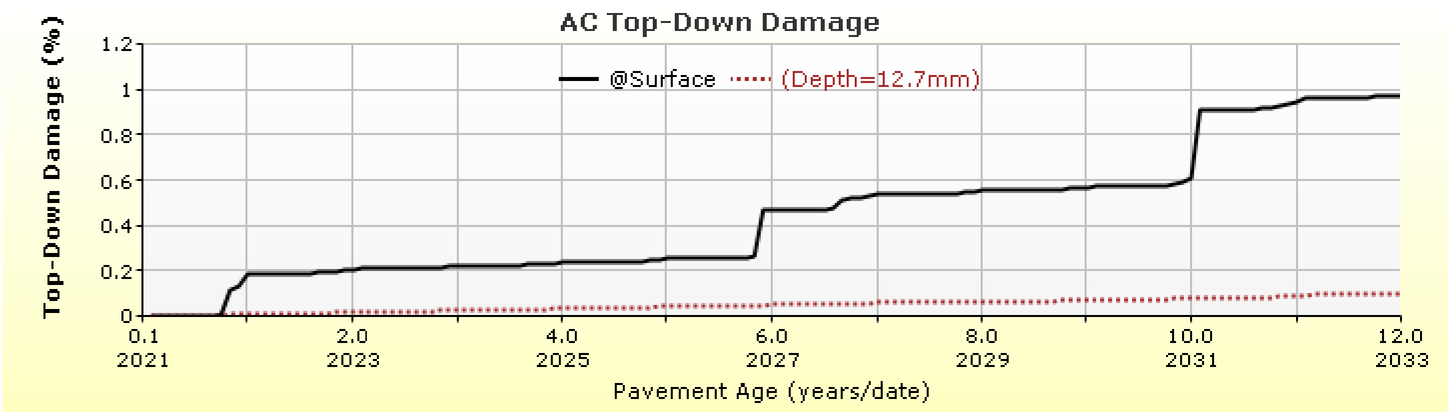

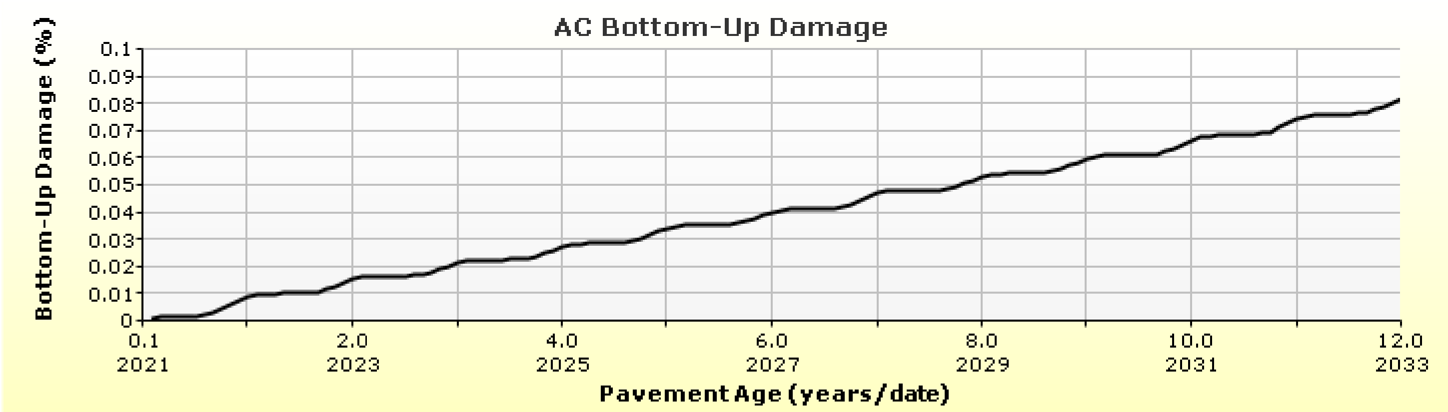

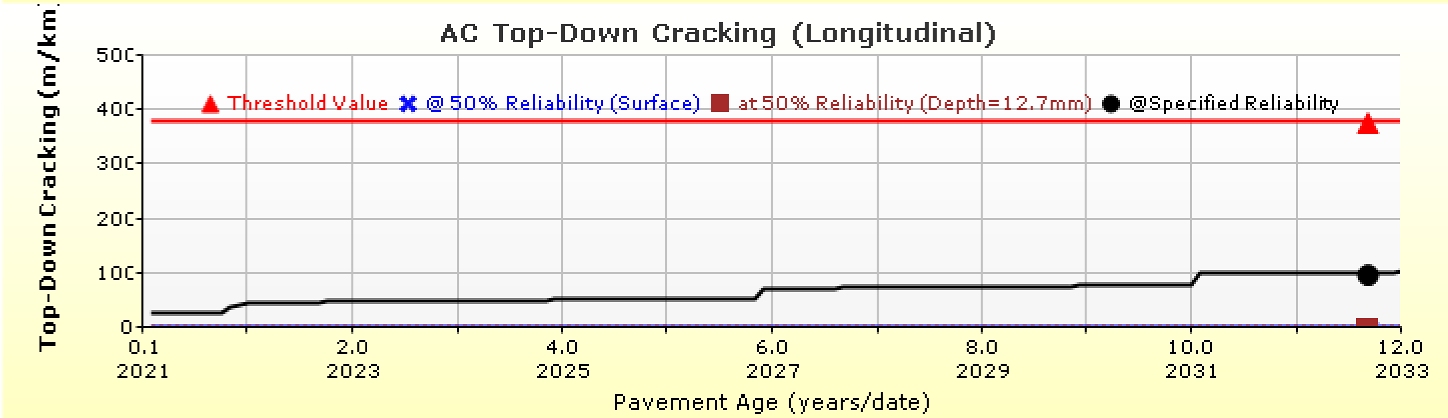

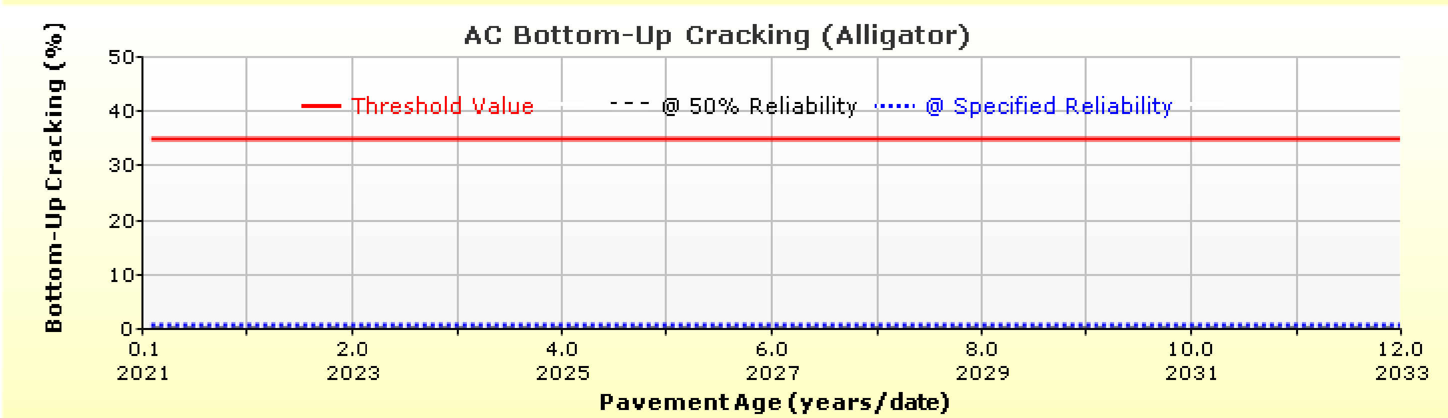

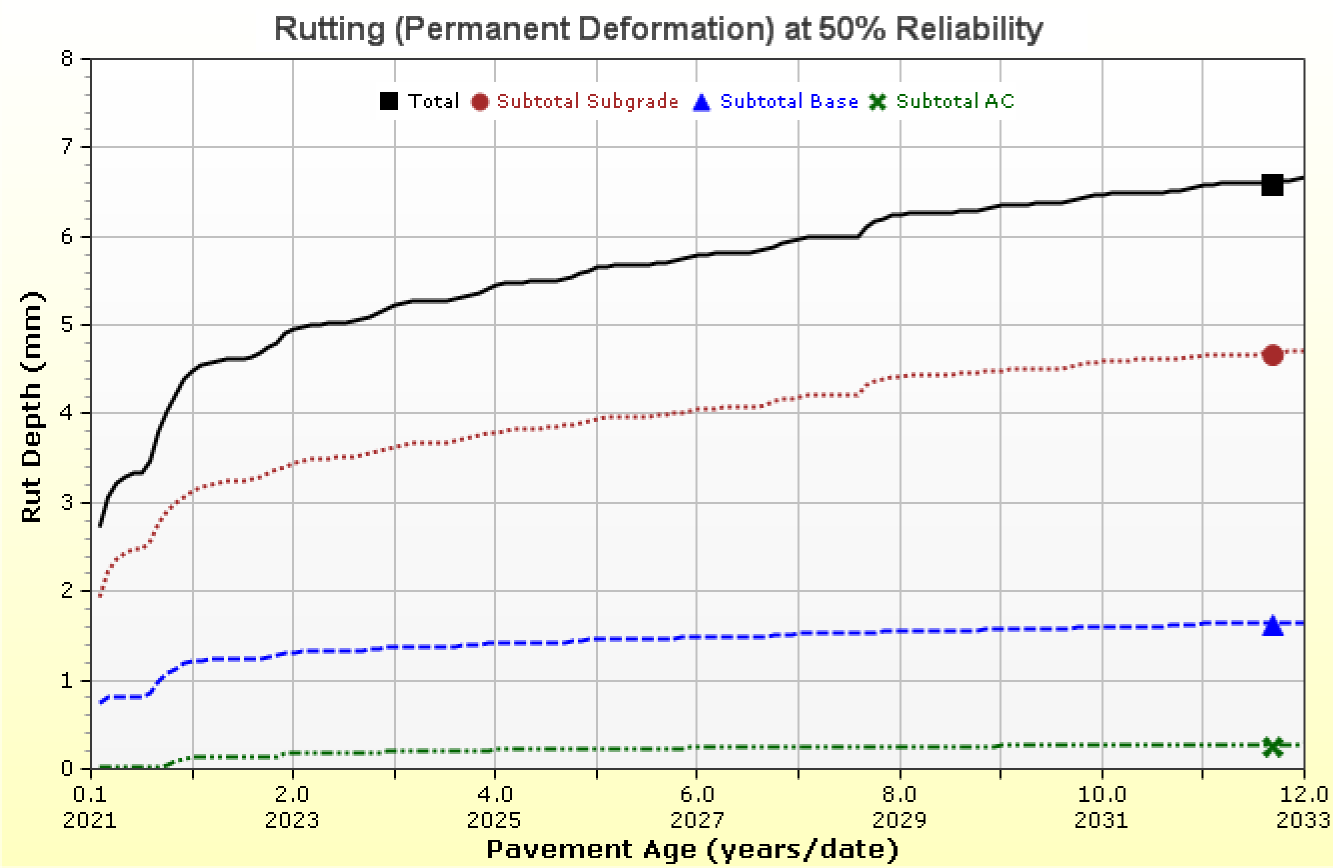
Rutting (Permanent Deformation) at 50% Reliability
Total
Subtotal Subgrade
Subtotal Base
Subtotal AC
Rut Depth (mm)
Pavement Age (years/date)
0
1
2
3
4
5
6
7
8
0.1
2021
2.0
2023
4.0
2025
6.0
2027
8.0
2029
10.0
2031
12.0
2033

LVR_400AADT_CIR_1.5%-12 years December 2019

File Name: C:\Users\admin\Desktop\Taha M2\LVR_400AADT_CIR_1.5%-12 years December 2019.dgpx

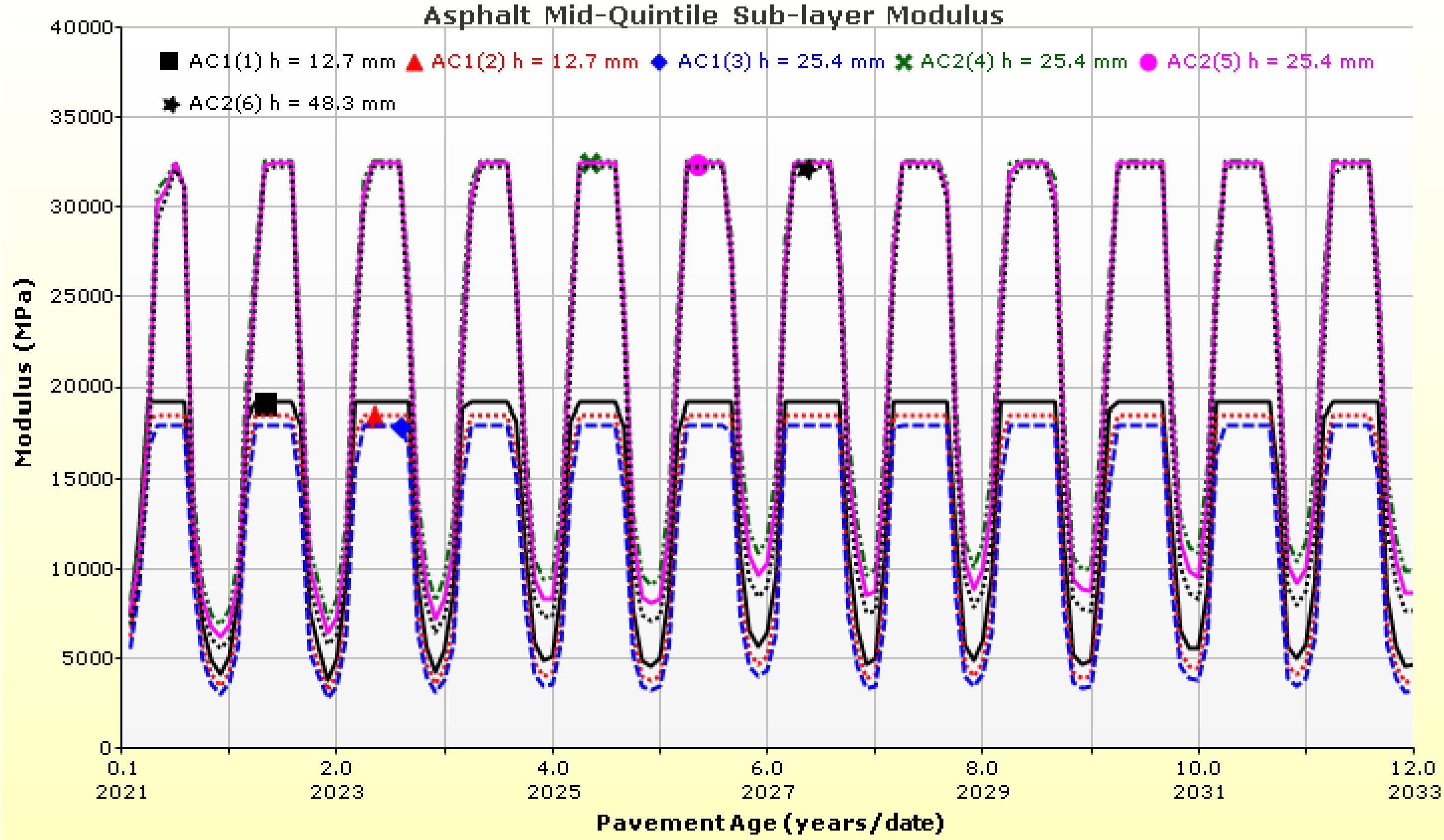

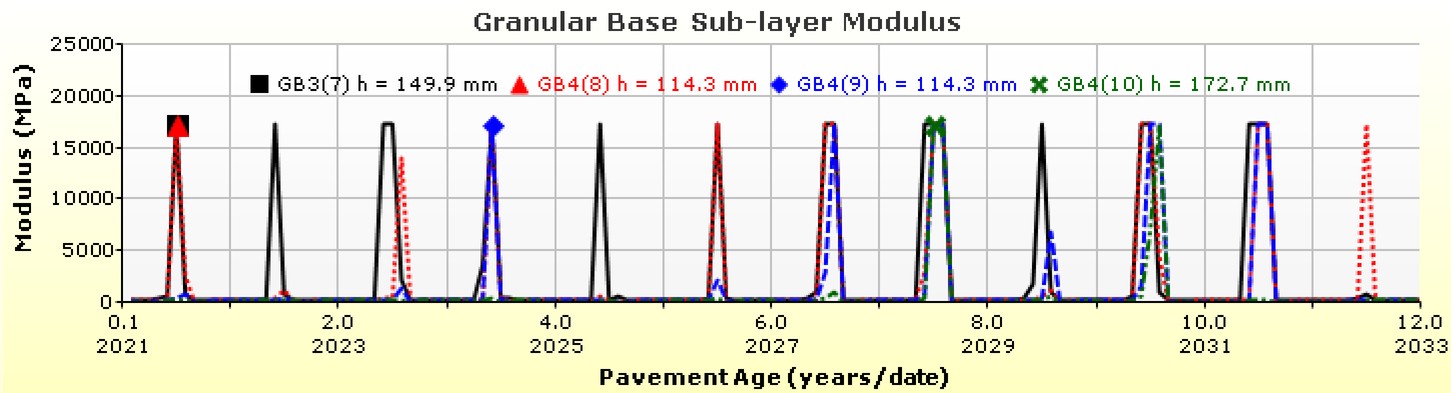

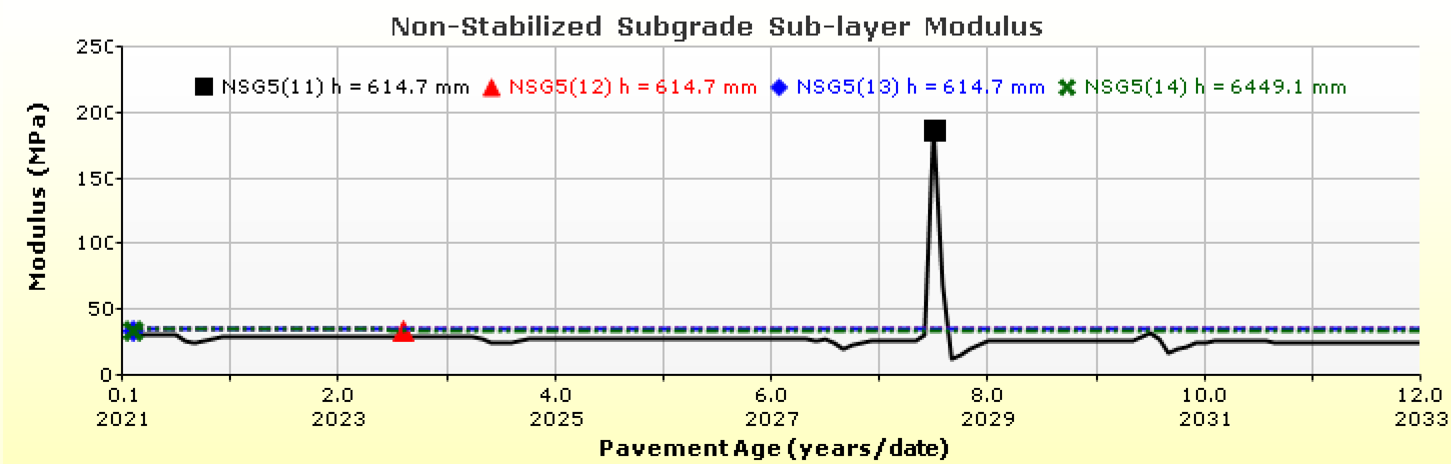

Layer Information

Layer 1 Flexible : Default asphalt concrete

Asphalt		
Thickness (mm)	50.0	
Unit weight (kgf/m^3)	2460.0	
Poisson's ratio	Is Calculated?	False
	Ratio	0.35
	Parameter A	-
	Parameter B	-

Asphalt Dynamic Modulus (Input Level: 3)

Gradation	Percent Passing
19 mm sieve	100
9.5 mm sieve	83.2
4.75 mm sieve	54
0.075mm sieve	4

Asphalt Binder

Parameter	Value
Grade	Superpave Performance Grade
Binder Type	64-28
A	10.312
VTS	-3.44

General Info

Name	Value
Reference temperature (ºC)	21.1
Effective binder content (%)	11.8
Air voids (%)	7
Thermal conductivity (watt/meter-kelvin)	1.16
Heat capacity (joule/kg-kelvin)	963

Identifiers

Field	Value
Display name/identifier	Default asphalt concrete
Description of object	
Author	
Date Created	9/16/2010 1:00:00 AM
Approver	
Date approved	9/16/2010 1:00:00 AM
State	
District	
County	
Highway	
Direction of Travel	
From station (km)	
To station (km)	
Province	
User defined field 1	
User defined field 2	
User defined field 3	
Revision Number	0

Layer 2 Flexible : Default asphalt concrete

Asphalt		
Thickness (mm)	100.0	
Unit weight (kgf/m^3)	2460.0	
Poisson's ratio	Is Calculated?	False
	Ratio	0.35
	Parameter A	-
	Parameter B	-

Asphalt Dynamic Modulus (Input Level: 1)

T (ºC)	0.1 Hz	0.5 Hz	1 Hz	5 Hz	10 Hz	25 Hz
-10	11985.41	13748.86	14880.45	16994.82	18141.93	19409.35
4	5924.617	7369.854	8011.166	9822.414	10737.41	11711.86
21	1434.219	2293.610	2807.905	3983.936	4602.746	5750.611
57	1434.219	2293.610	2807.905	3983.936	4602.746	5750.611

Asphalt Binder

Temperature (ºC)	Binder Gstar (Pa)	Phase angle (deg)
4.4	5494.5	57
12.8	1919	59.3
21.1	490.2	61.6
29.4	161.2	62.4
37.8	39.9	62.7
46.1	15.2	62.7

General Info

Name	Value
Reference temperature (ºC)	21.1
Effective binder content (%)	11.2
Air voids (%)	7
Thermal conductivity (watt/meter-kelvin)	1.16
Heat capacity (joule/kg-kelvin)	963

Identifiers

Field	Value
Display name/identifier	Default asphalt concrete
Description of object	
Author	
Date Created	9/16/2010 1:00:00 AM
Approver	
Date approved	9/16/2010 1:00:00 AM
State	
District	
County	
Highway	
Direction of Travel	
From station (km)	
To station (km)	
Province	
User defined field 1	
User defined field 2	
User defined field 3	
Revision Number	0

Layer 3 Non-stabilized Base : A-1-a

Unbound	
Layer thickness (mm)	150.0
Poisson's ratio	0.35
Coefficient of lateral earth pressure (k0)	0.5

Modulus (Input Level: 3)

Analysis Type:	Modify input values by temperature/moisture
Method:	Resilient Modulus (MPa)

Resilient Modulus (MPa)
250.0

Use Correction factor for NDT modulus?	-
NDT Correction Factor:	-

Identifiers

Field	Value
Display name/identifier	A-1-a
Description of object	Default material
Author	AASHTO
Date Created	1/1/2011 12:00:00 AM
Approver	
Date approved	1/1/2011 12:00:00 AM
State	
District	
County	
Highway	
Direction of Travel	
From station (km)	
To station (km)	
Province	
User defined field 1	
User defined field 2	
User defined field 3	
Revision Number	0

Sieve

Liquid Limit	6.0
Plasticity Index	0.0
Is layer compacted?	False

	Is User Defined?	Value
Maximum dry unit weight (kgf/m^3)	False	2038.2
Saturated hydraulic conductivity (m/hr)	False	2.376e-02
Specific gravity of solids	False	2.7
Water Content (%)	False	5.7

User-defined Soil Water Characteristic Curve (SWCC)	
Is User Defined?	False
af	3.0201
bf	2.5984
cf	0.7539
hr	100.0000

Sieve Size	% Passing
0.001mm	
0.002mm	
0.020mm	
0.075mm	5.0
0.150mm	
0.180mm	
0.250mm	
0.300mm	13.5
0.425mm	
0.600mm	
0.850mm	
1.18mm	27.5
2.0mm	
2.36mm	
4.75mm	45.0
9.5mm	61.5
12.5mm	77.5
19.0mm	92.5
25.0mm	100.0
37.5mm	
50.0mm	
63.0mm	
75.0mm	
90.0mm	

Layer 4 Non-stabilized Base : A-1-b

Unbound	
Layer thickness (mm)	400.0
Poisson's ratio	0.35
Coefficient of lateral earth pressure (k0)	0.5

Modulus (Input Level: 3)

Analysis Type:	Modify input values by temperature/moisture
Method:	Resilient Modulus (MPa)

Resilient Modulus (MPa)
150.0

Use Correction factor for NDT modulus?	-
NDT Correction Factor:	-

Identifiers

Field	Value
Display name/identifier	A-1-b
Description of object	Default material
Author	AASHTO
Date Created	1/1/2011 12:00:00 AM
Approver	
Date approved	1/1/2011 12:00:00 AM
State	
District	
County	
Highway	
Direction of Travel	
From station (km)	
To station (km)	
Province	
User defined field 1	
User defined field 2	
User defined field 3	
Revision Number	0

Sieve

Liquid Limit	11.0
Plasticity Index	0.0
Is layer compacted?	False

	Is User Defined?	Value
Maximum dry unit weight (kgf/m^3)	False	1981.7
Saturated hydraulic conductivity (m/hr)	False	7.17e-03
Specific gravity of solids	False	2.7
Water Content (%)	False	7.9

User-defined Soil Water Characteristic Curve (SWCC)	
Is User Defined?	False
af	5.0954
bf	2.5384
cf	0.8464
hr	100.0000

Sieve Size	% Passing
0.001mm	
0.002mm	
0.020mm	
0.075mm	4.0
0.150mm	
0.180mm	
0.250mm	
0.300mm	33.5
0.425mm	
0.600mm	
0.850mm	
1.18mm	55.0
2.0mm	
2.36mm	
4.75mm	60.0
9.5mm	
12.5mm	
19.0mm	
25.0mm	75.0
37.5mm	
50.0mm	
63.0mm	
75.0mm	
90.0mm	

Layer 5 Subgrade : A-6

Unbound	
Layer thickness (mm)	Semi-infinite
Poisson's ratio	0.3
Coefficient of lateral earth pressure (k0)	0.5

Modulus (Input Level: 3)

Analysis Type:	Modify input values by temperature/moisture
Method:	Resilient Modulus (MPa)

Resilient Modulus (MPa)
35.0

Use Correction factor for NDT modulus?	-
NDT Correction Factor:	-

Identifiers

Field	Value
Display name/identifier	A-6
Description of object	Default material
Author	AASHTO
Date Created	1/1/2011 12:00:00 AM
Approver	
Date approved	1/1/2011 12:00:00 AM
State	
District	
County	
Highway	
Direction of Travel	
From station (km)	
To station (km)	
Province	
User defined field 1	
User defined field 2	
User defined field 3	
Revision Number	0

Sieve

Liquid Limit	18.0
Plasticity Index	4.0
Is layer compacted?	False

	Is User Defined?	Value
Maximum dry unit weight (kgf/m^3)	False	1992.5
Saturated hydraulic conductivity (m/hr)	False	1.095e-06
Specific gravity of solids	False	2.7
Water Content (%)	False	8.8

User-defined Soil Water Characteristic Curve (SWCC)	
Is User Defined?	False
af	26.3898
bf	1.0483
cf	0.8553
hr	332.0000

Sieve Size	% Passing
0.001mm	
0.002mm	8.0
0.020mm	
0.075mm	29.0
0.150mm	
0.180mm	58.0
0.250mm	
0.300mm	
0.425mm	72.0
0.600mm	
0.850mm	
1.18mm	
2.0mm	84.0
2.36mm	
4.75mm	90.0
9.5mm	94.0
12.5mm	97.0
19.0mm	98.0
25.0mm	100.0
37.5mm	
50.0mm	
63.0mm	
75.0mm	
90.0mm	

Calibration Coefficients

AC Fatigue

$N_f = 0.00432 * C * \beta_{f1} k_1 \left(\frac{1}{\varepsilon_1}\right)^{k_2\beta_{f2}} \left(\frac{1}{E}\right)^{k_3\beta_{f3}}$	k1: 3.75
	k2: 2.87
$C = 10^M$	k3: 1.46
	Bf1: (5.014 * Pow(hac,-3.416)) * 1 + 0
$M = 4.84\left(\frac{V_b}{V_a + V_b} - 0.69\right)$	Bf2: 1.38
	Bf3: 0.88

AC Rutting

$$\frac{\varepsilon_p}{\varepsilon_r} = k_z \beta_{r1} 10^{k_1} T^{k_2\beta_{r2}} N^{k_3\beta_{r3}}$$
$$k_z = (C_1 + C_2 * depth) * 0.328196^{depth}$$
$$C_1 = -0.1039 * H_a^2 + 2.4868 * H_a - 17.342$$
$$C_2 = 0.0172 * H_a^2 - 1.7331 * H_a + 27.428$$

Where:
H_{ac} = total AC thickness(in)

ε_p = plastic strain(in/in)
ε_r = resilient strain(in/in)
T = layer temperature(°F)
N = number of load repetitions

AC Rutting Standard Deviation	0.24 * Pow(RUT,0.8026) + 0.001	
AC Layer 1	K1:-2.45 K2:3.01 K3:0.22	Br1:0.128 Br2:0.52 Br3:1.36
AC Layer 2	K1:-2.45 K2:3.01 K3:0.22	Br1:0.4 Br2:0.52 Br3:1.36

Thermal Fracture

$$C_f = 400 * N\left(\frac{\log C / h_{ac}}{\sigma}\right)$$
$$\Delta C = (k * \beta t)^{n+1} * A * \Delta K^n$$
$$A = 10^{(4.389 - 2.52 * \log(E * \sigma_m * n))}$$

C_f = observed amount of thermal cracking(ft/500ft)
k = refression coefficient determined through field calibration
$N()$ = standard normal distribution evaluated at()
σ = standard deviation of the log of the depth of cracks in the pavments
C = crack depth(in)
h_{ac} = thickness of asphalt layer(in)
ΔC = Change in the crack depth due to a cooling cycle
ΔK = Change in the stress intensity factor due to a cooling cycle
A, n = Fracture parameters for the asphalt mixture
E = mixture stiffness
σ_M = Undamaged mixture tensile strength
β_t = Calibration parameter

Level 1 K: ((3 * Pow(10,-7)) * Pow(MAAT,4.0319)) * 1 + 0	Level 1 Standard Deviation: 0.14 * THERMAL + 168
Level 2 K: ((3 * Pow(10,-7)) * Pow(MAAT,4.0319)) * 1 + 0	Level 2 Standard Deviation: 0.20 * THERMAL + 168
Level 3 K: ((3 * Pow(10,-7)) * Pow(MAAT,4.0319)) * 1 + 0	Level 3 Standard Deviation: 0.289 * THERMAL + 168

CSM Fatigue

$$N_f = 10^{\left(\frac{k_1 \beta_{c1}\left(\frac{\sigma_s}{M_r}\right)}{k_2 \beta_{c2}}\right)}$$

N_f = number of repetitions to fatigue cracking
σ_s = Tensile stress(psi)
M_r = modulus of rupture(psi)

k1: 0.972	k2: 0.0825	Bc1: 1	Bc2:1

Unbound Layer Rutting

$$\delta_a(N) = \beta_{s_1} k_1 \varepsilon_v h \left(\frac{\varepsilon_0}{\varepsilon_r}\right) \left| e^{-\left(\frac{\rho}{N}\right)^\beta} \right|$$

δ_a = permanent deformation for the layer
N = number of repetitions
ε_v = average veritcal strain(in/in)
$\varepsilon_0, \beta, \rho$ = material properties
ε_r = resilient strain(in/in)

Base Rutting		Subgrade Rutting	
k1: 0.965	Bs1: 1	k1: 0.675	Bs1: 1
Standard Deviation (BASERUT) 0.1477 * Pow(BASERUT,0.6711) + 0.001		Standard Deviation (BASERUT) 0.1235 * Pow(SUBRUT,0.5012) + 0.001	

AC Cracking

AC Top Down Cracking

$$FC_{top} = \left(\frac{C_4}{1 + e^{(C_1 - C_2 * log_{10}(Damage))}}\right) * 10.56$$

AC Bottom Up Cracking

$$FC = \left(\frac{6000}{1 + e^{\left(C_1 * C_1' + C_2 * C_2' log_{10}(D*100)\right)}}\right) * \left(\frac{1}{60}\right)$$

$$C_2' = -2.40874 - 39.748 * (1 + h_{ac})^{-2.856}$$

$$C_1' = -2 * C_2'$$

AC Top Down Cracking				AC Bottom Up Cracking		
c1: 7	c2: 3.5	c3: 0	c4: 1000	c1: 1.31	c2: (0.867 + 0.2583 * hac) * 1 + 0	c3: 6000

Top down AC Cracking Standard Deviation	Bottom up AC Cracking Standard Deviation
200 + 2300/(1+exp(1.072-2.1654*LOG10(TOP+0.0001)))	1.13 + 13/(1+exp(7.57-15.5*LOG10(BOTTOM+0.0001)))

CSM Cracking

$$FC_{ctb} = C_1 + \frac{C_2}{1 + e^{C_3 - C_4 * log_{10}(Damage)}}$$

C1: 0	C2: 75	C3: 2	C4: 2

CSM Standard Deviation

CTB*1

IRI Flexible Pavements

C1 - Rutting
C2 - Fatigue Crack
C3 - Transverse Crack
C4 - Site Factors

C1: 55	C2: 0.4	C3: 0.008	C4: 0.015

LVR_400AADT_CIR_3%-12 years December 2019

File Name: C:\Users\admin\Desktop\Taha M2\LVR_400AADT_CIR_3%-12 years December 2019.dgpx

Design Inputs

Design Life:	12 years	Base construction:	May, 2020	Climate Data Sources (Lat/Lon)	44, -78.75
Design Type:	FLEXIBLE	Pavement construction:	June, 2021		
		Traffic opening:	September, 2021		

Design Structure

Layer type	Material Type	Thickness(mm)
Flexible	Default asphalt concrete	50.0
Flexible	Default asphalt concrete	100.0
NonStabilized	A-1-a	150.0
NonStabilized	A-1-b	400.0
Subgrade	A-6	Semi-infinite

Volumetric at Construction:	
Effective binder content (%)	11.8
Air voids (%)	7.0

Traffic

Age (year)	Heavy Trucks (cumulative)
2021 (initial)	400
2027 (6 years)	424,055
2033 (12 years)	919,115

Design Outputs

Distress Prediction Summary

Distress Type	Distress @ Specified Reliability		Reliability (%)		Criterion Satisfied?
	Target	Predicted	Target	Achieved	
Terminal IRI (m/km)	2.70	1.75	75.00	99.85	Pass
Permanent deformation - total pavement (mm)	17.00	7.81	75.00	100.00	Pass
AC bottom-up fatigue cracking (percent)	35.00	0.76	75.00	100.00	Pass
AC thermal cracking (m/km)	190.00	21.65	75.00	100.00	Pass
AC top-down fatigue cracking (m/km)	380.00	309.38	75.00	80.70	Pass
Permanent deformation - AC only (mm)	6.00	0.44	75.00	100.00	Pass

LVR_400AADT_CIR_3%-12 years December 2019

File Name: C:\Users\admin\Desktop\Taha M2\LVR_400AADT_CIR_3%-12 years December 2019.dgpx

Distress Charts

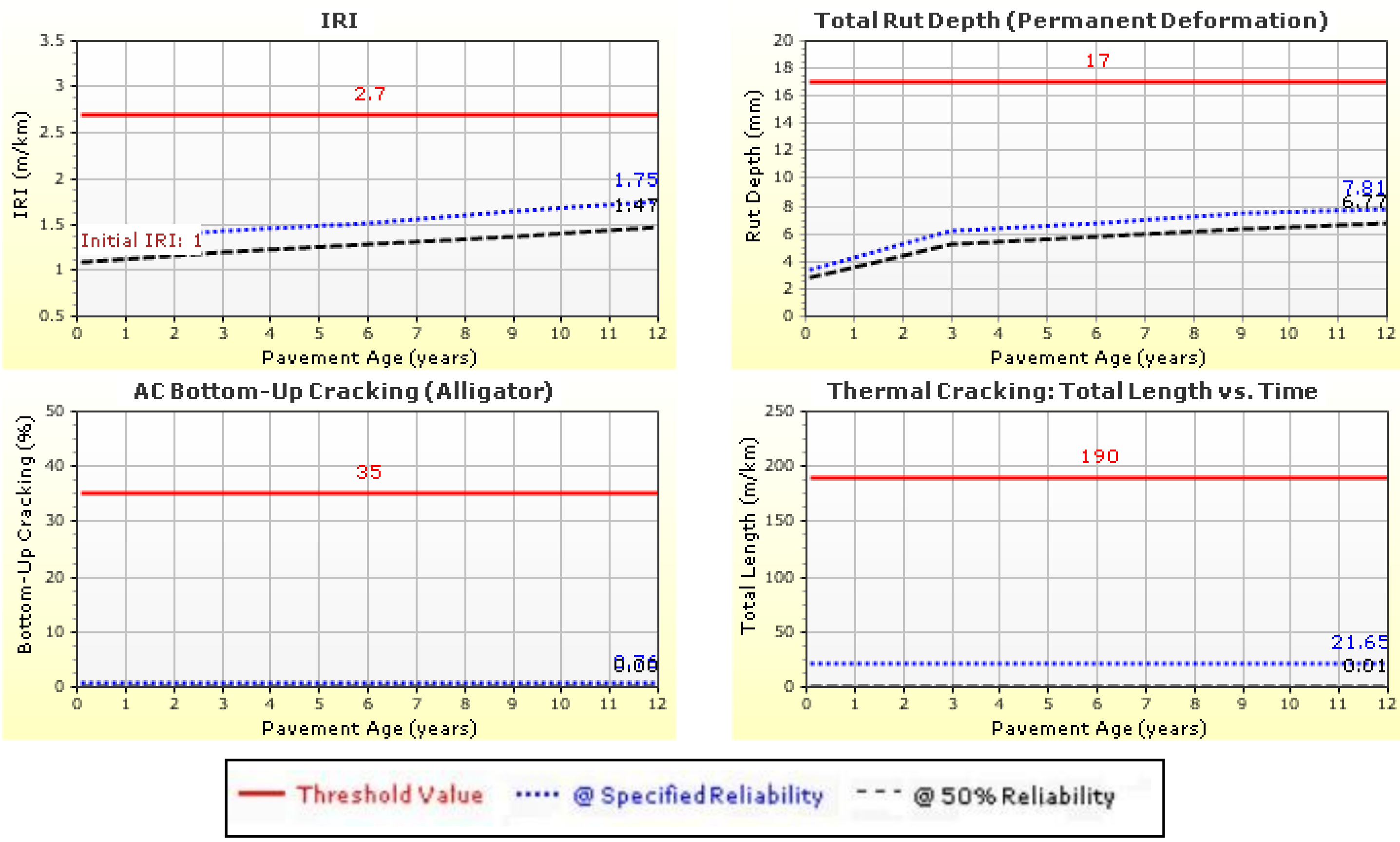

Traffic Inputs

Graphical Representation of Traffic Inputs

Initial two-way AADTT:	400	Percent of trucks in design direction (%):	50.0
Number of lanes in design direction:	2	Percent of trucks in design lane (%):	90.0
		Operational speed (kph)	80.0

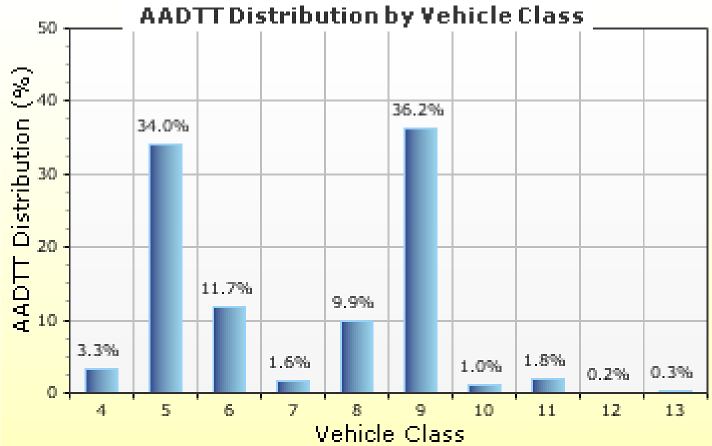

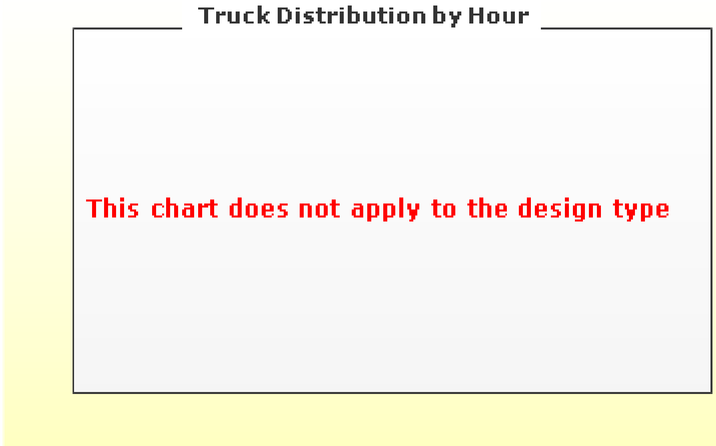

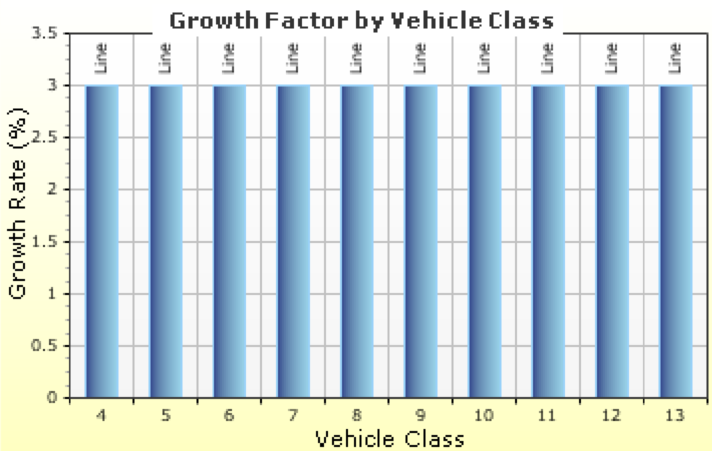

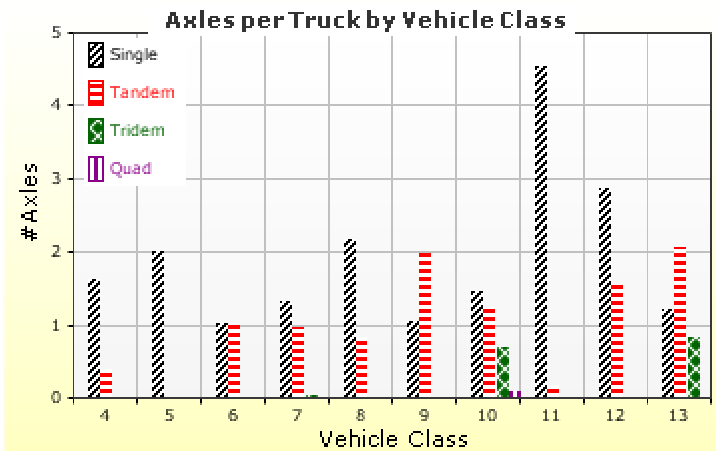

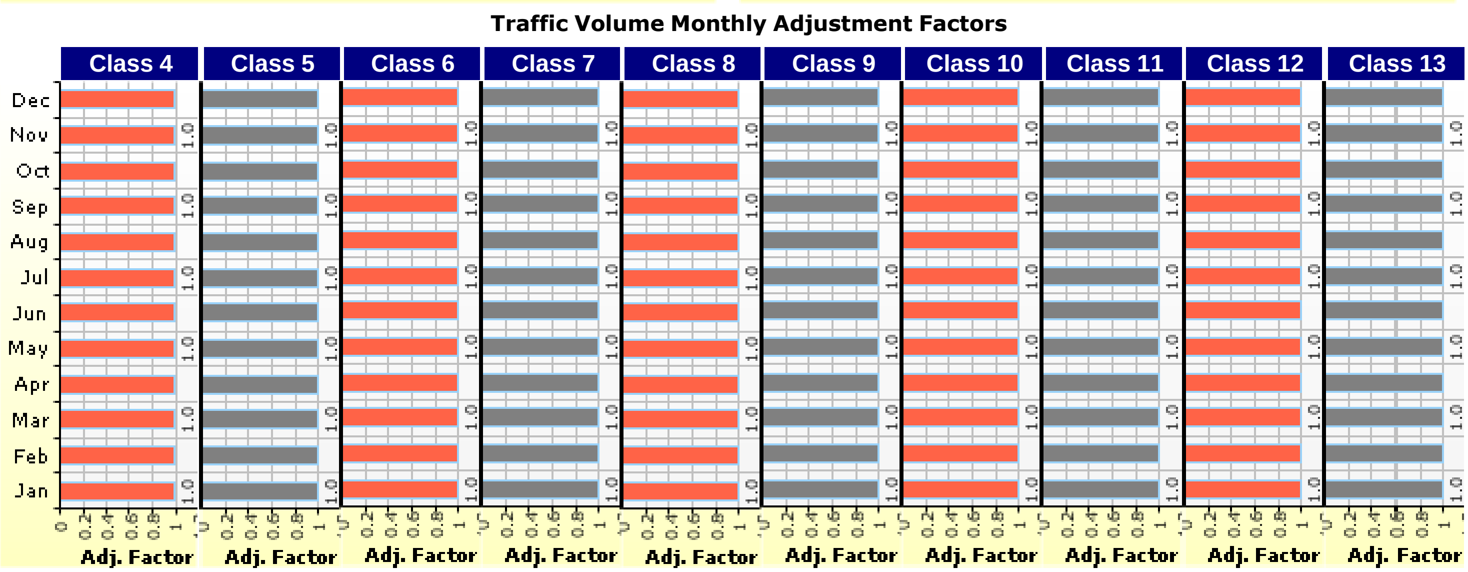

LVR_400AADT_CIR_3%-12 years December 2019

File Name: C:\Users\admin\Desktop\Taha M2\LVR_400AADT_CIR_3%-12 years December 2019.dgpx

Tabular Representation of Traffic Inputs

Volume Monthly Adjustment Factors

Level 3: Default MAF

Month	Vehicle Class									
	4	5	6	7	8	9	10	11	12	13
January	1.0	1.0	1.0	1.0	1.0	1.0	1.0	1.0	1.0	1.0
February	1.0	1.0	1.0	1.0	1.0	1.0	1.0	1.0	1.0	1.0
March	1.0	1.0	1.0	1.0	1.0	1.0	1.0	1.0	1.0	1.0
April	1.0	1.0	1.0	1.0	1.0	1.0	1.0	1.0	1.0	1.0
May	1.0	1.0	1.0	1.0	1.0	1.0	1.0	1.0	1.0	1.0
June	1.0	1.0	1.0	1.0	1.0	1.0	1.0	1.0	1.0	1.0
July	1.0	1.0	1.0	1.0	1.0	1.0	1.0	1.0	1.0	1.0
August	1.0	1.0	1.0	1.0	1.0	1.0	1.0	1.0	1.0	1.0
September	1.0	1.0	1.0	1.0	1.0	1.0	1.0	1.0	1.0	1.0
October	1.0	1.0	1.0	1.0	1.0	1.0	1.0	1.0	1.0	1.0
November	1.0	1.0	1.0	1.0	1.0	1.0	1.0	1.0	1.0	1.0
December	1.0	1.0	1.0	1.0	1.0	1.0	1.0	1.0	1.0	1.0

Distributions by Vehicle Class

Vehicle Class	AADTT Distribution (%) (Level 3)	Growth Factor	
		Rate (%)	Function
Class 4	3.3%	3%	Linear
Class 5	34%	3%	Linear
Class 6	11.7%	3%	Linear
Class 7	1.6%	3%	Linear
Class 8	9.9%	3%	Linear
Class 9	36.2%	3%	Linear
Class 10	1%	3%	Linear
Class 11	1.8%	3%	Linear
Class 12	0.2%	3%	Linear
Class 13	0.3%	3%	Linear

Truck Distribution by Hour does not apply

Axle Configuration

Traffic Wander	
Mean wheel location (mm)	460.0
Traffic wander standard deviation (mm)	254.0
Design lane width (m)	3.7

Axle Configuration	
Average axle width (m)	2.6
Dual tire spacing (mm)	305.0
Tire pressure (kPa)	827.4

Average Axle Spacing	
Tandem axle spacing (m)	1.5
Tridem axle spacing (m)	1.7
Quad axle spacing (m)	1.3

Wheelbase does not apply

Number of Axles per Truck

Vehicle Class	Single Axle	Tandem Axle	Tridem Axle	Quad Axle
Class 4	1.62	0.39	0	0
Class 5	2	0	0	0
Class 6	1.01	0.993	0	0
Class 7	1.314	0.989	0.03	0
Class 8	2.163	0.845	0	0
Class 9	1.055	1.968	0.003	0
Class 10	1.446	1.234	0.7	0.088
Class 11	4.546	0.168	0	0
Class 12	2.857	1.526	0	0
Class 13	1.201	2.058	0.848	0.024

AADTT (Average Annual Daily Truck Traffic) Growth

*** Traffic cap is not enforced**

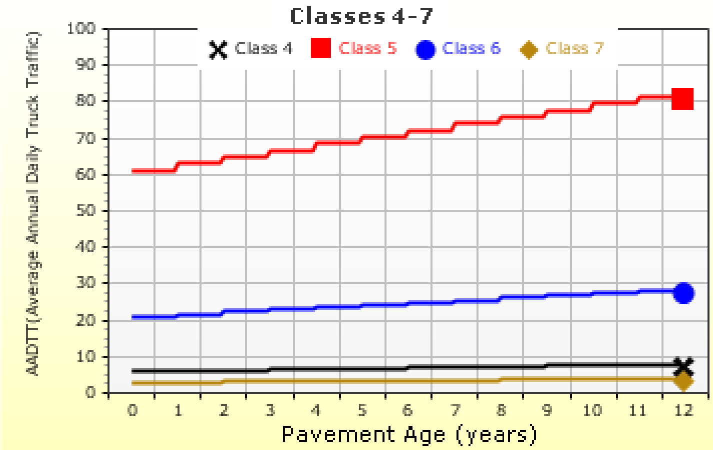

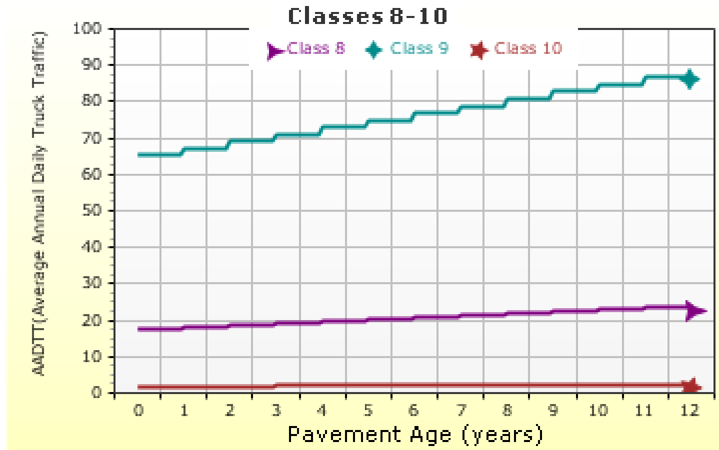

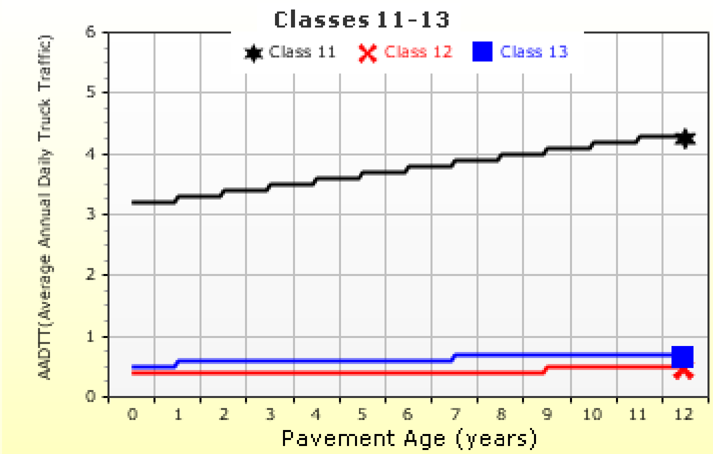

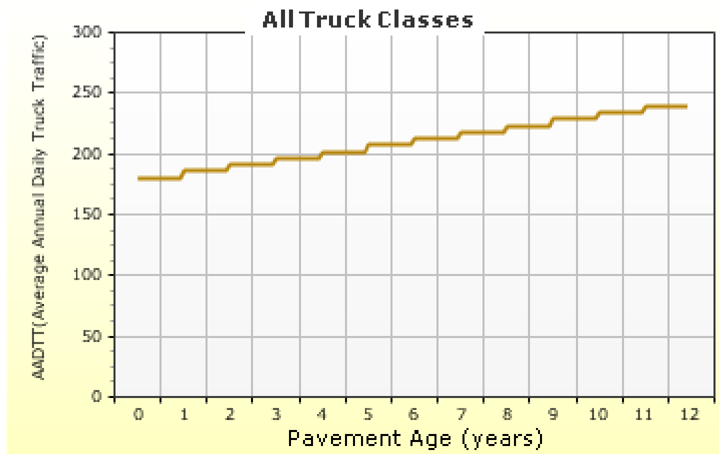

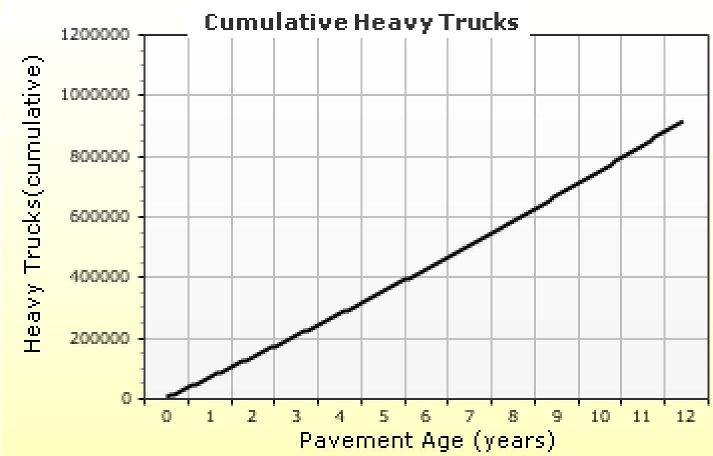

Climate Inputs

Climate Data Sources:

Climate Station Cities:	Location (lat lon elevation(m))
CA, ON	44.00000 -78.75000 193

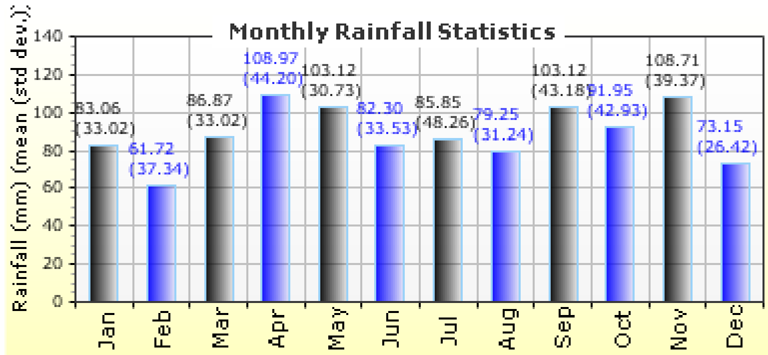

Annual Statistics:

Mean annual air temperature (ºC)	7.62
Mean annual precipitation (mm)	1068.32
Freezing index (ºC - days)	573.75
Average annual number of freeze/thaw cycles:	77.00
Water table depth (m)	10.00

Monthly Climate Summary:

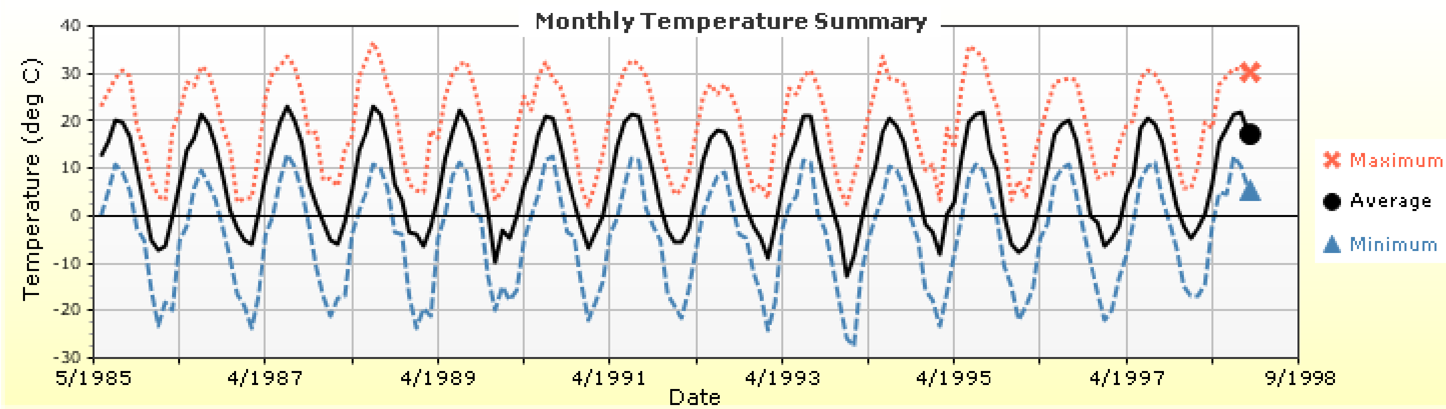

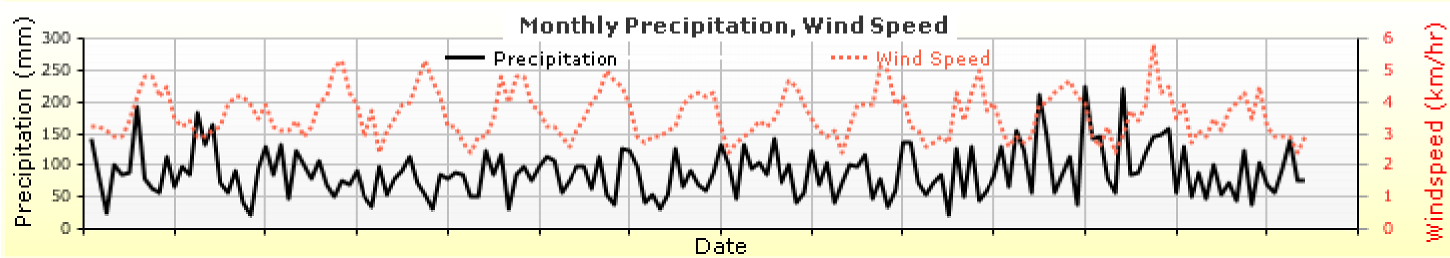

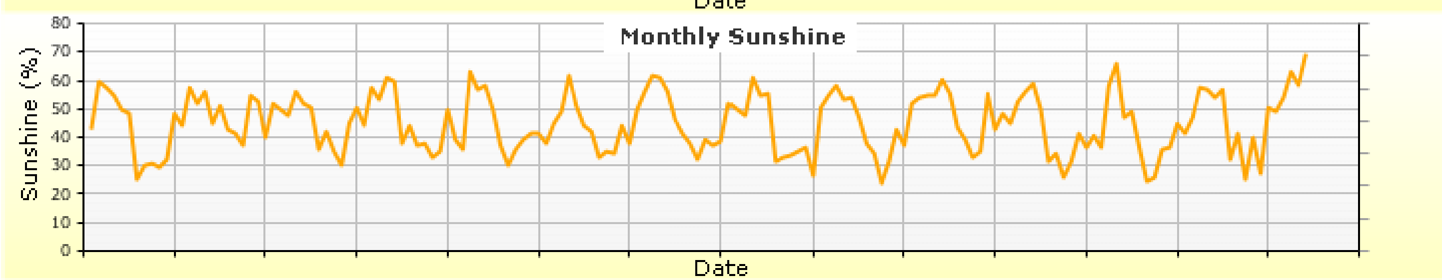

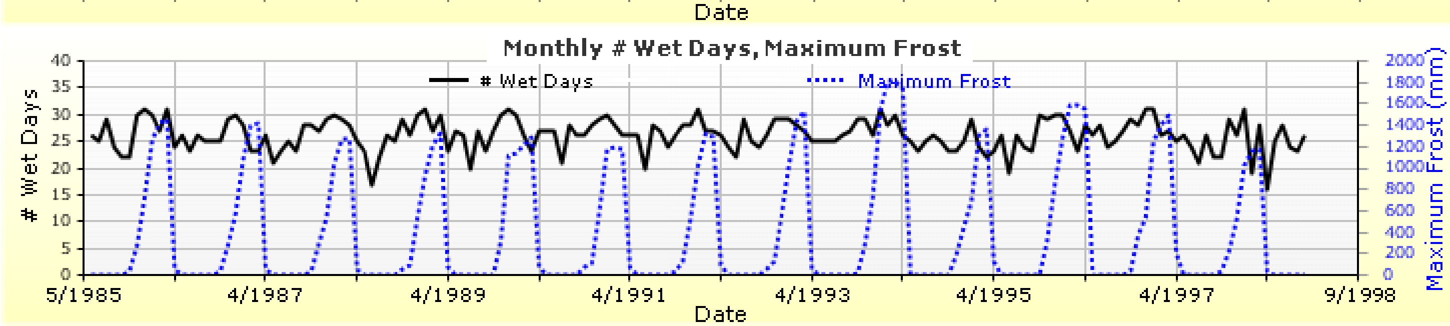

LVR_400AADT_CIR_3%-12 years December 2019

File Name: C:\Users\admin\Desktop\Taha M2\LVR_400AADT_CIR_3%-12 years December 2019.dgpx

Hourly Air Temperature Distribution by Month:

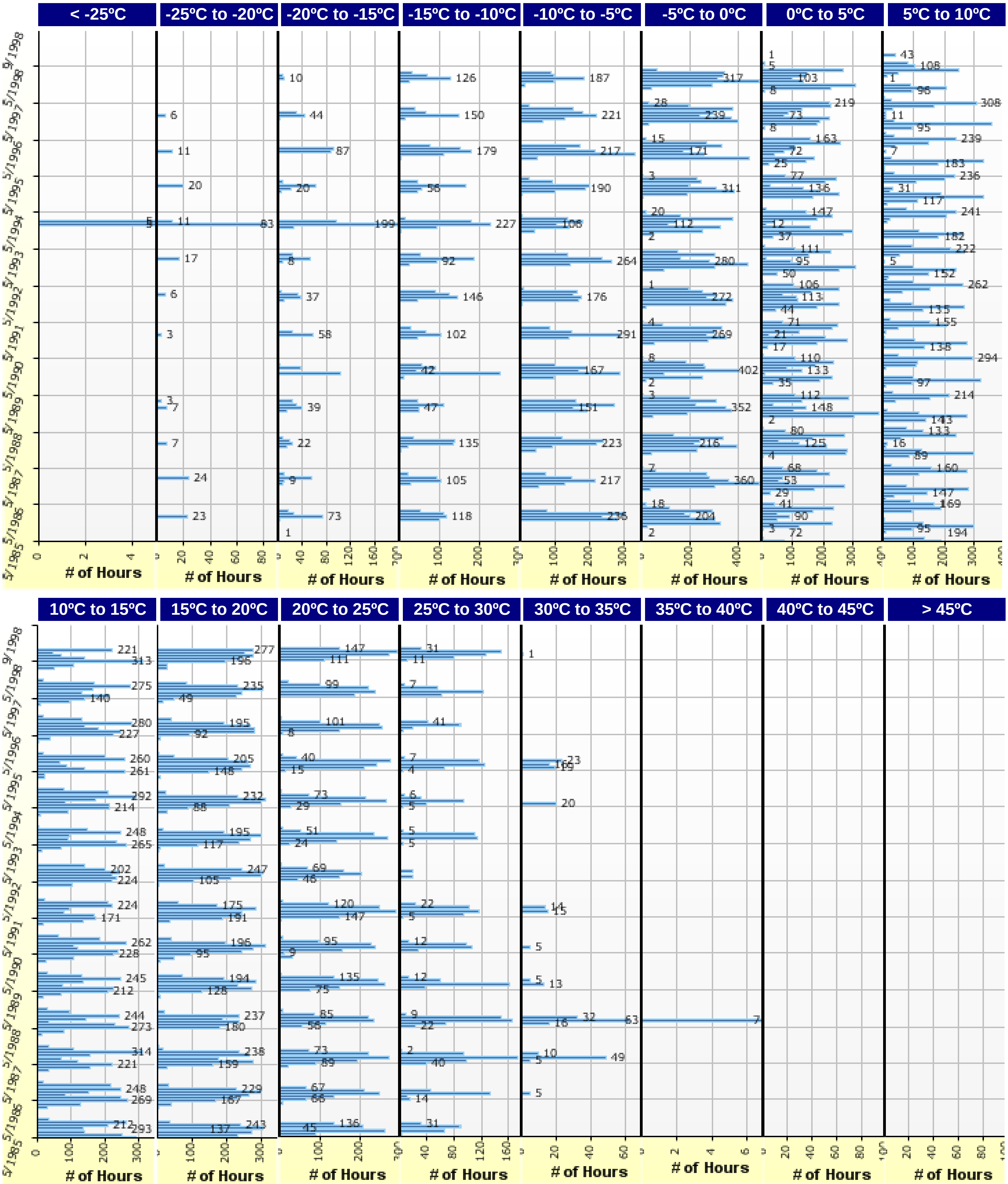

Design Properties

HMA Design Properties

Use Multilayer Rutting Model	False
Using G* based model (not nationally calibrated)	False
Is NCHRP 1-37A HMA Rutting Model Coefficients	True
Endurance Limit	-
Use Reflective Cracking	True

Structure - ICM Properties	
AC surface shortwave absorptivity	0.85

Layer Name	Layer Type	Interface Friction
Layer 1 Flexible : Default asphalt concrete	Flexible (1)	1.00
Layer 2 Flexible : Default asphalt concrete	Flexible (1)	1.00
Layer 3 Non-stabilized Base : A-1 -a	Non-stabilized Base (4)	1.00
Layer 4 Non-stabilized Base : A-1 -b	Non-stabilized Base (4)	1.00
Layer 5 Subgrade : A-6	Subgrade (5)	-

Thermal Cracking

Thermal Contraction	
Is thermal contraction calculated?	True
Mix coefficient of thermal contraction (mm/mm/ºC)	-
Aggregate coefficient of thermal contraction (mm/mm/ºC)	9.0e-006
Voids in Mineral Aggregate (%)	18.8

Indirect Tensile Strength (Input Level: 3)	
Test Temperature (ºC)	Indirect Tensilte Strength (Mpa)
-10.0	2.79

Creep Compliance (1/GPa) (Input Level: 3)			
Loading time (sec)	-20 ºC	-10 ºC	0 ºC
1	5.57e-002	8.57e-002	1.16e-001
2	6.17e-002	1.01e-001	1.51e-001
5	7.07e-002	1.25e-001	2.15e-001
10	7.83e-002	1.48e-001	2.80e-001
20	8.68e-002	1.74e-001	3.65e-001
50	9.94e-002	2.16e-001	5.19e-001
100	1.10e-001	2.55e-001	6.77e-001

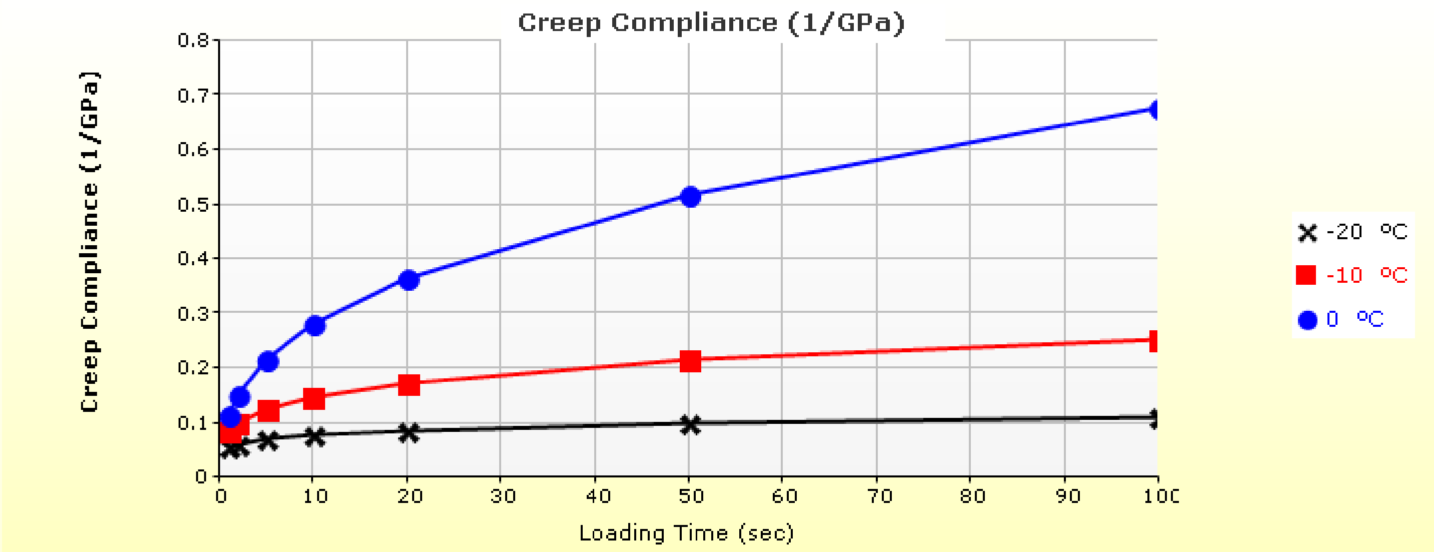

LVR_400AADT_CIR_3%-12 years December 2019

File Name: C:\Users\admin\Desktop\Taha M2\LVR_400AADT_CIR_3%-12 years December 2019.dgpx

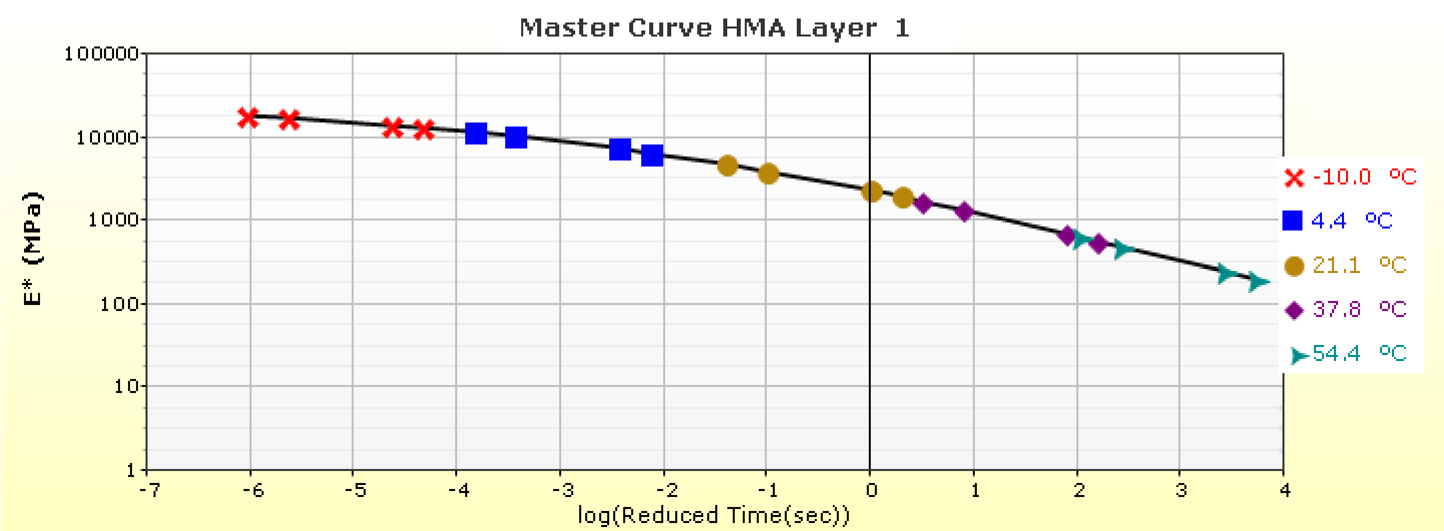

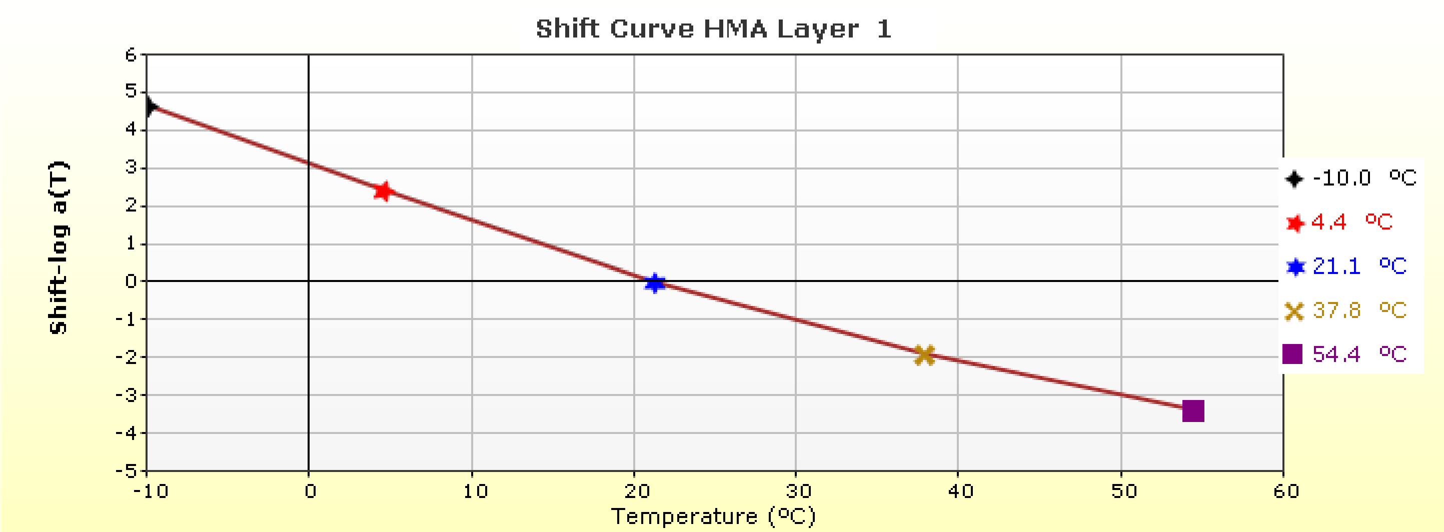

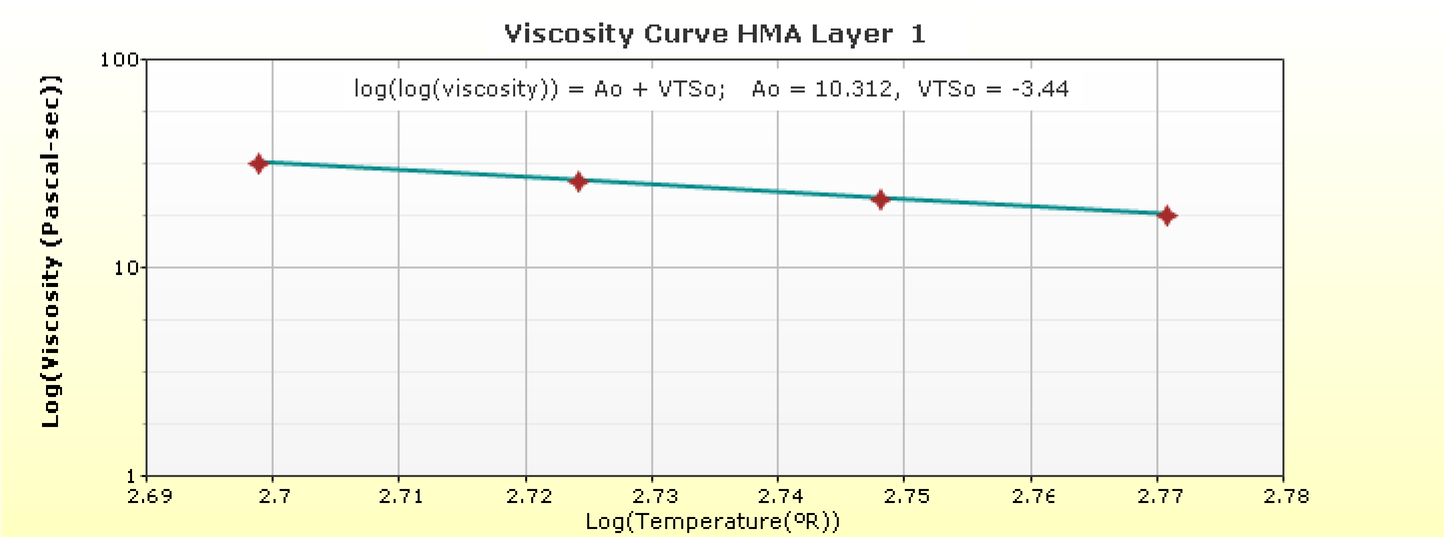

HMA Layer 2: Layer 2 Flexible : Default asphalt concrete

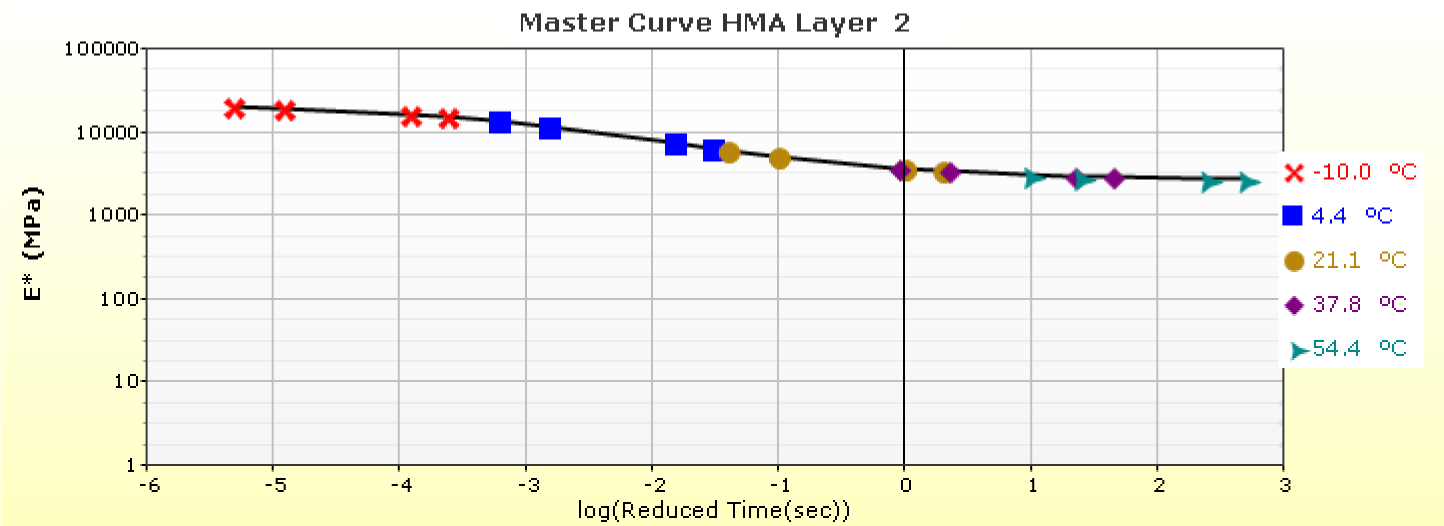

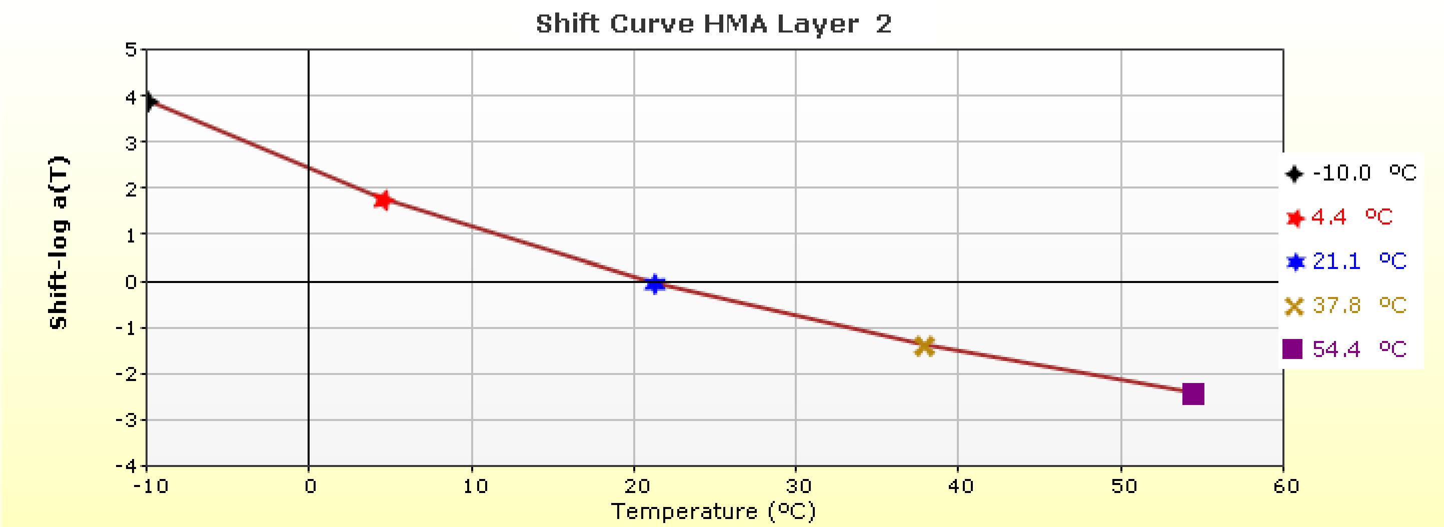

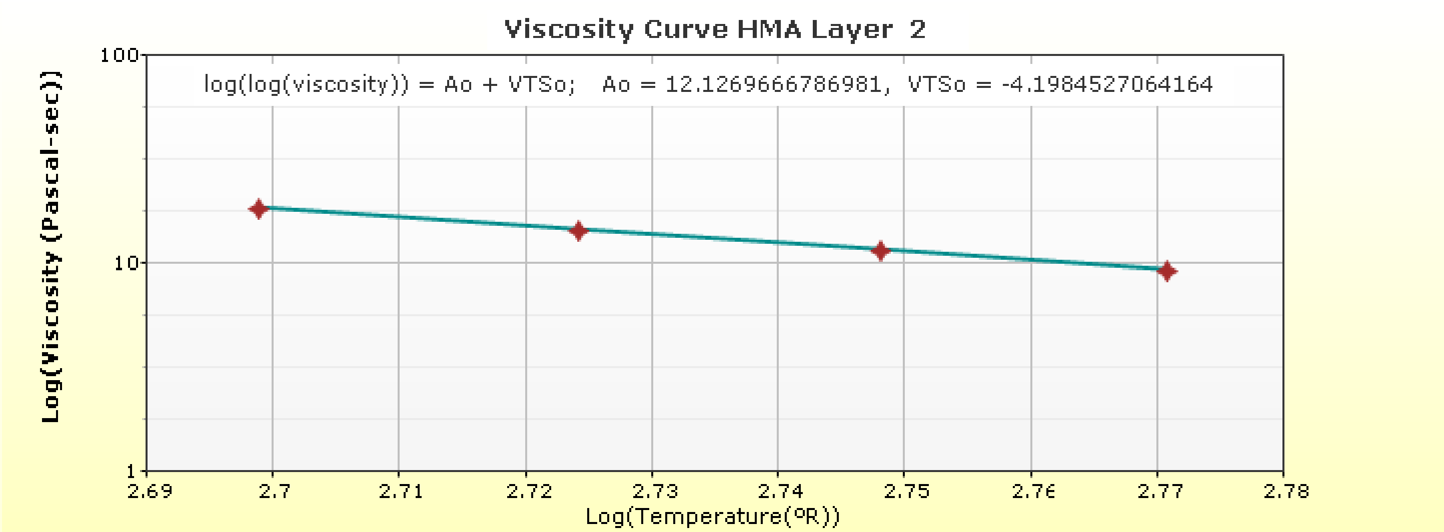

LVR_400AADT_CIR_3%-12 years December 2019

File Name: C:\Users\admin\Desktop\Taha M2\LVR_400AADT_CIR_3%-12 years December 2019.dgpx

Analysis Output Charts

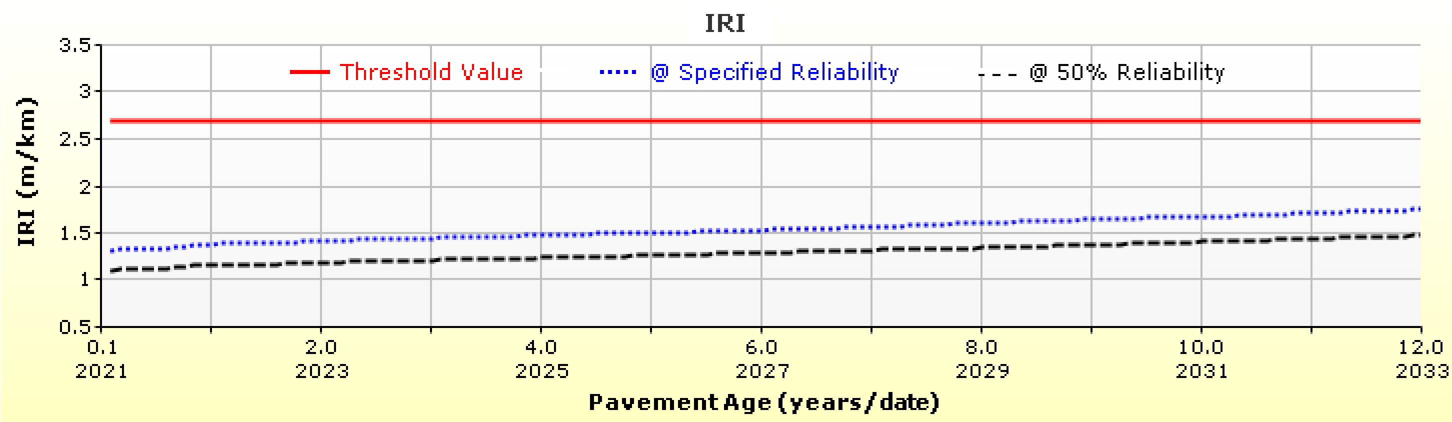

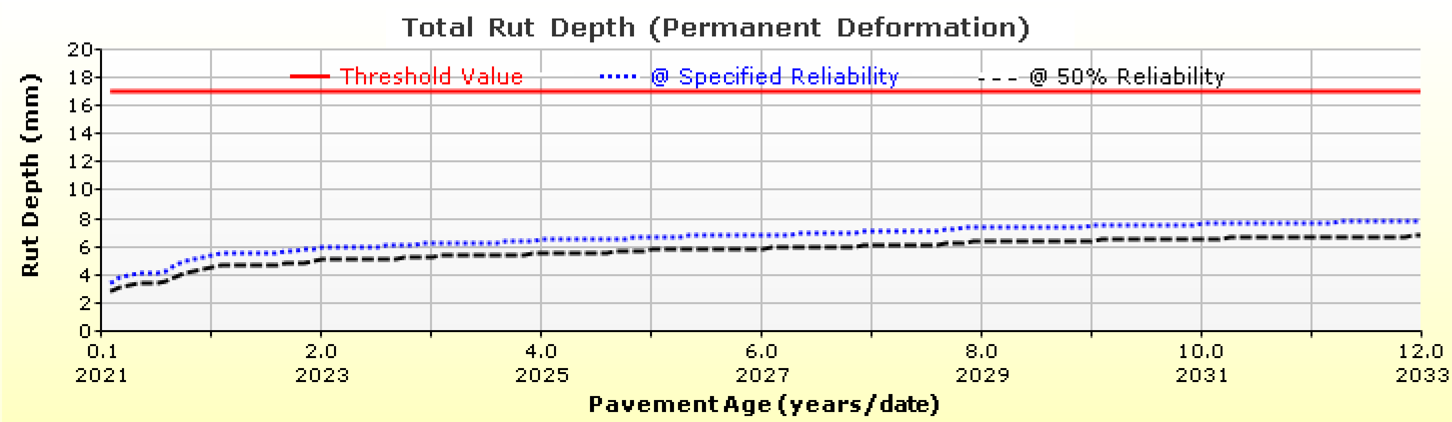

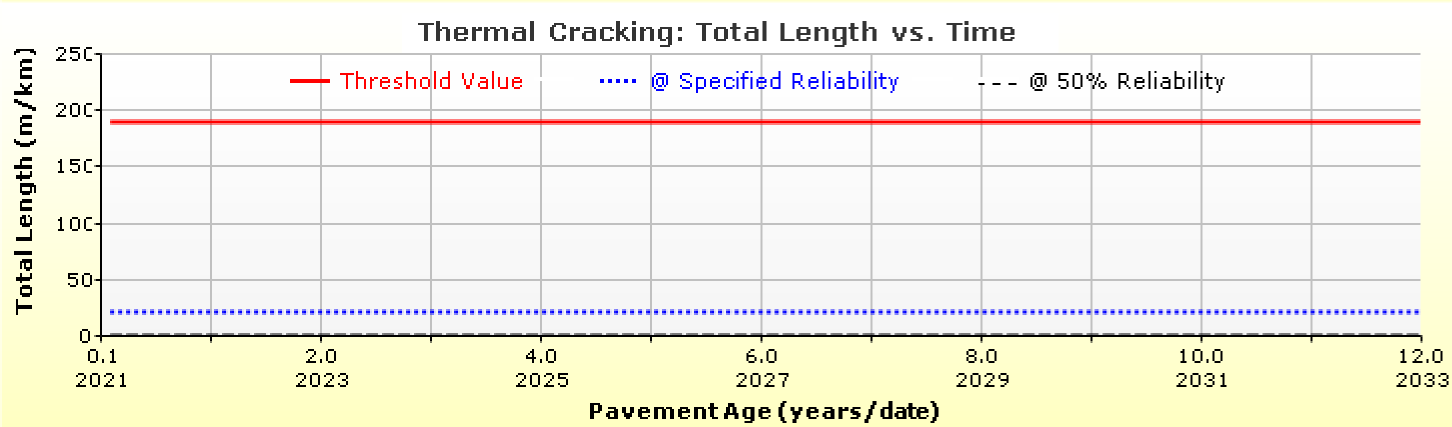

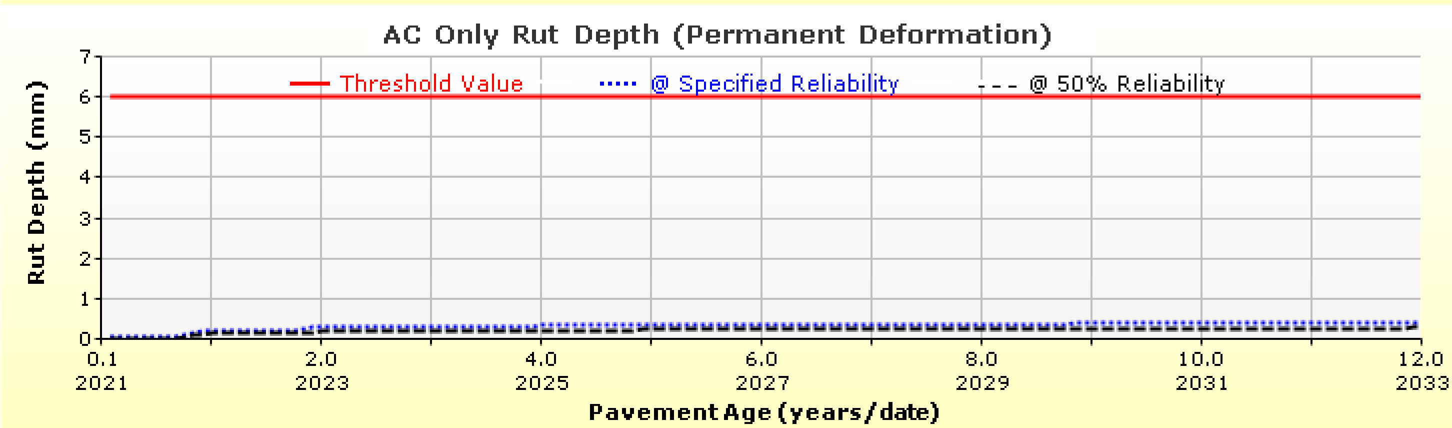

LVR_400AADT_CIR_3%-12 years December 2019

File Name: C:\Users\admin\Desktop\Taha M2\LVR_400AADT_CIR_3%-12 years December 2019.dgpx

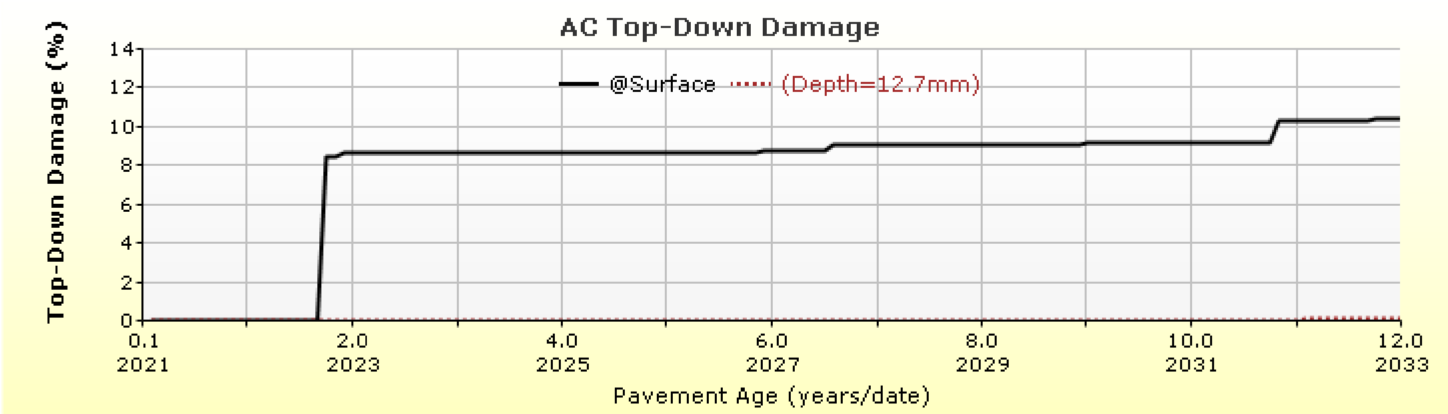

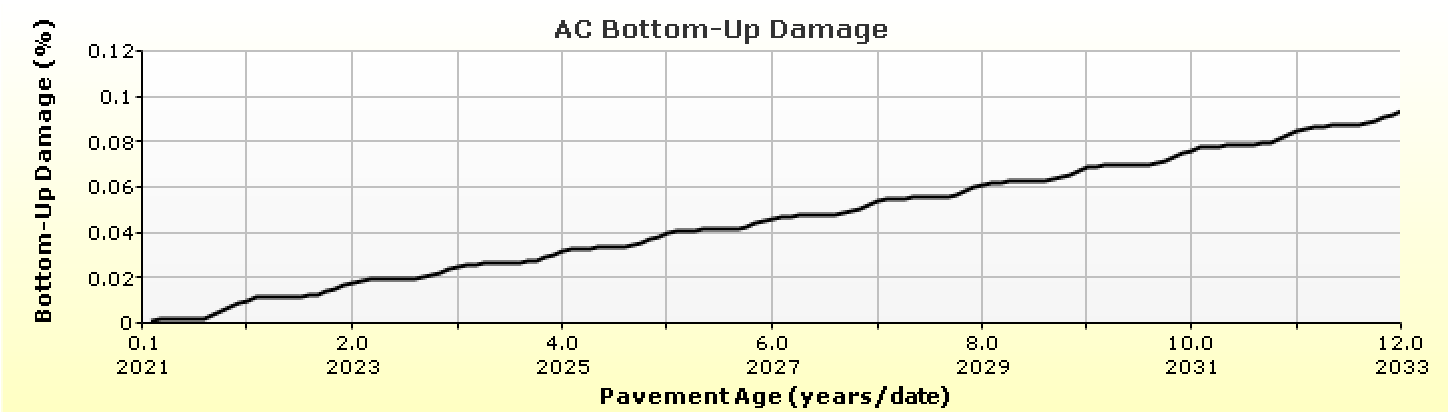

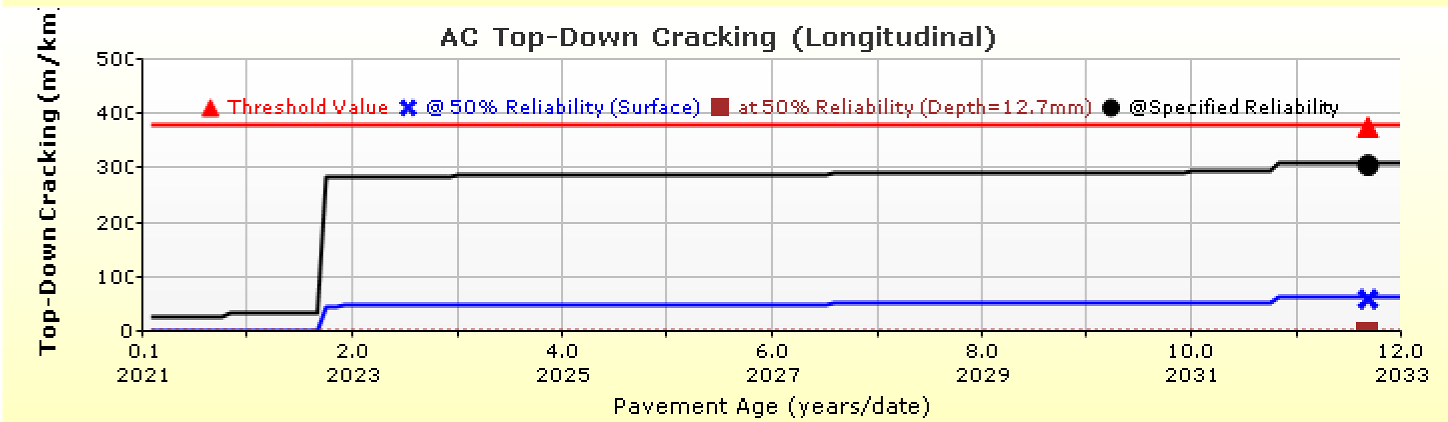

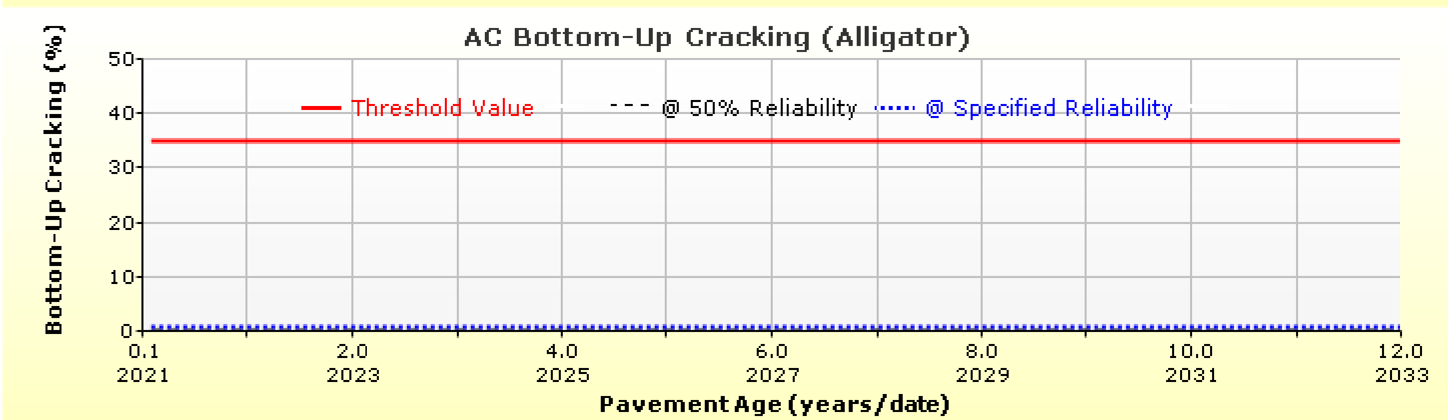

LVR_400AADT_CIR_3%-12 years December 2019

File Name: C:\Users\admin\Desktop\Taha M2\LVR_400AADT_CIR_3%-12 years December 2019.dgpx

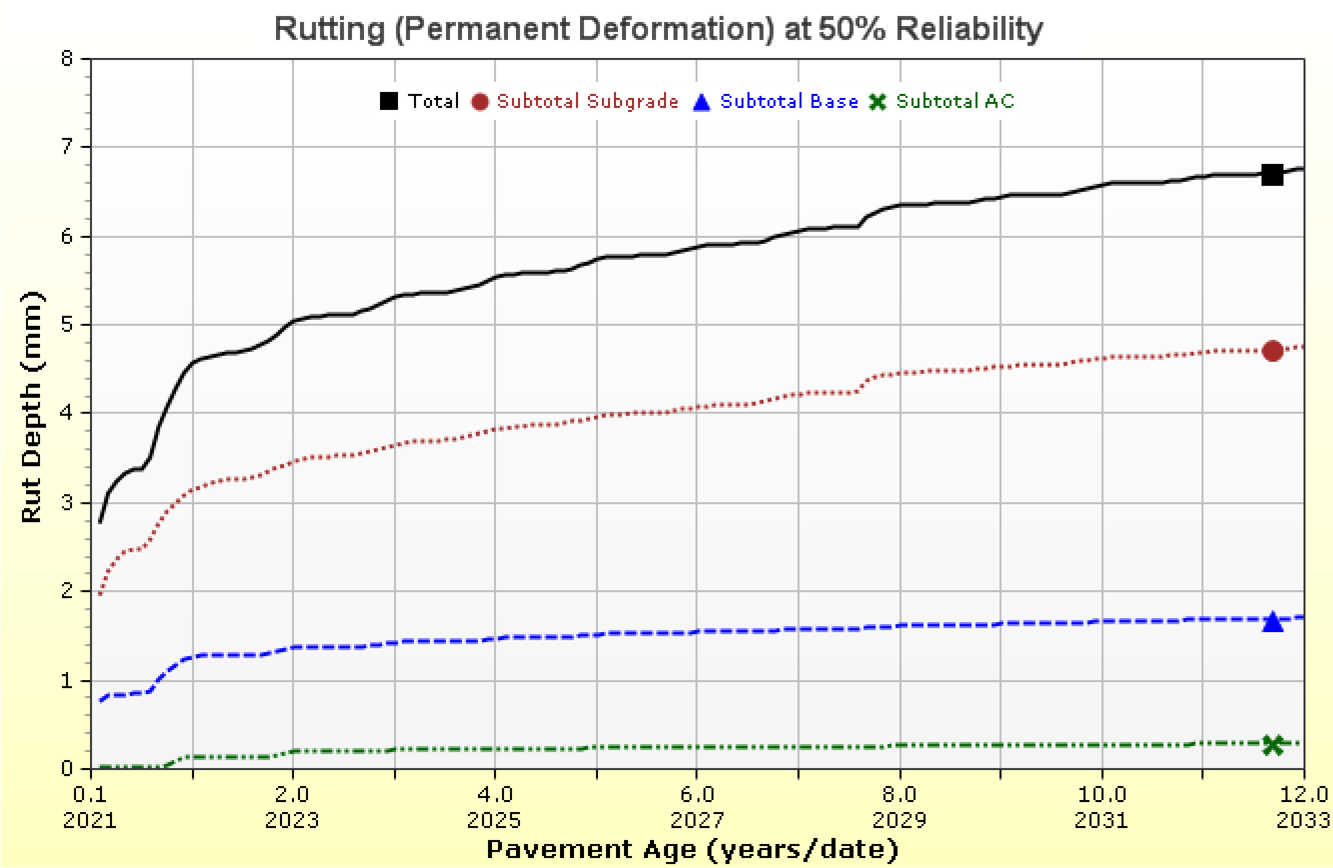

LVR_400AADT_CIR_3%-12 years December 2019

File Name: C:\Users\admin\Desktop\Taha M2\LVR_400AADT_CIR_3%-12 years December 2019.dgpx

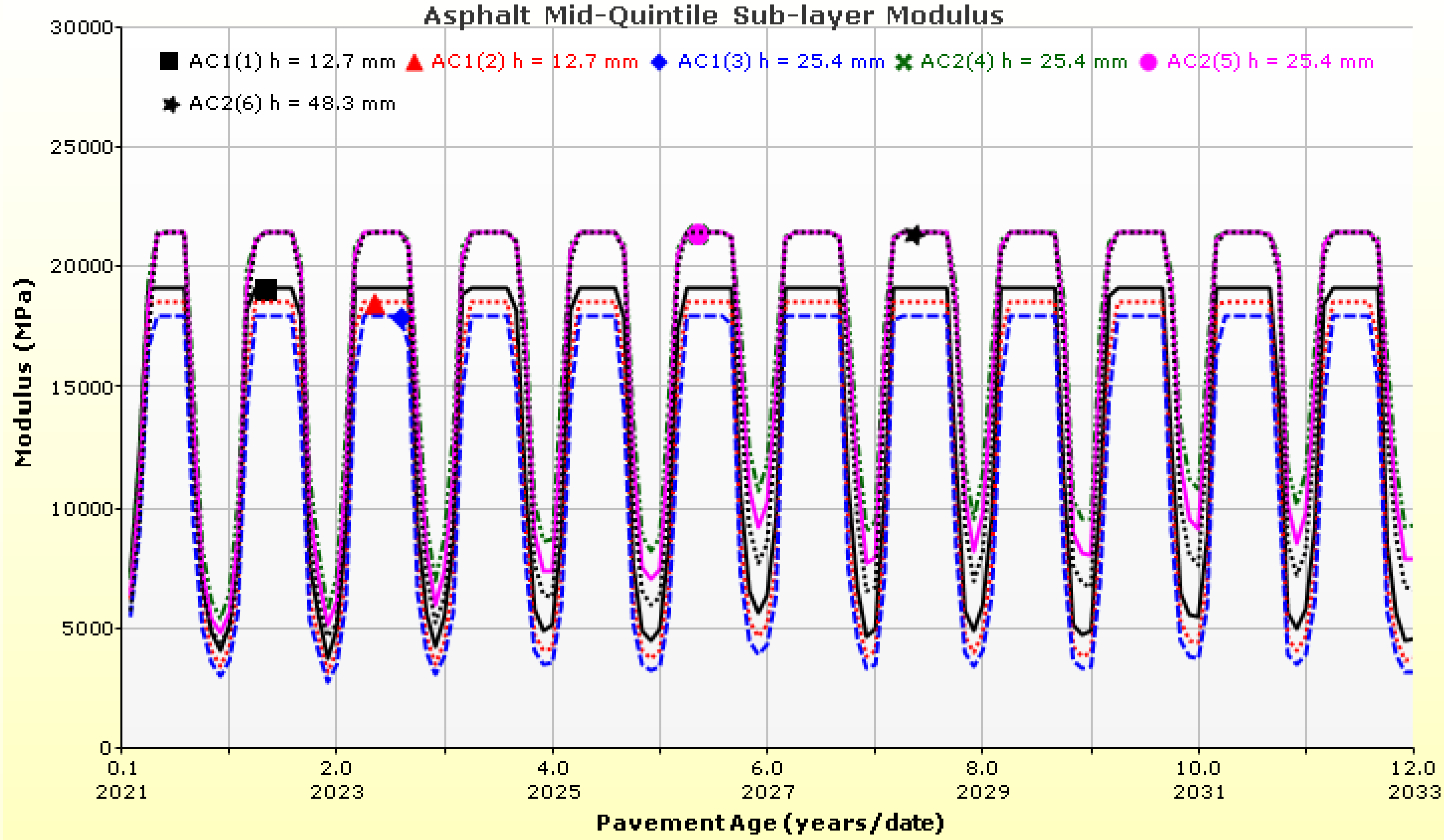

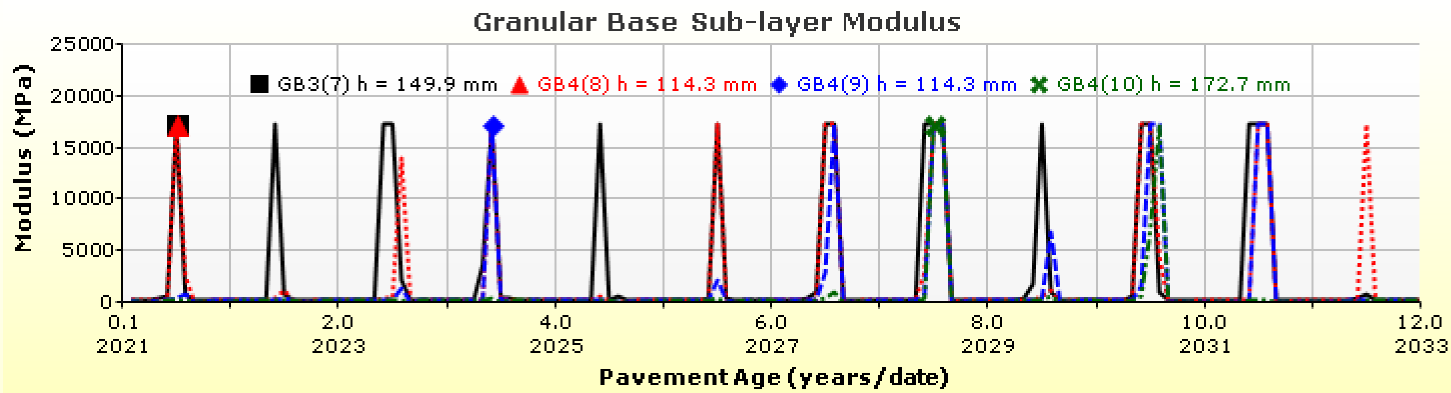

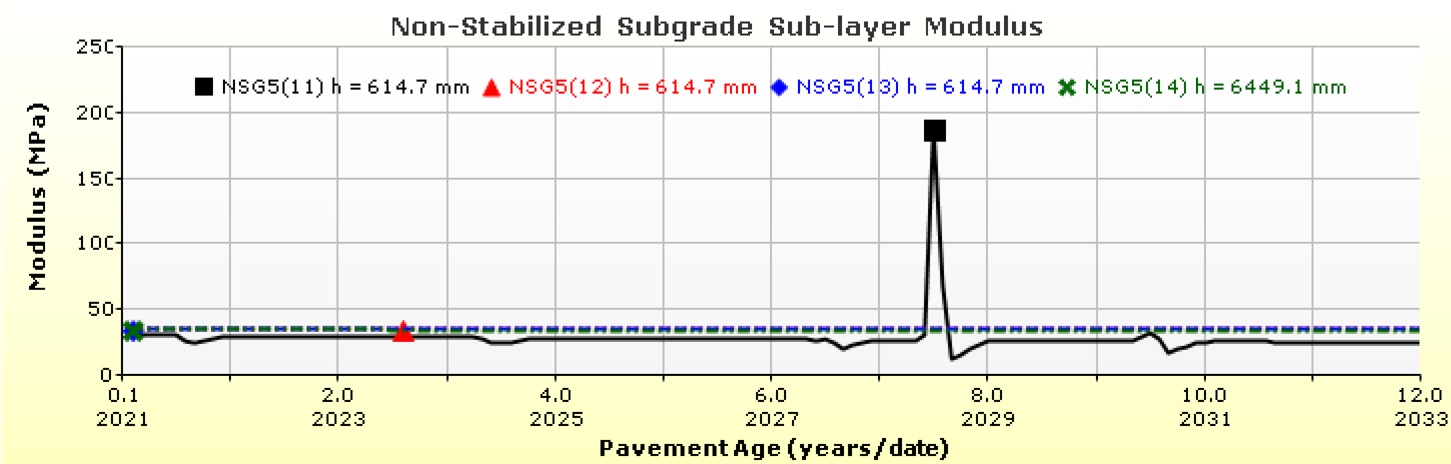

Layer Information

Layer 1 Flexible : Default asphalt concrete

Asphalt		
Thickness (mm)	50.0	
Unit weight (kgf/m^3)	2460.0	
Poisson's ratio	Is Calculated?	False
	Ratio	0.35
	Parameter A	-
	Parameter B	-

Asphalt Dynamic Modulus (Input Level: 3)

Gradation	Percent Passing
19 mm sieve	100
9.5 mm sieve	83.2
4.75 mm sieve	54
0.075mm sieve	4

Asphalt Binder

Parameter	Value
Grade	Superpave Performance Grade
Binder Type	64-28
A	10.312
VTS	-3.44

General Info

Name	Value
Reference temperature (ºC)	21.1
Effective binder content (%)	11.8
Air voids (%)	7
Thermal conductivity (watt/meter-kelvin)	1.16
Heat capacity (joule/kg-kelvin)	963

Identifiers

Field	Value
Display name/identifier	Default asphalt concrete
Description of object	
Author	
Date Created	9/16/2010 1:00:00 AM
Approver	
Date approved	9/16/2010 1:00:00 AM
State	
District	
County	
Highway	
Direction of Travel	
From station (km)	
To station (km)	
Province	
User defined field 1	
User defined field 2	
User defined field 3	
Revision Number	0

LVR_400AADT_CIR_3%-12 years December 2019

File Name: C:\Users\admin\Desktop\Taha M2\LVR_400AADT_CIR_3%-12 years December 2019.dgpx

Layer 2 Flexible : Default asphalt concrete

Asphalt		
Thickness (mm)	100.0	
Unit weight (kgf/m^3)	2460.0	
Poisson's ratio	Is Calculated?	False
	Ratio	0.35
	Parameter A	-
	Parameter B	-

Asphalt Dynamic Modulus (Input Level: 1)

T (ºC)	0.1 Hz	0.5 Hz	1 Hz	5 Hz	10 Hz	25 Hz
-10	13075.60	14979.82	16113.52	18302.70	19249.60	20458.31
4	5859.390	7463.947	8334.234	10265.16	11207.22	12766.28
21	1684.922	2423.819	2983.831	4149.485	4721.115	5919.668
57	1684.922	2423.819	2983.831	4149.485	4721.115	5919.668

Asphalt Binder

Temperature (ºC)	Binder Gstar (Pa)	Phase angle (deg)
4.4	5494.5	57
12.8	1919	59.3
21.1	490.2	61.6
29.4	161.2	62.4
37.8	39.9	62.7
46.1	15.2	62.7

General Info

Name	Value
Reference temperature (ºC)	21.1
Effective binder content (%)	11.2
Air voids (%)	7
Thermal conductivity (watt/meter-kelvin)	1.16
Heat capacity (joule/kg-kelvin)	963

Identifiers

Field	Value
Display name/identifier	Default asphalt concrete
Description of object	
Author	
Date Created	9/16/2010 1:00:00 AM
Approver	
Date approved	9/16/2010 1:00:00 AM
State	
District	
County	
Highway	
Direction of Travel	
From station (km)	
To station (km)	
Province	
User defined field 1	
User defined field 2	
User defined field 3	
Revision Number	0

Layer 3 Non-stabilized Base : A-1-a

Unbound	
Layer thickness (mm)	150.0
Poisson's ratio	0.35
Coefficient of lateral earth pressure (k0)	0.5

Modulus (Input Level: 3)

Analysis Type:	Modify input values by temperature/moisture
Method:	Resilient Modulus (MPa)

Resilient Modulus (MPa)
250.0

Use Correction factor for NDT modulus?	-
NDT Correction Factor:	-

Identifiers

Field	Value
Display name/identifier	A-1-a
Description of object	Default material
Author	AASHTO
Date Created	1/1/2011 12:00:00 AM
Approver	
Date approved	1/1/2011 12:00:00 AM
State	
District	
County	
Highway	
Direction of Travel	
From station (km)	
To station (km)	
Province	
User defined field 1	
User defined field 2	
User defined field 3	
Revision Number	0

Sieve

Liquid Limit	6.0
Plasticity Index	0.0
Is layer compacted?	False

	Is User Defined?	Value
Maximum dry unit weight (kgf/m^3)	False	2038.2
Saturated hydraulic conductivity (m/hr)	False	2.376e-02
Specific gravity of solids	False	2.7
Water Content (%)	False	5.7

User-defined Soil Water Characteristic Curve (SWCC)	
Is User Defined?	False
af	3.0201
bf	2.5984
cf	0.7539
hr	100.0000

Sieve Size	% Passing
0.001mm	
0.002mm	
0.020mm	
0.075mm	5.0
0.150mm	
0.180mm	
0.250mm	
0.300mm	13.5
0.425mm	
0.600mm	
0.850mm	
1.18mm	27.5
2.0mm	
2.36mm	
4.75mm	45.0
9.5mm	61.5
12.5mm	77.5
19.0mm	92.5
25.0mm	100.0
37.5mm	
50.0mm	
63.0mm	
75.0mm	
90.0mm	

Layer 4 Non-stabilized Base : A-1-b

Unbound	
Layer thickness (mm)	400.0
Poisson's ratio	0.35
Coefficient of lateral earth pressure (k0)	0.5

Modulus (Input Level: 3)

Analysis Type:	Modify input values by temperature/moisture
Method:	Resilient Modulus (MPa)

Resilient Modulus (MPa)
150.0

Use Correction factor for NDT modulus?	-
NDT Correction Factor:	-

Identifiers

Field	Value
Display name/identifier	A-1-b
Description of object	Default material
Author	AASHTO
Date Created	1/1/2011 12:00:00 AM
Approver	
Date approved	1/1/2011 12:00:00 AM
State	
District	
County	
Highway	
Direction of Travel	
From station (km)	
To station (km)	
Province	
User defined field 1	
User defined field 2	
User defined field 3	
Revision Number	0

Sieve

Liquid Limit	11.0
Plasticity Index	0.0
Is layer compacted?	False

	Is User Defined?	Value
Maximum dry unit weight (kgf/m^3)	False	1981.7
Saturated hydraulic conductivity (m/hr)	False	7.17e-03
Specific gravity of solids	False	2.7
Water Content (%)	False	7.9

User-defined Soil Water Characteristic Curve (SWCC)	
Is User Defined?	False
af	5.0954
bf	2.5384
cf	0.8464
hr	100.0000

Sieve Size	% Passing
0.001mm	
0.002mm	
0.020mm	
0.075mm	4.0
0.150mm	
0.180mm	
0.250mm	
0.300mm	33.5
0.425mm	
0.600mm	
0.850mm	
1.18mm	55.0
2.0mm	
2.36mm	
4.75mm	60.0
9.5mm	
12.5mm	
19.0mm	
25.0mm	75.0
37.5mm	
50.0mm	
63.0mm	
75.0mm	
90.0mm	

Layer 5 Subgrade : A-6

Unbound	
Layer thickness (mm)	Semi-infinite
Poisson's ratio	0.3
Coefficient of lateral earth pressure (k0)	0.5

Modulus (Input Level: 3)

Analysis Type:	Modify input values by temperature/moisture
Method:	Resilient Modulus (MPa)

Resilient Modulus (MPa)
35.0

Use Correction factor for NDT modulus?	-
NDT Correction Factor:	-

Identifiers

Field	Value
Display name/identifier	A-6
Description of object	Default material
Author	AASHTO
Date Created	1/1/2011 12:00:00 AM
Approver	
Date approved	1/1/2011 12:00:00 AM
State	
District	
County	
Highway	
Direction of Travel	
From station (km)	
To station (km)	
Province	
User defined field 1	
User defined field 2	
User defined field 3	
Revision Number	0

Sieve

Liquid Limit	18.0
Plasticity Index	4.0
Is layer compacted?	False

	Is User Defined?	Value
Maximum dry unit weight (kgf/m^3)	False	1992.5
Saturated hydraulic conductivity (m/hr)	False	1.095e-06
Specific gravity of solids	False	2.7
Water Content (%)	False	8.8

User-defined Soil Water Characteristic Curve (SWCC)	
Is User Defined?	False
af	26.3898
bf	1.0483
cf	0.8553
hr	332.0000

Sieve Size	% Passing
0.001mm	
0.002mm	8.0
0.020mm	
0.075mm	29.0
0.150mm	
0.180mm	58.0
0.250mm	
0.300mm	
0.425mm	72.0
0.600mm	
0.850mm	
1.18mm	
2.0mm	84.0
2.36mm	
4.75mm	90.0
9.5mm	94.0
12.5mm	97.0
19.0mm	98.0
25.0mm	100.0
37.5mm	
50.0mm	
63.0mm	
75.0mm	
90.0mm	

Calibration Coefficients

AC Fatigue

AC Fatigue	
$N_f = 0.00432 * C * \beta_{f1} k_1 \left(\frac{1}{\varepsilon_1}\right)^{k_2 \beta_{f2}} \left(\frac{1}{E}\right)^{k_3 \beta_{f3}}$	k1: 3.75
	k2: 2.87
$C = 10^M$	k3: 1.46
	Bf1: (5.014 * Pow(hac,-3.416)) * 1 + 0
$M = 4.84\left(\frac{V_b}{V_a + V_b} - 0.69\right)$	Bf2: 1.38
	Bf3: 0.88

AC Rutting

$$\frac{\varepsilon_p}{\varepsilon_r} = k_z \beta_{r1} 10^{k_1} T^{k_2 \beta_{r2}} N^{k_3 \beta_{r3}}$$

$$k_z = (C_1 + C_2 * depth) * 0.328196^{depth}$$

$$C_1 = -0.1039 * H_a^2 + 2.4868 * H_a - 17.342$$

$$C_2 = 0.0172 * H_a^2 - 1.7331 * H_a + 27.428$$

Where:

$H_{ac} = total\ AC\ thickness(in)$

$\varepsilon_p = plastic\ strain(in/in)$

$\varepsilon_r = resilient\ strain(in/in)$

$T = layer\ temperature(^\circ F)$

$N = number\ of\ load\ repetitions$

AC Rutting Standard Deviation	0.24 * Pow(RUT,0.8026) + 0.001	
AC Layer 1	K1:-2.45 K2:3.01 K3:0.22	Br1:0.128 Br2:0.52 Br3:1.36
AC Layer 2	K1:-2.45 K2:3.01 K3:0.22	Br1:0.4 Br2:0.52 Br3:1.36

Thermal Fracture

$$C_f = 400 * N\left(\frac{\log C / h_{ac}}{\sigma}\right)$$

$$\Delta C = (k * \beta t)^{n+1} * A * \Delta K^n$$

$$A = 10^{(4.389 - 2.52 * \log(E * \sigma_m * n))}$$

$C_f = observed\ amount\ of\ thermal\ cracking(ft/500ft)$
$k = refression\ coefficient\ determined\ through\ field\ calibration$
$N(\,) = standard\ normal\ distribution\ evaluated\ at(\,)$
$\sigma = standard\ deviation\ of\ the \log\ of\ the\ depth\ of\ cracks\ in\ the\ pavments$
$C = crack\ depth(in)$
$h_{ac} = thickness\ of\ asphalt\ layer(in)$
$\Delta C = Change\ in\ the\ crack\ depth\ due\ to\ a\ cooling\ cycle$
$\Delta K = Change\ in\ the\ stress\ intensity\ factor\ due\ to\ a\ cooling\ cycle$
$A, n = Fracture\ parameters\ for\ the\ asphalt\ mixture$
$E = mixture\ stiffness$
$\sigma_M = Undamaged\ mixture\ tensile\ strength$
$\beta_t = Calibration\ parameter$

Level 1 K: ((3 * Pow(10,-7)) * Pow(MAAT,4.0319)) * 1 + 0	Level 1 Standard Deviation: 0.14 * THERMAL + 168
Level 2 K: ((3 * Pow(10,-7)) * Pow(MAAT,4.0319)) * 1 + 0	Level 2 Standard Deviation: 0.20 * THERMAL + 168
Level 3 K: ((3 * Pow(10,-7)) * Pow(MAAT,4.0319)) * 1 + 0	Level 3 Standard Deviation: 0.289 * THERMAL + 168

CSM Fatigue

$$N_f = 10^{\left(\frac{k_1 \beta_{c1} \left(\frac{\sigma_s}{M_r}\right)}{k_2 \beta_{c2}}\right)}$$

$N_f = number\ of\ repetitions\ to\ fatigue\ cracking$
$\sigma_s = Tensile\ stress(psi)$
$M_r = modulus\ of\ rupture(psi)$

k1: 0.972	k2: 0.0825	Bc1: 1	Bc2:1

LVR_400AADT_CIR_3%-12 years December 2019

File Name: C:\Users\admin\Desktop\Taha M2\LVR_400AADT_CIR_3%-12 years December 2019.dgpx

Unbound Layer Rutting

$$\delta_a(N) = \beta_{s_1} k_1 \varepsilon_v h \left(\frac{\varepsilon_0}{\varepsilon_r}\right) \left| e^{-\left(\frac{\rho}{N}\right)^{\beta}} \right|$$

δ_a = permanent deformation for the layer
N = number of repetitions
ε_v = average veritcal strain(in/in)
$\varepsilon_0, \beta, \rho$ = material properties
ε_r = resilient strain(in/in)

Base Rutting		Subgrade Rutting	
k1: 0.965	Bs1: 1	k1: 0.675	Bs1: 1
Standard Deviation (BASERUT) 0.1477 * Pow(BASERUT,0.6711) + 0.001		Standard Deviation (BASERUT) 0.1235 * Pow(SUBRUT,0.5012) + 0.001	

AC Cracking

AC Top Down Cracking

$$FC_{top} = \left(\frac{C_4}{1 + e^{(C_1 - C_2 * log_{10}(Damage))}}\right) * 10.56$$

c1: 7	c2: 3.5	c3: 0	c4: 1000

AC Bottom Up Cracking

$$FC = \left(\frac{6000}{1 + e^{(C_1 * C_1' + C_2 * C_2' log_{10}(D*100))}}\right) * \left(\frac{1}{60}\right)$$

$$C_2' = -2.40874 - 39.748 * (1 + h_{ac})^{-2.856}$$

$$C_1' = -2 * C_2'$$

c1: 1.31	c2: (0.867 + 0.2583 * hac) * 1 + 0	c3: 6000

Top down AC Cracking Standard Deviation	Bottom up AC Cracking Standard Deviation
200 + 2300/(1+exp(1.072-2.1654*LOG10(TOP+0.0001)))	1.13 + 13/(1+exp(7.57-15.5*LOG10(BOTTOM+0.0001)))

CSM Cracking

$$FC_{ctb} = C_1 + \frac{C_2}{1 + e^{C_3 - C_4 * log_{10}(Damage)}}$$

C1: 0	C2: 75	C3: 2	C4: 2

CSM Standard Deviation
CTB*1

IRI Flexible Pavements

C1 - Rutting
C2 - Fatigue Crack
C3 - Transverse Crack
C4 - Site Factors

C1: 55	C2: 0.4	C3: 0.008	C4: 0.015